Ductile Fracture and Structural Integrity of Pipelines & Risers

by

Kirki N. Kofiani

Submitted to the Department of Mechanical Engineering
in partial fulfillment of the requirements for the degree of
Doctor of Philosophy in Mechanical Engineering
at the
MASSACHUSETTS INSTITUTE OF TECHNOLOGY
February 2013

Author .....
Department of Mechanical Engineering
January 1, 2013

Certified by .....
Tomasz Wierzbicki
Professor, Applied Mechanics, Committee Chairman
Thesis Supervisor

Certified by .....
Paul D. Sclavounos
Professor, Mechanical Engineering & Naval Architecture, Committee Member
Thesis Supervisor

Certified by .....
Henry S. Marcus
Professor, Mechanical Engineering & Marine Systems, Committee Member
Thesis Supervisor

Accepted by .....
David E. Hardt
Chairman, Department Committee on Graduate Thesis

To the memory of my beloved uncle and godfather

Ductile Fracture and Structural Integrity of Pipelines & Risers

by

Kirki N. Kofiani

Submitted to the Department of Mechanical Engineering
on January 1, 2013, in partial fulfillment of the
requirements for the degree of
Doctor of Philosophy in Mechanical Engineering

Abstract

The Oil and Gas (O&G) industry has recently turned its interest towards deep and ultra-deep offshore installations in order to address the global increase of energy demand. Pipelines and risers are key components for the production and transportation of oil and gas both in the offshore and onshore environment. The structural integrity and fracture control of pipes, which are major components for the exploration, production and transportation of fossil fuels have been the subject of extensive analysis in the past decade using classical fracture mechanics approaches, especially for the offshore case. The main driving force for this line of research was the fact that both the cost and the technical challenges increase disproportionally with water depth. In the deep and ultra-deep water environment the technical challenges include higher permanent and operational loads, extreme environmental conditions and the presence of corrosive agents. All the above mentioned parameters demand the use of modern fracture mechanics approaches. At the same time, the inaccessibility to structures located at depths of two to three kilometers, results in extreme repair costs. Due to the magnitude of environmental and financial consequences in the event of failure, the industry has established extremely conservative safety requirements resulting from outdated approaches for those types of structures. Furthermore, the O&G industry is reluctant to adopt novel fracture models, unlike other industries, such as the automotive and aerospace. Pipelines and risers need to be evaluated both from a structural and a financial perspective. The current thesis is proposing a new physics-inspired technology and computational capability for the prediction of fracture and structural failure of pipelines and risers operating in extreme conditions, such as deep and ultra-deep water environments subjected to extreme conditions and accidental loads. The computational tool employed in the current study is derived from a variational principle, combined with a cumulative measure of damage that is developed to control the fracture initiation. The calibration process of this methodology is achieved through a hybrid numerical experimental procedure. The material selection for this study was chosen naturally from the O&G and pipeline community. Traditionally, the O&G and pipeline industries have been using not only conventional

fracture methods, but also conventional low-grades of steels for pipelines and risers, such as X60 and X70. However, deep and ultra-deep applications and the demand for increase of daily flow production pose new challenges in terms of harsh environmental conditions, increase of external diameter and higher operational loads. The industry is well aware of the fact that Advance High Strength Steels (AHSS), such as X100 and X120, can address those issues, but is not yet ready to introduce them, due to incomplete understanding of their material properties and structural behavior in the plastic and near failure range. Therefore, the current thesis offers a comprehensive study of two representative grades from both categories (X70 and X100), comparing their mechanical properties and completing a preliminary analysis quantifying the financial difference between the two for pipeline construction. Pipeline and riser installations are extremely capital intensive. They need to be evaluated both from a structural and a financial perspective, so that operating companies can quantify the integrity of their investments. The proposed thesis will develop a method using representations of oil prices and material costs along with a fracture mechanics model to improve the decision process of the material, the design, and the operating conditions of pipeline installations. This technique will not only attempt to account for the mechanical properties and structural integrity of the tubular component of interest but also to quantify the financial benefit of AHSS in the Oil and Gas community.

Thesis Supervisor: Tomasz Wierzbicki
Title: Professor, Applied Mechanics, Committee Chairman

Thesis Supervisor: Paul D. Sclavounos
Title: Professor, Mechanical Engineering & Naval Architecture, Committee Member

Thesis Supervisor: Henry S. Marcus
Title: Professor, Mechanical Engineering & Marine Systems, Committee Member

Acknowledgments

First of and foremost, I would like to thank my advisors Professor Tomasz Wierzbicki, Professor Henri Marcus and Professor Paul Sclavounos for their guidance, encouragement and discussions on both research and non-research related matters. Especially, I would like to thank Professor Wierzbicki who taught me the importance of real-world applications, the significance of collaborations both within our lab and in the wide-academic community. This thesis would not have been possible without the support of Dr. Young-Woong Lee, who believed in this project early on and supported this work through the MIT/Shell project. Acknowledgements are also due to Dr. Bo Cerup Simonsen for his contribution to the project and for offering me the first real world perspective on my work and Dr. Aida Nonn that has been a valuable colleague, advisor and friend. Also, I want to deeply thank the VFRL and ICL families for their immense contribution in my transformation from a Hydro researcher to an Experimental and Computational Fracture Mechanics researcher. Especially, I would like to thank Wenting Xiao (Dr.), Sankha Banerjee (Dr.), Grgur Tokic, Tea Zakula, Bryce Campbell, Meng Liu (Dr), Elham Sahraei (Dr.), Allison Beese (Dr.), Matthiew Dunand, Stephane Marcadet, Kai Wang, Keun Hwan Pack and Xiaowei Zhang for the support, discussions and long explanations of initially foreign concepts and also Themis Resvanis for the jump-start of this project with the ROV picture of the Deepwater Horizon leak location. I owe additional thanks to Ms. Barbara Smith for her amazing help in all types of problems and matters during my PhD years and for her (and dear Benjamin's) encouragement in times of extreme stress. I would also like to thank my immediate and extended family/friends for their love and support on this work. Specifically, thanks are due to my cousins Konstantina and Theodora and Eleni for teaching me humility and forgiveness, Anastasia Kefiridou and Giorgos Papadakos for offering to me their unconditional love and support, my closest friends Eirini Liotou, Ivi Tsantili and Konstantina Georgaki for their time and encouragement, my thesis group Dr. Hsi, Gabie, Timea and Razan. Also, Chun for inspiring and guiding me towards becoming a Fracture Mechanics researcher, my mother and

father for teaching me perseverance and self-worth, my grandmother who taught me human kindness and my grandfather who taught me honor. This worked would have been impossible with out you all.

Contents

List of Figures

List of Tables

Abbreviations

ABS American Bureau of Shipping

AHSS Advanced High strength Steel

Al2O3 Aluminium Oxides

API American Petroleum Institute

BG British Gas

BP British Petroleum

BV Bureau Veritas

CAPEX Capital Expenditures

CaS Calcium Sulphide

CBA Cost Benefit Analysis

CCS China Classification Society

CDF Crack Driving Force

ClassNK Nippon Kaiji Kyokai

COD Crack Opening Displacement

CRES Center for Reliable Energy Systems

CSM Centro Sviluppo Materiali

CT Compact Tension

CTOA Crack Tip Opening Angle

CTOD Crack Tip Opening Displacement

CVN Charpy V Notch Tests

DIC Digital Image Correlation

DnV Det Norkse Veritas

DWTT Drop Weight Tear Tests

EAW Electric Arc Welding

ECSC European Coal and Steel Community

EMSA European Maritime Safety Agency

EPRG European Pipeline Research Group

ERW Electric Resistance Welding

FAD failure assessment diagram

FE Finite Element

FEM Finite Element Modeling

GL Germanischer Lloyd

GMA Gas Metal Arc

GoMOS Gulf of Mexico Oil Spill

GTN Gurson-Tvergaard-Needleman model

HAZ Heat Affected Zone

High Pressure/ High Temperature HP/HT

HSAW Helical Submerged Arc Welded

IACS International Association of Classification Societies

ICL Impact and Crashworthiness Lab

ISOPE International Society of Ocean (Offshore) and Polar Engineering

JIP Joint Industrial Project

KR Korean Register of Shipping

LOM Light Optical Microscopy

LR Lloyd's Register

LSAW Longitudinal Submerged Arc Welded

MC Mohr-Coulomb

MMC Modified Mohr-Coulomb

NK Nippon Kaiji Kyokai (ClassNK)

NPV Present Value

O&G Oil and Gas

OD Outside Diameter

OMAE International Conference on Ocean, Offshore and Arctic Engineering

OPEC Organization of the Petroleum Exporting Countries

R&D Research and Development

R-curve Resistance curve

RINA Registro Italiano Navale

ROV Remotely Operated Vehicles

ROW Right of Way

RS Russian Maritime Register of Shipping

SAW Submerged Arc Welded

SBD Strain-Based Design

SEM Scanning Electron Microscope

SENB Single Edge Notched under Bending

SENT Single Edge Notched under Tension

SOLAS Safety Of Life at Sea

TiN Titanium Nitride

TOCA Transfer of Class Agreement

Chapter 1

Introduction

This chapter starts with setting the background of the current thesis, highlighting the transition from fracture technology for the automotive industry towards fracture for the oil and gas industry. More importantly, the focus of this study will be the transition from investigation of plasticity and fracture behavior of metal sheets to thick-walled pipes. The next step will be stating the hypothesis of the applicability of the Modified Mohr-Coulomb (MMC) model for the structural evaluation of pipelines and risers. The significance of this research area will be presented including the motivation and contribution to both academic and real world problems. The correct and reliable safety assessment of pipes and risers for complex loading scenarios lies in the extension of a powerful fracture technology to a new set of problems. Finally, the financial implications of comparing high and low strength API grades for both existing and future newbuildings infrastructure for cost assessment is presented for two specific pipeline cases. Finally, the outline of the thesis is presented, including the proof of the hypothesis and the benefits stemming from it.

1.1 Setting the Background for the Research

Pose question that the thesis will answer!

Over the past 10 years the Impact and Crashworthiness Lab (ICL) at MIT has developed a complete fracture predictive technology for steel sheets under the spon-

sorship of the worldwide steel and automotive industries. This technology has now reached a stage of full maturity that allows for the reliable and high accuracy prediction of any sheet metal forming and crashworthiness application. This technology has been developed and evaluated as an important predictive tool for both the automotive and steel industries. The applicability of this technology remains to be evaluated, however, for cases of thick-walled structures, where the stress state conditions significantly vary through the thickness and also throughout the loading process. This new set of problems remains to be studied, so that the MIT fracture predictive technology can be applied to new fields of engineering with stress states that significantly depart from the plane stress state region. Also, this modern approach is required to be compared to the standard fracture mechanics methodologies currently used for the assessment of thick tubular components. The main objective of the current thesis originally aimed to test the hypothesis of applying the MIT technology to general cases of fracture prediction and strain based design of pipelines and risers. However, due to inherent differences in the setting of the problem in the case of heavy-walled tubular components, primary research focused on extending the applicability of the MIT fracture technology to cover a much larger range of stress states [58]. The most important difference between sheets and thick tubes lies in the fact that in plasticity and fracture characterization of steel sheets, the stress state is close to plane stress, which simplifies the underlying equations, both for the description of the plasticity and fracture behavior of the material. At the same time, in the case of heavy-walled pipes, the material properties and stress state during operation and failure depends largely on the wall thickness and loading setting. Another important difference is the fact that in the current study, the material is characterized as an end product, rendering the manufacturing process an important factor that affects immensely the plasticity, anisotropy and fracture behavior of the final metal structure of interest. Different industries focus on different engineering and design parameters. In previous research, ICL was interested in understanding how the originally produced sheet would sustain the manufacturing process loading during sheet metal-forming and also the dynamic loading during accidental impact. In the current line of work, the main

interest is to understand how the manufacturing process affects the safety and life expectancy of the final product. In the Oil and Gas (O&G) industry, pipelines and risers have a special value in the industry's supply chain. The safe extraction, production and transportation of oil and gas greatly depends on these critical components, affecting managerial decisions and also the oil and gas market itself. There are examples of safety breaches of pipelines and risers that led to disturbance of oil and gas flow that subsequently affected also the financial market. For example, the recent Gulf of Mexico, Deepwater Horizon accident, led to a significant decrease of O&G companies' market value. It was estimated by Bloomberg in 2010 in that companies that were associated with the Gulf of Mexico Oil Spill (GoMOS) lost $(US)95bn (see Fig. 1-1). The effect of failure of pipelines and risers is significant and additional work is required to fully understand how material properties and loading may lead to a structural collapse and the subsequent event of leak. The result of the intense in-depth research conducted in 2011 by National Commission report on the BP Deepwater Horizon Oil Spill and Offshore Drilling, resulted in the following statement:
"Deepwater energy exploration and production, particularly at the frontiers of experience, involve risks for which neither industry nor government has been adequately prepared, but for which they can and must be prepared in the future."
Therefore, understanding and reliably reconstructing extreme case scenarios and designing the correct procedures for minimizing the environmental effect due to catastrophic events has not only a pragmatic environmental but also financial and economic effect. The current study explores in depth the technical part and touches upon the financial implications of responsible and safe engineering, so that technological advances may lead to large-scale adoption of oil and gas as a safe energy source even when explored and produced in highly dangerous locations.

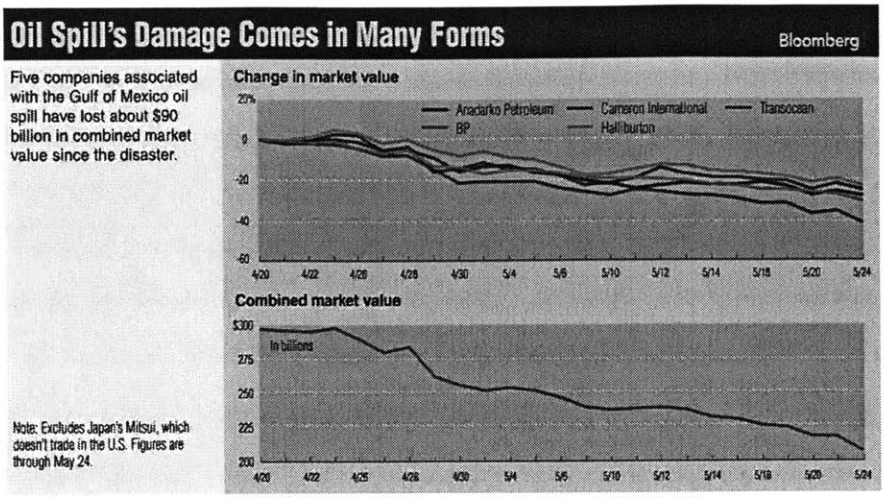

Figure 1-1: Deepwater Horizon accident negative effect on market value of companies associated with the oil spill [84].

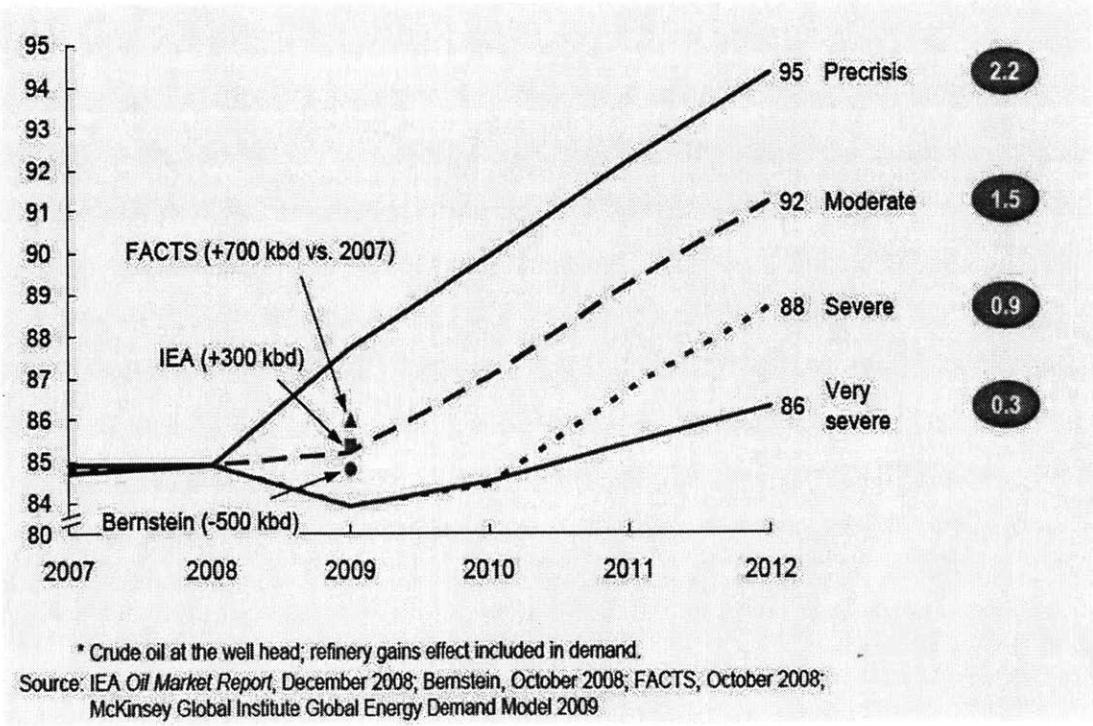

Figure 1-2: Oil demand predictions for different market projection scenarios ranging from conservative to optimistic [28].

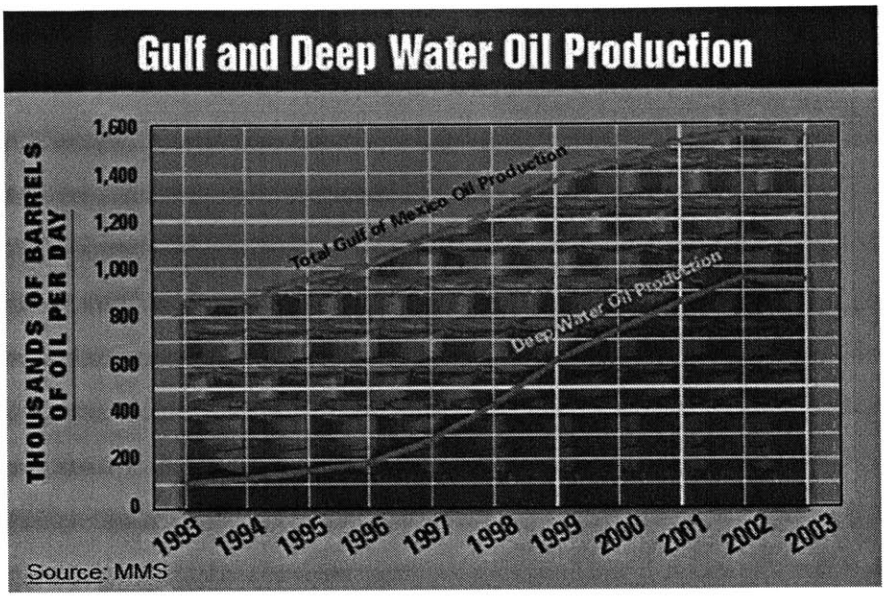

Figure 1-3: Exploration and production trend towards deep and ultra deepwater territories [68].

All the above are combined with a unique set of events that lead to an increased demand for energy resources (see Fig. 1-2), similar as the rise of new markets like China and India. The oil and gas industry is riding the wave of surging demand in which the risers and key pipelines are reshaping the global economy in terms of exploration and transportation of oil and gas. The structural integrity of those components is therefore an important parameter that is required to be thoroughly investigated with the state of the art technical tools such as the MIT fracture predictive technology. That results in a massive expansion of oil and gas demand forcing O&G companies to move into more hostile environment-located reservoirs (ultra deep water and arctic) to match the existing supply [36] as it is shown in Fig. 1-3.

It is also important to mention that it is predicted by the US Energy Information Administration's World Energy Outlook that fossil fuels will remain the primary sources of energy, meeting more than 90% of the increase in future energy demand that is assessed to rise by about 1.6% per year, from 75 millions of barrels of oil per day (mb/d) in 2000, to 120 mb/d in 2030. As far as the natural gas consumption demand is concerned, it is expected to double between now and 2030. In this highly lucrative

business, safety poses a barrier and a competitive advantage to oil companies. Data from previous years show that companies like Exxon Mobil (the world-leading oil company that announced in January 2006 profits of $US36 billion) and Shell Oil (that announced a record profit for a British company of $US23 billion, in February 2006) are more open to new technologies that will provide the competitive edge and thus the necessary licenses to explore even more demanding fields. The growth in energy demand was and will continue in the future to be supported by extensive expansion of the pipeline infrastructure. Over approximately the last 50 years, the pipeline network has grown by a factor of 10 and is expected to be up by 7% per year over the next 15 years. This means over 8000 km/yr of pipeline being built in the USA alone, at a cost of $(US)8 billion/yr. The structural integrity of pipelines becomes very important especially taking into account that the main causes of pipeline failure in the USA is accidental loading (external force) leading to environmental catastrophes and casualties, as shown in Fig. 1-4.

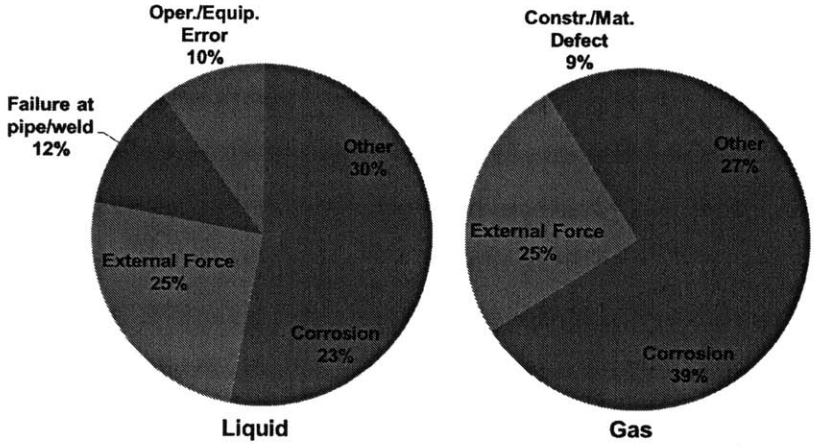

Figure 1-4: Percentage breakdown of main failure causes the US pipeline infrastructure [52].

Pipes are designed to withstand multiple operating, installation, environmental and accidental loads. An important and traditional design parameter is the internal

pressure that is related to the circumferential (hoop) stress, σ_{hoop} defined in Eq. (1.1).

$$\sigma_{hoop} = \frac{pD}{2t} = a\sigma_{yield} \tag{1.1}$$

where p is the internal pressure, t is the thickness of the pipe, a is the design safety factor and σ_{yield} is the yield strength of the base material.

However, the above-mentioned formula leads to over-engineered pipes taking into account only the plasticity information of the base material. As the demands of safe pipes increase and the loading conditions become more extreme, new models are needed that take into account the detailed mechanical characteristic of the pipe material. Other industries, like the automotive, were forced to move faster towards modern approaches for economic reasons that required the decrease of the vehicle weight that is easily translated into gasoline consumption per mile traversed. In the case of the O&G industry, the improvement of the understanding and modeling of the material behavior is driven by the increasing requirements for safer and more economic design in extreme environments, like the arctic and ultra-deep underwater locations. This industry is notorious for its reluctance towards new methods and its support to over-engineering as the best alternative to a complex and modern approach. Although change is not welcomed by O&G community, however, it is required especially after the GoMOS effect in the offshore drilling legislation and in the market value of related oil companies. There is one of the driving forces towards achieving not only the structural integrity but also the economic design and reduction of over-engineering. Also, as new grades of steel continue to emerge, it is important to have a reliable fracture predictive tool that allows for a comparison and assists the designing process both from a technical and economical point of view.

1.2 Pipelines and Risers

The current thesis is primarily concerned with the investigation of the structural integrity of pipelines and risers. In the offshore exploration, production and trans-

portation of oil and gas, pipes play a very significant role. Pipes are used in offshore and onshore installation both vertically, connecting the production facility with the reservoir and also horizontally, connecting remote wells to the location of processing or to the transportation hub. Pipelines are the most effective means of transportation for oil and gas. They offer a vast array of reasons favoring them against others means like transportation by tankers, trucks, rail etc. The main advantages of pipeline use for transportation of oil and gas are both economic and social. More specifically, pipelines offer a large throughput over extended hostile territories with low maintenance costs at a fraction of the cost of transportation compared to other means previously mentioned. They also offer the second best value proposition for transportation of oil and gas, as it shown in Fig. 1-5.

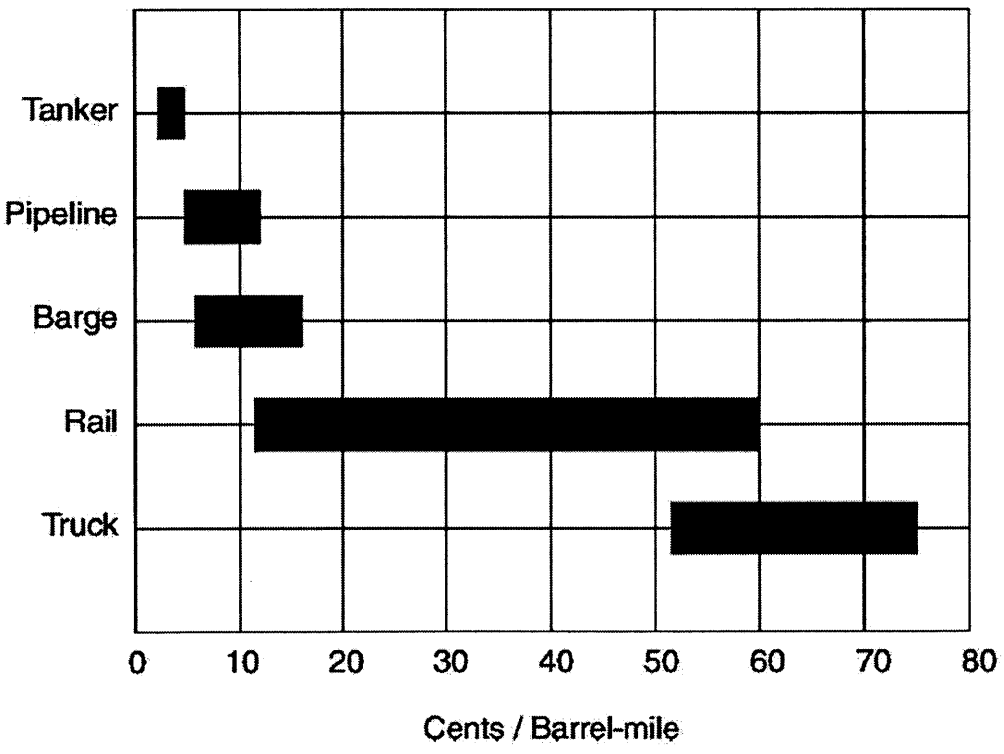

Figure 1-5: Comparison of transportation cost between major logistics methods for petroleum.

Table 1.1: Comparison of Energy Intensiveness between different means of oil and gas transportation.

Airplane	37,000
Truck	2300
Railroad	680
Waterway/Barge	540
Oil Pipeline	450

Pipelines have also very low energy intensity, that is defined as the energy consumed in transporting a unit weight of cargo over unit distance (such as Btu per tonne mile), see Table. 1.1. It is finally important to mention that the safe operation of pipelines is environmental friendly. However, when their safety is breached, the pollution affects greatly the surrounding environment. Risers on the other hand connect the reservoir that is located in the bottom of the ocean floor to the platform without contaminating the surrounding environment. According the location of the well, the depth, the ocean wave profile in the specific location and the well characteristics, risers are designed appropriately to connect the production site to hub for further transport or immediate processing. The length of risers are not usually so extensive as in the case of pipelines.

The manufacturing process for pipelines and risers is the same. Pipelines and risers can be referred to as tubes or tubular components. There are mainly two types of tubes used extensively in the transportation of oil and gas, classified based on the method of pipe manufacturing.

- Seamless pipes
  - Pilger mill process
  - Plug mill process
  - Push mill process
  - Continuous mandrel mill process
- Welded pipes

- Hot pressure welding
- Electric resistance welding
- Electric arc welding

The seamless pipe manufacturing process starts with the heating of the solid billets using the Mannesmann process. Depending on the final diameter and thickness, one of the four following processes one of the following process is used i) continuous casting of round billets, the pug mill, the mandrell mill and the pilger mill. As far as the welded pipes are concerned, there are many categorizations based on the i) forming process, ii) the welding process, iii) the nomenclature, iv) the type of weld and v) the size range.

The manufacturing process plays a critical role in the mechanical characteristics of the end-product. Therefore, in the long run the industry should undertake a comprehensive project of transferring the data and the numerical analysis from the manufacturing phase to the final operating conditions of the pipe installation. The situation facing the O&G industry is somewhat similar to the one studied by and on behalf of the steel and the automotive industries. Computational models were developed to monitor the evolution of the stress and strain tensors during the forming process of components from sheets. The end data of the above-mentioned simulations was the input in the finite element analysis for the prediction of the crashing process. The history of deformation caused during the manufacturing phase of tubes is not included directly in the analysis, but rather indirectly through analyzing the mechanical properties of the pipe material after it has underwent the manufacturing process.

1.3 Structural Integrity of Pipelines and Risers

Offshore pipelines and risers installed in the ultra-deep water depth nowadays are exposed to high external pressure and temperatures. The large plastic deformations may arise during pipe installation (reeling, S-lay, J-lay), under operational conditions

such as free-spans due to uneven seabed topography and wave motion causing sway movement or due to temperature variations leading to local failure due to extreme localized strains. This work focuses on the base material analysis as the first main step illustrating the efficacy and importance of this modern fracture approach for pipe structural integrity assessment. In the recent years, the strain-based approach has been introduced mainly for pipelines. This approach is more appropriate for dealing with global large plastic deformations when compared to the traditional stress-based approaches. Assuming that the pre-service defects resulting from manufacturing, installation (e.g. girth weld defects) and operational process cannot be avoided, these approaches have been extended to allow for flaw assessment. The procedure used by the industry for the assessment of flawed structures is based on the Failure Assessment Diagram (FAD) representing the limit curve of toughness and strength controlled failure. It is implemented in standards and recommended practice such as [31] , [19], [47] and [29]. In case of strain-based flaw assessment, the strain capacity equations (e.g. [33] and UGent equations [38] and [42] and ExxonMobil procedures [59] have been developed to quantify design and allowable strains in dependence of different geometry (pipe diameter, wall thickness, flaw size, etc.) and material parameters (ultimate tensile strength UTS, Y/T ratio, ultimate elongation UEL, weld strength mismatch, toughness, etc.). If the material shows ductile tearing in the stable way prior to final fracture, the fracture toughness is considered in terms of failure Resistance curve (R-curve) instead of single threshold values (Jmat or CTODmat). The resistance curves depend on both the material properties and on the crack tip constraint for the given geometry and loading situation. As shown in [23] they can be normalized by the constraint parameter T-stress. For the derivation of failure criterion, the onset of the unstable crack growth is identified using traditional tangency criterion which requires comparison of Crack Driving Force (CDF) and R-curves. Since the experimental determination of the R-curves for full-scale tests can be very time- and cost-intensive, especially in the view of parametric studies for different pipe geometry, numerous computational fracture models have been developed within the finite element framework aiming to characterize ductile fracture propagation of steel

materials for small and full-scale tests. There are two groups of models, fracture mechanics and damage mechanics based models. A typical example of the former is the mapping approach which interpolates ductile tearing between results of several simulations with fixed but different crack sizes [50]. There are several major limitations of the fracture toughness approach. First, it requires the presence of initial cracks and it will not work to predict initiation of fracture in crack-free bodies. Secondly, it only provides information of initial crack growth, thus fails to predict post-failure behavior of a given component all the way to a complete separation. Thirdly, no constraint effect is considered explicitly, but has to be included via constraint normalized R-curve. Fourthly, no direction of the crack propagation including crack path deviation can be predicted without a user-defined criterion. Finally and most importantly, the approach is restricted to the stress states at the crack tip generating merely Mode I fracture. By contrast, damage mechanics theory is able to describe crack initiation and propagation by allowing the damage evolution to take into account both the influence of local stress and strain variables. Hence, ductile crack propagation can be fully represented within a single simulation. One of these models is Gurson-Tvergaard-Needleman (GTN) model [48], [78]; and [79] and its subsequent modifications. The GTN model and its extensions have removed all above mentioned limitation of the fracture mechanics based models but introduced several new issues. The micromechanics-based GTN model describes the failure mechanism as a sequence of void nucleation, growth and coalescence. Recent modifications of GTN, e.g. to account for shear-stress dominated fracture [56]; [14]; [16] lead to an increase of the additional phenomenological parameters and therefore lost its original appeal. The number of free parameters of the shear modified GTN model has increased to 13 from the original 7 in the GTN model. This creates difficulties in the calibration procedure which should be an integral part of all fracture modeling. Several disposable parameters in the GTN model are responsible for the coupling of fracture with plasticity. Recently [41] showed that this large set of parameters is not necessary for achieving a good correlation in the plastic and fracture range for low triaxiality levels. Another finding was that the GTN model and its derivative cannot predict fracture

in the combined regime of shear and compression loading. The next step in the development of fracture technology is the Modified Mohr-Coulomb model that is the methodology proposed in this thesis. This is a phenomenological but physics-inspired model. It requires the calibration of three free parameters and it is applicable to the whole spectrum of stress states from tension and tension/shear to pure shear, all the way to shear and compression. It has been proven for metal sheet applications and it is proposed for the prediction of failure for pipeline and riser applications. The two parameters are defining the classical Mohr-Coulomb fracture model and the third parameter is responsible for the local shape of the yield condition, introduced by [26]. It was successfully applied for the prediction of ductile fracture initiation and propagation in advanced high-strength sheet and low-strength aluminum materials [24]. This extended model describes the equivalent strain to fracture depending on stress triaxiality and Lode angle that is the normalized third invariant of deviatoric stress tensor. To derive the three-dimensional fracture locus, it is necessary to calibrate only three model parameters by at least the same number of experiments. The suitability of the MMC model to characterize ductile fracture has been demonstrated in many publications, primary for the ranges of low stress triaxiality ($\eta < 2/3$) see (e.g. [24], [41]). On the other hand, there is little information about the accuracy of the model prediction for the high triaxiality range, $\eta > 1.0$, which is very important for analysis of cracked structures. Recent results on the case on API X100 were given in [62] validated by compact specimen experimental and numerical results. The present thesis is explaining in detail the extension of the applicability of the MMC model to the range of high stress triaxiality. This is the area so far dominated almost exclusively by the fracture toughness method and the GTN approach.

1.4 Major Pipeline and Riser Problems

It is important to note that the O&G community is facing a number of important challenges that command for modern fracture prediction methods for the safe design and operation of pipes. Independent of the specifics of the application, pressing is-

sues call for a new method to address existing and future development scenarios and challenges. Ranging from Deep to Ultra Deep Water, pipeline installations down to three kilometers or more are required to address the expansion of subsea system development. The material properties along with external hydrostatic pressure which becomes the main design parameter, the geometric imperfections and the complex loading conditions exerted by neighboring structural components significantly affect the structural integrity of the pipe. That combined with hostile environmental and operational loading conditions create a dangerous mix. Risers in the same environment face the same challenges as pipelines, with the addition of severe cyclic loading due to platform sway movements consequent to wave, wind, currents and tidal loading and also due to vortex shedding induced vibrations directly acting on the riser line due to currents. In this study we will focus on monotonic loading and consider that cyclic loading and additional loading component can be studied independently. High Pressure combined with High Temperature (HP/HT) for cases of exposed pipes into the sea bottom or buried are additional application that need to be investigated. Thermal expansion and lateral bending deformation randomly located or at specific locations along the pipeline route and vertical weight and lateral movement of the superstructure connecting the well to the free-surface are more examples of complex problems that need to be addressed by the community. Finally, abrupt dislocation of parts of the pipe, such as in gauging cases in the arctic environment and ground movement due to seismic excitation leading to large local strains, demand a new methodology that focuses on strain based design. All the above mentioned issues are combined with the continually aging infrastructure for exploration, production and transportation of fossil fuels and the continued evolution and development of new grades of steel toward Advanced High Strength Steel (AHSS) grades. In the following sections more information of how these two aspects create the appropriate environment for research focusing in the structural integrity assessment of thick tubular components will be presented.

1.4.1 Aging of Oil & Gas Infrastructure

One of the most important problems facing the O&G industry, is the fact that the pipeline and marine riser infrastructure is reaching and exceeding their assumed design life span. Over 50% of the USA oil and gas pipeline system (1M km) is over 40 years and 20% of Russians oil and gas system is nearing the end of its design life according to the Mineral Management Service database. The correct assessment of the structural integrity and the remaining life of this infrastructure is important in order to tactically replace older, or more damaged components first and cause the minimum amount of interruptions of flow due to failure events. After the world's pipe infrastructure reaches their life expectancy, the oil and gas community will have to face the challenge of replacement. As environmentally related legislation becomes more stringent, it is important to develop tools that reliably assess any additional operational life of an existing asset and that they are fit for purpose. Therefore, a proactive integrity management of onshore and offshore pipe assets and a re-evaluation of their fitness-for-purpose is essential, making sure that at the end of their predicted operational life there exist proactive measures to pick up the demand for transportation for the next 50 years. In about 15 years, more that half of the existing infrastructure will be at the end of its design life Therefore, care for our aging assets is a major engineering challenge and structural integrity assessments will be a key tool in the near future.

1.4.2 Trend towards API AHSS Grades of Steel

Among many engineering problems involving ductile fracture, the heavy-wall seamless pipelines, risers and drilling pipes present a class of their own. Deep and ultra-deep offshore exploration and productions pose many challenges to the O&G industry. Of particular interest are the choice of the right material and the determination of structural integrity under normal and accidental loading. A grim reminder of the potential hazards is the recent accident of the BP Deepwater Horizon drill platform. There has been a debate within the O&G industry on the right choice of material

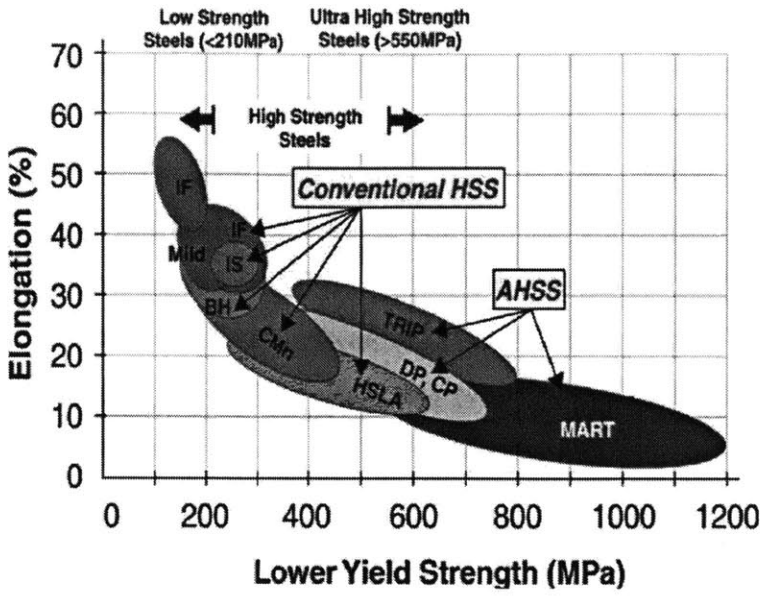

Figure 1-6: Trend towards AHSS observed in the automotive industry.

for ultra-deep water installations. The trend within the automotive industry is to replace conventional grades of steel by Advanced High Strength Steels. The trade-off between the strength and ductility, illustrated by the so-called "banana plot" in Fig. 1-6, gives a clear indication of the dilemma. For comparison, a similar plot for the O&G industry grades of steel was constructed, see Fig. 1-6. The ICL at MIT embarked on a comparative study of the advantages of higher grade steels, including cost implications under the partial support of Shell. The pipeline and riser community proceeded with a different pace and with different objectives. The pipeline industry on one hand is interested in large diameter (internal diameter) to maximize flow. Because of that, the application of AHSS was only for onshore installations where the thickness could be reduced in a similar way as in the automotive industry. The design of offshore pipeline installations, however, are driven by hydrostatic pressure and for that reason the reduction of thickness is not considered in this case due to pipe collapse issues. The pipeline thickness is a critical parameter, that for a certain depth of operation/external pressure, once it reaches a critical value it causes structural collapse and interruption of the transportation of oil or gas. However, new grades of API steel for the construction of pipelines and risers are developed and the

trend is obviously similar to that of the automotive industry (Fig. 1-7).

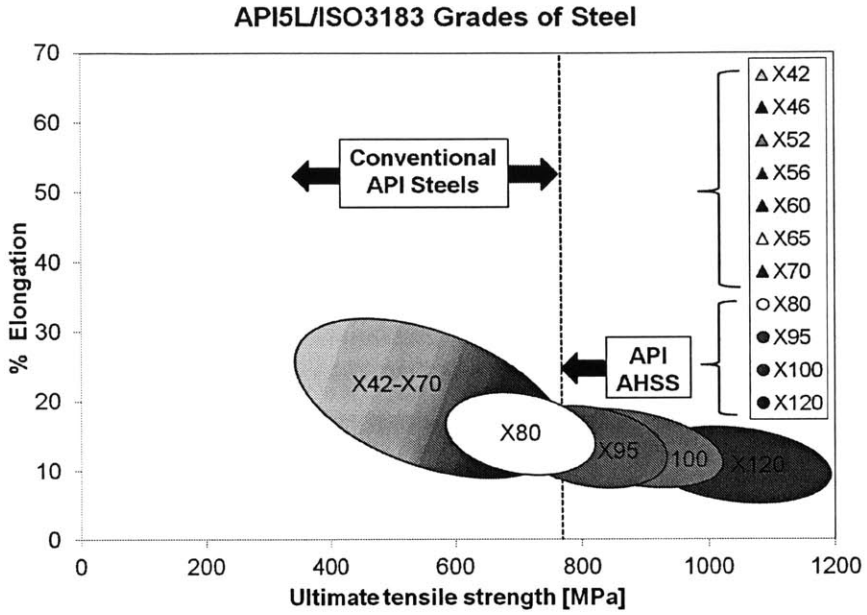

Figure 1-7: Trend towards AHSS observed for API pipeline grades of steel.

1.5 Thesis Outline

The current thesis consists of seven chapters. In the first chapter the setting of the general background of this thesis/research will be presented posing the question of interest (hypothesis), explaining the significance of the research area (motivation/contribution) and finally describing the path/road map of the thesis (outline). In the second chapter the critical parameters of the pipeline and riser applications will be identified and explored in terms of design, manufacturing and operating processes so that the modeling of the problem is complete. In the sequence, chapter 3 will describe the landscape for this research project and presenting the current state of the art and areas of contribution for the present thesis. Chapter 4 will focus on the comprehensive study of the mechanical properties of two important API grades of steel covering both the traditional and Advanced High strength Steel grades while in chapter 5, the validation of the MMC model as a fracture predictive tool in cases

of pipelines and risers will be covered. Finally, in chapter 6 will be the financial assessment of pipelines using structural integrity considerations. Finally, chapter 7 will explore the landscape for new areas of research stemming from this work and make recommendations to the interested industries.

Chapter 2

Oil & Gas Pipelines and Risers

Finally, it should be noted that a pipeline is part of a very large and complex system that includes the linepipe pumps, storage facilities, valves, etc. This chapter considers the pipeline, and not the associated plant. Deep and ultra-deep water applications use medium- and thick- wall pipes for the construction of pipelines and risers. In onshore installations, the wall thickness further reduces and the trend in terms of material selection converges to that of the automotive and aerospace industries. Offshore and onshore pipes are subjected to a large range of operational, environmental and oftentimes environmental loading such as hydrostatic pressure, wave current and environmental loads both during installation and service. As the applications become more demanding and the external conditions more hostile, there is a need for higher strength grades of steels with good weldability and corrosion resistance. The structural integrity and fracture control of pipelines and risers have been the objective of extensive study and analysis in the past using classical fracture techniques. However, these methods lack the potential for the direct connection between the material properties and the processes that it needs to undergo. The proposed study will offer a new, modern fracture technology and computational capability for the prediction of material fracture and structural failure of this class of structures. The model will be applied to two different grades of steel, i) a conventional material extracted from a seamless pipe (API X70) and ii) an advanced high strength steel material extracted from a UOE pipe (API X100). API refers to the American Petroleum Institute. In

the following sections more information of the options for material selection, design and manufacturing process will be presented. A short account of the installation methods for pipelines will be presented and finally the loading for both pipelines and risers will be covered.

2.1 Manufacturing Process of Pipelines and Risers

As it was mentioned in the introduction, the manufacturing process greatly affects the mechanical properties of tubular components. Both pipelines and risers have to comply to a certain set of requirements. The required properties are achieved by a carefully designed manufacturing process. The tubular components used in the O&G industry are either seamless or welded. The first category aims applications with required outside diameter up to 16 inches (406.4 mm). For larger diameters, the UOE and JCO processes are used for up to 64 inches (1625.5 mm) for the outside diameter. For the intermediate range of pipes up to 24 inches (609.6 mm) a continuous process is used to produce Electric Resistance Welded (ERW) tubes. There is typically another manufacturing process of tubes which is the spiral welded process, but is mainly used for water pipes. We have selected to characterize two pipeline materials, one coming from a seamless pipe (X70) and one from a welded pipe using the UOE method (X100). In this manner, information on the effect of the manufacturing process on the mechanical properties will be collected to be compared in terms of anisotropic plasticity, and fracture resistance. More information will be provided in the following paragraphs on the types of different manufacturing processes available for pipe construction.

2.1.1 Seamless pipes

The seamless pipe manufacturing process was invented by the Mannesmann brothers around the 1880s that led to the industrialization of the pipe production. As the patent life has expired, new methods for the manufacturing of seamless pipes have evolved over the years including the i) The pilger mill process, ii) the plug mill,

iii) the continuous mandrel and iv) the stretch reducing mill. The dividing factor between methods lies on the geometric features of the pipe. In Fig. 2-1, it is clear that there are overlaps between the possible geometric features of the tubes that can be achieved through the various manufacturing methods. It is important to note that each tube manufacturer has specific restrictions, ranges and offers a personalized in-house methodology for the manufacturing of tubes, trying to offer a competitive advantage in terms of the mechanical properties and resistance against fracture of the end product to their clients. This competitive environment calls for a modern approach to fracture that can be used to characterize the end product and deduce the damage of the base material during the manufacturing process.

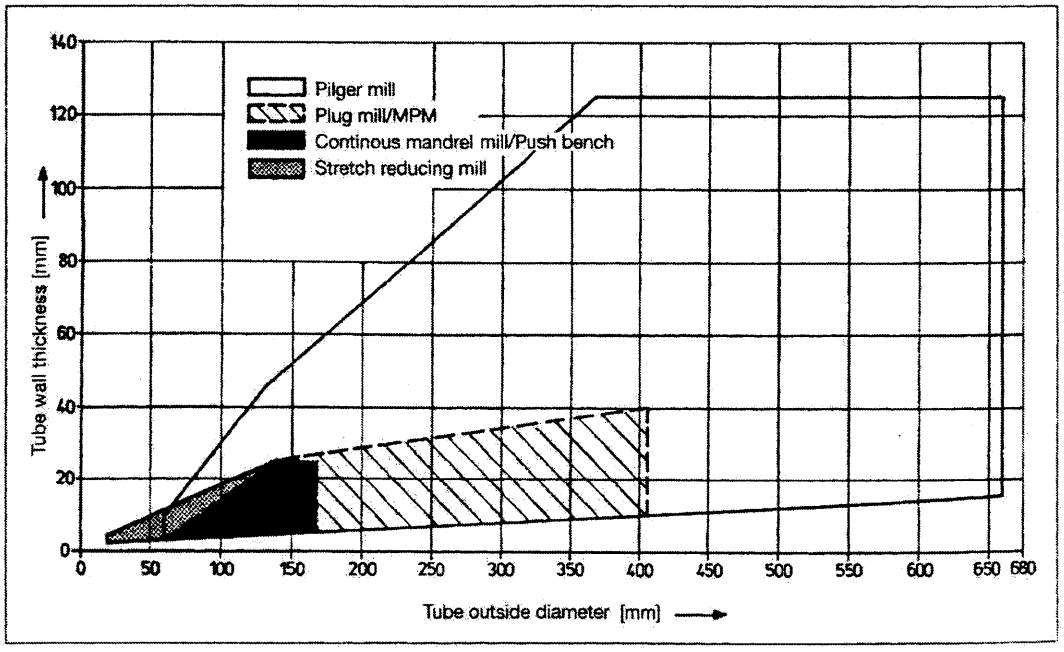

Figure 2-1: Seamless pipe manufacturing process as a function of outside diameter and thickness [64].

The similarities and differences between the four main methods for manufacturing seamless pipes are evident in Figures 2-2, 2-3, 2-4 and 2-5 and are summarized in the following paragraph. The pilger mill method was the original manufacturing process that was proposed by the Mannesmann brothers offering a wide range of Outside

Diameter (OD) and pipe thicknesses. All processes initiate with the heating of the billets using the Mannesmann process. The general description of the manufacturing procedure for seamless pipe included i) the heating of the billets, ii) the piercing of the billet to produce a hollow cell, iii) resizing to the final requirements and iv) the cooling process. The differences lie mainly in the piercing technique ranging from mandrell, hydraulic and pneumatic. It is important to underline that the size of the mill dictates the maximum size that can be achieved. The schematic of a mill using the pilger method is shown in Fig. 2-2 from the initial heating process until the final cooling of the pipe.

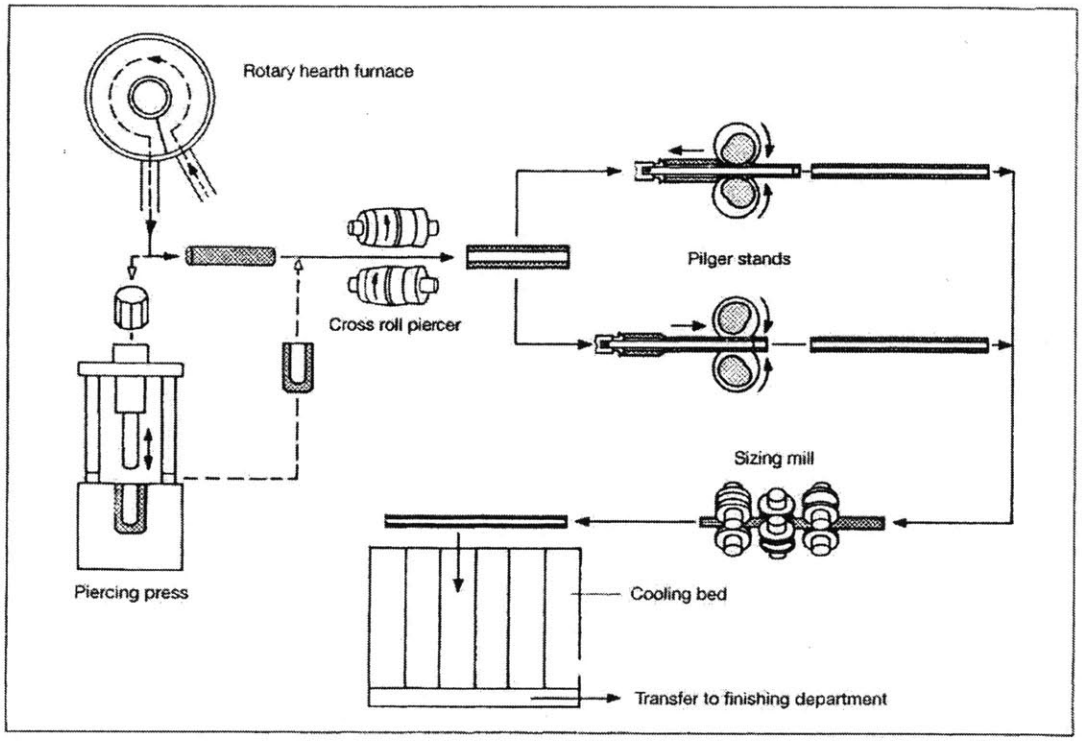

Figure 2-2: Schematic representation of the pilger mill manufacturing process [64].

The schematic of a mill using the plug method is shown in Fig. 2-3 from the initial heating process until the final cooling of the pipe. The schematic of a mill using the mandrel method is shown in Fig. 2-4 from the initial heating process until the final cooling of the pipe. The last schematic is that of the continuous push bench method is shown in Fig. 2-5 from the initial heating process until the final cooling of

the pipe. This technique appeared at the turn of the century offering a more efficient alternative of seamless construction.

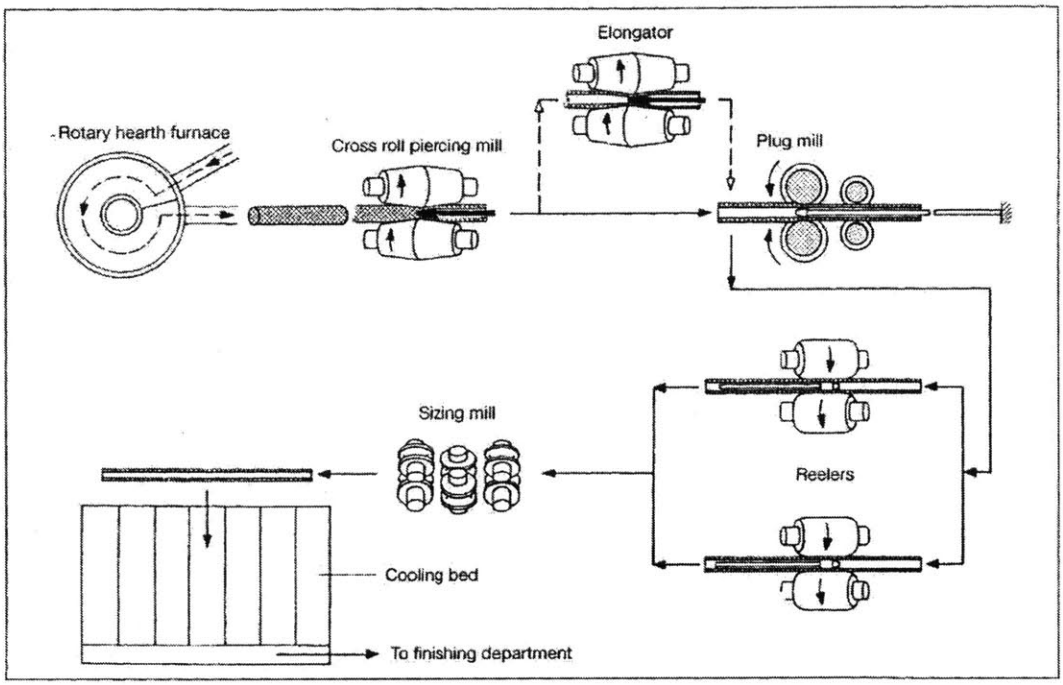

Figure 2-3: Schematic representation of the plug mill manufacturing process [64].

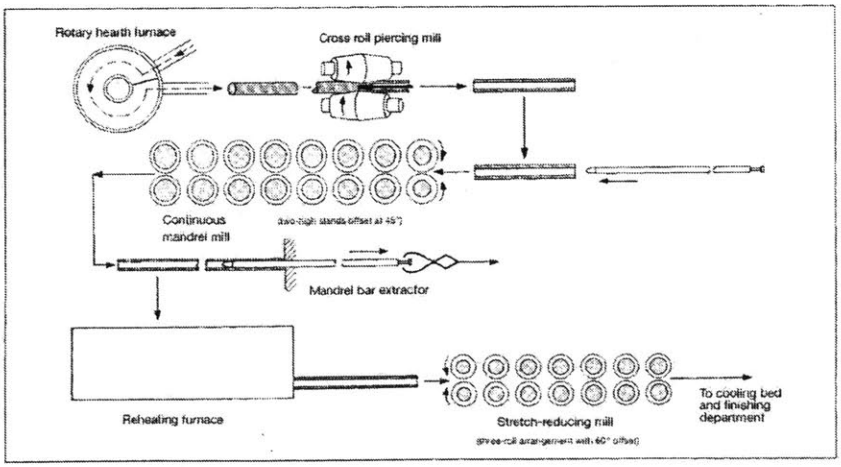

Figure 2-4: Schematic representation of the continuous mandrel mill manufacturing process [64].

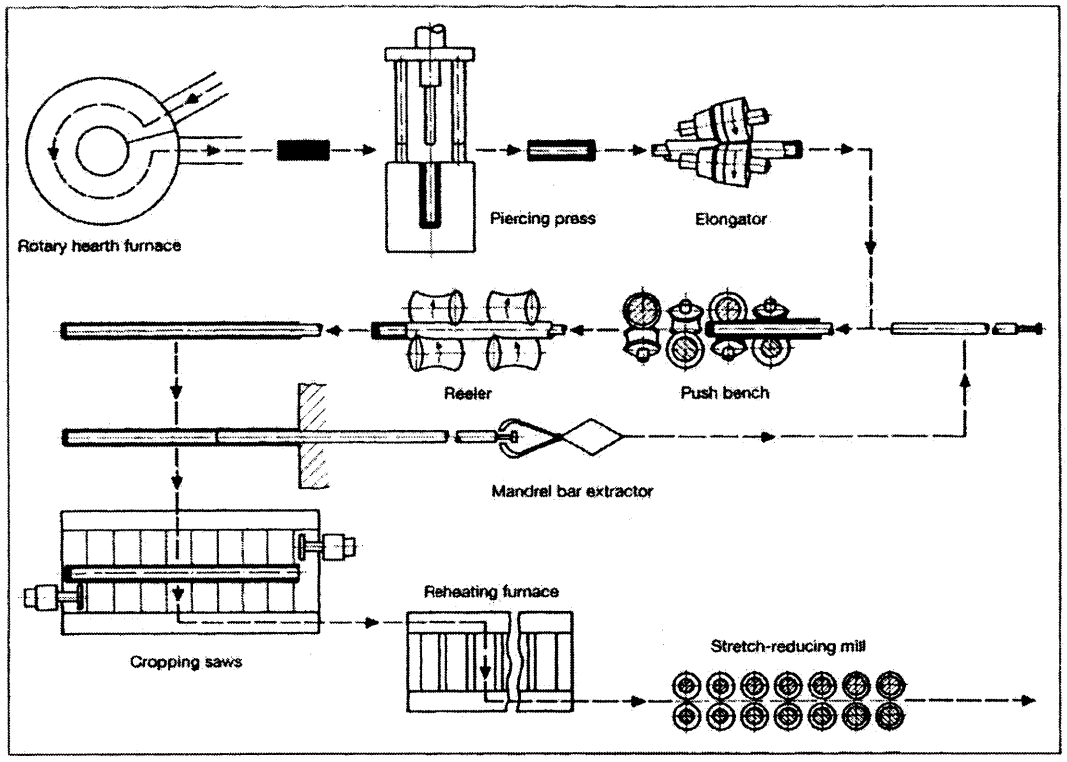

Figure 2-5: Schematic representation of the continuous push bench manufacturing process [64].

2.1.2 Welded pipes

Another alternative for manufacturing pipes of larger outside diameters that cannot be constructed in the seamless mill, is manufacturing employing the welding technology that initiated back in 1825 in Great Britain by J. Whitehouse, the first patent owner of welded pipes. Welded pipes can be categorized based on many criteria, such as the forming process, the welding process and the range of the OD size. As far as the forming process is concerned, there are i) continuous, ii) single forming operation using C-pressing and iii) single forming operation using U/O-pressing. As far as the welding process is concerned, the different available types are i) hot pressure welding, ii) Electric Resistance Welding and iii) Electric Arc Welding (EAW). The hot pressure welding is also referred to as Fretz-Moon process and uses the base mate-

rial as the weldment. The electric resistance welding process can be sub-categorized depending to the frequency of the current used for the welding to direct current, low-frequency and high-frequency. The electric arc welding processes has evolved into a complicated set of sub-processes that include i) Submerged Arc Welding (SAW), ii) Gas Metal Arc (GMA) that are mainly used for either longitudinal and spiral welded pipes. An example of a spiral weld pipe mill is presented in Fig. 2-6.

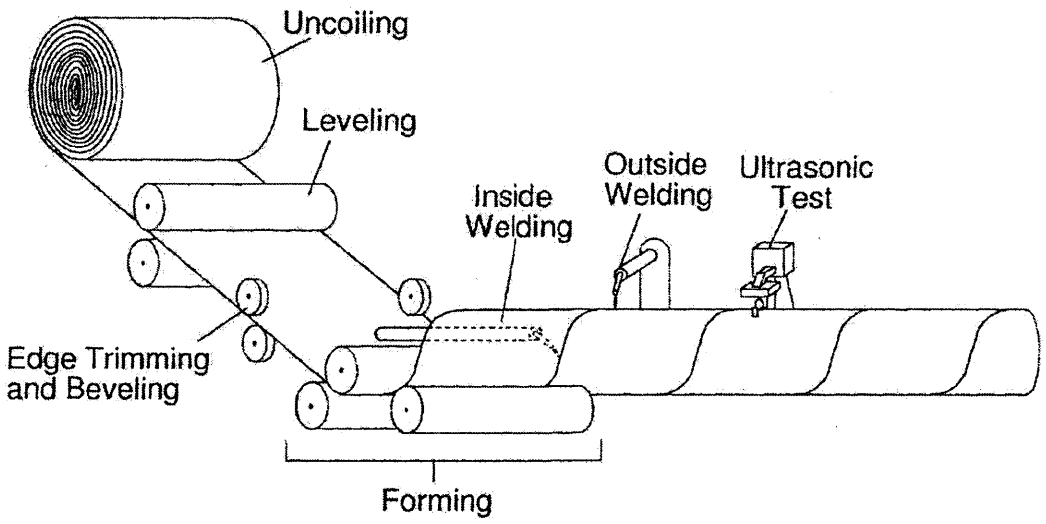

Figure 2-6: Schematic representation of the spiral weld mill manufacturing process [64].

The patents for the welded pipes are numerous dating back to 1931 with the introduction of the Fretz-Moon process, continuing with E. Thomson's discovery of electrical welding in the mid 1880s to the recent-year patents that usually a mill develops in order to manufacture pipes. The diagram of an ERW mill is presented in Fig. 2-7. The fact that the mechanical properties of final pipe are important for the customer led to the development of several welding processes with the objective to standardize and automatize the process as well as to control the effect of the method on the mechanical properties of the pipe. The significance for the current thesis is the fact that the proposed method offers a general approach able to characterize the mechanical properties of the final pipe independently of the manufacturing process.

It is important to note that each different manufacturing method accumulates very different plastic strain histories that changes the pipe resistance against fracture. Therefore, the material properties of the original plate used for the pipe before the welding and the remaining processes, is very different than that of the pipe itself.

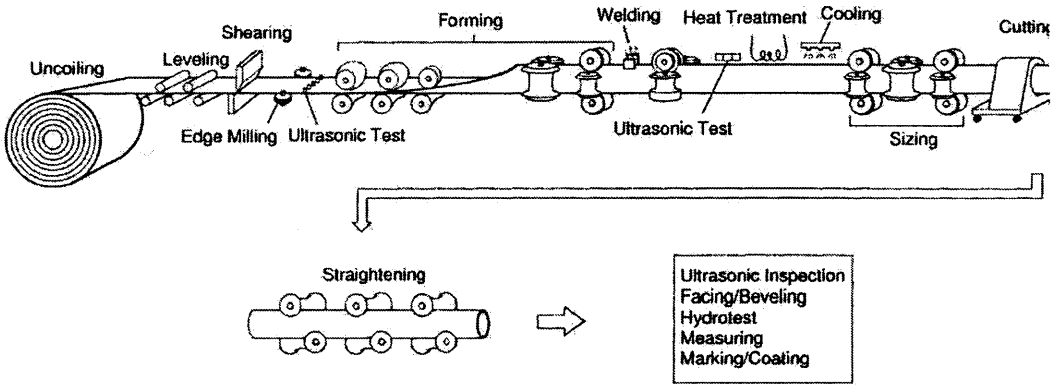

Figure 2-7: Schematic representation of the ERW manufacturing process [64].

The UO method is called after the characteristic shape that the original plate takes during the formation process. As it is shown in Fig. 2-8, the plate is subjected to extreme bending. This is called U-ing process. Then, the bent plate is forced through a mold to give it a close to circular shape. This is the O-ing process followed by the expansion process, where the pipe is sized to its final requirements using internal pressure. The total process is referred to as UOE, where E stands for expansion.

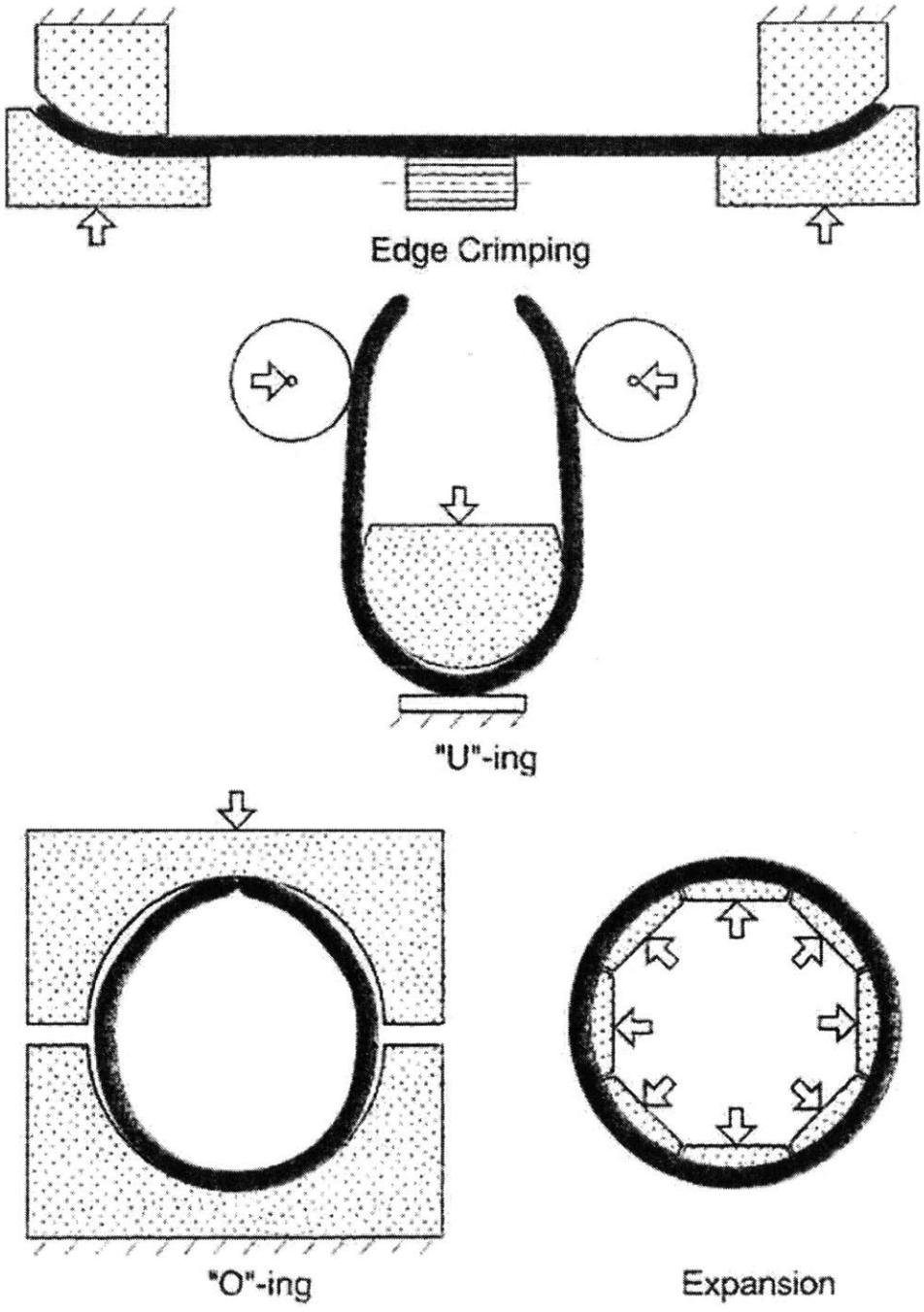

Figure 2-8: Schematic representation of the UOE manufacturing process [64].

2.2 Material Selection for Pipelines and Risers

This line of research has drawn parallels from the automotive industry to the pipeline and general O&G industries. In order to make that step, it was required that certain initial investigations would take place, collecting data to investigate the steel grade trend for the new area of interest. The first step was to identify the material of ICL that were characterized from previous researcher and place them in the original Fig. 1-6. The results of this investigations are presented in Fig. 2-9. Seven grades of steel have been characterized at ICL that include ThyssenKrupp TRIP700, POSCO TRIP 780, POSCO DP590, ArcelorMittal DP980, US Steel DP780, ThyssenKrupp MS and ArcelorMittal SS301LN. The material characterization capability ranges from low to high strength grades for the automotive and steel industries that was developed over the past 10 years.

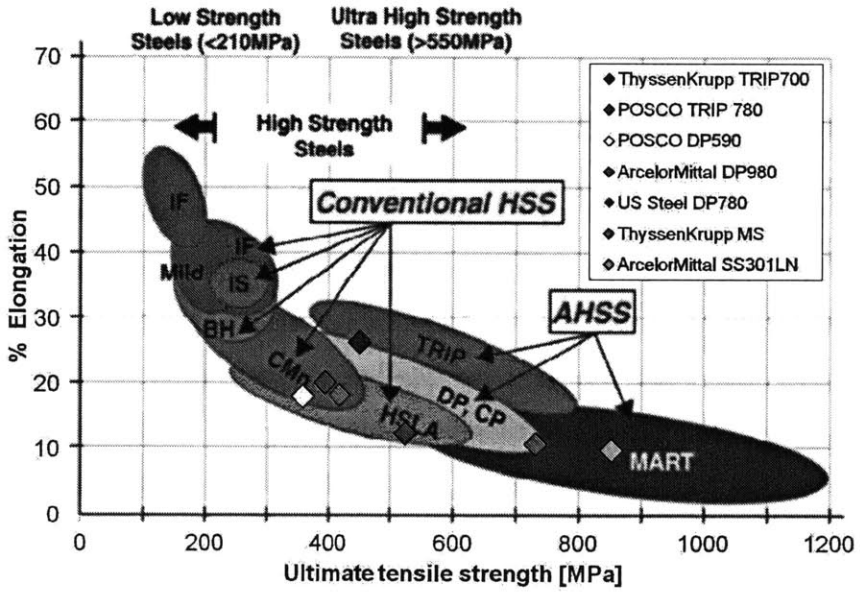

Figure 2-9: ICL characterized materials inserted in the automotive trend banana plot.

The next step was to gather information regarding the trend for the API grades of steel. Following the [19] the following graph was created. The area of each API grade is calculated based on the minimum and maximum specifications determined in the API guide. The results are plotted along with the data from the automotive

industry to assess whether ICL will be proficient in characterizing material for the O&G industry. It is concluded that it is possible to pursue a characterization for the range of API steels, at least as far as the plasticity specs is concerned.

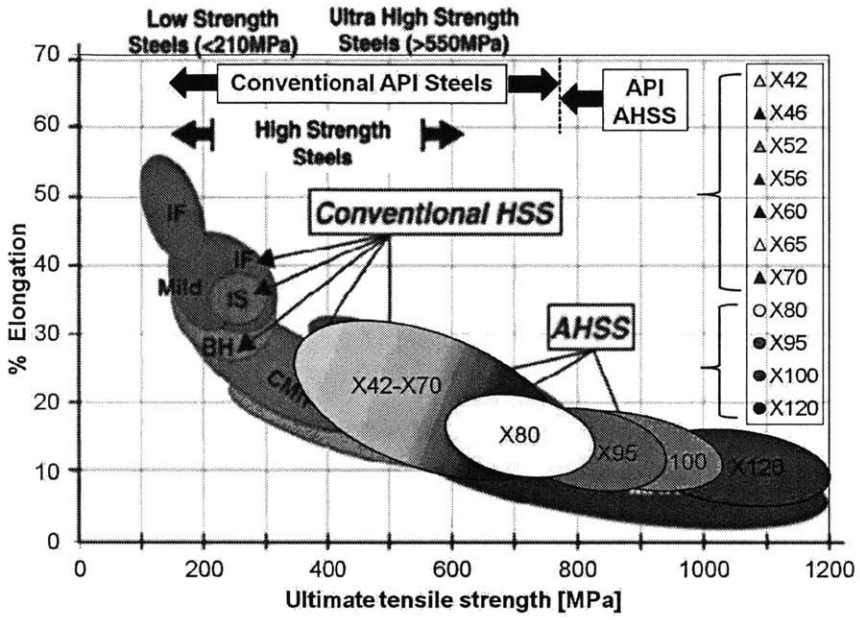

Figure 2-10: Combination of the automotive and pipeline trend towards advanced high strength grades of steel.

It is also possible in order to jump start the research for the O&G to use ICL characterized steel for the automotive industry as a first estimate for qualitative comparison and to explore the capabilities of the proposed model to pipeline and riser applications. The first case study attempting to apply the proposed methodology to an oil and gas application was the reconstruction of the Gulf of Mexico accident. The material that was used for the investigation was Thyssen Krupp TRIP 700, the material properties of which were thoroughly investigated and characterized at ICL in the past. The result of this analysis is presented in details in Chapter 5. The International High Strength Steel community along with the International Society of Ocean (Offshore) and Polar Engineering (ISOPE) welcomed the results recognizing not only the need of a modern method but also the development of a database for the API grades.

2.3 Installation Methods for Offshore Pipelines

After the selection of the geometry, the material and the manufacturing process of the pipe, another critical process that affects the damage and fracture resistance of the pipelines and risers is the installation process that is followed. The laying operations of pipelines are also a source of repeated plastic strain cycling. For instance, when reel-laying technique is used then the the pipe is subjected to 4-5 loading/unloading cycles. The choice of installation technique (i.e. S-lay, J-lay and others) can affect the finally fracture resistance. Important stress controlled loads are often involved and these could become risky when combined with other sources of loading (e.g. deep water laying: bending moment at touch down zone of J-lay combined with external pressure acting on the pipeline). These challenging scenarios have a strong impact on pipeline material requirements especially for very thick wall pipes (up to 50 mm). Increased resistance with respect to fatigue, plastic deformation and fracture, even at low temperature for both base material and welded joint are essential for the safe operation of pipes and adequately detailed models are required to model and predict

.

2.4 Loading of Pipelines and Risers

The loading that pipelines and risers have to sustain is of many different types. The most common type of loading is i) permanent loading that includes among others the weight of permanent equipment, the hydrostatic forces like the buoyancy and hydrostatic pressure; ii) operational loading like the weight of non-permanent equipment, the drilling and mooring forces, iii) environmental forces, like wind and wave forces. One of the most challenging applications for pipes is the offshore/arctic environment because the combination of static and dynamic forces applied on the pipes combine all the possible environmental and operational loading. Also, the accidental loading and subsequent fracture of a pipe is directly translated to environmental disaster. After the Deepwater Horizon accident the community is becoming more inviting to new

methods that not only can benchmark the pipe performance for standard operational conditions but that would also offer the possibility of using a detailed account of the conditions (boundary condition and loading history) to investigate numerically accident scenarios reliably. The current thesis focuses on monotonically increasing loading (tensile/shear) and presents a case study for accidental loading conditions similar for the case of a sinking platform. The monotonic loading choice is related with benchmarking the new proposed method with respect to other structural integrity methods offered in the pipeline and oil and gas industry.

Chapter 3

Structural Integrity against Ductile Fracture of Oil & Gas Pipelines and Risers

3.1 Structural Integrity against Ductile Fracture

Integrity assessment is an old topic for pipelines and risers ensuring their safety and security. This term usually encompasses not only the design of the pipe, but also its functionality ensuring its continuing normal operation. In the current thesis, the focus will be on the design of pipes for safe operation. The design of pipelines and risers includes two main aspects, i) the material selection and ii) the geometric design. The material is required to offer to the structure an adequate level of strength, to support the operational and accidental loads, but also enough ductility, to allow for deformations that may occur due to environmental, or accidental factors. Such reasons may be lateral movement due to earthquake events for the case of a pipeline and sinking of the supporting platform for the case of a riser. The name of grades is characterized by X and a number that refers to the minimum yield stress of the base material in ksi.

Traditionally, ductility protects against sudden brittle fracture ensuring that fail-

ure, if it occurs, is governed by tension and not by toughness (ductile and not brittle fracture). It is important to mention that for metal structures there is a certain set of conditions that may cause a transition from ductile to brittle fracture. Among others the main factors include dynamic rate of strain, extreme temperature variations and high constraints for the stress state at the critical location of fracture initiation. The current thesis will focus on the triaxial state of stress factor to validate the proposed methodology for the case of Single Edge Notched under Tension (SENT) specimens with a pre-existing fatigue crack at the end of the notch. Other traditional tests used to assess the ductility of the material include Drop Weight Tear Tests (DWTT) and Charpy V Notch (CVN) Tests. These tests are used to measure ductility in terms of energy absorption due to impact, aiming the estimation of crack arrest of pipelines mostly. However, these methodologies due to their simplicity, were used extensively to benchmark pipes in general, through codes and guidelines. An interesting part of the use of the above tests (SENT, DWTT and Charpy V) is the correlation of these results to large-scale testing results to assess the range of applicability of small-scale tests for the prediction of failure in the actual pipe. Requirements for SENT tests guarantee that pipes can resist Mode I fracture (see Fig. 3-1). This is a new step in the so-called strain-based design area, while DWTT and Charpy V are typical design approaches of the classical fracture methodologies. These are used to ensure that the design and material selection offer adequate crack arrest properties so that if failure occurs, propagation will be limited and brittle fracture will be avoided. The results for the aforementioned guidelines can be found described in detail at [15], [71] and [5]. Other than the guidelines and codes there is also a set of publications that are basically rules of thumb to ensure the fitness for purpose of pipes. Among the main publications in that mindset are [19], [30] and [39]. After recent developments, the last two publications have been proven to be conservative resulting to over-engineered pipes. All these approaches are based mostly on experimental data and empirical approaches. However, new physics-based methods for predicting and characterizing fracture are necessary for new, challenging applications as it was mentioned in Chapter 1. This is where the current thesis fits in. It offers a physics-based

methodology, that was developed for the automotive industry, for pipe applications. This method is taking into account the underlying physics of the material and was extended to provide a broad capability of numerical analysis for metal structures of any geometry and loading conditions including bursting, puncture, overload, structural collapse/buckling, fatigue, and fracture.

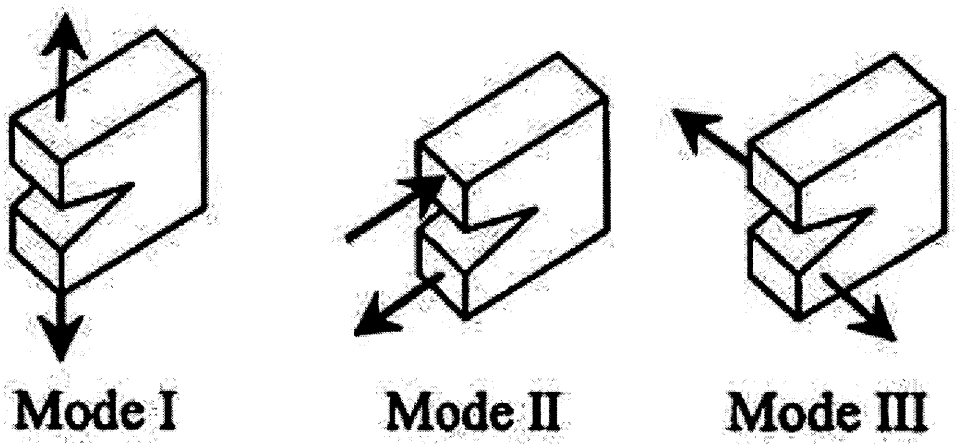

Figure 3-1: The three typical fracture modes i) Opening, ii) Sliding and iii) Tearing.

Pipes are characterized by their geometric features (i.e. diameter and wall thickness), the grade of material used (i.e. X70 which refers to the minimum specified yield strength of 70ksi/483MPa) and its manufacturing technique (seamless, longitudinally welded, spirally welded). Other than the characteristics of the pipe, there are many factors that need to be taken into consideration and that could potentially pose a risk to the safe operation of pressurized pipes. The major factors include

1. complex state of combined loading (tension, compression, bending, internal pressure)
2. cyclic loads (reeling installation bending/re-bending)
3. thickness reduction due to corrosion
4. embedded material imperfections

5. defects of girth welds

6. unexpected localized loads (dropped object)

7. tectonic motion and sediment settlement

8. accidental over-pressure

9. extreme environmental events (hurricane, tsunami etc)

The combination of the above parameters has led in the past to severe offshore accidents. For example, the accident of the Piper Alpha that occurred due to pump leakage that led to gas ignition, multiple explosions, widespread fire and riser failure, a total of 167 casualties, a significant environmental impact and a financial cost for $1.27 billion for the operating company. Due to the magnitude of environmental and financial consequences in the event of failure, the industry has extremely strict safety requirements for platforms and their constitutive parts. A more recent accident, the Deepwater Horizon oil leak, also shocked the O&G community not only due to the immense damage to the environment but also due to the fact that the unexpected loading conditions led to failure of the material of both the drill pipe and casing and subsequent oil leak in a remote location that was discovered long after the accident took place. That led to a delay in reaction to contain the pollution and secure the weld. With the use of new models and modern computational tools that can simulate and reconstruct reliably such events, immediate action can take place without unnecessary delays due to uncertainty of the magnitude of the damage of the pipe system. It is important to note that structural integrity assessment cannot take into account all the design and loading features for every different case of pipeline and riser installation. Alternatively, the creation of a material data base for API grades, that will be characterized for plasticity and fracture for tubular section taking into account their manufacturing process will offer a strong advantage for simulating any combination of boundary and loading condition. That can be a valuable and inexpensive assessment tool for pipes. This can be the first step towards a new era of proactively safe, physics-based and economic pipe design. The base material analysis

can be extended to classification of weldments and introduction of corrosion features as an additional parameter in wall thickness calculations. In this analysis corrosion will be neglected under the assumption that it can be added as a safety factor that will increase the wall thickness.

3.2 Classical Standards and Guidelines on Fracture

3.2.1 Toughness testing

Classical methodologies of fracture resistance focus on an important material parameter that is usually used for the classification of materials, that is the fracture toughness of a steel. To quantify it, Charpy V notch impact tests are conducted to assess the amount of energy absorbed at impact at a specific temperature. The energy is calculated by Eq. 3.1.

$$\Delta E_k = \frac{energy}{volume} = \int_0^{\epsilon_f} \sigma d\epsilon \tag{3.1}$$

where ϵ is the plastic strain, ϵ_f is the strain at the onset of failure and σ is total stress. A geometric representation of the fracture toughness is the area under the stress-strain curve up to the fracture initiation instance. It is extensively used for the study of transition from brittle to ductile fracture. CVN test was named after its inventor, G. Charpy, back in 1905. It was originally used for the study of catastrophic failure events on ships during WWII but its applicability expanded to other areas rapidly due to the simplicity of the testing process. The working principle of CVN test is based on the transaction of mechanical energy between the hammer and the specimen before and after impact (see Fig. 3-2).

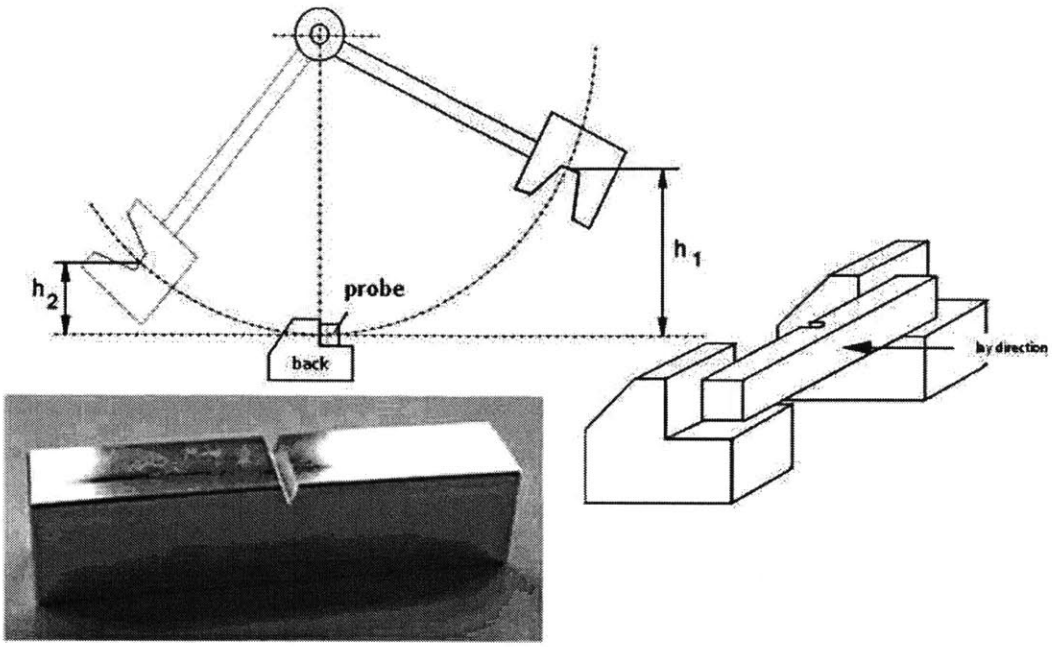

Figure 3-2: Typical graphical representation of Charpy V notched test.

3.2.2 Small-scale testing

Usually in the framework of classical fracture mechanics, fracture toughness tests on Compact Tension (CT), SENB and SENT specimens are used to measure crack extension resistance. In the area of pipelines, there exist recommended practices that resulted from the Fracture Control Joint Industrial Project (JIP) that will be described in the next section in detail. The suggested geometry of the compact specimens selected for the toughness evaluation differs from one practice to another. In the case of pipelines, a typical SENT specimen can be seen in Fig. (3-3). Both SENT and SENB specimens are commonly used to estimate the fracture resistance of the corresponding pipe. Usually, an SENT/SENB test is corresponding to a pipe if the specimen is cut for the same pipe (or the same batch of pipes) and its width, W is approximately the equal to the thickness of the pipe. In [30] the experimental process is presented along with a suitable calculation process for crack resistance customized for thick structures. The experimental resistance curves are produced to assess the resistance of the pipe against crack extension.

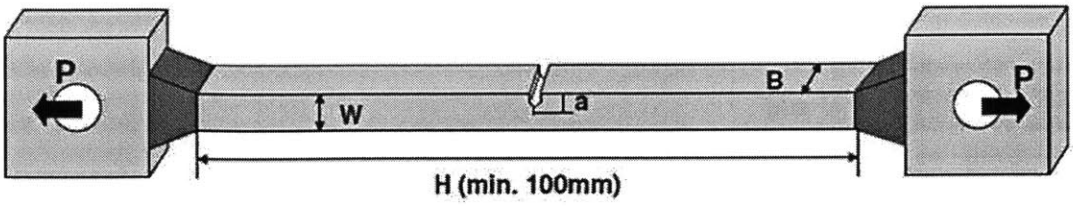

Figure 3-3: SENT specimen sketch with pin loading applied at the ends of the specimens.

Both SENT and SENB specimens are used for the same purpose however, the SENT specimens are thought to be more suitable to measure fracture toughness properties of pipes that are exposed to bending, tensile or pressure loading as it was shown by many groups including by [15]. Depending on the investigating team, both longitudinal strips and round-bar specimens are usually used for testing. SENB and SENT tests are performed either on pipe material or weldments. In this study only SENT specimens from pipe material (base material) were tested for the range of high values of stress triaxiality $\eta > 1.0$. The obtained experimental data were subsequently used for the validation of the proposed fracture model for the case of two API grades of steel X70 and X100. The reason for selecting those two grades for the current study was the enhancement our team's material database with API grades, both in the conventional and advance strength steel ranges, with an objective to analyze numerically typical large-scale offshore and offshore structures (see Chapter 5). In the current work, SENB specimens were not used since SENT specimens were proven to be more suitable to measure fracture toughness properties of pipes exposed to bending, tension or pressure loading. Compared to SENB specimens, SENT specimens are able to represent the constraint that is actually observed in the pipe more realistically. Furthermore, the observed load in the pipe can better be described in a small-scale test by a tensile load rather than by a bending load. In small-scale testing, the experimental data are then used to determine the Resistance curves using multiple specimen method in accordance with [30]. During this process, multiple specimens are loaded monotonically to various loading levels and then fully unloaded after reaching

different amounts of stable crack growth. Thereafter, the specimens are broken by using liquid nitrogen to measure different crack extensions. The geometry of the tested specimens is defined by the length, L without welded grips and the square cross-section of WxH and a/W (Fig. (3-3). Two opening displacements are usually recorded continuously during testing by using clip-gauges mounted at two heights with respect to the specimen surface in order to deduce the Crack Opening Displacement (COD). The final initial crack size is established by inserting a fatigue pre-crack. Typically, the evaluation of the ductile fracture resistance of SENT specimens is conducted to determine the toughness values in terms of Crack Tip Opening Displacement (CTOD) or J-integral versus crack extension. These methodologies have served the community well for many years and are offering a conservative but well-understood evaluation process. The main focus of small-scale tests is to connect their results to large scale results from actual pipe in order to avoid spending extreme amounts of time and funds on the latter.

3.2.3 Large-scale testing

The final benchmark of small-scale tests, presented in the previous section, is usually completed through the comparison to full-scale tests on pipes subjected to internal pressure and/or tension/bending. Full-scale tests are very expensive and require a large team of researchers to coordinate and process the acquired data. Laboratories around the world such as Centro Sviluppo Materiali (CSM)and Tenaris Research and Development (R&D) offer the capability for large-scale testing for interested parties. The testing facility of CSM is shown in Fig. 3-4 and it has been active in full-scale testing of pipes for many years. Many research groups have worked on that area extensively and produced results connecting small- and large-scale testing for pipes in the past. More specifically, [15] demonstrated that the SENT specimens offer a better small-scale comparable.

Figure 3-4: Full-scale multi-Axial Load Testing Machine [Courtesy of CSM].

Large-scale tests are usually conducted under the scope of industrial collaborations (JIP) not only to spread the cost across many contributing companies, but also to provide a common benefit to the entire industry that will lead to improvement of standards for the safe operation of pipes under the supervision of standardization houses, such as classification societies. Large scale tests are not only used for research reasons but also to assess the remaining margins of safety of existing pipe systems that have been under operation for a number of years. Classification societies play an important role in standardization of procedures and for that reason the next paragraph includes the necessary information on them.

3.2.4 Classification Societies

A classification society, also called class in-short, is a non-profit organization in the shipping and offshore industry that sets the standards for the construction and classification of ships and offshore structures. It supervises constructions and carries out regular surveys to ensure compliance with safety standards. In order to avoid liability,

classification societies do not take responsibility for the safety, fitness to purpose and seaworthiness of the ship and offshore structure. In the scope of this work, we will focus on classification societies' role as the providers of standards for the safe operation of pipes, mainly offshore. Other services offered by classes are surveys through the asset's commercial life to ensure that standards are continually met. Classification societies also certify offshore platforms such as oil platforms, and submarines. The standards include hull and machinery. The history of classification societies start in the second half of the 18th century when London merchants, captains and shipowners felt the need of having some standardization of assessing the value of a ship, so that they can issue insurances to minimize risk of the trade. Register society was formed in 1760 (evolving to Lloyds Register) and published an annual registry of ships. The publication tried to assess the quality of the ship hull and equipment. An attempt was made to evaluate vessels annually including assessment for the hull the condition of which was classified as A, E, I, O or U, according to the state of its construction and its adjudged continuing soundness and equipment was classified as G, M, or B that is simply, good, middling or bad. In time, G, M and B were replaced by 1, 2 and 3, which is the origin of the well-known expression 'A1', meaning 'first or highest class'. The purpose of this system was not to assess safety, fitness for purpose or seaworthiness of the ship, but to evaluate risk. This function has changed over the years into a safety standard institution. The list of Classification Societies includes i) London 1760 Lloyds Register (1834 Lloyd's Register of British and Foreign Shipping and Lloyds Register of Shipping), ii) Antwerp 1828 Bureau Veritas (Paris 1932 Bureau Veritas, (BV)), iii) 1864 Det Norske Veritas (DNV), iv) 1867 Germanischer Lloyd (GL), v) 1899 Nippon Kaiji Kyokai (ClassNK) and vi) 1913 Russian Maritime Register of Shipping (RS). Recently DnV and GL have joined forces forming a joint class. On the other hand open Registers include the i)1916 Panama and the ii) 1948 Liberia registries. The increasing competition between classes led to a relaxation of the standards and Transfer of Class Agreement (TOCA) was introduced to counteract the hopping between classes and support the integrity of the societies. In order to reverse that atmosphere, the International Association of Classification

Societies (IACS) formed in 1968 (11 September 1968) dedicated its purpose to safe ships and clean seas and led to the international convention for the Safety Of Life at Sea (SOLAS). The membership of the IACS club includes i) ABS American Bureau of Shipping, ii) BV Bureau Veritas, iii) CCS China Classification Society, iv) DNV Det Norske Veritas, v) GL Germanischer Lloyd, vi) KR Korean Register of Shipping, vii) LR Lloyd's Register, iiiv) NK Nippon Kaiji Kyokai, ix) RINA Registro Italiano Navale and x) RS Russian Maritime Register of Shipping. The European Maritime Safety Agency (EMSA) on the other hand is a European Union agency charged with reducing the risk of maritime accidents, marine pollution from ships and the loss of human lives at sea by helping to enforce the pertinent European Community legislation. It is headquartered in Lisbon. All the above entities press for new modern models and have a significant reason for investing in the improvement of the assessment tools of offshore structures and pipelines and risers in specific.

3.3 Joint Industrial Projects on Structural Integrity and Fracture Control

Research in the area of fracture resistance assessment is important to the industrial representatives of the pipeline and wide oil and gas community. The latter in particular recognizes the importance of correctly treating complex states of loading which may introduce significant amount of plastic deformation into the pipe material and girth weld even, leading to component failure. This interest is evidenced by numerous presentations on recent international conferences as well as organization and participation in several sponsored projects. Almost the entire O&G industry is participating in some Joint Industrial Projects. Presently, there are three concurrent JIPs related to pipeline fracture:

1. Fracture Control Offshore Pipelines, Phase II led by Dr. Erling Ostby of SINTEF.

2. Flaw Tolerance in Pipeline Girth Welds Subjected to Axial Straining and In-

ternal Pressure, organized by TWI and directed by Dr. Henryk Pisarski.

3. Validation and Documentation of Tensile Strain Limit Design Models for Pipelines organized by Dr. Yong-Yi Wang of the Center for Reliable Energy Systems (CRES).

A common denominator of these projects is the consideration of a wide range of surface and embedded circumferential flaw sizes, as well as the study of the impact of main material tensile properties (strain hardening exponent, yield to tensile ratio, etc.) onto fracture limits. These projects address a typical scenario of bending, internal pressure and combined axial and circumferential loading. They are based on a combination of Finite Element Modeling (FEM), laboratory and full-scale testing. Another feature is the reliance on one parameter fracture models such as fracture toughness, CTOD, Crack Tip Opening Angle (CTOA), J-integral or line spring. These models were developed in 70's and 80's and have been serving the community well for more than two decades. The influence of plastic strain cycling on material properties is the issue which is actually being addressed by a number of R&D efforts (including the three JIPs mentioned above). However, the problem is still far from being solved. Cyclic loading, or overloads in plastic regime can cause accumulated plastic straining and associated severe pipeline damage (pipeline walking, ratcheting) with the final result that can be loss of serviceability and reduction of the safety factor even if fracture is not reached. The evaluation of the influence of cyclic plastic loading on pipe safety is difficult in particular when multi-axial load cases are considered. In this respect, the above mentioned JIPs are not expected to fill such gap by providing a comprehensive interpretative model but just to give indications for specific cases (as for instance a girth weld subjected to axial strain). JIP steering committee usually chooses the most representative cases that will be used for working out plastic strain cycling to be used as reference for predictive modeling set-up and calibration and in the full-scale testing. Recently, new plasticity and fracture models, developed under the sponsorship of the steel and automotive industry have reached a state of maturity. In the automotive community, fracture of sheets has to be avoided

during car body part stamping operations and it must be controlled in crash loading. The worldwide automotive and steel industry invested huge resources of their own R&D departments, as well as provided ample support to the leading academic and government labs. These types of new approaches along with novel testing and calibration procedures and advances in FE simulations, offer a great generality and accuracy. The two lead labs in the automotive and steel area applications include the Impact and Crashworthiness Lab at MIT, as well as the Research Institute, Centro Sviluppo Materiali in Italy. Other labs with application in the aerospace industry include the Politecnico di Milano that focuses on helicopter applications. Time has come to present the new fracture predictive technology to the O&G industry. It is recognized that the new, general theories will have to compete with less general, but well-established models. Therefore, one of the tasks of the present thesis is to prove the potential of the new approach in terms of accuracy and computational efficiency. By using this technique one will significantly reduce very expensive full-scale testing of pipes and lead to more economic and less over-engineered pipe designs. In short, the underlying reason of the above advantages of the proposed method is that the new theory is based on first principles and recent advances in experimental mechanics. Once plasticity and fracture parameters are determined for a given pipe material any boundary conditions, loading histories, type of surface or embedded flaws, corrosion damage could be easily introduced into the FEM. The calculations will provide the resulting displacement and strain fields, the amount of constraint at the crack tip (as measured by the stress triaxiality and the Lode angle), location of a possible initiation site and the crack path and evolution of the safety factor. Several leading FE codes such as ABAQUS, LS-DYNA, PAM-CRASH and RADIOSS have already introduced the MIT fracture model in their respective material model libraries or user defined subroutines have been developed. However, the direct application is not doable without an extension for the case of thick structures. In the past, extensive research covered the sheet metal forming and crashing issues, limiting the analysis to plane stress conditions. In order to offer the fracture technology to the O&G community, a special consideration is necessary to include new features stemming from the general

stress state during loading and up to fracture. Fracture of offshore installations is a rare occurrence but its effects could be devastating. The industry has recognized the importance of fracture research. Currently, there are two ongoing Joint Industry Programs in this area. One on Fracture Control which is lead by Dr. Erling Ostby of SINTEF, in Norway. The participating institutes include apart from SINTEF; Shell, Gassco, ConocoPhillips, ENI, Technip, StatoilHydro, ExxonMobil, Tenaris NKK and DNV. The second JIP is entitled Heavy Wall SEVEN. The name of the program suggests that thick pipelines will be used for ultra-deep water exploration and production applications. The members of this consortium are Tenaris, Agip KCO, ENI, EXXON Mobil, CVX, SAIPEM, Total, EWI and CSM. BP is not a part in either of the above consortiums, but it participated earlier in full-scale burst tests on X100 and X120 linepipes. Specifically, BP teamed up with Advantica and commissioned in 2003, a full-scale fracture propagation test using X100 pipes. Earlier, in 2000, the same company took part in the JIP together with Alliance Pipeline, BG and TransCanada Pipelines. Clearly there has been a lot of interest within oil and gas companies globally in fracture control.

3.4 Research Projects on Structural Integrity and Fracture Control

Other than the JIP research work, independent research teams have been working in the area of structural integrity of pipes with the objective to derive empirical relations that could predict the onset of fracture in pressurized pipes. One of the main concerns of these teams is failure due to localization of damage because of thickness reduction caused by corrosion. That area has been vastly explored as it was demonstrated by the number of publication on the matter. More specifically, one of the leading teams from Puc/Rio university produced a series of papers focusing on the analysis and study of pipe structural integrity affected by corrosion. In [9], a finite element model was developed for the prediction of the bursting behavior of externally

corroded pipes for the elastic-plastic range. The material of the original welded tubes was API5L X60 and the dimensions of original welded tubes were $D = 323.9mm$, $t = 9.53mm$, $L = 6m$. Specimens in both the longitudinal and transverse direction were extracted for the study and the experiments were modeled using a finite element model (ANSYS 5.3) with actual elastic-plastic stress-strain behavior obtained from the experiments neglecting the geometric nonlinearities. In this paper, when von Mises equaled the true ultimate strength of the material rupture occured. This line of work produced a number of different publications including corrosion analysis for thickness reduction patches used to represent corrosion areas of the pipes. In [40], another finite-element method was developed and experimental tests were used to analyze stress and strain data for the case of pipelines that suffered thickness metal loss, loaded with internal pressure. An analytic model was developed to predict the burst pressure of longitudinally corroded pipes and results from that model were compared to experimental data gathered from full-scale hydrostatic tests and finite element results. The reason for developing the analytic model was to predict ductile burst pressure of corroded/eroded pipe. The corrosion was represented by extensive longitudinal areas of approximately constant depth. The same bursting criterion was used for the Von Mises yield stress as in [9]. This publication addressed a number of issues including the comparison of yield and burst behavior of pipes under laboratory test conditions to pipelines in field operation using finite element procedure and also verified the capability of the analytic models in predicting the finite element and experimental results. However, the interaction of different imperfection areas was not addressed, which led to more publication in that area. A series of publications was published in that area to cover that gap, including [43], [45], [74], [46] with the intent of exploring pipe fracture control for corroded pipes with the main objective to assess interaction of corrosion patches bursting of pipes. In [43], tests were performed on full-size and scaled tubular specimens to a) evaluate the accuracy of standard used equations for safe ensuring operation of pipelines, b) determine the remaining safety factor, c) obtain the time history of hydrostatic versus stress-strain, d) determine effectiveness of composite reinforcement techniques

and finally to e) validate FE models. The results were presented for the experimental elastic and plastic strain analysis for the benchmark for both analytic models and FE results. In [45], the data acquired from corroded pipe segments that were tested under internal pressure up to rupture were presented. The concept of long and short defects was again addressed. The behavior of a defect of a certain length was related to the support that the surrounding full-thickness material offers to it. Level-1 methods are employed of assessment of the remaining strength of corroded pipelines. Results for pipeline segments under internal pressure up to rupture were presented and compared with similar results computed by the standards ASME and DNV RP-F101 concluding that the DNV standard is a conservative but reasonable method for the prediction of bursting pressure. The bursting pressure was found to increase as the defect length decreases, up to a certain limit, beyond which the failure pressure was found to be weakly influenced by the increase of the defect length. Finally, a general publication of the group [44] came to shed light on the economics of pipes and structural integrity and at the same time gather information on different experimental techniques used in the areas of pipeline integrity. In [74], bursting tests of a number of tubular specimens subjected to internal pressure and irregular-shaped real corrosion defects. The specimens originated from pipelines that were on operation for several years. The corrosion patterns were identified by using results from a series of tests and compared to different test methods. All predicted burst pressure results were conservative when compared to the actual failure pressures with minor exception related to DNV RP-F101 methods for complex-defects. The so-called in the pipe industry level-1 methods were found to be the most conservative, while the DNV RP-F101 method for single defects presented the smallest deviation from real measurements. Some differences occurred due to the flow stress formulation in level-2 methods. This paper addressed a long overdue question on which series of standards and guideline methods are more conservative, thus producing over-engineered pipes and which method is the most appropriate for the calculation of the bursting pressure of tubular specimens that contain real corrosion defects. More papers were produced in the area, among others [46] concluding that all four methods used for the prediction

of bursting pressure (ASME B13G, RSTRENG effective area, DNV RP-F101, API 579) were over-conservative. Also an interaction between different defects has been verified. The most important variable was shown to be the distance between different depth defects. The distance seemed to have an important effect on the magnitude of the failure pressure. This publication indicated that new methods of evaluating fracture for pressurized pipes are necessary. Additional publications in the area of fracture control by the Battelle Memorial Institute team were published focusing on the new challenges in the area of pipe fracture control for new grades of high strength steels [6]. The economic viability of new long-distance high-capacity pipelines was reviewed taking into account the material costs reduction (up to 15%) through the use of higher strength steels. The important outcome of this line of research was that since the 1950's pipe manufacturers and designers have been working on a progressive evolution of pipe grades (with X65 been the classical grade and X80 recent and evolutionary). X65 and X80 grades of steel are not adequately strong for the new applications. X100 and X120 are the new alloys that are evaluated and most of their design, construction and operation performance have been addressed. Key concern in the pipeline and O&G industries is the prevention of crack propagation and fracture. The introduction of welding exacerbated the fracture issue since fracture could run through the whole component leading to fracture of entire steel structures. In order to address these issues full-scale fracture propagation experiments were conducted by the Battelle Memorial Institute in 1953. Due to higher design pressures and lower operation temperatures, higher strength steels were introduced. Fracture initiation models were developed in the early 1970s by Battelle and Shannon. The emerging advance high strength steel alloys stimulated the research on structural integrity in the area of high strength steels and posed questions on the suitability of existing methods for the new frontier of pipe applications in the onshore and offshore environment. Other areas of interests include hydrogen embrittlement for AHSS grades for pipe construction [49]. British institutions also address the defect due to corrosion for pipe design [18]. This section concludes the overview of work on structural integrity on pipes using classical methods.

3.5 Modern Approaches to Ductile Fracture

It is important to mention that a major limitation of current approaches to fracture within the O&G industry, that were described above, is the treatment of constraints at the crack tip. Calibration of fracture models in all existing JIPs, including the TWI [70] the SINTEF [69] and the CRES [34] projects is based on a single test (CT, SENB and more recently SENT). Such testes are representative only to one value of stress triaxiality ([72], [57], [42]). Recent work at the Impact and Crashworthiness Lab at MIT ([2], [85] and [27]) proved that the amount of constraint at a given material point is fully characterized by not one but two parameters which are the stress triaxiality η and the Lode angle $\overline{\theta}$, defined by

$$\eta = \frac{-p}{q} \tag{3.2}$$

$$\overline{\theta} = (\frac{r}{q})^3 \tag{3.3}$$

where r and q are the second and third invariant of the stress deviator and p is the first invariant of the stress tensor. This methodology offers a complete map of possible stress states at the crack tip. For example, bending superposed on tension in pipes gives one value of the constrain while the application of internal pressure another value. A complex history of external loading and possible crack propagation will lead to variable amount of constraints. Thus, real life loading situations cannot be represented by one simple SENT test. Other research centers have independently arrived in the same formulation. More specifically, CSM allows too for two different parameters in the definition of the local stress state [37]. The MIT fracture model accounts for an arbitrarily variable constraint condition. The calibration of this model requires several (three to five) different tests to cover a wide range of stress states encountered in engineering practice. In the case of pipe applications subjected to a complex load history the MIT approach offers additional capability in detecting the real critical condition. This was the objective of the current thesis. The damage model including both stress triaxility and the Lode angle sensitivity was

applied to two grades of API steel X70 and X100 that originated from a seamless and a UOE pipe respectively. By the way, once acquired the suitable awareness of material behavior and constraint evolution in specific scenarios, the most suitable single-test configuration should be identified, which better reproduce the constraint conditions involved in the specific application. This is done to combine highly sound scientific approach, involving its intrinsic predictive reliability, with industrial need to have practical and easily repeatable testing procedures. The important capabilities that are required for these applications include i) Multiple loading, unloading, reverse reloading cycles, ii) Critical Assessment of Classical Fracture Models and iii) Finite Element Implementations. It is recognized that reeling operations as well as some in service situations involve several loading/unloading reverse reloading plastic straining cycles in the pipe. The plasticity model should account for this important effect. Furthermore, fracture initiation is the end-point of damage accumulation during plastic straining. No mention is made, in the otherwise well written, TWI proposal about this important effect. The SINTEF proposal on the other hand refers to tension-compression tests but does not explain how their fracture model accounts for complex loading histories. The proposed fracture model is based on the concept of accumulated plastic strain modified by the variable amount of constraints. For that reason it is particularly suited to accommodate large variation in loading histories. As above mentioned, the approach to fracture by all current JIP investigating teams is based on classical elastic-plastic fracture mechanics. For example the TWIs strain-based Failure Assessment Diagram is deeply entrenched in the K/J-integral philosophy, as it is based on the paper by [32]. Similarly, the SINTEF approach uses the concept of line springs, developed in 70s and significantly improved since then. Similar limitations exist in the CRES project. This is not to say that the application of these classical methods to pipelines are incorrect; they have been serving well the community but they come with all their limitations which were not clearly stated by the respective proposals. In this context the new 3-dimensional approach to fracture is breaking new grounds because it is not subjected to the limitations of the classical methods and is applicable to a wide range of engineering problems. The MIT fracture

predictive technology has been implemented into several leading commercial codes in close co-operation with the developers of those codes. The program RADIOSS, owned by Altair, was first to introduce the MIT fracture model in its commercial version. Two user-defined subroutines in solid and shell elements for ABAQUS are available to sponsoring institutions of the MIT projects. The general purpose FE codes, LS-DYNA and PAMCRASH have recently introduced the MIT fracture model in their updated commercial versions. The above programs are very popular amongst O&G companies. In this way the MIT fracture technology is automatically available to a large number of industrial users. Finally, the proposed technique applies to both un-cracked as well as cracked bodies (pipelines). All previous methods used by existing JIP requires that the initial crack size and orientation be defined beforehand. A first step for the demonstration of the capabilities of the proposed method in predicting initiation and propagation of cracks was the pilot study on API 5L X45 seamless pipe of 2.5 m length, 0.457 m diameter and 6.35 mm thickness from a pipeline transporting oil onshore for several years. The pipe was subjected to internal pressure, developed localized a bulge and burst soon after as shown in Fig. (3-5). Many authors in the past were able to evaluate the busting pressure but none could predict the slant nature of the cracked surface. The unique characteristic of the proposed method is the capability to predict slant fracture. Numerical simulations for the problem of 4-point bending of a pipe with an initial circumferential crack. Test results performed by [35] demonstrated that the crack path was curved and slant rather than straight fracture developed. All those features were nicely predicted at [85]. This new approach offers many advantages but needs to be further investigated and tested in order for its potential to be proven to the oil and gas community. This was undertaken in the current work and the results will be presented in detail in the following chapters.

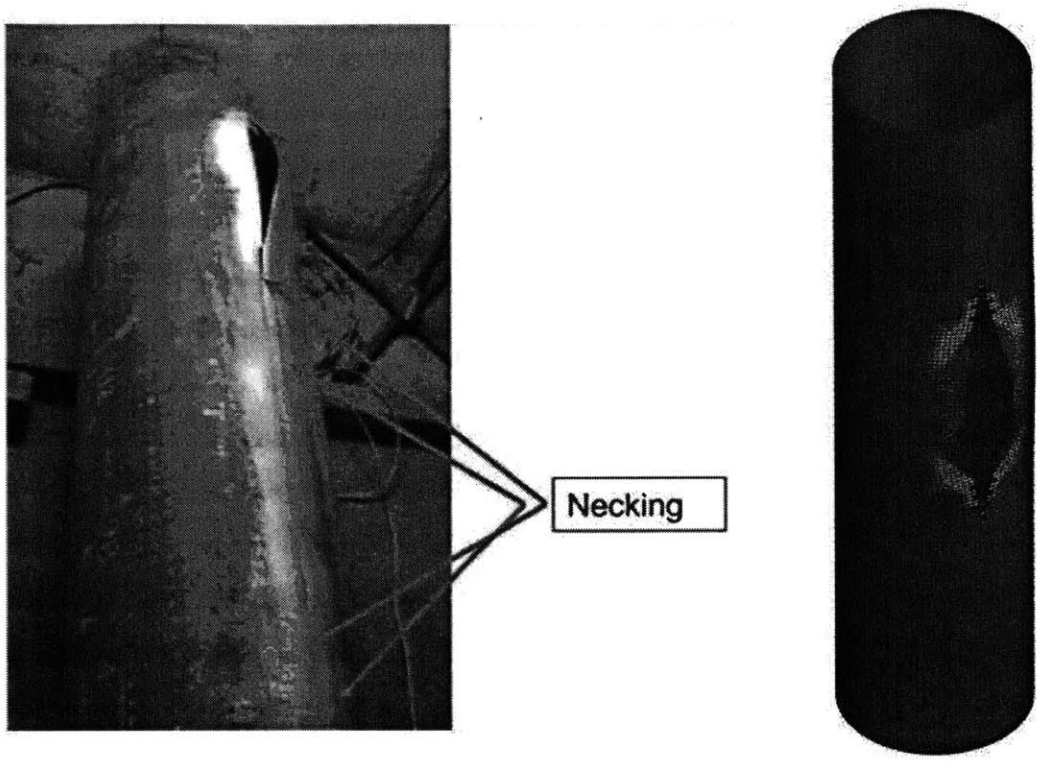

Figure 3-5: Bulging pipe subjected to internal pressure taken from [40].

3.6 Objectives and Contribution

After the brief description of the MMC model, a comprehensive experimental program is described to characterize anisotropic plasticity and fracture in the wide range of stress triaxiality $0 > \eta > 2$. The FE models of all fracture specimens are developed and the model identifications are performed using the hybrid experimental/computational method using a weighted average optimization method to calculate the fracture parameters. Finally, the calibrated model is used to predict fracture initiation and propagation on SENT tests with very good accuracy. In order to make a convincing case to the O&G industry, all specimens were cut from offshore pipes made of API X70 and X100 grade steel. The major benefit of using the MMC model is the capability to predict failure in both crack-free and pre-cracked bodies and the detailed evolution of crack surface for both initiation and propagation. Using the

above physics-based model, fracture in a wide range of loading conditions including shear can be predicted with a good accuracy. The aim of the thesis is to develop an advanced material testing procedure and modeling for pipelines and risers for strain-based design applications through the modeling and calibration of plastic and fracture properties under monotonic, reverse loads and complex loading histories (multi-axial).

A new plasticity and fracture methodology will be used to assess structural performance and safety of pipelines and risers under operational and extreme loading. The proposed methods and procedures are much more general and accurate than those studied under the existing JIPs led respectively by SINTEF, TWI and CRES. This line of research will be concerned with both seamless and pipes manufactured using a UOE approach for deep and ultra deep water applications. The objective of this thesis is to propose a methodology that extends across the field of experimental and computational mechanics and the field of financial engineering. Crack initiation, propagation and arrest will be studied in pressurized seamless pipes to develop a performance index taking into account the pipeline material and design. A finance model will then be developed incorporating the above performance index together with representatives of oil prices and material costs to improve the decision process of the pipeline design, material selection and operating parameters and to quantify the benefits of replacing conventional types of steel with higher grades in offshore pipeline installations. This study will include three interrelated parts. The first is the experimental determination of the plasticity and fracture parameters of two grades of API steel. This has not been done before on these grades. Then, the computational model will employ the material data to predict crack initiation and propagation in pressurized seamless pipelines. The merit of this new approach is the prediction of failure and bursting of both crack-free pipelines and pipelines with arbitrary type of imperfections. Existing numerical approaches within the O&G industry work only with the presence of a predefined crack. The final contribution will be to validate this new methodology as it will be compared to classical fracture mechanics approaches that are well-established in the pipe community and demonstrate the potential that the new model can offer. Finally, the calibrated and validated model

will be used for real, large-scale pipeline and risers simulation for the reconstruction of the Deepwater Horizon oil leak. The final contribution will be the development of a cost-benefit model that will provide guidelines for management and investment decisions.

Chapter 4

Mechanical Properties of API Grades X70 and X100

4.1 Theoretical Part

In this section the fundamental underlying theory selected for the current thesis is presented for both the anisotropic plasticity and fracture modeling of steel pipe materials. The scope of this chapter is the comprehensive mechanical characterization of API grades of steel, X70 and X100, used for pipe manufacturing. The material anisotropic placticity is modeled using Hill's anisotropic yield condition, introduced in 1948 paired with an associate flow rule and an isotropic-kinematic hardening law. The last theoretical component is the modeling of fracture. The mechanical properties of both grades are studied focusing on the feasibility of replacing conventional grades (X70) by higher grade steels (X100). This trend is prominent in the automotive industry with main contributing drivers the vehicle weight and fuel consumption reduction provided that formability remains adequate for sheet metal forming and crash applications.

In the case of pipe design, after a number of accidents, the most recent and devastating of which was the Gulf of Mexico accident, the analysis of pipe failure under accidental loading became a pressing issue for energy companies, with respect to the integrity assurance of their pipe infrastructure. Interestingly, the failure assessment

diagrams approach extensively used by the O&G industry, encountered difficulties in predicting failure under complex stress states, especially in defect-free cases. Classical fracture mechanics methods used for crack resistance assessment require the consideration of an initial crack. However, in accidental cases, such as extreme bending, overpressure and abrupt ground movement, damage could localize and lead to failure in an intact location. Due to severe financial damages to non-compliant companies responsible for environmental pollution, oil and gas companies turned their attention towards modern integrity assessment tools that could inclusively address both operational and accidental conditions in defected and intact cases.

Efforts have been made to develop alternative inclusive methodologies to predict complex failure modes for pipe applications. A widely model used for the simulation of the damage evolution in pipelines is GTN model ([48], [78], [79]). More specifically, recent work on ductile fracture modelling of API X100 material using the GTN model in the high stress triaxiality range ([76], [67], [54]) demonstrated the capabilities of damage evolution models. Recent extensions of the GTN model, accounting for shear-stress dominated fracture ([56], [14], [16]), led to an increase of the number of calibrating parameters and of the challenge of finding a representative parameter set.

As an alternative to the GTN model, the modified Mohr-Coulomb model has been introduced in [24] and was successfully applied for the prediction of ductile fracture initiation and propagation in advanced high-strength sheet and low-strength steel materials ([63]). This extended model describes the fracture initiation criterion in terms of equivalent strain that depending on stress triaxiality and Lode angle. The Lode angle parameter is related to the normalized third invariant of stress deviator. In the work of [17] a comparison has been conducted in the range of low triaxiality stress proving the additional capabilities of the MMC model compared to the GNT model ([26], [17]). The large range of triaxility capabilities of the MMC model has been presented in [58] and [62] for the case of crack propagation in SENT specimens. In the front end of the full material characterization lies the plasticity modeling which is presented in the following subsection.

4.1.1 Plasticity modeling

The plasticity behavior of a given material can be fully modeled by a trinity of components, the yield surface combined with the flow rule and an appropriate hardening law. In this current work, Hill's orthotropic yield surface is employed ([51]), with the associated flow rule. Hill '48 model is the extension of the Von Mises ([4]) yield criterion for materials that exhibit anisotropy. Isotropic hardening law was used for the material modeling of the hardening behavior of both API grades. The anisotropic yield condition can be written in the form

$$f([\sigma], k) = \overline{\sigma} - k = 0 \tag{4.1}$$

where $[\sigma]$ is the Cauchy stress tensor, $\overline{\sigma}$ is the equivalent stress, defined in Eq. (4.2) and k is the deformation resistance of the material.

$$k = \sqrt{F(\sigma_{22} - \sigma_{33})^2 + G(\sigma_{33} - \sigma_{11})^2 + H(\sigma_{11} - \sigma_{22})^2 + 2L\sigma_{23} + 2M\sigma_{31} + 2N\sigma_{12}} \tag{4.2}$$

This expression reduces to Eq. (4.3) for plane stress condition.

$$\overline{\sigma} = \sqrt{(G + H)\sigma_{11}^2 - 2H\sigma_{11}\sigma_{22} + (F + H)\sigma_{22}^2 + 2N\sigma_{12}^2} \tag{4.3}$$

In metal sheet applications, this is the expression that is used for anisotropy calibration through flat dogbone tensile tests cut in the principal 0, 45 and 90 degree directions defined with respect to the rolling direction. The same methodology for anisotropy calibration will be used for both API X70 and X100 grades. The principal direction (0 degrees) will be the direction of the length of the pipe. This is a common approach accounting for pipe material directionality and it has been employed by previous groups ([citation for anisotropy]). The equivalent stress can also be written in the form of Eq. (4.4).

$$\overline{\sigma} = \sqrt{([R][\sigma]) \cdot [\sigma]} \tag{4.4}$$

where $[\sigma] = [\sigma_{ij}]$, σ_{ij} is the stress in the i-direction acting on the j-plane and $[R]$ is a symmetric, positive-definite tensor that in the plane stress condition reduces to Eq. (4.5).

$$[R] = \begin{bmatrix} R_{11} & R_{12} & 0 \\ R_{21} & R_{22} & 0 \\ 0 & 0 & R_{33} \end{bmatrix} \tag{4.5}$$

The elements of $[R]$ are described in terms of the anisotropic parameters F, G, H and N of the reduced Hill model presented in Eq. (4.2). The equivalent description using the R_{ij} parameters is given by Eq. (4.6).

$$k = \sqrt{R_{11}\sigma_{11}^2 - 2R_{12}\sigma_{11}\sigma_{22} + R_{22}\sigma_{22}^2 + R_{33}\sigma_{12}^2} \tag{4.6}$$

The relation between the F, G, H and N and the R_{ij} parameters are given by Eqs. (4.7), (4.8), (4.9) and (4.10).

$$F = R_{22} + R_{12} \tag{4.7}$$

$$G = 1 + R_{12} \tag{4.8}$$

$$H = -R_{12} \tag{4.9}$$

$$N = \frac{1}{2}R_{33} \tag{4.10}$$

Alternative $[R]$ is given by Eq. (4.11)

$$[R] = \begin{bmatrix} G+H & -H & 0 \\ -H & F+H & 0 \\ 0 & 0 & 2N \end{bmatrix} \tag{4.11}$$

The calibration of the above-mentioned model will be presented in detail in the

experimental part. In brief, for the calculation of the anisotropic parameters F, G, H and N, tensile test data from the dogbone specimens on 0, 45 and 90 degrees are used for both grades to calculate the Lankford ratios assuming an associated flow rule. The last component of the material model includes the isotropic-kinematic hardening rule modeled by Eq. (4.12).

$$k = A \cdot (\bar{\epsilon}_p + \epsilon_o)^n \tag{4.12}$$

where $\bar{\epsilon}_p$ denotes the corresponding work-conjugate equivalent plastic strain and A, ϵ_o and n are the fitting parameters of the Swift law, determined through uniaxial tensile dogbone specimen cut in the principal direction (longitudinal direction). For the combination of the plasticity theory and the fracture model which will be presented in the following subsection, the hardening rule used is the power law, assuming $\epsilon_o = 0$ for both API grades. In reality, the difference between the Swift and power law localizes close to the elastic to plastic transition area.

4.1.2 Fracture Criterion

The unique characteristic of the MIT fracture technology lies on the physics-inspired, Mohr-Coulomb (MC) fracture criterion illustrated in Fig. 4-1. Eq. (4.13) dictates that fracture occurs at the plane where the combined sum of the shear stress modified by the normal stress, σ_n becomes maximum (location-wise), at the instance that this sum reaches a critical value (time-wise).

$$max(\tau + C_1\sigma_n) = C_2 \tag{4.13}$$

There are two limiting cases of the above model. Shear localization and growth/linkage of voids. In the first case, the normal stress is almost zero, Fig. 4-1 (left), whereas in second the shear stress tends to zero and fracture is controlled by the hydrostatic (tensile) pressure, Fig. 4-1 (right). In reality, a combination of both states Fig. 4-1 (middle) occurs. The Mohr-Coulomb criterion is a simple expression, however the determination of C_1 and C_2 is not straight forward considering this formulation. In

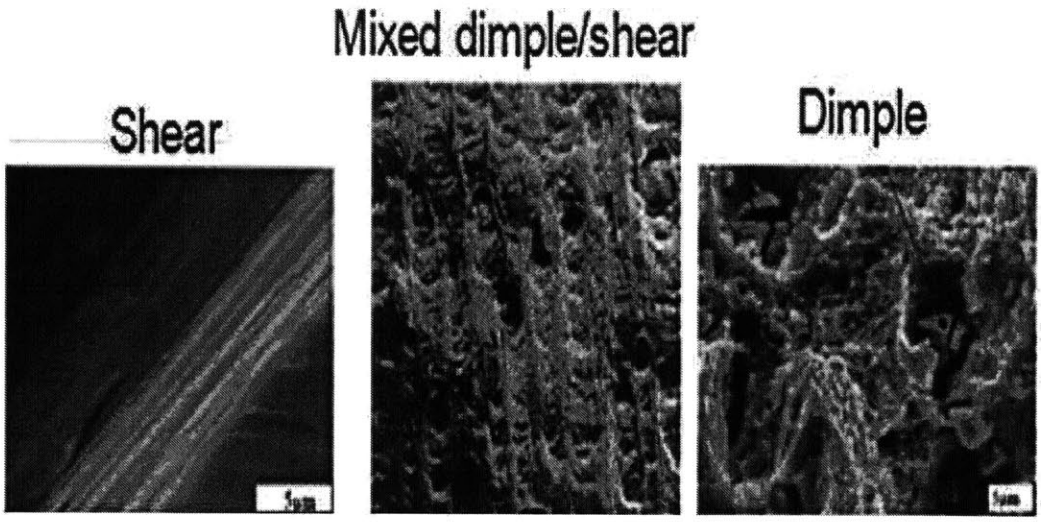

Figure 4-1: Two different types of fracture mechanisms controlled respectively by the shear stress and normal stress and their combination.

2008, this criterion was reformulated into the so-called MMC criterion and the calibration of the fracture parameters was expressed in a physics-based manner. The reformulation of the MC criterion is described in detail along with the calibration of the fracture parameters process for metal sheets in [24].

A brief account of the reformulation of the Mohr-Coulomb model is presented, starting from the basic stress tensor definition. The Cauchy stress tensor, $[\sigma]$ represents completely the stress state for every material point. For isotropic materials, the stress tensor can be fully described by the following three invariants.

$$I_1 = (\sigma_1 + \sigma_2 + \sigma_3) \tag{4.14}$$

$$J_2 = (1/2)[s] : [s] \tag{4.15}$$

$$J_3 = det([s]) \tag{4.16}$$

where $[s]$ is the deviatoric stress tensor, $[s] = [\sigma] - \frac{1}{3}tr([\sigma])[I]$, σ_1, σ_2 and σ_3 are the principal stresses, $tr(.)$ is the trace operator and $[I]$ is the 3x3 identity tensor. An

equivalent representation of the stress state is in the cylindrical coordinate system through the stress triaxiality, η and the normalized Lode angle, $\overline{\theta}$. Stress triaxiality and Lode angle are defined in Eqs. (4.17) and (4.18).

$$\eta = -\frac{p}{\sqrt{3J_2}} \tag{4.17}$$

$$\overline{\theta} = 1 - \frac{6}{\pi}\left(\frac{1}{3}\arccos\left(\frac{3\sqrt{3}J_3}{2(J_2)^{3/2}}\right)\right) \tag{4.18}$$

where p is hydrostatic pressure, $p = -(1/3)I_1$. From now on, the normalized Lode angle will be referred to as simply Lode angle. The stress representation with respect to triaxiality and Lode angle is given by Eq. (4.19).

$$\overline{\sigma} = C_2\left(\sqrt{\frac{1+C_1^2}{3}}cos\left(\frac{\overline{\theta}\pi}{6}\right) + C_1\left(\eta + \frac{1}{3}sin\left(\frac{\overline{\theta}\pi}{6}\right)\right)\right)^{-1} \tag{4.19}$$

This is a stress representation, however the resolution of the onset of ductile fracture is higher for a strain representation of the Mohr-Coulomb criterion. To this end, one must express the equivalent stress in terms of equivalent strain. This will be done in the present section for monotonic loading and a assuming a power law material hardening function. In [25] a generalized hardening rule with Lode angle dependence was proposed, in the form

$$\overline{\sigma} = A\overline{\epsilon}^n\left(C_3 + \frac{\sqrt{3}}{2-\sqrt{3}}(1-C_3)\left(sec\left(\frac{\overline{\theta}\pi}{6} - 1\right)\right)\right) \tag{4.20}$$

where C_3 is the third parameter to be determined from tests. Inverting Eq. (4.20) and eliminating equivalent stress between Eqs. (4.19) and (4.20), the final form of the 3D fracture criterion can be derived in terms of equivalent plastic strain at fracture location and instance, normalized stress triaxiality and Lode angle, as presented in Eq. (4.22).

$$\bar{\epsilon}_f = \left\{ \frac{A}{C_2} \left\{ C_3 + \frac{\sqrt{3}}{2-\sqrt{3}}(1-C_3) \left(\sec\left(\frac{\bar{\theta}\pi}{6}\right) - 1 \right) \right\} \right. \tag{4.21}$$

$$\left. \left(\sqrt{\frac{1+C_1^2}{3}} \cos\left(\frac{\bar{\theta}\pi}{6}\right) + C_1 \left(\eta + \frac{1}{3} \sin\left(\frac{\bar{\theta}\pi}{6}\right) \right) \right) \right\}^{-1/n} \tag{4.22}$$

where C_1, C_2 and C_3 are the fracture parameters. The limiting values, $C_3 = 1$ and $C_3 = \sqrt{3}/2$ correspond to the Von Mises and Tresca yield conditions, respectively. Eq. (4.22) represents a locus in the three-dimensional space of all possible fracture strains reached under proportional loading for which η and $\bar{\theta}$ are constant. For general non-proportional loading the damage evolution rule is employed in order to account for non-proportional loading.

$$D = \int_0^{\bar{\epsilon}_f} \frac{d\bar{\epsilon}_p}{f(\eta, \bar{\theta})} \tag{4.23}$$

where each strain increment $d\bar{\epsilon}_p$, is normalized with respect to the value of the equivalent strain to fracture corresponding to the current value of the stress triaxiality and Lode angle. Other damage models are also used for the evaluation of onset of fracture ([73]). At the onset of fracture $\bar{\epsilon}_p = \bar{\epsilon}_f$ and $D = D_{crit} = 1$. In order to characterize the fracture properties of a certain material, a series of tests are conducted for different stress states, namely for different combination of $(\eta, \bar{\theta})$. At least three fracture tests are required for the calibration of the fracture parameters C_1, C_2 and C_3. If additional test data are available, then they are used for the verification of the calculated parameters. It is important to note that in the case of plain stress, there is a unique relation between the Lode angle and triaxiality parameters given by Eq. (4.24).

$$\cos\left(\frac{\pi}{2}(1-\bar{\theta})\right) = -\frac{27}{2}\eta\left(\eta^2 - \frac{1}{3}\right) \tag{4.24}$$

The present method belongs to the class of extended strain-based fracture criteria where the material ductility depends on both the stress triaxiality and the Lode angle.

The detailed calibration procedure will be presented in the following experimental part along with all the details regarding the tests conducted for the calibration and validation of the proposed methodology for the integrity assessment of pipelines and risers subjected to monotonic loading.

4.2 Experimental Part

Two different grades of offshore steels, API X70 and X100, were analyzed in the current thesis for anisotropic plasticity and fracture characterization using the MIT fracture predictive technology. Fro the characterization of both materials a comprehensive experimental program is carried out.

4.2.1 Preparation of specimens

Each material was received in pipe segments cut in 45 and 30 degree angles respectively for X70 and X100 from original, virgin pipes. The X70 pipe was a seamless pipe, while the X100 was a UOE pipe. The effect of the manufacturing process affected severely the anisotropy results. These curved pipe segments were sent to MIT Central Machine Shop (CSM) to produce specimens. The specimen manufacturing process included four steps.

1. Each curved pipe segment was partitioned and grinded to produce rectangular blocks of bulk material, Fig 4-3(left). The longitudinal axis of the pipe was noted on the blocks (see Fig. 4-2).

2. The cuboid blocks were then sliced resulting to several sheets of about 2.5 mm thick each (see Fig. 4-3).

3. The profile of each specimens was then cut from the machined sheets.

4. The thickness of each specimen was trimmed down to the desired value to produce the final specimens of the case of the butterfly specimens, to produce the complex double curvature surface.

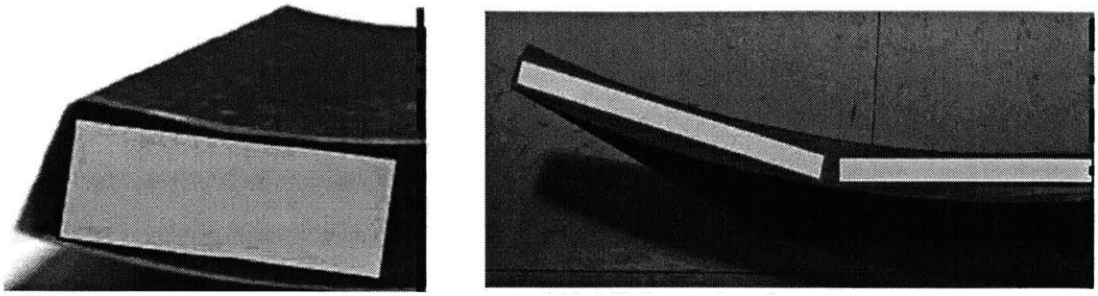

Figure 4-2: X70 (left) and X100 (right) pipe segment as received with cuboid cutouts.

After the completion of all tests it was found that there was significant in-homogeneity and anisotropy, especially for the case of X100 due to the UOE manufacturing process followed for the original pipe. For the case of X70 the results were similar across the thickness and around the circumference for the same type of specimen and loading conditions. The mechanical properties of the specimens cut for this study may present different properties from identical specimens cut from another location of the pipe due to in-homogeneity. In-homogeneity was not considered in this analysis. However, the results from this study offer accurate result for the modeling of the mechanical properties of these grades. In order to connect the inhomogeneity whith the manufacturing process followed, and additional analysis should be conducted, which is outside the scope of the current thesis.

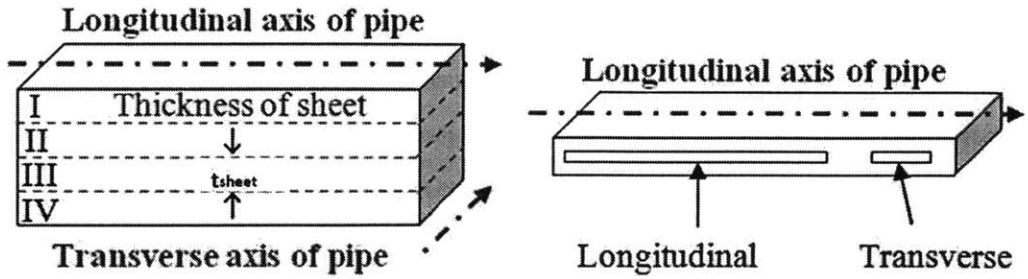

Figure 4-3: Graphical representation of steps 2 and 3 for the extraction of specimens with respect to the longitudinal direction of the pipe.

Table 4.1: Number and thickness per type of specimen for X70 API grade

Type of Specimen	# Specimens	t [mm]
Regular dogbone	4	1.50
Small dogbone	6	0.75
Notched R6.67	4	1.50
Central Hole	4	2.00
Butterfly	8	1.50
Disk	4	1.50

Table 4.2: Number and thickness per type of specimen for X100 API grade

Type of Specimen	# Specimens	t [mm]
Regular dogbone	6	1.50
Small dogbone	-	1.50
Notched R6.67	4	1.50
Central Hole	4	1.50
Butterfly	8	1.50
Disk	4	1.50

This will be demonstrate in Chapter 5. It is important to state that all specimens were tested in the longitudinal direction, except for the dog-bone specimens that were additionally cut and tested in the 45 and 90 degree (circumferential direction) angles to study anisotropy of the material. For the complete characterization of the offshore grades, five types of flat specimens were machined, dog-bone, notched R6.67, flat specimens with central hole, butterfly specimens and circular disk specimens. The geometrical specifications of each specimen will be presented in detail in the follwoing sections. The same profile geometry of specimens was used for both X70 and X100. In Table 4.1 and 4.2 the thickness of each type of flat specimen is given for X70 and X100. In addition to the flat specimens, round specimens with notches were tested also and used for the fracture calibration.

It is important to note that small dog-bone specimens were used to study anisotropy, in the case of X70 due to geometric restrictions of the received pipe segments. Their dimensions are scaled down by a factor of two with respect to regular dog-bone spec-

imens. The preparation method of specimens is responsible for the final roughness of the specimen surface. Therefore very fine finishing was selected to avoid non-smooth edges that would affect the results of the experiments. This was also reported by [41] for TRIP780. In the following section all the specimens used for the characterization of the two grades will be covered. There is always a challenge in extracting specimens from thick pipe segments because of variation of material properties through the pipe thickness due to manufacturing process and pre-existing strains. In order to minimize this effect, most of the specimens were narrow and were cut in the longitudinal direction. In the case of flat circular disks, this was not possible. Various parts of the disks had to come from different layers of the pipe. This difficulty was noticed in the data analysis, manifesting a spread of fracture strain from piece to piece.

4.2.2 Description of experimental apparatus and digital image correlation

Instron 8080 biaxial testing machine: ICL has developed a hybrid technique that combines experimental and numerical results for the understanding and the modeling of mechanical properties of metals. This method requires testing specimens under a broad range of loading conditions. In order to characterize plasticity and fracture, uniaxial and biaxial testing is required. In a joint effort with Instron Inc., the ICL team developed a unique testing machine which is capable of testing specimens under in-plane shear, compression/tension and any combination of these three loading patterns. This resulted in the ICL hydraulic machine (Instron 8080) with customized high pressure clamps. Instron 8080 is a unique dual-actuator system capable of biaxial testing of specimens extracted from sheet and pipe materials. The specimens are clamped, using appropriate grips, to a vertical actuator and a low-friction sliding table (Fig. 4-4). Using the horizontal actuator, for the application of shear load, it is possible to study the combination of Mode I and Mode II failure.

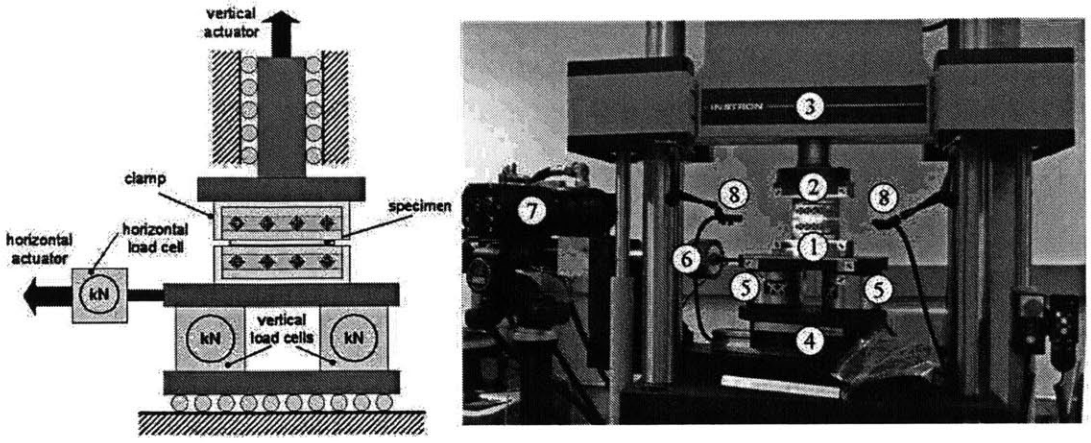

Figure 4-4: Main components of ICL, Instron 8080 customized dual actuator testing equipment.

The loading frame is designed such that the vertical actuator can carry both vertical and horizontal loads. The vertical and horizontal carrying capacities are 50 and 25kN respectively. At the same time, two loads cells are integrated into the sliding table measuring both the vertical force and the moment acting on the specimen. A third load cell measuring the shear force is placed between the horizontal actuator and the sliding table. During the testing process, both force and displacement controls are can be used to simulate complex loading paths.

The displacement and strain fields on the specimen surface are measured using two high resolution digital video cameras along with a 3D digital image correlation software while the force is monitored by the loading cells. The Instron testing machine is used for the testing of notched, central hole and butterfly specimens. Customized grips (Fig. 4-5) and spacers are used for the experiments to ensure adequate traction and uniform application of load along the width of the specimen.

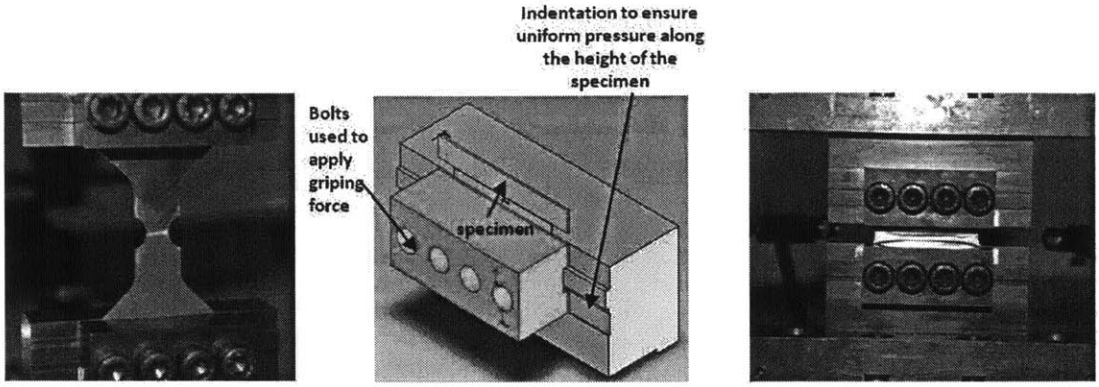

Figure 4-5: Instron 8080 customized pressure grips used for tensile test of a notched X100 specimen (left), schematic of the grip design (middle) and shear test of a butterfly X70 specimen (right).

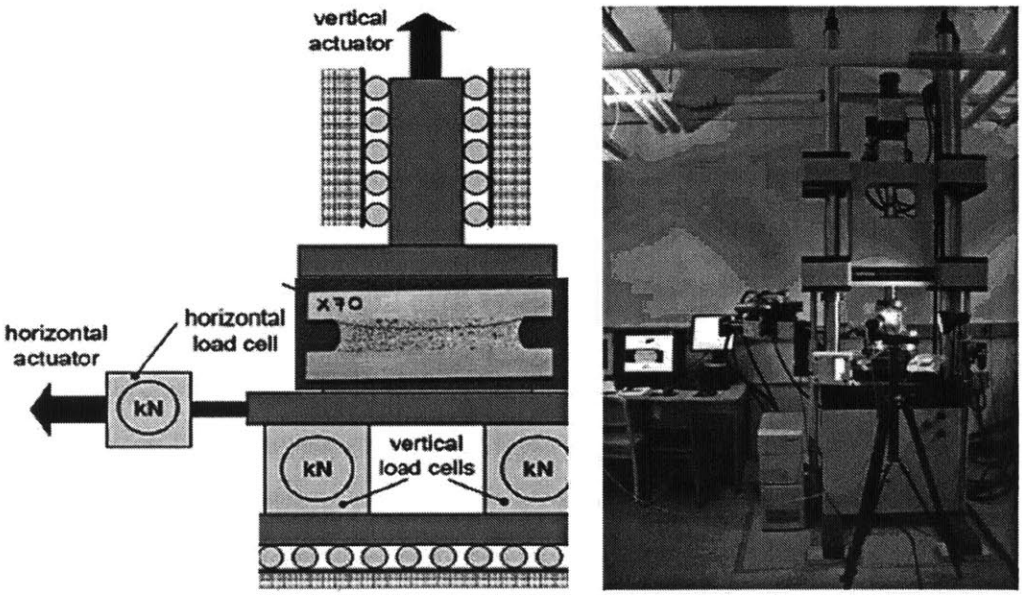

Figure 4-6: Schematic representation of dual actuator Instron 8080 with customized pressure grips (left), ICL biaxial testing facility (right).

MTS G45 uniaxial testing machine: The remaining two specimens, namely the dogbone and the circular disk specimens were tested using ICL's electro-mechanical universal testing machine (MTS, G45, Eden-Prarie), see Fig. 4-7. The carrying ca-

pacity of the machine is 200 kN with two different load cells of 10 and 200 kN. The dogbone specimens were tested up until fracture using the 10 kN load cell and wedge grips while the circular disk specimens were tested using the 100kN load cell and a circular die. Force and displacement were measured by the load cell and additional displacement measurements were taken by DIC and compared to load cell measurement.

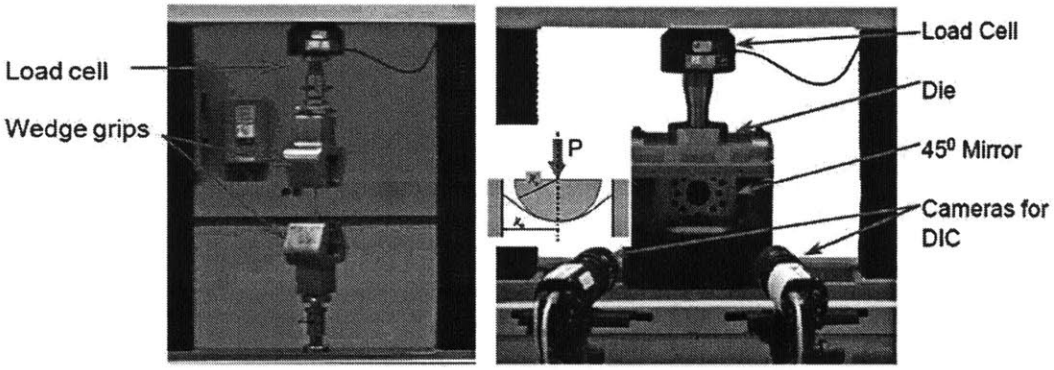

Figure 4-7: MTS uniaxial tensile wedge grips, b) MTS circular grips and die used for punch testing.

Digital Image Correlation Method: The displacement is monitored using Digital Image Correlation (DIC) by tracking the speckle applied in the gage section of each specimen with respect to time. The strain fields are then calculated and compared to the load cell measurements. One important advantage of using DIC is the flexibility of defining multiple virtual extensometers according to the location of interest after the completion of the experiment. Other advantages include the fact that the entire strain field can be readily computed for a selected window for both 2D and 3D deformations as well as the fact that sliding of the specimen, during the testing procedure, does not affect the results. This method is a contact-less measuring method for displacement monitoring. The necessary equipment for the calculation of displacements and strains include two digital cameras (QImaging Retiga 1300i with 105mm Nikon Nikkor lenses) that are able to take approximately 500 pictures of 1300x1030 pixels resolution of the speckle painted on the gage surfaces of the

specimen and appropriate lighting units see Fig.4-8(left). For flat specimens only one camera is required while for the punch test both cameras are used to monitor the 3D deformation of the surface of the disk, see Fig. 4-8(right). The average speckle size is about 80μm. The gage section of the specimen is initially painted white and then a black speckle pattern is sprayed on top (Fig. 4-9). The VIC-2D/VIC-3D software is then used to track the change on the pattern of the speckles either for prescribed positions (virtual extensometers) or entire window areas (Fig. 4-9). The high speed capability is more important for dynamic testing dealing with high strain rates.

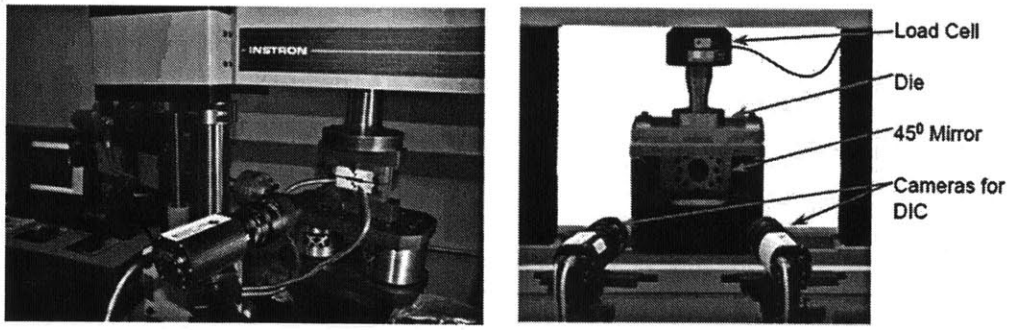

Figure 4-8: 2D DIC monitoring the displacement field of flat specimen (left) and 3D DIC monitoring the 3D deformation field of the disk specimen (right).

The working principle of this method is the comparison of each frame in time to the original frame. The location of the virtual extensometers varied for different specimens. For the notched, central hole and butterfly specimens subjected to tension, one extensometer was used. The ends of the extensometer were set on the horizontal centerline of the specimen placed symmetrically with respect to the fracture surface.

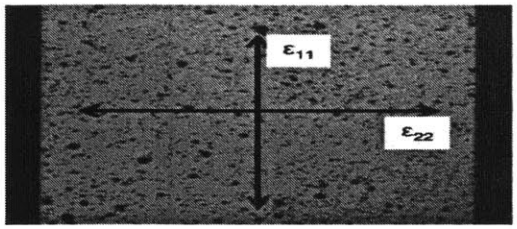

Figure 4-9: Example of speckle pattern on a dogbone specimen and indication of virtual vertical and horizontal extensometers.

For the dogbone under tension and the butterfly under pure shear and additional extensometer was prescribed horizontally measuring the lateral displacement of two points on the vertical centerline. Depending on the distance of the camera from the specimen and on the zooming settings, both global and local strains near the location of onset of fracture can be measured. The displacement field is calculated by DIC (VIC2D, Correlated Solutions) based on the assumption of a quadratic transformation of the 35x35 pixel neighborhood of each point of interest. The engineering axial and shear strains at the center of the specimen are computed from the displacements measured using VIC-2D.

4.2.3 Metallurgical and chemical analysis

This section will present the metallurgical and chemical properties for both API grades. X70 is a typical grade used for the manufacturing of pipelines transporting oil and gas. This particular material was provided to MIT by Shell Oil for the complete plasticity and fracture characterization. The metallurgical properties of this grade were studied by Salzgitter Mannesmann Forschung GmbH (SZMF) to extract information regarding the micro-structure and the content of different Fe phases. An important property of this material is relatively low strain hardening exponent, $n = 0.1$. The chemical composition is given in Table 4.3 and the microstructure is shown in Fig. 4-10. The microstructure of X70 is characterized by polygonal ferrite (white areas in Fig. 4-10) with smaller regions of bainitic ferrite (black areas) Fig. 4-10.

Table 4.3: Chemical analysis of X70

C [%]	Si [%]	Mn [%]	P [%]	Al [%]
0.06	0.30	1.48	0.01	0.04

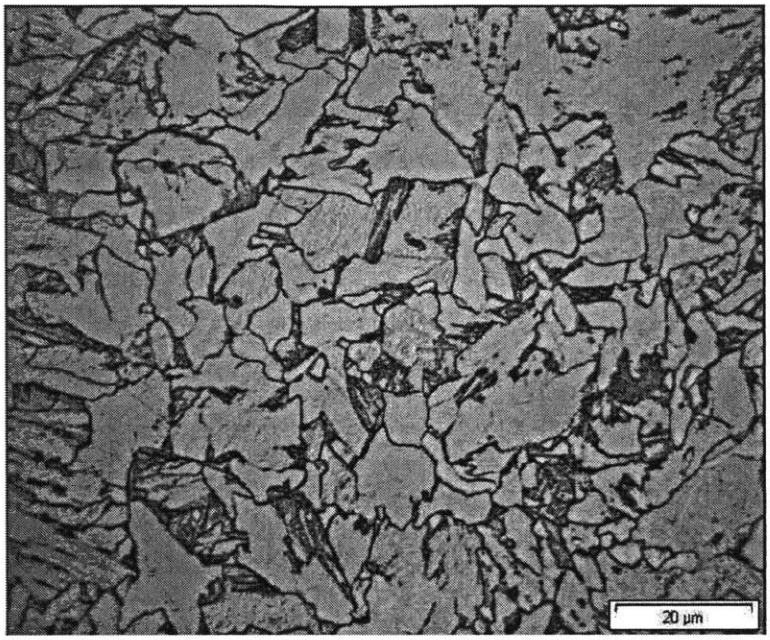

Figure 4-10: Surface microstructure analysis of API X70 by Salzgitter Mannesmann Forschung.

The microstructural length scales such as the distance between two neighbored microvoids or average nearest neighbor distance between inclusions can be used as a characteristic or critical lengths for the estimation of the mesh size in the damage modeling based on studies, like in [75] and [8]. The mesh size has been treated as an additional parameter of the applied local damage model which is related to the deformation energy per crack elongation. Furthermore, this energy depends on the hardening behavior and microstructural length. The relation between this characteristic length and the mesh size is not directly proportional. It should be noted that these analyses with mesh size as additional parameter have been performed on specimens with high stress triaxiality levels (i.e. round specimens). By decreasing the

Table 4.4: Chemical analysis of X100

C [%]	Si [%]	Mn [%]	P [%]	Al [%]
0.058	0.306	1.771	0.012	0.016

stress triaxiality and increasing the material hardening, the mesh sensitivity becomes less relevant. The results from the tests with high hardening exponent, in the range of low stress triaxiality, [41] showed that the mesh size effect is very weak leading to rapid convergence of plastic equivalent strain to fracture, triaxiality and Lode angle.

The X100 material for the investigations has been extracted from the same section and location (approx. 6 o'clock) as that of X70 of the large diameter pipe section with outer diameter $D = 1219mm$ (48 inches) and wall thickness $t = 18.4mm$ (0.72 inches). The longitudinally welded pipe has been manufactured by Europipe GmbH using the UOE process from the thermo-mechanically rolled plate. The chemical composition of X100 material is given in Table 4.4. The mechanical properties in terms of yield and tensile strengths have been obtained from flat dogbone specimens for both grades and will be presented in the plasticity section. Additional tensile tests on the smooth round bar specimens, for both grades have been conducted for verification. The geometry of these round tested specimen is defined by diameter $D = 8mm$ and gauge length of $L = 40mm$. The course of the resulting engineering stress-strain curves for X70 and X100 exhibits a wide range of Luders strain. Since both pipe materials were subjected to a coating process after the pipe production, it is assumed that thermal aging effects lead to manifested pronounced yield strength and significant Luders plateau compared to an un-treated pipe. The metallographic analyses have been performed with objective to identify and quantify the relative microstructure entities, which might be used for the damage modeling. The Light Optical Microscopy (LOM) on the polished and HNO3 etched sample shows ferritic-bainitic microstructure for X100 steel characterized by ferrite grains aligned in the rolling direction and bainite bands, shown in Fig. 4-11. By applying LOM on the polished unetched sample of X100, the large inclusions with diameter $d > 1\mu m$ have been made visible. Inclusions

of the type Calcium Sulphide (CaS), Titanium Nitride (TiN) and Aluminium Oxides (Al2O3) are expected due to the chemical composition of the material. In contrast to above-mentioned inclusions, the detachment of the particles with diameters $d < 1\mu m$ leading to formation of secondary voids for larger strains. There are two major types of particles contributing to the nucleation of secondary voids, bainite packages, which consists of finest precipitated iron carbides (Fe3C, cementite), and M-A-constituents (combination of martensite + retained austenite). These two microstructural entities can be observed by SEM of HNO3 etched surfaces at high magnifications, as it is demonstrated in Fig 4-11.

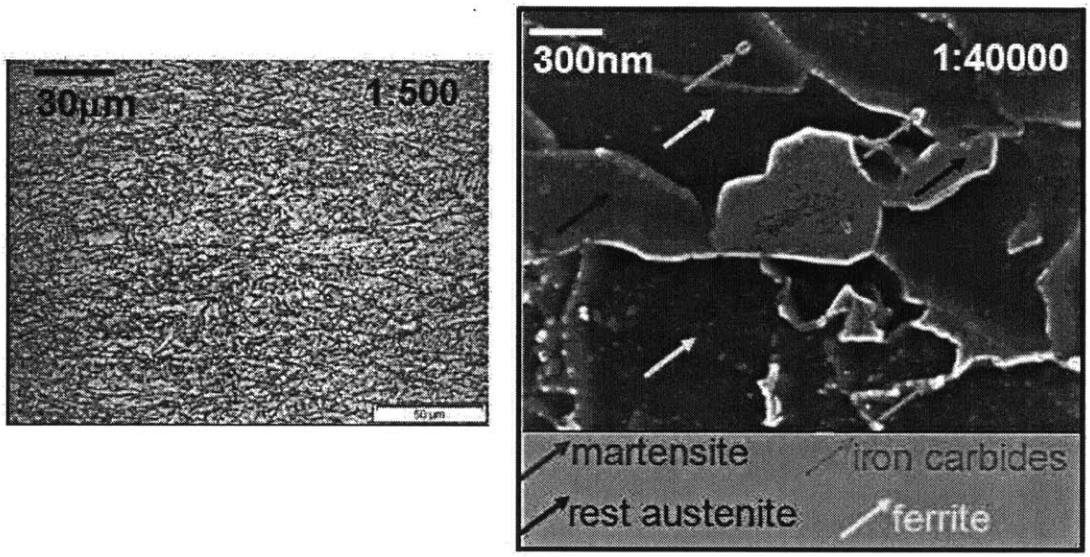

Figure 4-11: Microstructure of X100 from LOM (left) and SEM (right) analyses.

4.2.4 Plasticity

The raw experimental data are usually applied force and cross-head displacement. For each experiment, force is measured by the load cell and displacement is measured by both the load cell and DIC. The DIC method provides flexibility in terms of positioning the extensometers near or far away from the failure area, measuring global or local strains and also setting the virtual extensometers after the completion of each experiment allowing for multiple measurements from a single test. For this study, DIC

displacement measurements were chosen. In order to ensure repeatability of experimental data measurements, a minimum of three specimens were tested per specimen type. The first piece of data acquired, is the force displacement curves for each test. Then, engineering stress versus strain curves are calculated. When load reaches the ultimate strength of the material, diffused necking initiates and the cross-section area is reduces with respect to the original cross-sectional area. For low levels of strain, the two curves for engineering and true stresses coincide. As the strain increases further, the cross-section collapses and true stresses exceed engineering stresses for the same amount of strain. All stress versus strain graphs depicted in this chapter represent true quantities. The next step is the identification of onset of fracture on the specimen surface. Crack initiation occurs in the center of the specimen, however, for flat specimens, crack instantly reaches the external surface. Pictures frames are taken constantly at a prescribed frequency throughout the duration of each experiment. At the same time, load and displacement measurements are stored to a computer unit. The frequency of taking pictures was 1 frame/sec for all tests. After the completion of the test, the displacement to fracture is identified as the displacement for the frame where the first surface discontinuity is visible. The displacement at the initiation of fracture, δ_{frac} measurements are essential for the inverse calibration of plasticity in the post-necking range, as well as for the fracture calibration. Displacement to fracture measurements were not used the dogbone specimens. In the case of dogbone specimens, the exact location of first failure cannot be a priori defined. Numerical simulations were not developed for this type of specimen. The fracture displacement is given as input for the numerical simulations of each specimen, prescribing the maximum travelling distance of the grips for the Finite Element (FE) model. The final measurement taken from the tested specimens is the thickness measurements at the failure location up to initiation of fracture. For identical specimens, δ_{frac}, varied by maximum 5% for X70 tests and 8% for X100. The fracture displacement considered for each type of specimen was the minimum measured for each specimen category. In the subsequent sections, comparison of the experimental and FEM data will be presented for each specimen type.

The material experiences elastic deformations up to the point that the stress reaches the yield stress of that given material. The investigation of material behavior under certain loading conditions is a very important area that allows us to evaluate the integrity of a structure constructed by that specific material. Two important material properties for metals are (i) the yield strength and (ii) the ultimate strength. The yield strength of a material is defined as the maximum stress under which the material can deform elastically, while the ultimate strength is the corresponding stress to the maximum tensile load. In the elastic regime, after unloading the material it regains its original form without any energy dissipated in the material. Above the yield stress, the material starts deforming plastically. The ultimate strength of a material indicates the initiation of the neck formation. This is the maximum stress that a material can specimen. In order to evaluate those material parameters a tensile test has to be conducted. Standard test pieces are subjected into slowly increasing (quasi-static loading conditions), axial tensile stress up until failure. Dogbone tensile specimens were used for the determination of the pre-necking plastic behavior of the two materials.

In plane stress conditions, which were extensively studied at the ICL for the automotive industry, the stress triaxiality cannot exceed $\eta = 2/3$. By contrast, in heavy-walled pipes, much higher triaxiality values may occur, especially in the Heat Affected Zone (HAZ) and the near defect areas (welding zone, pitting corrosion etc.) where pre-existing cracks alter the stress field locally. At the same time, low triaxiality values must also be studied in order to correctly represent shear dominated failure of pipes. Anisotropy is also an important feature due to the manufacturing process of the pipes. Therefore, the needs of the pipe applications require the choice of the necessary experimental program so that the material parameters are calibrated covering all the range of stress triaxialities encountered in pipe applications.

For the complete characterization of the material, five types of flat specimens were selected, namely flat dog-bone, flat notched with $R = 6.67mm$, flat specimens with central hole, butterfly specimens and circular disk specimens for the low triaxiality region; and also three round specimens with notch-radii of $R = 0.2$, 0.5 and 1.0 mm

to cover the higher triaxiality values. For the latter two specimens (R = 0.5 and 1.0 mm) fracture initiates at the center of the specimen cross-section, while for the case of $R = 0.2mm$ fracture initiated at the root of the notch, where the stress state was not axisymmetric ($\overline{\theta}$= 1). For that reason, it was decided that only R = 1.0 and 0.5 mm would be used for the fracture calibration. The flat specimens have a stress triaxiality ranging from zero, for pure shear (butterfly specimens) up to 2/3 for equibiaxial tension (circular disk specimens). The initial stress triaxiality in the round notched specimens can be estimated by the Bridgman equation. The stress triaxiality at the center of the cross-section, which is usually the fracture initiation location is defined in Eq. (4.25).

$$\eta = \frac{1}{3} + \ln\left(1 + \frac{\alpha}{2R}\right) \tag{4.25}$$

where R is the local radius of the notch in the round specimen and α is the radius of the minimum cross-section at the notch root. For the case of notch radii, $R = 0.2mm$, due to the fact that fracture initiates at the root of the notch and not at the middle of the cross-section, therefore Eq. 4.25 is not applicable. According to the Bridgman equation, the triaxialities in the center of the round notched specimens for R = 0.5 and 1.0 mm are η = 1.432 and 1.026. The corresponding values from the numerical simulations are higher 1.73 and 1.39 respectively, than the analytic values calculated using the Bridgman equation. This difference is due to the fact that the analytic expression calculates the evolution of stress triaxiality as a function of necking radii and not global radii.

The pipe segments of API X70 originated from a pipe of outside nominal diameter, $D = 355.6mm$ and thickness, $t = 25.4mm$, cut in 45 degree segments. The specimen manufacturing process was design specifically to take into account through-thickness variation of material properties. The results presented here are taken from the outer extracted sheet/layers of X70. For isotropic material, the yield stress ratios in the in-plane directions are equal to unity. It seems that from the point of view of the plastic flow, the effect of anisotropy of API X70 is small. The studied material comes

from a seamless pipe as it was mentioned earlier, for which the effect of anisotropy is much less pronounced than for typical UOE pipes. For all subsequent numerical simulation X70 was considered to be isotropic.

In the case of X100, the pipe segments originated from a large diameter pipe manufactured at Europipe. The outside pipe diameter is $D = 1219.2mm$ (48 inches) and wall thickness, $t = 18.4mm$ (0.72 inches) cut in 60 degree angle curved segments. Due to the UOE manufacturing process the resulting bulk material presented significant anisotropy.

The above representation is valid up to the point of ultimate tensile strength. In order to determine the plasticity behavior in the post-necking region an iterative process was followed. The diffused necking occurs at strain equal to the hardening exponent, $\epsilon = n$. The final flow curve was calibrated using an iterative process, where force-displacement measurements from tested notched and flat specimens with central hole are compared to the numerical simulation data. In each step the flow curve was modified to match the numerical results to the actual experimental measurements. The post necking flow curve lies between the power law and the flat extensions. As the material presents little hardening, the difference between those two limit cases is very small. The power law overestimates the force level after the ultimate strength, while the flat extension underestimates it.

Plasticity Calibration: Dogbone specimens tested for three principle directions, namely 0, 45 and 90 degrees with respect to the longitudinal axis of the pipe. For X70 grade, both regular ASTM 6mm wide and 32mm long gage section and ASTM 3mm wide and 16mm long gage section specimens were tested. The first type was cut in the longitudinal axis and the latter in all three directions. The smaller dogbone specimens were used to accommodate the geometrical restriction of the received pipe segment and also to minimize the through the thickness variation of the mechanical properties in the calibration of anisotropy. The scaling ratio between small and regular dogbone specimens is two. For the X100 grade, the pipe curvature was larger, therefore allowing for all the usage the regular ASTM 6mm wide and 32mm long gage section dogbone specimens for all directions. The information regarding the

plasticity behavior of both X70 and X100 is taken from the regular 0 degree dogbone tests up to the point of necking initiation. The experimental data beyond that point are discarded. The results from the tests for X70 and X100 are presented below in Figs. 4-12 and 4-13. For every grade, three different specimens were tested to ensure repeatability. The good repeatability of both grades justifies presenting only one set of results, namely the one for which fracture occurred for the smallest value of displacement. Data of X70 material are depicted using red color, while data of X100 material are shown in blue. The true stress strain curves are calculated using

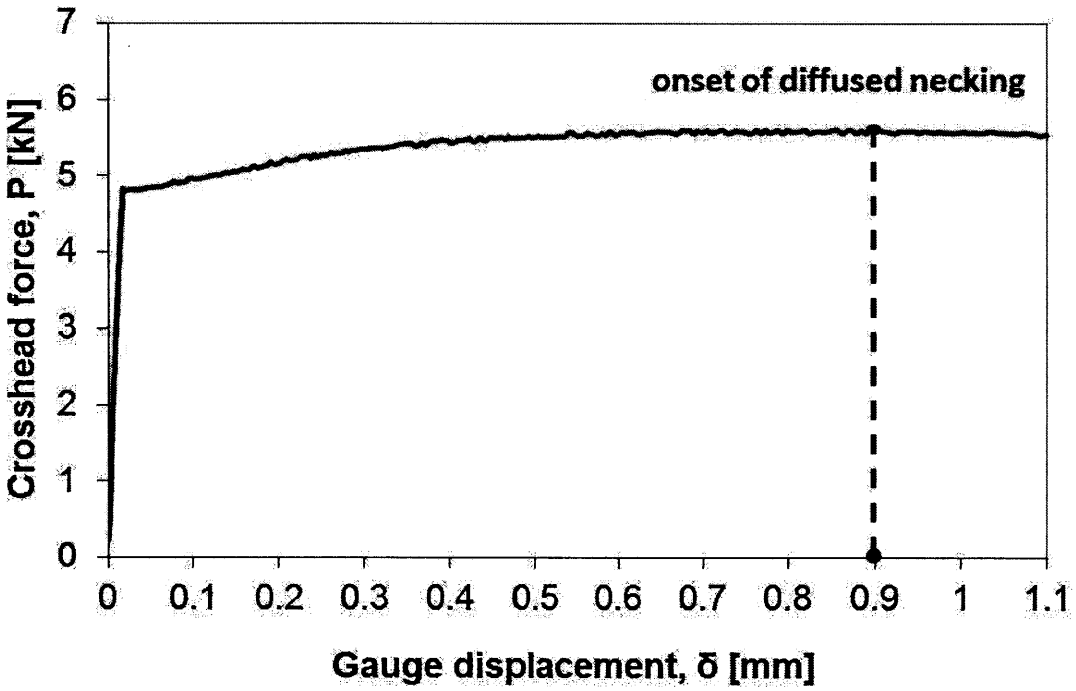

Figure 4-12: Force versus displacement of dogbone specimen experimental data for API X70 steel.

the DIC displacement measurements and presented below for dogbone specimens longitudinally cut from X70 and X100 offshore grades.

The stress versus strain curve is extended beyond the ultimate strength using two additional piece-wise linear sections. The iterative process is partitioned in two subsections. The first range focuses on strains beyond the necking point but not

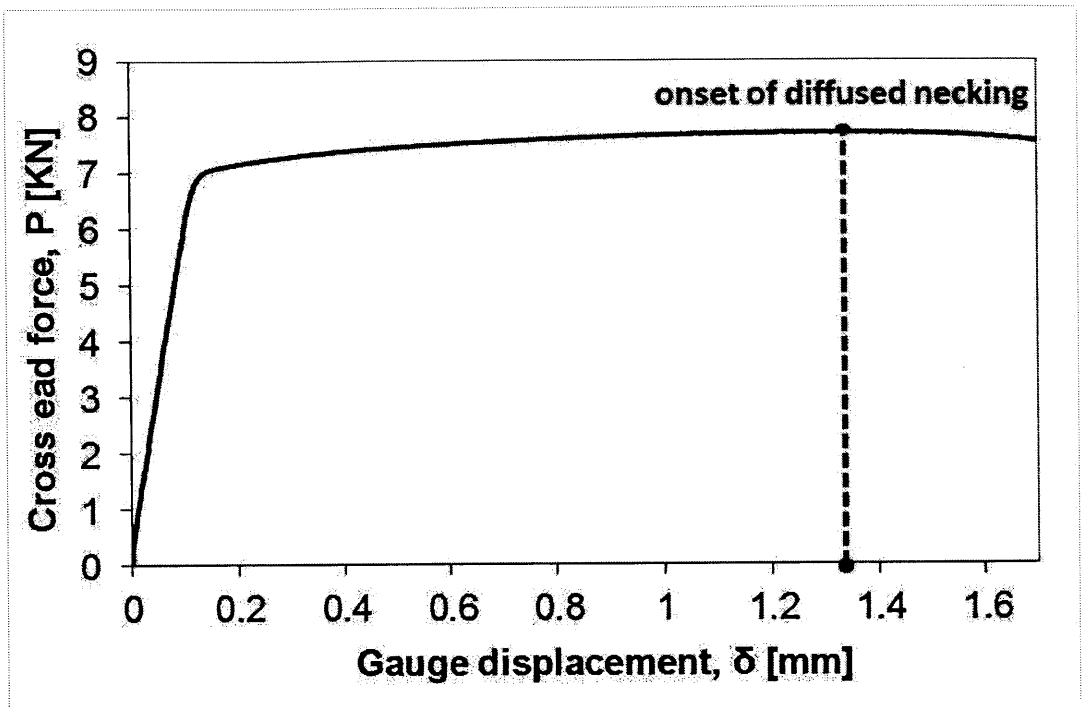

Figure 4-13: Force versus displacement of dogbone specimen experimental data for API X100 steel.

Table 4.5: Pre-necking plasticity parameters calibrated for X70 and X100 grades.

Hardening parameters	X70	X100
A [MPa]	844.6	1006.5
n	0.0984	0.0384
ϵ_o	0.005	0.0008

exceeding the fracture strain in specimen with central hole subjected to tension. The second range includes much higher strains only attainable in the disk specimens subjected to equi-biaxial tension.

The ultimate stress occurs at about 10% of strain for X70 and 3.8% of strain for X100. For X70 the upper range of strain was 25% while for X100 is was 10%. The calibration was done based on an inverse trial and error method.

Several slopes were considered in the numerical simulations and the one that follows more closely the experimental load displacement curve was used to define the

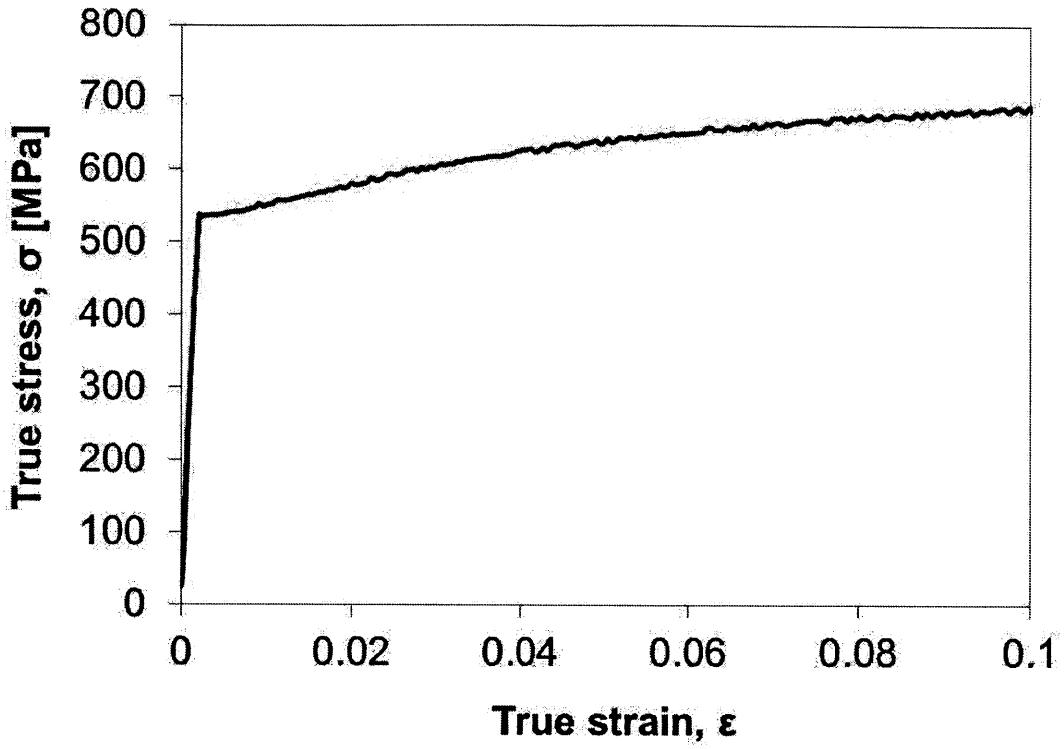

Figure 4-14: Calculated true stress versus strain curve of dogbone specimen for API X70 grade of steel.

post-necking slope. The final corrected stress strain curves for the two materials are shown in Figs. 4-18 and 4-19.

The calibration process was done manually. However, a more automatic process combining experimental results and numerical simulations in an iterative loop until final convergence of experiments with simulations is been developed to make the process less intricate and more easily introduced in industrial integrity assessment applications.

This analysis is essential to ensure the reliability of the model at following the material's behavior closely. The range of the hardening law was extended for large strains through punch tests data. The iterative procedure still works well. The results are shown in Figs. 4-20 and 4-21. However, several other effects such as in-homogeneity, anisotropy and friction affect the simulated load displacement curve.

The range of large displacements is becoming increasingly important, especially in

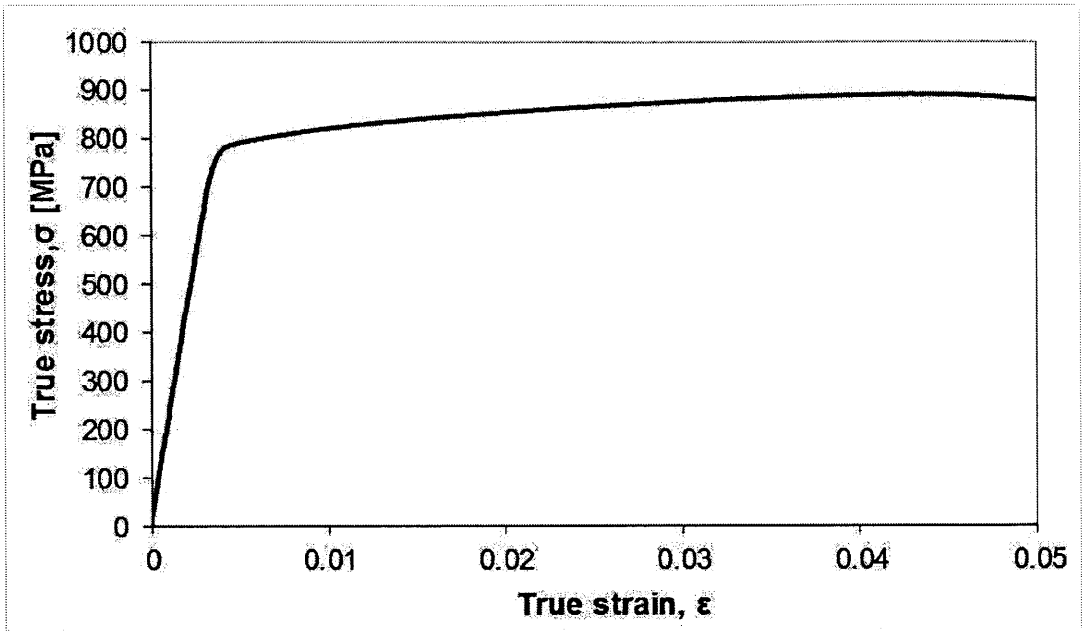

Figure 4-15: Calculated true stress versus strain curve of dogbone specimen for API X100 grade of steel.

the case of offshore, arctic pipelines, where ground movement enforces large strain on the body of pipe. Therefore, the calibration in this range becomes an essential part of the material description. For that reason punch experiments conducted at MIT along with the corresponding numerical simulation model was an important part of the process. An important parameter that affects the final outcome is the friction considerations for the experiment and the FE model. As a first attempt, the interaction between the circular quarter of the disk and of the modeled die is assumed friction-less in the FE simulation. However, during the experimental procedure, friction is not equal to zero. It was significantly reduced using Teflon sheets between the punch die and the disk specimen. In the future a parametric study should be carried out to investigate the effect of adding a friction coefficient to describe the interaction properties of the die-disk system. Another direction would be to conduct identical punching tests in a hydraulic bulging system and compare results for the same material and geometry between the ICL mechanical system and the numerical output.

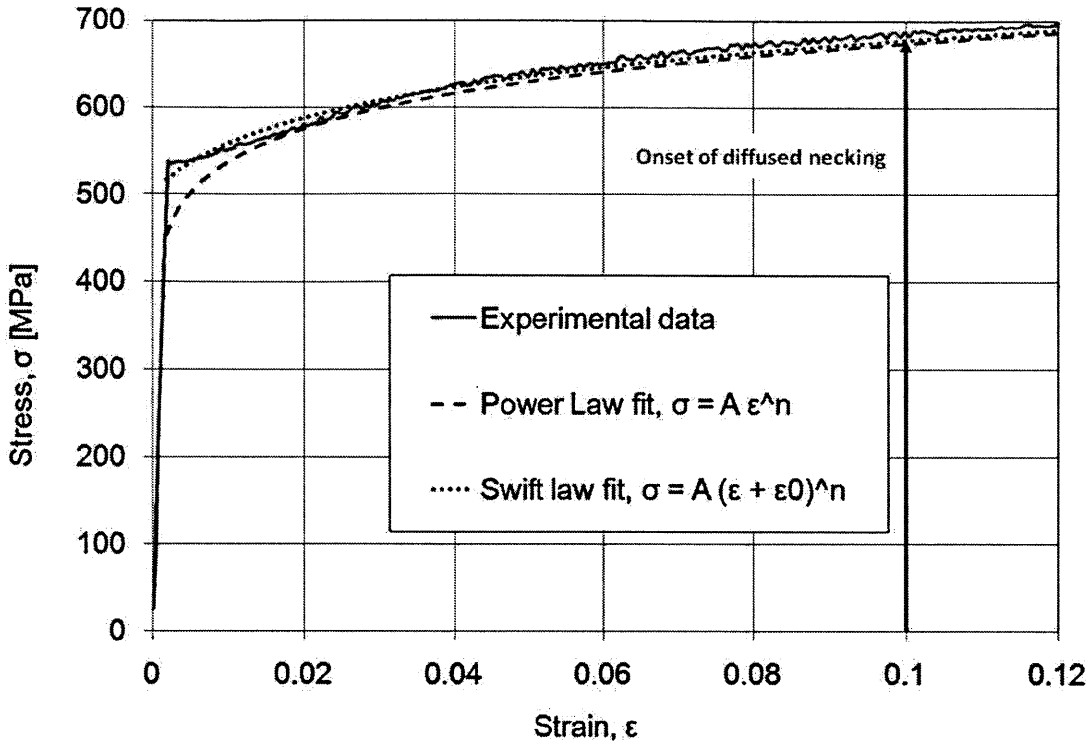

Figure 4-16: Hardening rule fitting for the longitudinal dogbone tensile specimen made by API X70.

Anisotropy Testing Procedure: For the study of anisotropy, dogbone specimens, cut in three principal directions were tested in order to define the amount of anisotropy for each material. The force versus displacement is presented for 0, 45 and 90 degrees using small-scale dogbone specimens, Fig. 4-22. The extreme behavior observed in the circumferential direction could be due to several factors such as thermal ageing effect and anisotropy due to manufacturing process used. This is also observed by other research groups [12] and [66] working in the area of Strain-Based Design (SBD). More analysis and testing are required to better understand the anisotropic features of the material in connection to the manufacturing process. Dogbone specimens in the longitudinal direction are used. The parameters are summarized in Table 4.5 for plasticity and Table 4.6 for anisotropy.

As it was mentioned above, dogbone specimens were cut in three main directions with respect to the longitudinal axis of the pipe. The displacement history data was

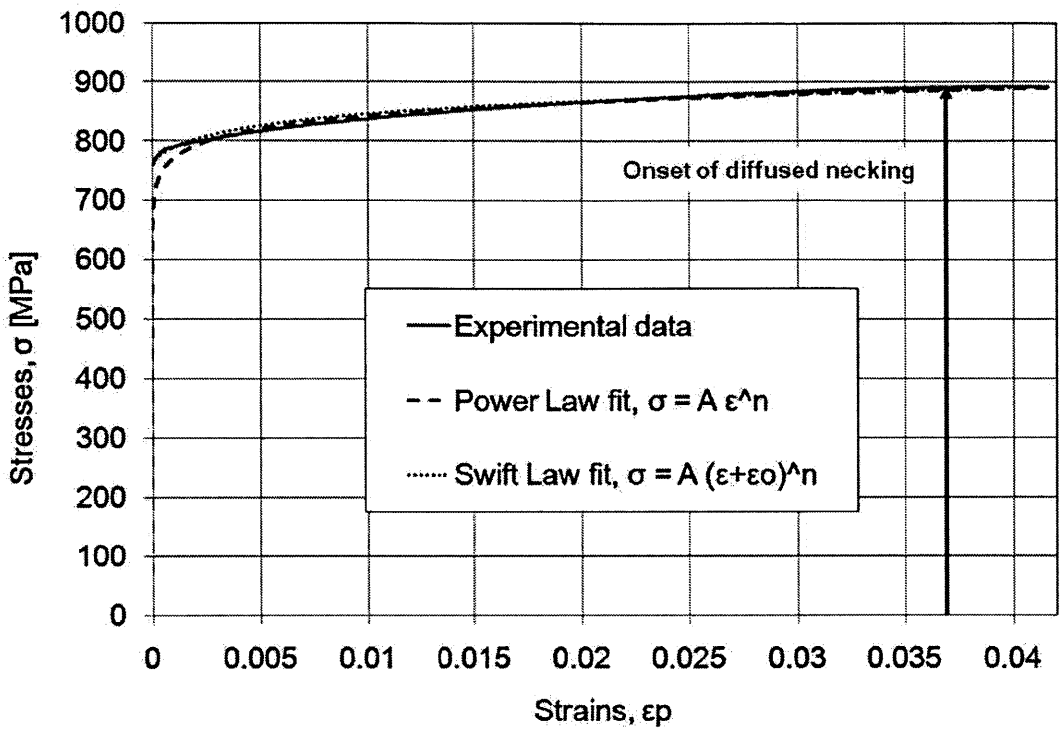

Figure 4-17: Hardening rule fitting for the longitudinal dogbone tensile specimen made by API X100.

used to compute the engineering and true strain history. The Lankford coefficients, r_0, r_{45}, r_{90} in the longitudinal, the 45 degree and the circumferential direction were then calculated based on true-strain data.

This process is performed for both grades and the results are presented in Table 4.6 in terms of yield ratios that are going to be used in the FEM as input. Anisotropy is pronounced in the transverse direction for X100. The linear regression correlations, R2 are high indicating that the Lankford coefficients values calculated correct. The lowest correlation is for X70 in the 45 degree direction. Anisotropic hardening behavior will not be taken into account in this study. The Lankford coefficients characterize plastic anisotropy through the definition of the yield surface.

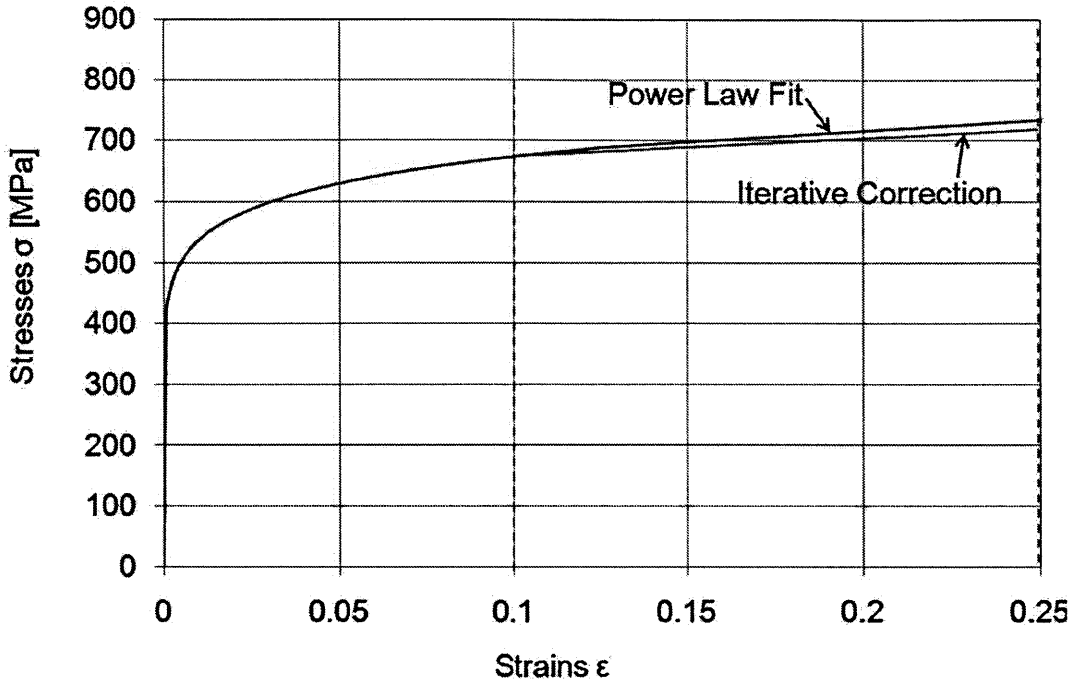

Figure 4-18: Material behavior after initiation of diffused necking for X70.

Table 4.6: Lankford coefficients and yield stress ratios for X70 and X100.

API grade	r_0	r_{45}	r_{90}	R_{11}	R_{22}	R_{33}	R_{12}	R_{13}	R_{23}
X70	0.7706	0.6950	0.8398	1	1.024	0.961	1.077	1	1
X100	0.988	1.035	0.482	1	1.047	0.871	0.861	1	1

4.2.5 Fracture

Out of many types of fracture tests that have been used in the past at ICL, this study focused on those tests that have been proven to be the most reliable for modeling of plane stress state conditions. This set of specimens was enhanced by specimens used for bulk material representation. This combination was able to provide the necessary mix of information for the calibration of the fracture parameters of X70 and X100. There is a great deal of know-how in designing specimens and fixtures for fracture testing at ICL. One issue is to make sure that first crack initiates at the centre of the specimens rather than from its boundaries. For that purpose the concept of butterfly specimen was invented in 2002 and subsequently improved over the years.

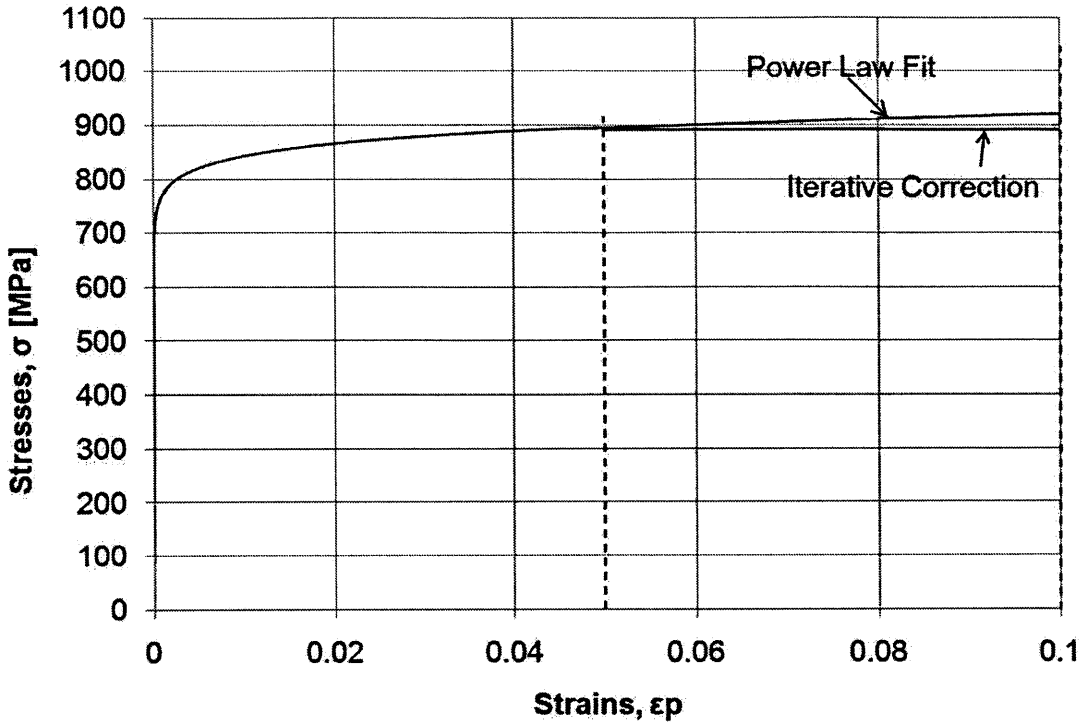

Figure 4-19: Material behavior after initiation of diffused necking for X100.

The strain field and in particular the equivalent plastic strain at fracture is determined with high accuracy using DIC. The stress tensor at the point of fracture is evaluated through an inverse method by running a FE simulation for which a precise plasticity model is needed. While tests using butterfly specimens cover a wide range of stress states, a number of complementary tests are needed that can extend the range of validity of the fracture model to higher stress triaxialities, that is usually the case for thick-walled components or specimens with sharp cracks. The objective of all of the above tests is to find a 3D-fracture envelop. The fracture characterization is a hybrid experimental-numerical procedure. The cross-head displacement and force are monitored, as before throughout the experiment and the displacement at the instance of fracture initiation is determined. Then, numerical simulation of each fracture experiment is developed and used to extract information on the history of plastic equivalent strain and stress tensor at the vicinity of fracture location up to the initiation of the first crack. The history of equivalent plastic strain, triaxiality

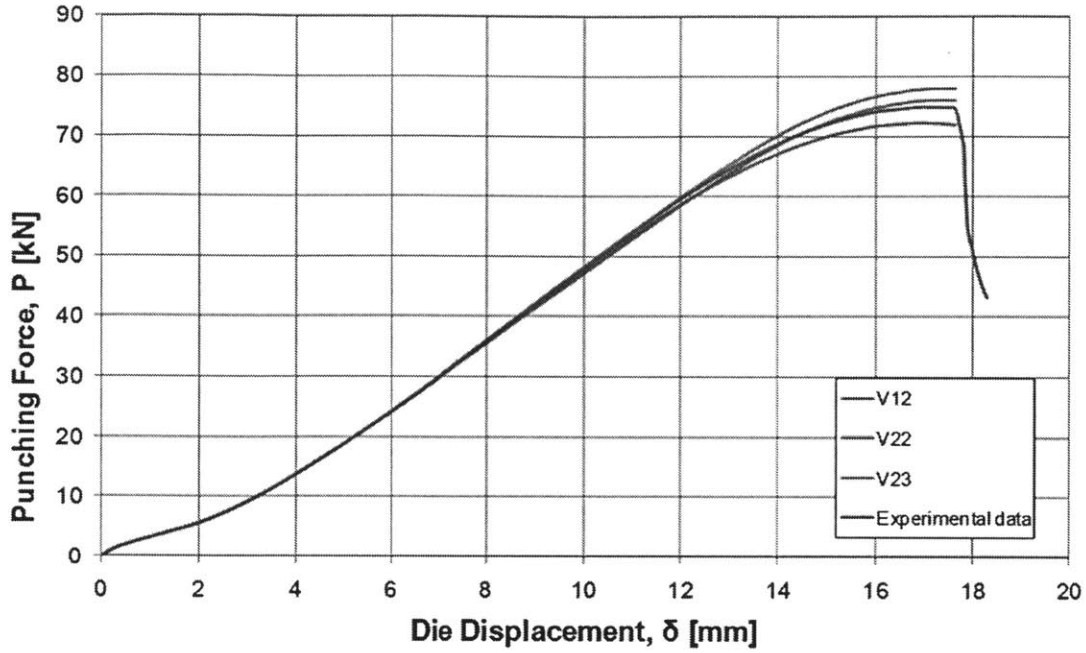

Figure 4-20: Load vs. displacement curve from punch simulations for X70.

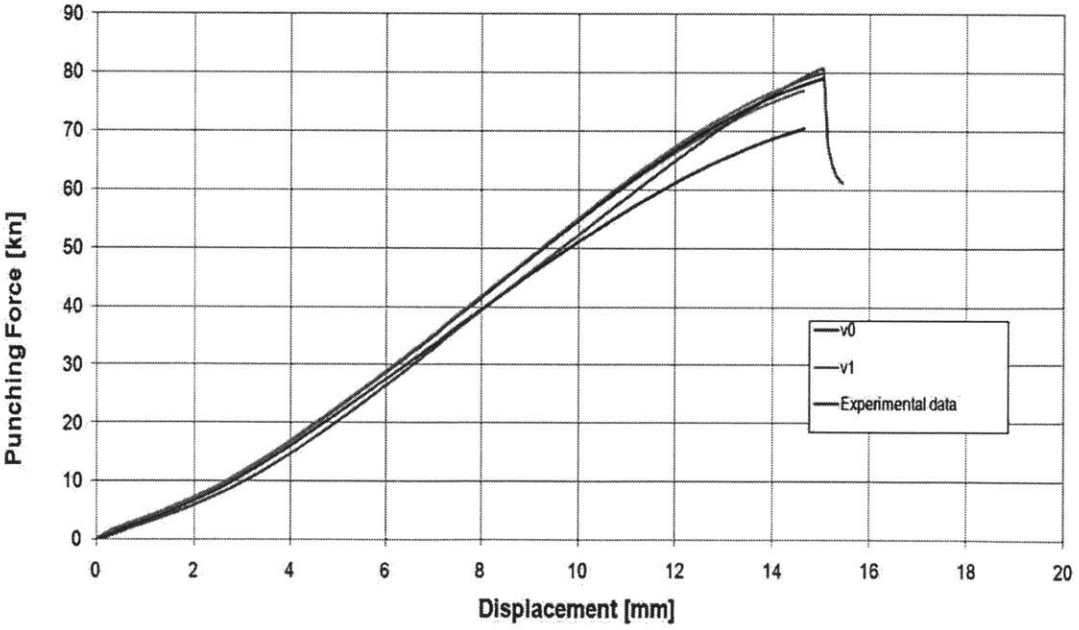

Figure 4-21: Load vs. displacement curve from punch simulations for X100.

and Lode angle are determined for each calibration test up to the onset of fracture. These results are used for the final fracture calibration. In some cases the fracture

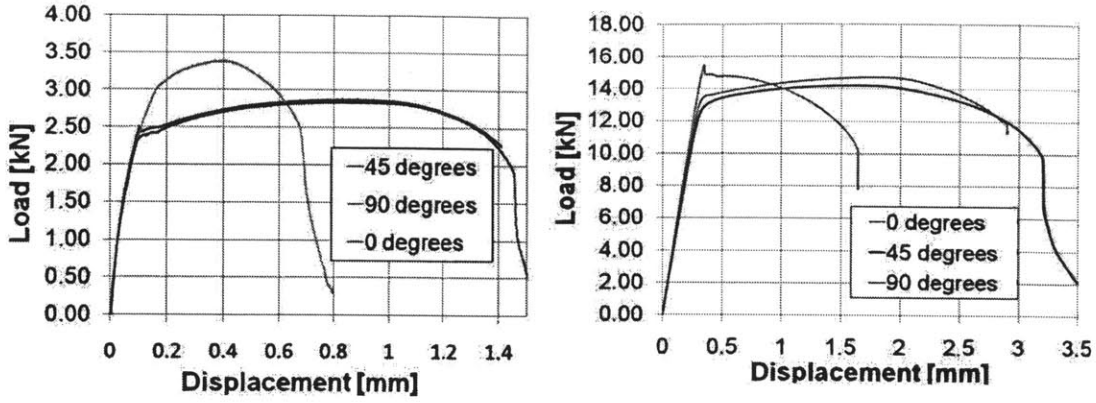

Figure 4-22: Force versus displacement for three principal directions of X70 (left) and X100 (right).

strains from the above hybrid method are checked against DIC measurements and direct thickness measurements. In the following section all fracture specimens will be presented. This includes flat speciment with central hole, flat notched specimens with notch radii, $R = 6.67mm$, flat butterfly specimens subjected to both tension and pure shear, flat disk specimens and round specimens with three different notch geometries.

Flat tensile specimens with central hole: This specific specimen geometry drives the crack initiation slightly away from the hole edge, where the initial stress state is close to uniaxial tension ($\eta = 0.33$). The dimensions of the specimen are depicted in Fig. 4-23. Specimens with central hole were cut in the longitudinal direction only and were used for fracture and post necking plasticity calibration.

The ICL hydraulic machine is capable of biaxial testing of specimens extracted from sheet and pipe materials, with customized high pressure clamps, see Fig. 4-23 (right). It offers the capability of testing specimens under in-plane shear, compression/tension and any combination of these three loading patterns.

The specimens are clamped to a vertical actuator and a low-friction sliding table. Using the horizontal actuator for the application of shear load, it is possible to study the combination of Mode I and Mode II failure.

Notched R6.67 tensile specimens: Flat tensile specimens with circular cutouts were also used for the characterization of fracture and post necking plasticity. The

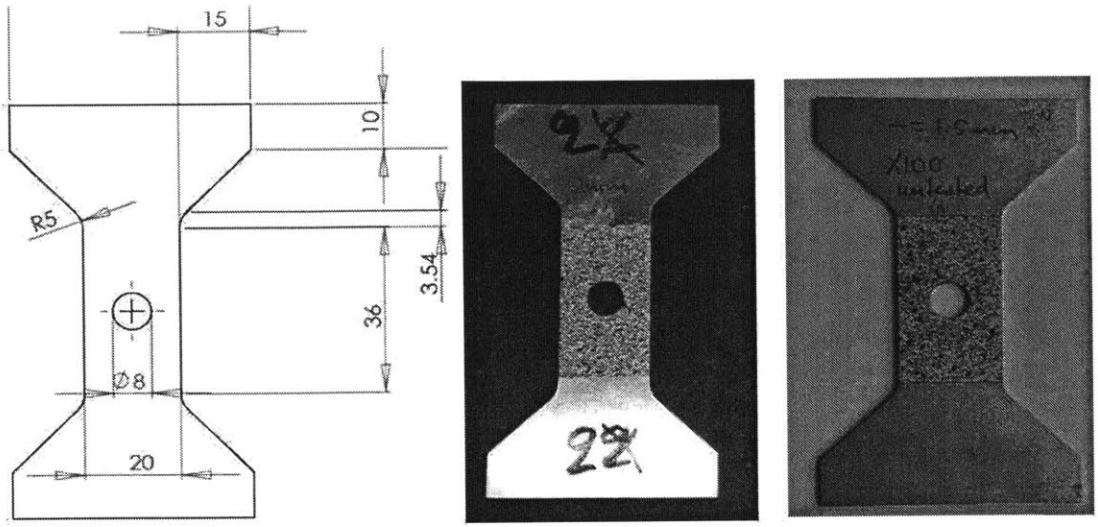

Figure 4-23: Blueprints of flat specimens with central hole and dyed specimens used for API X70 and X100.

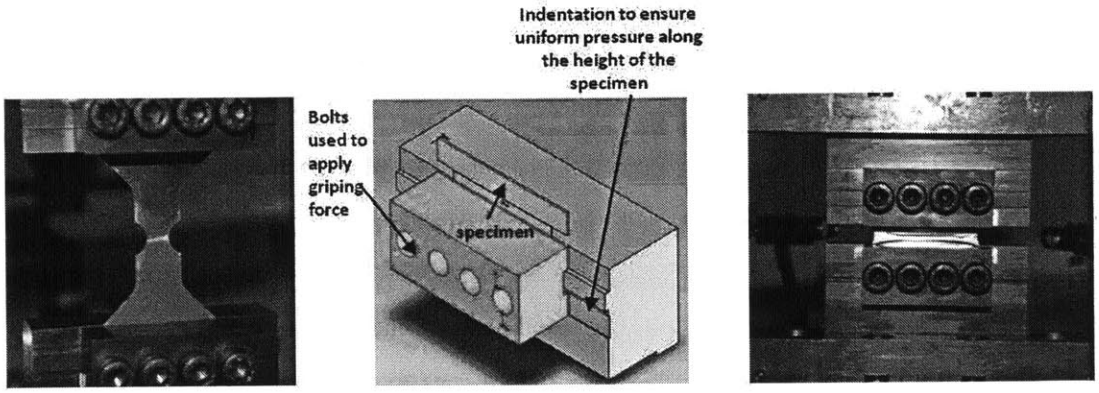

Figure 4-24: Instron 8080 customized pressure grips used for tensile test of a notched specimen (left), schematic of the grip design demonstrated in the case of a butterfly specimen.

stress state up to the point of necking at the location of crack initiation (center of the specimen) is a function of the radius of the cutouts ranging from uniaxial tension for $R \geq 20mm$, to plane strain for $R \leq 6.67mm$.

For isotropic materials, the triaxialities observed range from 0.33 to 0.58. In this study a radius of $R = 6.67mm$ was selected as shown in Fig. 4-25. Experiments were carried out using displacement control in the static regime with speed of cross-head of 0.2 mm/min same as for the central hole and butterfly specimens.

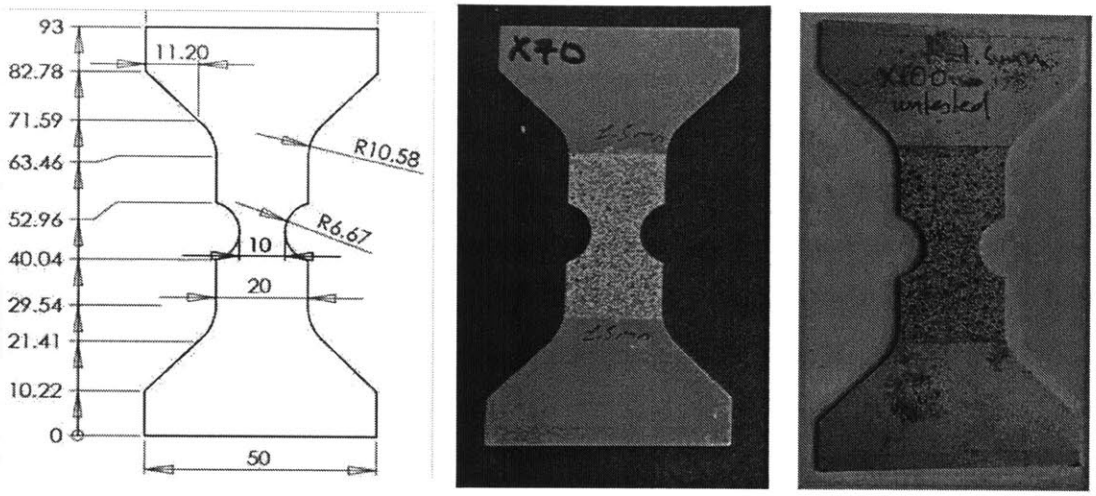

Figure 4-25: Blueprints of flat specimens with notch $R = 6.67mm$ and dyed specimens used for API X70 and X100.

Butterfly specimens: The next set of low triaxiality fracture tests was the tensile and shear tests of the butterfly specimens. The complex 3D geometry of the specimens (see Fig. 4-26) was developed at ICL to study multi-axial loading using biaxial testing machine. One of the unique features of this design is that by applying different combinations of horizontal and vertical displacements, or forces, a variety of stress states can be achieved in the gage section. In order to achieve pure shear ($\eta = 0$) the horizontal motion of the sliding table was displacement controlled while the vertical motion was force controlled with zero prescribed force. The curved profile of the boundaries was designed to prohibit edge crack initiation.

Circular disk specimens: Finally, the circular disk specimens were used for punch tests to simulated equibiaxial tension conditions. The actual specimen cut from X70 and X100 is shown in Fig. 4-27. The outer diameter of the disk is $127mm$, the bolt circle diameter is $87.884mm$ and the second bolt circle diameter is $106.934mm$. Several layers of Teflon sheets were used to eliminate friction between the punch and the disk. Fracture was observed slightly away from the pole due to the presence of material imperfection and friction, for X70, while for X100, fracture initiated in the specimen center.

A fine speckle pattern of $80\mu m$ was used for the DIC analysis for the extraction

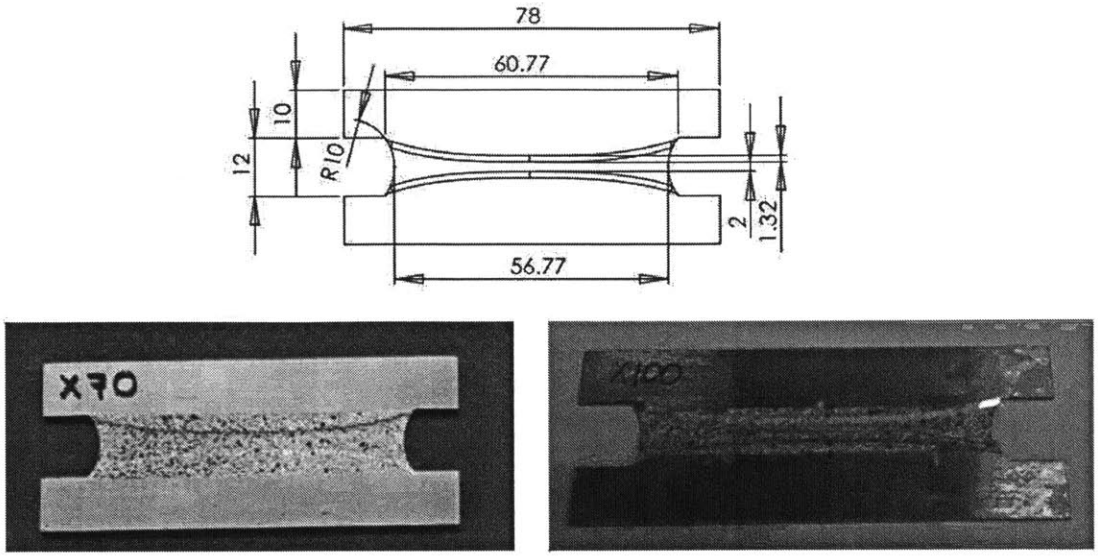

Figure 4-26: Blueprints of flat specimens with notch $R = 6.67mm$ and dyed specimens used for API X70 and X100.

of information about the strain field at the punching area. Similar speckle patterns were used in all other flat specimens ranging between 80 and 100μm. A digital camera was used to monitor the speckle pattern (Fig. 4-28). Direct thickness measurements were also used for the estimation of the fracture strain and correlation with the DIC values.

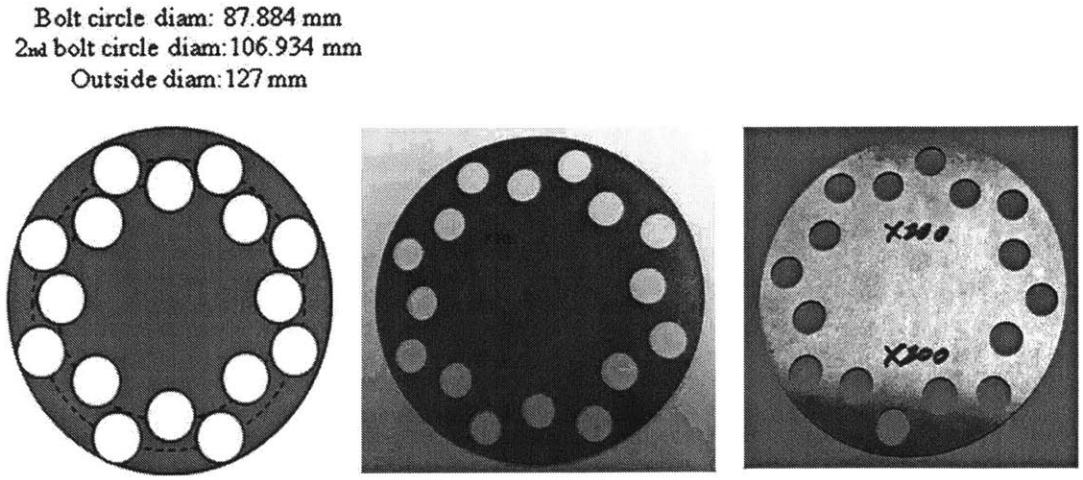

Figure 4-27: Blueprints of disks for the punch experiments and dyed specimens used for API X70 and X100.

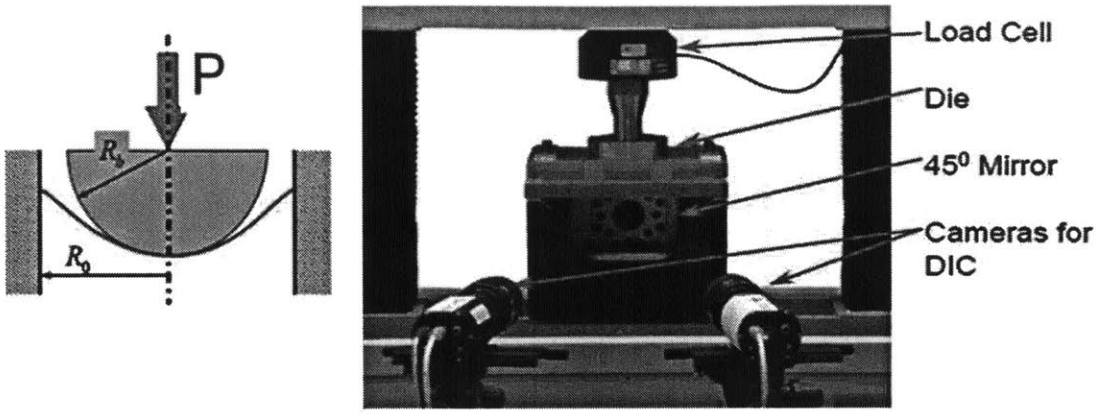

Figure 4-28: MTS uniaxial tensile wedge grips (left), MTS circular grips and die used for punch testing (right).

In the past, the MMC fracture model was applied mainly to thin walled structures for sheet metal forming applications, where the range of stress parameters is limited ($0 < \eta < 2/3$). In the present paper, the calibration of the MMC fracture locus was performed from tests covering a wide range of stress states ($-1 < \overline{\theta} < 1$ and $0 < \eta < 2$).

The following section explains the testing process of notched round bar specimens. Material information in the range of the stress states of $\eta > 1$ is needed to analyze the crack propagation of the SENT specimen and assess the capability of the MMC in bodies with pre-existing cracks. At the center of the SENT specimen, which is the targeted application, plane strain prevails while at the edge of the specimen the material points are essentially in plane stress. Therefore, a large gradient of constraints exists through the thickness of the specimen requiring a sophisticated model that is capable of taking into account complex stress state history that it changes during the experimental procedure.

Round notched specimens: Three different notch geometries, with notch radii $R = 0.2$, 0.5 and 1.0 mm, were tested at SZMF, leading to different stress triaxiality levels at crack initiation. Only two were finally used in the calibration process, $R = 0.5$ and 1.0mm. The geometry of the investigated standard B8x40 specimens is shown in Fig. 4-29. It is well known that in general fracture of round specimen starts from the

center and propagates outward for large notches. However, for sharp notches radii $R < 0.5mm$, fracture may initiate from the root of the notch.

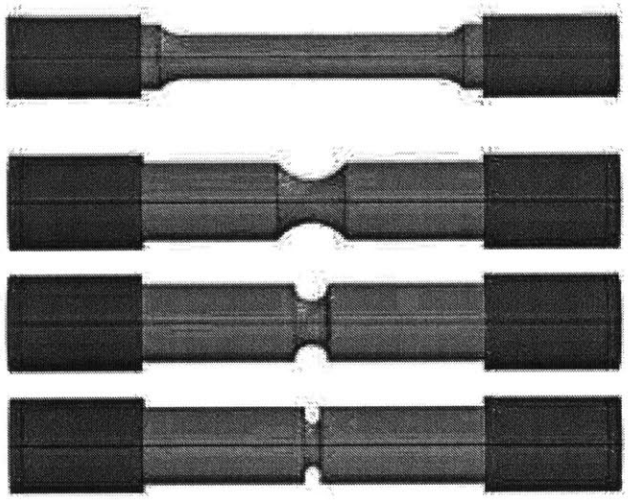

Figure 4-29: Schematic graph of the notched round bar specimens..

Therefore, the fracture strain definition is quite vague and the best way to determine the fracture onset is to conduct a series of interrupted test to determine the critical value of R for which fracture transitions from the center to the edge. In this study, the point of fracture is identified as the instant of the first microscopically recognizable void coalescence. Usually, three specimens per geometry type are required to identify fracture initiation using the interrupted tests technique. The first sample is loaded up to the point when the first crack appears on the outer surface of the notch for determining the force-deformation behavior of individual geometry. The second specimen is unloaded shortly before the fracture occurs, cut in the lengthwise direction to observe the fracture pattern by means of Scanning Electron Microscope (SEM). If the void coalescence is identified microscopically, further specimens are unloaded earlier during the test. This is a far more precise but also time-consuming procedure and its effectiveness should be assessed against the cost. This procedure was followed in the fracture test program on X100 steel [67]. For the case of API X70, only one specimen was tested per notch radii due to good repeatability, established from flat specimen testing results. The onset of fracture is assumed to be a few time

steps before the drop load.

4.3 Numerical Part

Finite element models assuming elastic and plastic material behavior were developed to determine the fracture strain by matching the calculated maximum FEM strain, at the instance when the measured critical displacement, δ_{frac} was reached. C3D8R, eight-node brick element with reduced integration (1 Gauss point) were selected for all specimens.

The post-necking calibration of the plasticity behavior is achieved using an iterative process. This process includes the numerical simulation of the notched, central hole and circular disk specimens. The calibration of the flow curve up to the point of maximum load was completed using measurement from the dogbone specimens cut in the longitudinal direction. Numerical models were also developed to simulate the butterfly specimens subjected to both tension and shear load to characterize fracture. All numerical simulations for the calibration of fracture were performed in Abaqus 6.9 Explicit.

The numerical results are used for two distinct processes. The first one is the calibration of the post-necking plasticity behavior. For this endeavor, numerical models are developed for the notched R 6.67, the circular disk and the flat specimen with central hole. Once the displacement to fracture is measured for all three types of specimens, it is prescribed as the final position in the FE code and the model is run. Force and displacement is monitored and the results are compared to experimental measurements. The plasticity behavior is thus calibrated in the post-necking range. For small displacements and strains, the notched and the flat specimen with central hole are used. For large displacement and strains, the circular disks are used. This method is iterative, i.e. the material behavior is calibrated using a trial and error process, the FE model is then re-run until the numerical prediction of the force displacement curve coincides with the experimental data in the area beyond the diffused necking has taken place.

The second process is the characterization of fracture. After the material behavior is defined, then it is inserted as input files and numerical simulations are run for all specimens. Triaxiality, equivalent strain and other stress-related parameters are monitored up to the point of fracture. This process is used to calculate certain variables that cannot be measured/calculated from experiments.

For the numerical modeling of all specimens solid elements were used. For each type of specimen different number of elements through the thickness has been used. The mesh size was chosen approximately 0.1mm near the fracture initiation area following the study regarding mesh size effect by. A parametric study of the effect of mesh size by [41] supported that selection to maximize time and computational efficiency of the numerical models. The flat specimen with central hole and the notched specimen R6.67 presented symmetry features justifying modeling 1/8th of the actual specimen (Fig. 4-30). The butterfly specimens are modelled in full while only 1/4th of the circular disk specimen was modeled taking into account symmetries in the x and y lateral directions.

In the case of the notched specimen, there are three planes of symmetry, allowing for modeling of only 1/8th of the specimen. Symmetric boundary conditions are prescribed. The top side of the specimen is forced to move until the displacement δ_{frac} is reached.

For the modeling of the flat specimen with central hole identical numerical model is used. The only difference is the geometry of the profile and the mesh structure.

The punch test simulation requires defining an appropriate surface-to-surface interaction behavior between the disk, the punch and the die. The die is considered a rigid body and the contact interaction is assumed to be friction-less to simulate the actual experiment.

The same model is used for the butterfly in shear and tension testing. The difference lies solely on the loading and the boundary conditions. In the tensile case, positive vertical displacement of the upper edge of the specimen is prescribed. Clamped boundary conditions are defined at the bottom edge, while the sides remain free. In the shear case, the top edge is forced to move towards the left, while requiring no

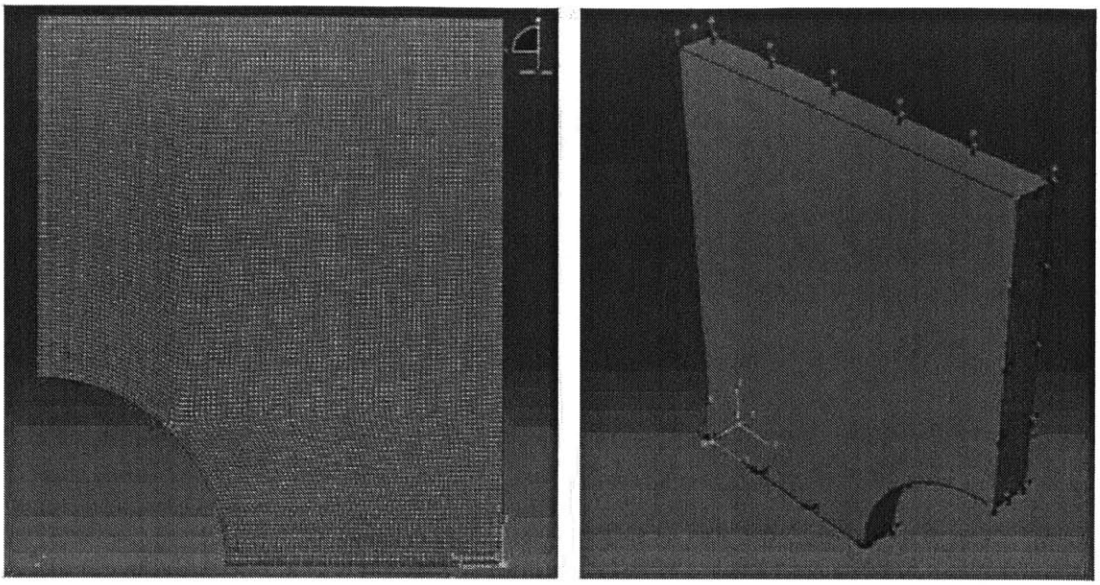

Figure 4-30: Flat tensile specimens with central hole finite element model. Mesh of model (left), boundary condition and loading (right).

vertical force. This is achieved by freeing the vertical boundary condition at the top edge. The bottom edge and the sides are as in the tensile case.

We assume that fracture occurs at the position/element where the equivalent strain is largest at the last frame of the simulations. In all cases the fracture location was close to the center of the specimen except for shear simulation, where the position of maximum equivalent strain was near the free sides.

The material elastic and plastic behavior including the post-necking information is incorporated in the FE model. True stress and plastic strain information is given in tabular form to define the hardening behavior. The first pair corresponds with the onset of plasticity ($\sigma_y = 0$, ϵ_y).

4.3.1 Comparison of experimental and numerical results

The first results to be presented are the force displacement curves from FE simulations for all specimens compared to the experimental findings. The material input to the numerical simulation is power law extension after neck formation. All numerical results follow the experimental data closely up to the maximum load for all specimens.

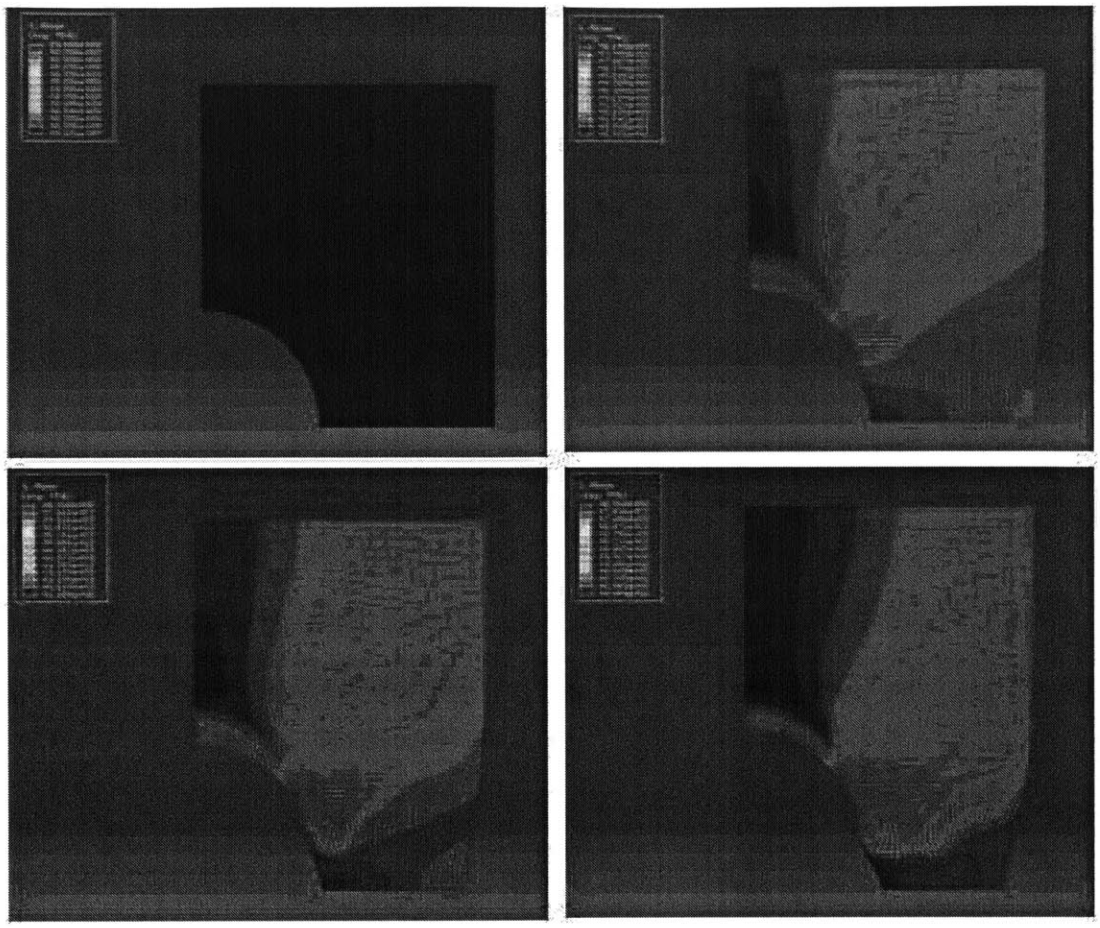

Figure 4-31: Frames of the simulation of experimental procedure of flat tensile specimens with central hole.

The punch specimen comparison presented the larger deviation between numerical and experimental results before the drop load occurred.

In order to extract information on plastic equivalent strain at fracture, Lode angle and triaxiality histories up to the point of fracture initiation, simulations are run with the fracture option turned off.

Small differences between predicted and measured forces and displacements in the pre-fracture-onset can be explained due to the variations of properties across the thickness of the original pipe, small anisotropy, the assumption of quadratic yield condition and also due to specimen machining procedure. The onset of fracture is depicted in every graph by a colored circle.

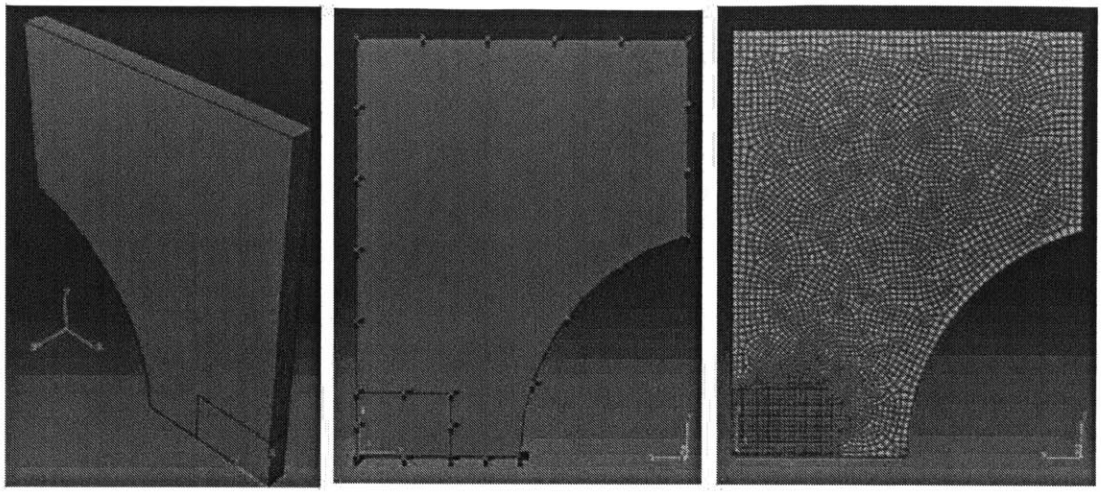

Figure 4-32: Notched R6.67 tensile specimen finite element model. Modeling 1/8th of specimen (left), boundary condition and loading (right)

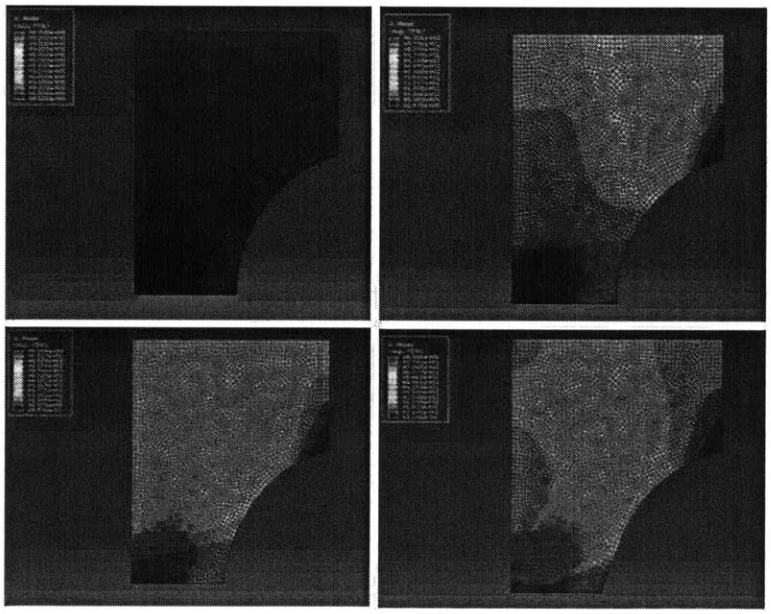

Figure 4-33: Frames of the simulation of experimental procedure of flat tensile specimens with notch R6.67.

4.3.2 Calibration process

The fracture behavior of both material is determined by three fracture parameters C_1, C_2 and C_3 through the definition of the 3D fracture surface. In the present study aiming the ductile fracture study of pipelines and risers, it is necessary to cover

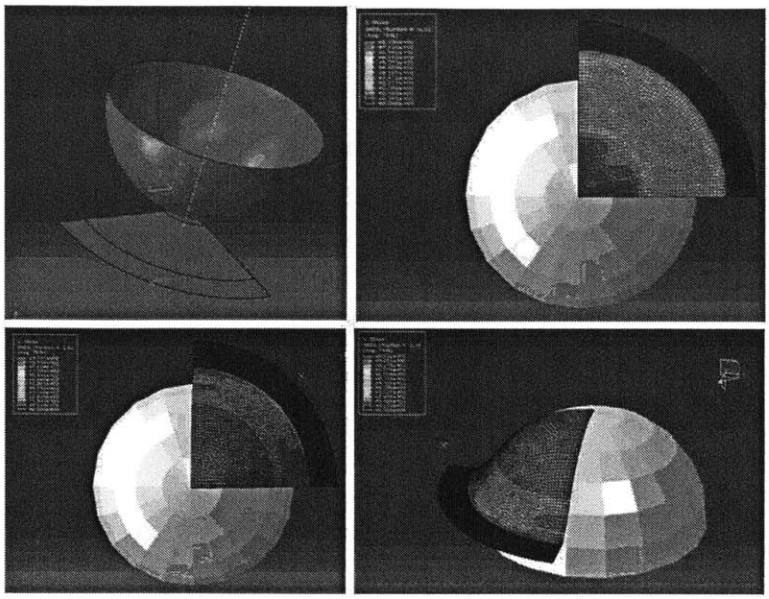

Figure 4-34: Notched Circular disk specimens finite element model. Geometrical configuration (up-left), frames of the simulation of experimental procedure (rest).

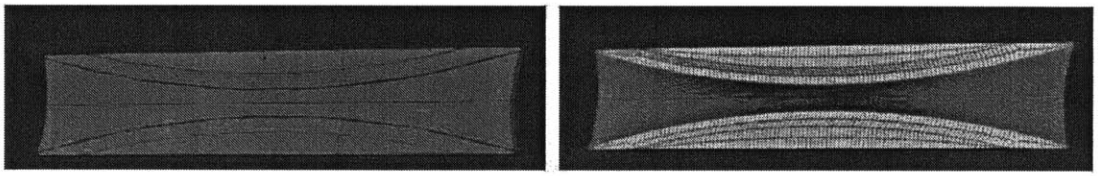

Figure 4-35: Butterfly specimens finite element model. Modeling of the gauge area (left), mesh of model (right).

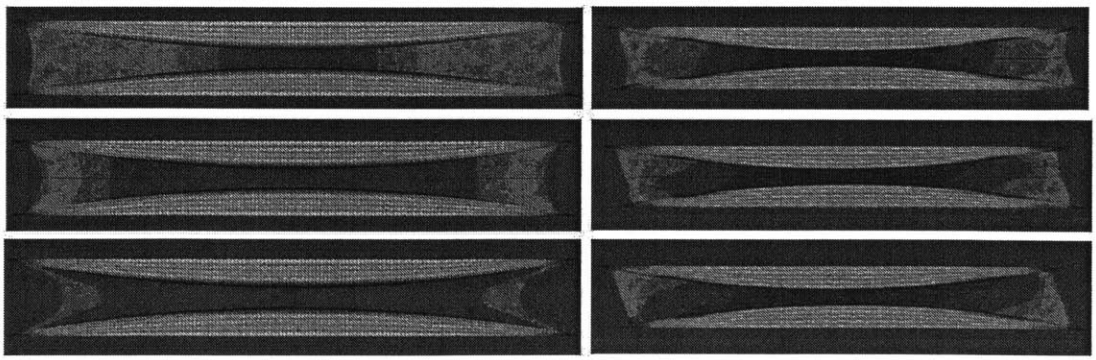

Figure 4-36: Butterfly specimens finite element model. FEM results for tensile (left column) and shear (right column) butterfly specimens.

the range of stress triaxiality values, $-1/3 < \eta < 2$. Originally, only flat specimen fracture data were used for the material calibration. The range of triaxiality of the flat

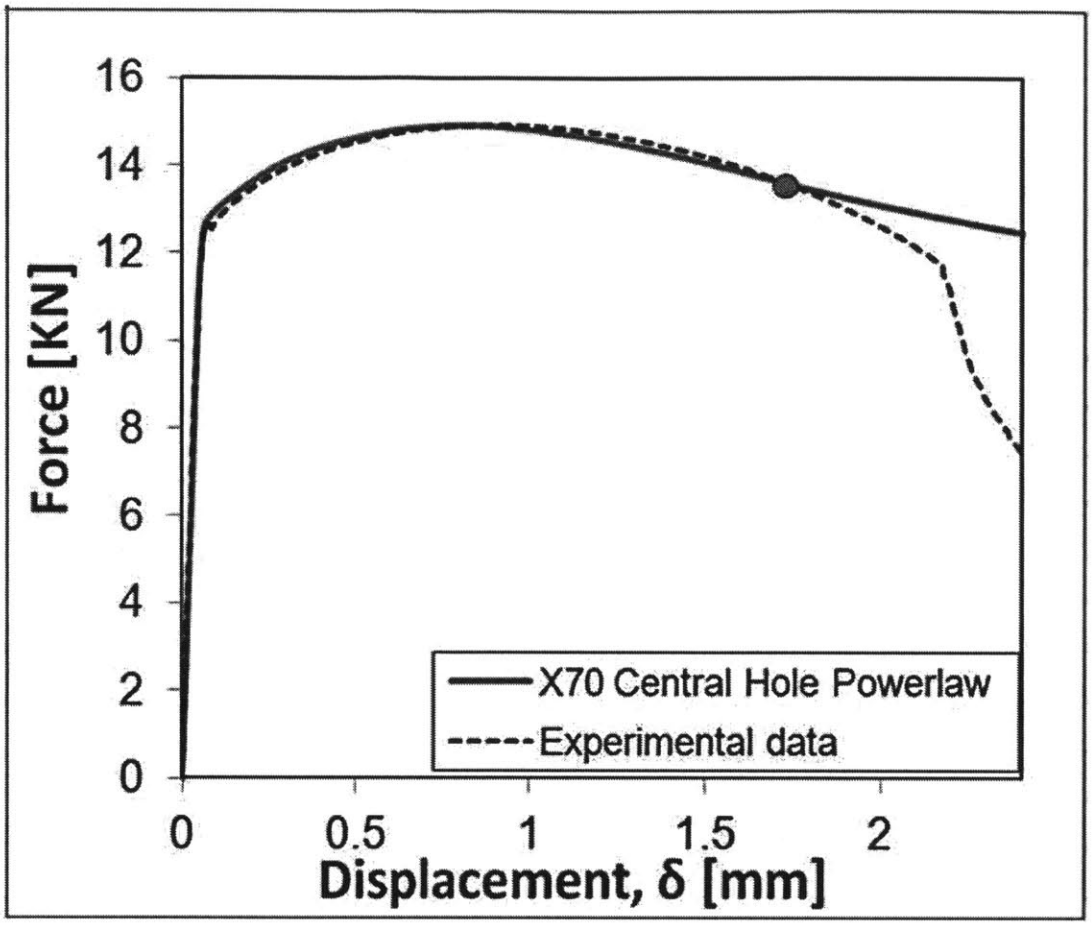

Figure 4-37: Comparison of experimental and numerical results for the central hole specimen made of API X70.

specimens was limited to $-1/3 < \eta < 2/3$. In order to model the material properties for applications that exhibits higher triaxiality values, the 3D fracture surface was initially extrapolated. However, this led to a set of fracture parameters C_1, C_2 and C_3, that could predict very well the fracture characteristics of the material within the fracture data range but predicted premature fracture for high triaxiality specimens and unstable crack propagation in areas with pre-existing cracks. This effect was not observed in experimental findings for Single Edged Notched Specimen subjected to Tension with pre-existing fatigue cracks at the notch edge. The round specimen fracture results provided the correct information for the fracture surface extrapolation to higher constrain states. The error minimization technique developed at ICL was

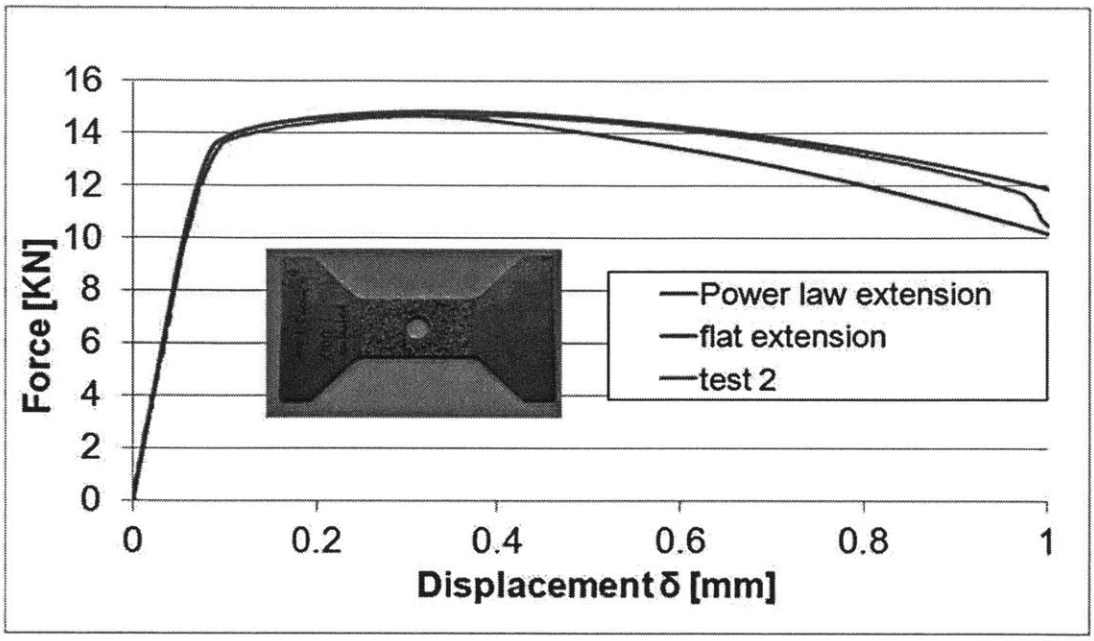

Figure 4-38: Comparison of experimental and numerical results for the central hole specimen made of API X100.

used to calculate the best values of the fracture constants developed by Dr. Luo and subsequently used at ICL. The minimization technique takes the following form

$$[C_1, C_2, C_3] = \min_{C_1,C_2,C_3} (\sum_{i=1}^{N} (1 - D(\eta, \overline{\theta}, \overline{\epsilon}_f))^2) \tag{4.26}$$

where D is the damage factor defined in the theoretical part. This problem is highly non-linear and sensitive to the initiation values of the fracture parameters. In order to improve this method, a Monte-Carlo component was added by the author in order to determine the global error minimum in a cube of $C_1 \in [0, 1]$, $C_2 \in [300, 800]$ and $C_3 \in [0.7, 1.1]$. The resulting material description for fracture was proven capable of addressing application in the range of high stress triaxiality.

In the case of plane stress specimens, finite element models assuming elastic and plastic material behavior were developed to determine the fracture strain, $\overline{\epsilon}_f$, by matching the calculated maximum strain from the FEM, at the instance when the critical displacement, δ_{frac} was reached. In all cases, the fracture location was close

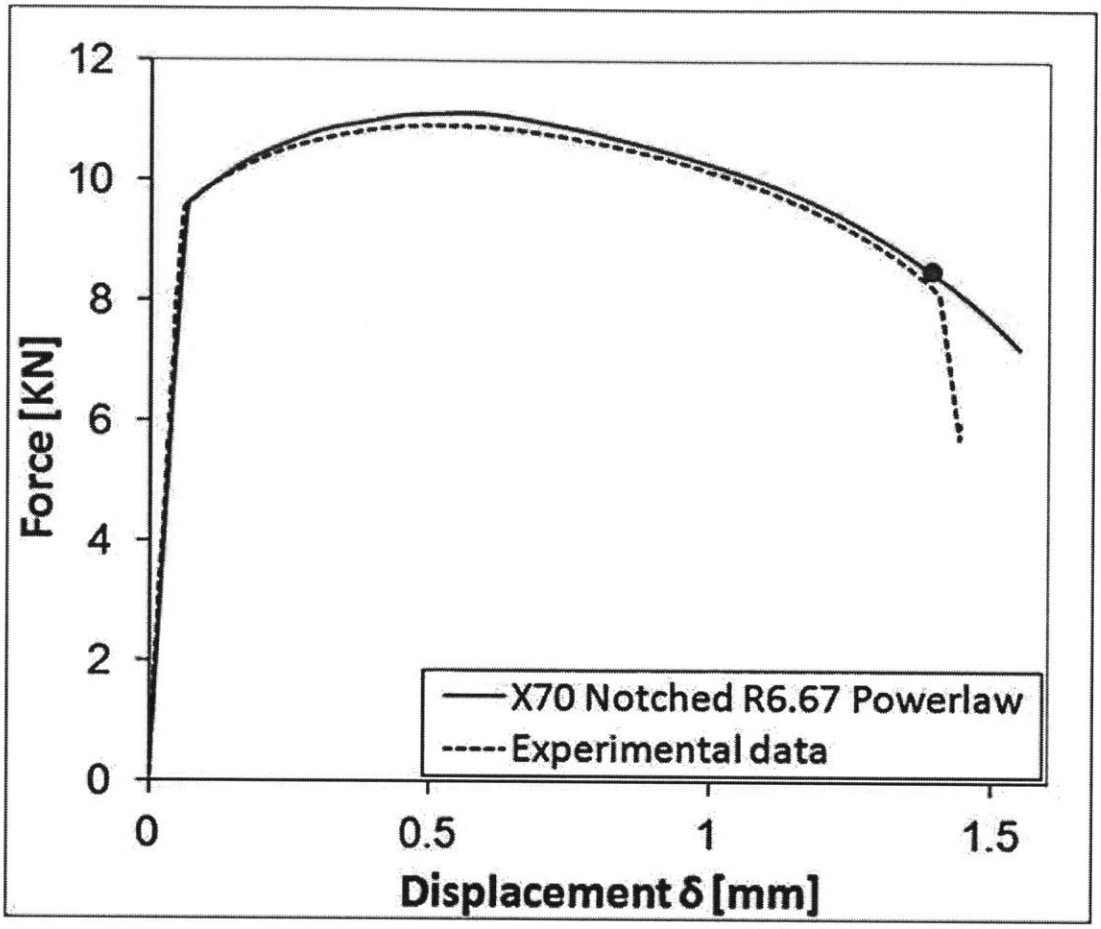

Figure 4-39: Comparison of experimental and numerical results for the central hole specimen made of API X70.

to the centre of the specimen except for the equi-biaxial punch test that the fracture occurred a bit further from the centre of the specimen for X100 that exhibited strong anisotropy (see Figs. 4-44 and 4-45).

The history of triaxiality and Lode angle with respect to plastic equivalent strain is presented in Figs. 4-46 and 4-50.

In most of integrity problems, pertinent to onshore and offshore pipeline systems and risers, exist initial cracks. Consequently, the calibration program was extended with the focus of representing, as close as possible, real world applications that undergo high constrains at the crack tip. SENT specimens have sharp notches followed by fatigue pre-cracks. This configuration gives rise to triaxiality parameter in the

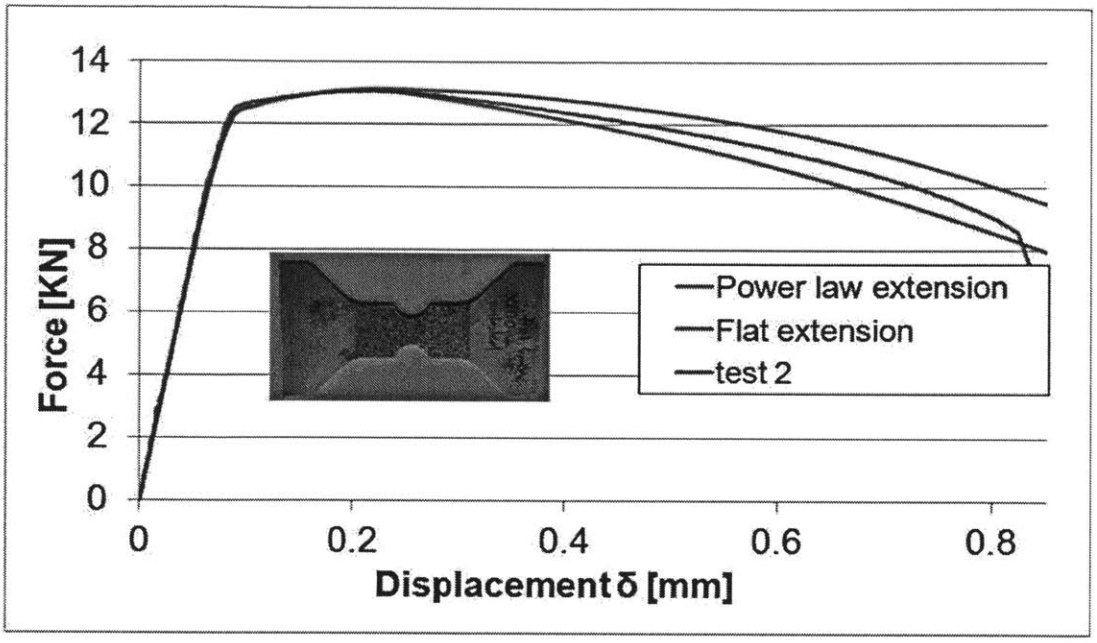

Figure 4-40: Comparison of experimental and numerical results for the central hole specimen made of API X100.

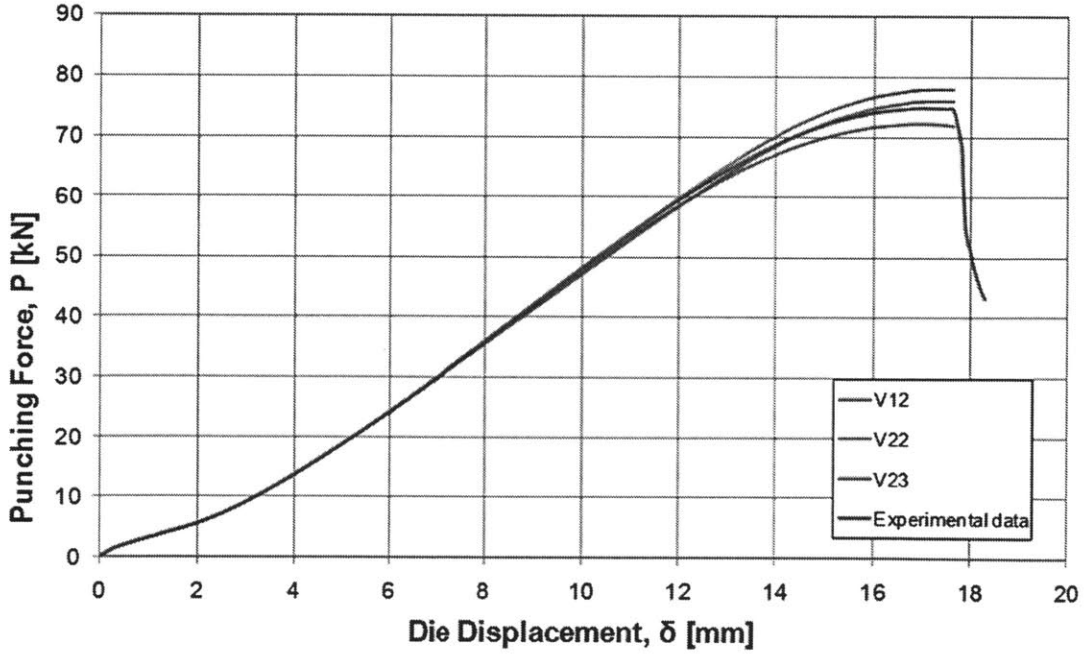

Figure 4-41: Comparison of experimental and numerical results for the punch specimen simulating bi-axial stress of state made of API X70.

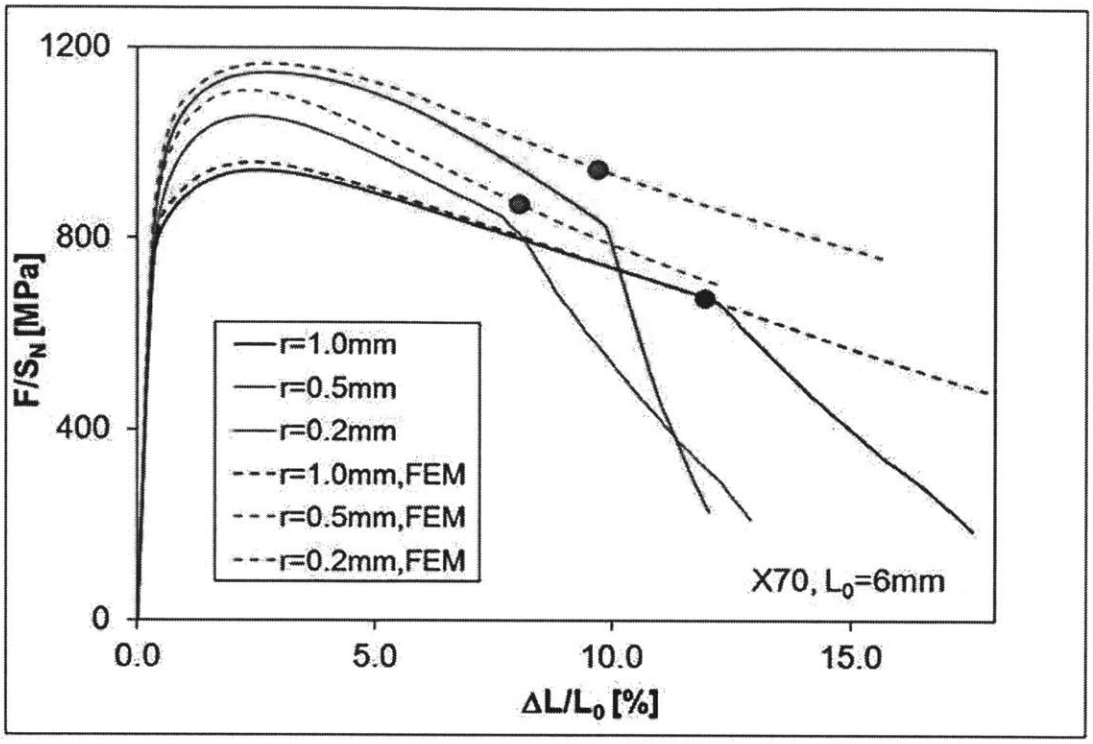

Figure 4-42: Comparison of experimental and numerical results for the round notched specimen, R=0.2, 0.5 and 1.0 simulating axi-symmetric conditions made of API X70.

range between one and two, which is much higher than the maximum achievable value of 2/3 for sheets. As it was mentioned previously, this extension included, the study of a new set of specimens (round notched specimens, Fig. 4-48).

In Figs. 4-49 and 4-50, the history of triaxiality and Lode angle with respect to plastic equivalent strain is shown.

The results of the fracture calibration are presented in Table 4.7. Using the calibrated plasticity and fracture parameters, the 3D fracture locus was constructed and is shown in Figs. 4-51 and 4-52. The results are also shown, in Table 4.7.

The red line corresponds to the plane stress condition, the yellow line corresponds to the axisymmetric condition and the black dots are the fracture data gathered from the calibration data. Flat specimens lie on the plane stress line, while the round notched specimens are on the axi-symmetric condition, = 1. It is important to note that none of the points lie exactly on the 3-D surface. The maximum error between

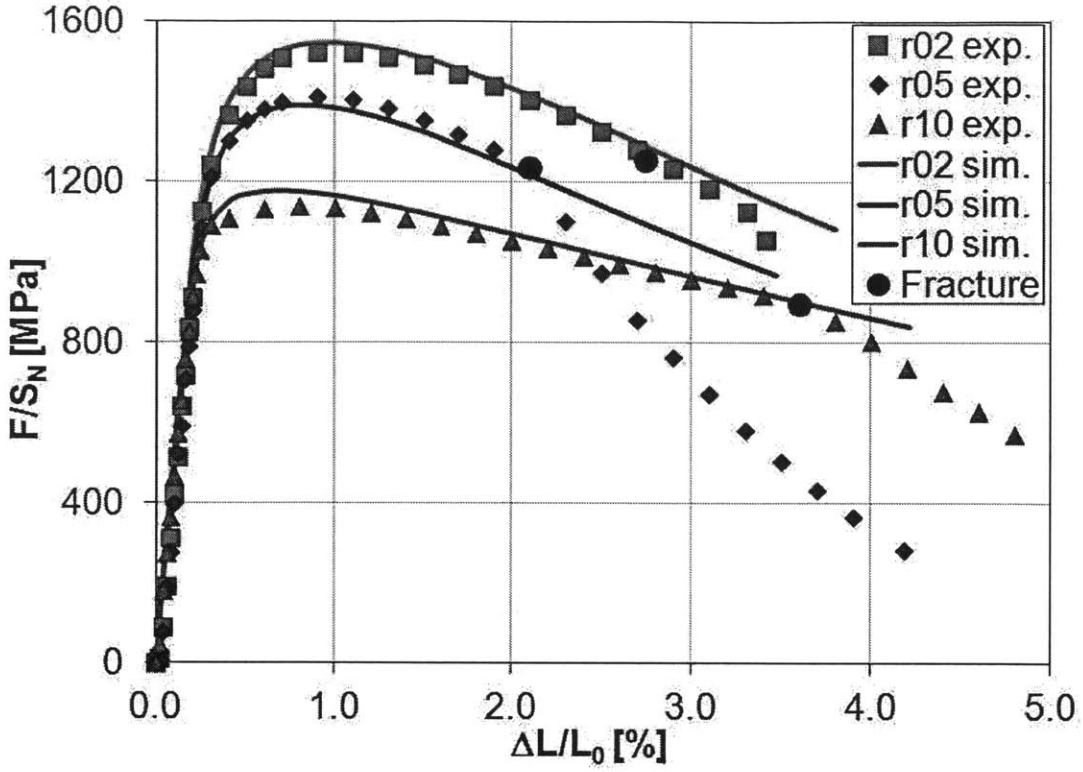

Figure 4-43: Comparison of experimental and numerical results for the round notched specimen, R=0.2, 0.5 and 1.0 simulating axi-symmetric conditions made of API X100.

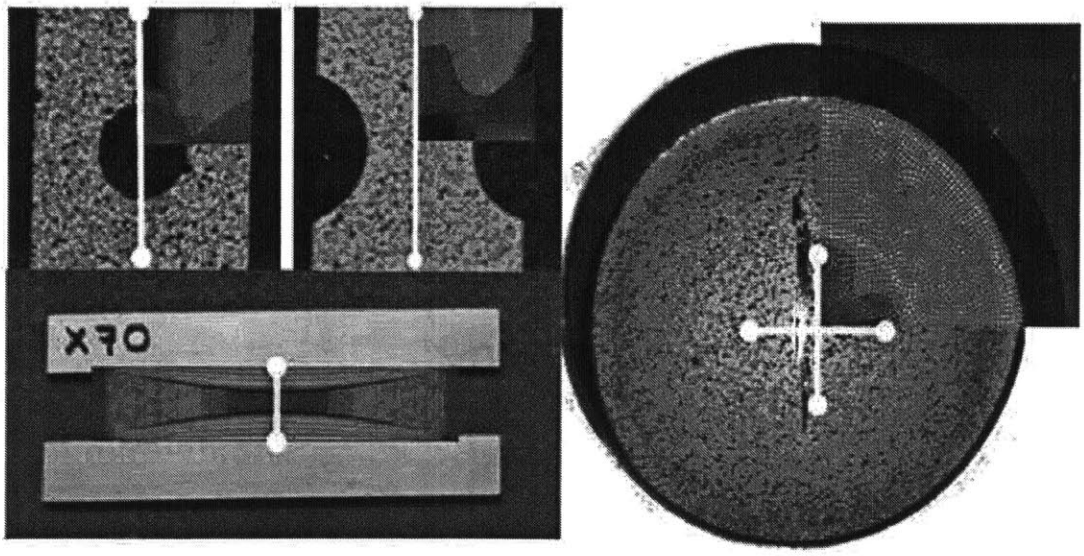

Figure 4-44: Experimental and numerical tested specimens for API X70.

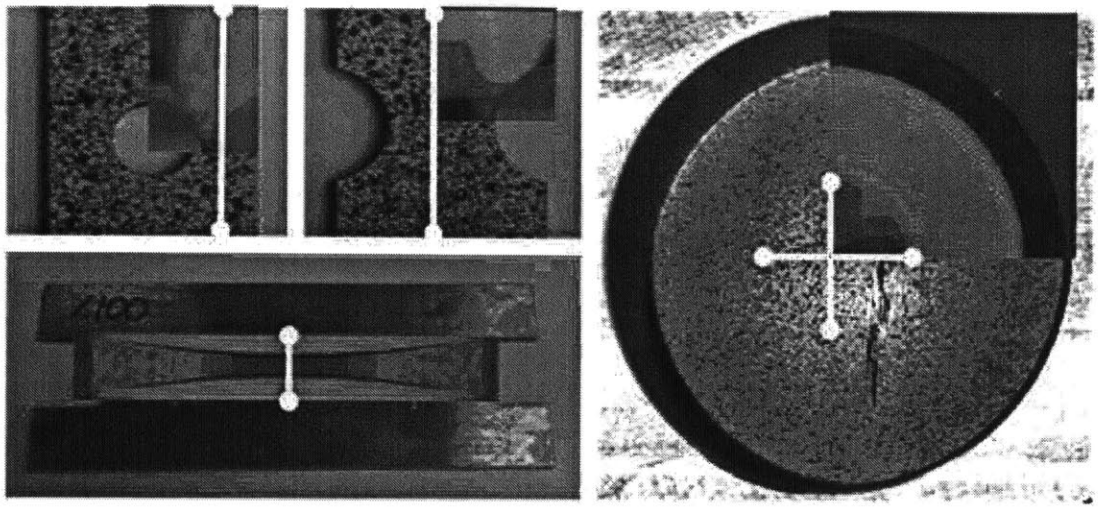

Figure 4-45: Experimental and numerical tested specimens for API X100.

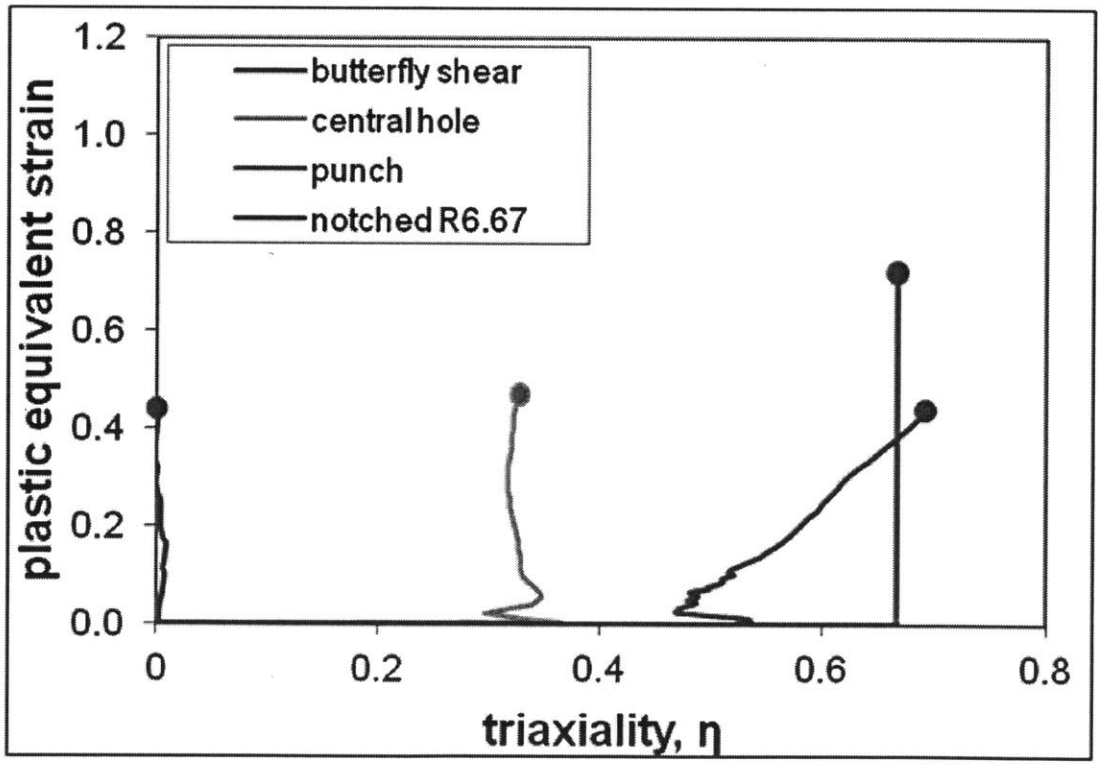

Figure 4-46: History of stress triaxiality as a function of equivalent strain at the location of failure initiation for X70 from numerical simulations of flat tests (strain shown in percentages).

the analytical fracture surface and the experimental data was 5%.

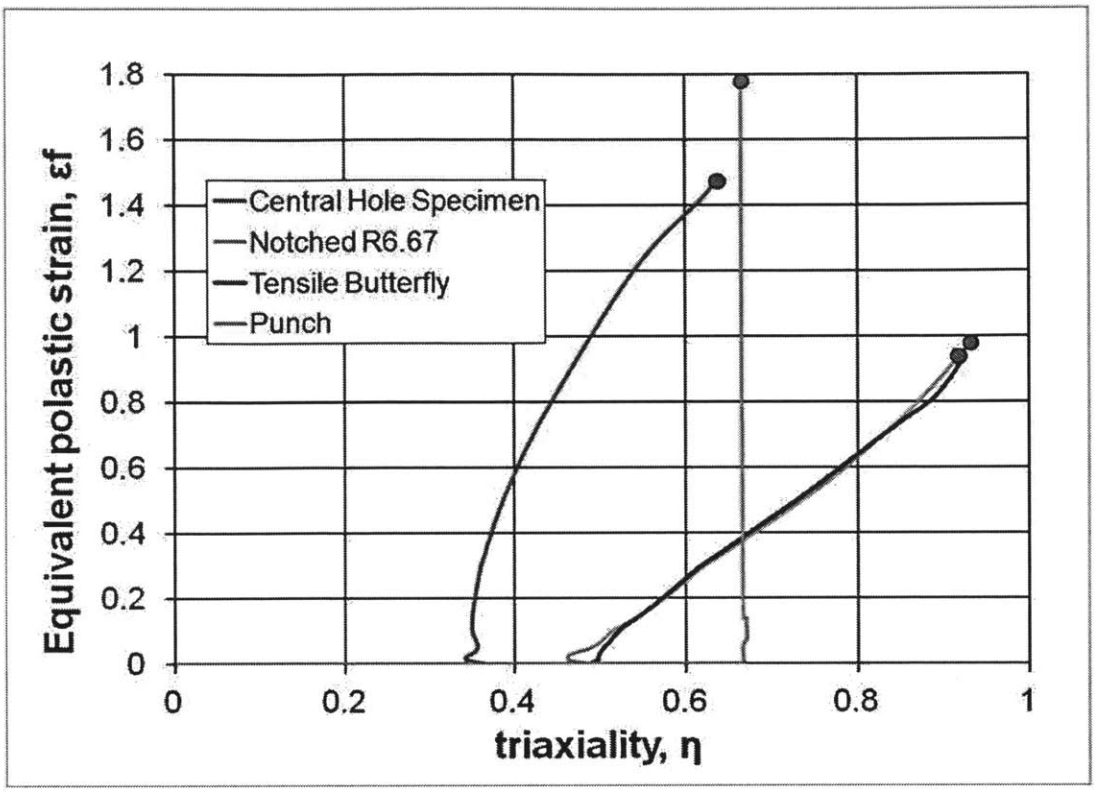

Figure 4-47: History of stress triaxiality as a function of equivalent strain at the location of failure initiation for X100 from numerical simulations of flat tests (strain shown in percentages).

4.3.3 Sensitivity analysis

After calibrating the plasticity and fracture parameters, a sensitivity analysis was conducted with respect to the normalized mesh size, $\Delta x/t$ and the hardening exponent, n on the example of the flat tensile central hole specimen tests. This analysis was conducted in two steps. In the first step, two real materials (TRIP780 and API X70) were chosen to represent, respectively, the high ($n = 0.204$) and low ($n = 0.098$) hardening exponent cases. The FE models of the central hole speciments were run for five different mesh sizes (0.075, 0.15, 0.3 and 0.6mm) while monitoring the key parameters in the fracture initiation location. The results are summarized in Fig. 4-53. It was found that there is almost no dependence of the mesh size on the triaxiality and Lode angle for both materials. That was expected because both of the above

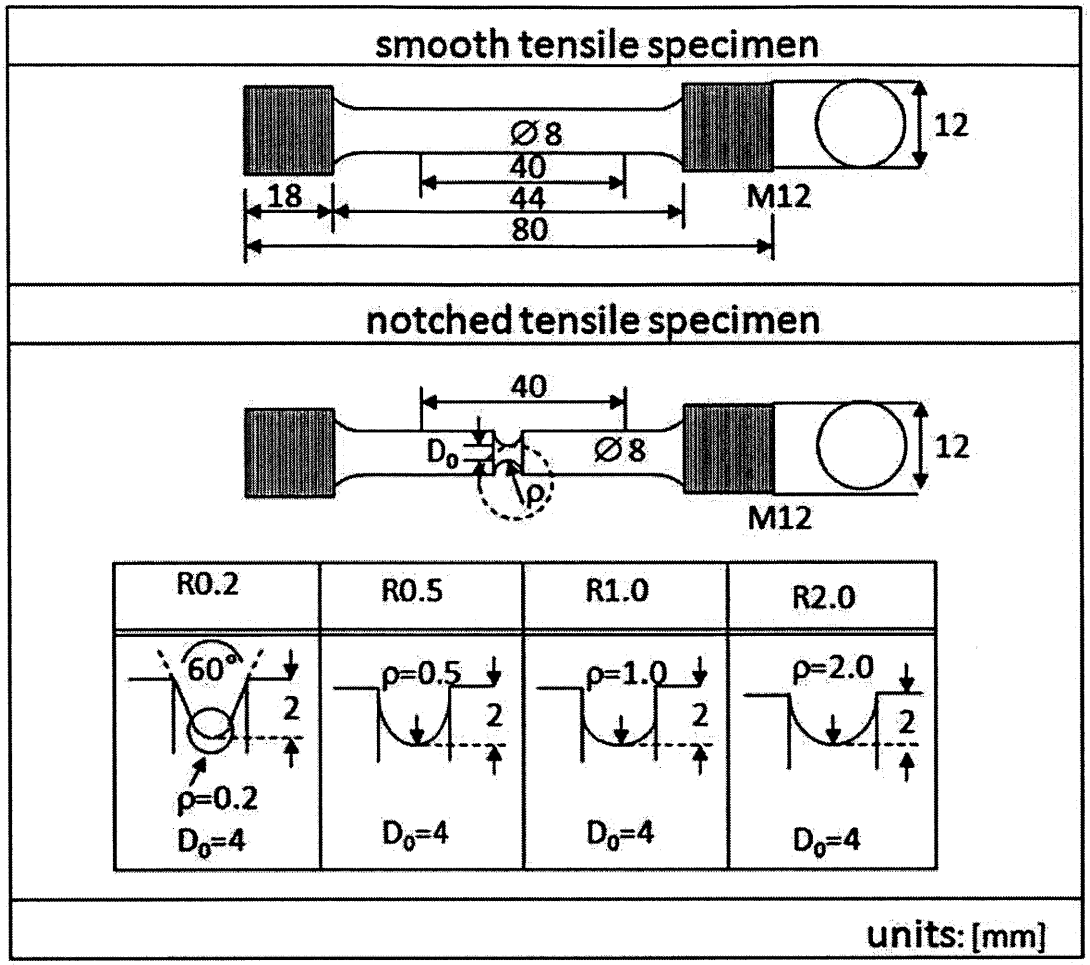

Figure 4-48: Geometry of additional round X70 and X100 specimens.

parameters are ratios of stress invariants. The numerators and denominators of the respective parameters change with mesh size, however, the ratios remain unchanged. At the same time, the plastic equivalent strain is affected by the mesh size. The degree to which it is affected, depends on the amount of hardening. For relatively high values of n, the mesh size effect is weak as shown by blue hollow diamonds in Fig 4-53. Such weak dependence with respect to the mesh size was reported for example by [26] for TRIP780.

Mesh Size Dependence: As an example of the mesh size dependence, API X70, which has much lower hardening than other metals studied at ICL will be used to explore this effect. It was found that there is a considerable mesh dependence on

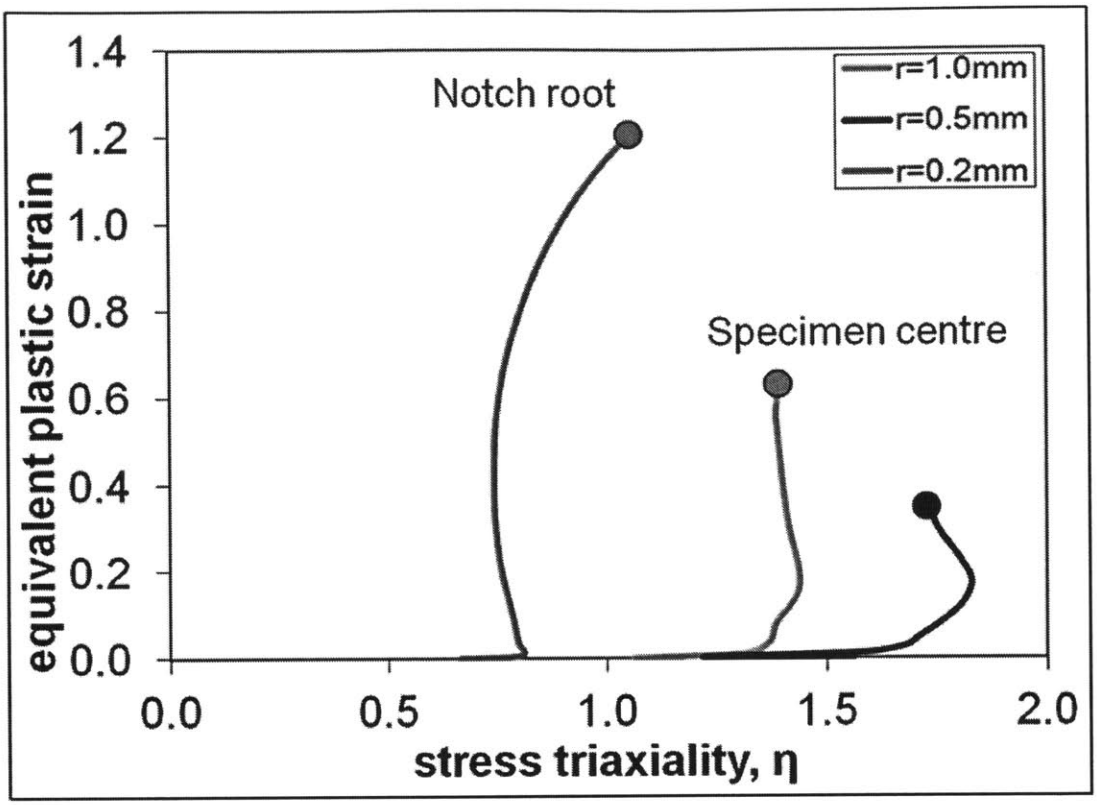

Figure 4-49: History of stress triaxiality as a function of equivalent strain at the location of failure initiation for X70 from numerical simulations of round tests (strain shown in percentages).

the equivalent plastic strain, which must be taken into account in calibration and applications simulations. This effect is even more severe in the case of X100.

This effect was found to be interrelated with the hardening exponent dependence. This effect was further studied in the second step of the sensitivity analysis. Five different values of the hardening exponent (n = 0.01, 0.05, 0.0984, 0.15 and 0.2) were considered for the mesh size of 0.1mm that was used for the fracture parameter calibration in the present paper. All other characteristics were kept the same as for API X70 (e.g. δ_{frac} and A). Therefore, these five materials can be considered as hypothetical variations of X70.

Hardening exponent dependence: The sensitivity analysis showed that the plastic equivalent strain was also affected by the hardening parameter, n. It was also found that the power law exponent influences the mesh size dependence. In Fig. 24,

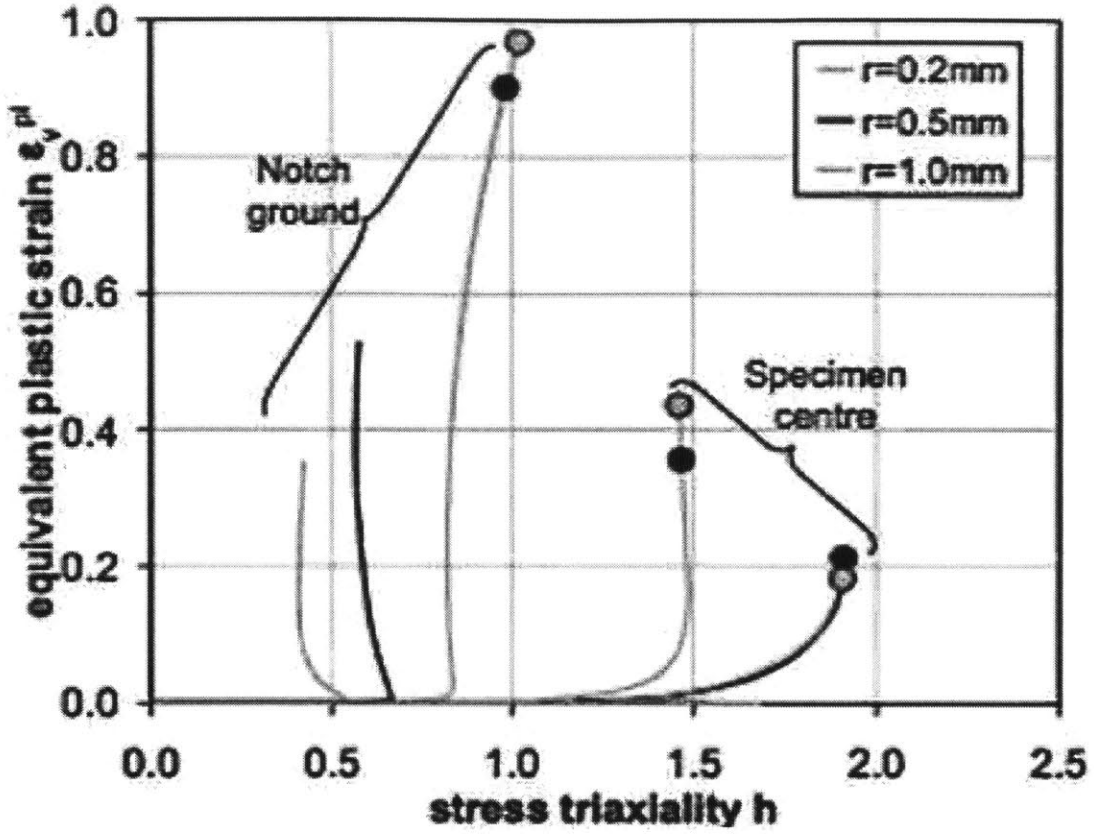

Figure 4-50: History of stress triaxiality as a function of equivalent strain at the location of failure initiation for X100 from numerical simulations of round tests (strain shown in percentages).

the blue bars represent the cumulative percentage of decrease of equivalent strain with respect to the equivalent fracture strain corresponding to the lowest considered hardening exponent ($n = 0.01$). The trend is increasing with n. The red bar shows the percentage change of between two concecutive hardening exponents, see Fig. 24. It is shown that the mesh size effect for exhibits a very interesting nonlinear relation, not previously reported in the literature. Mesh size dependence initially increases up and then decreases. The history of η and $\overline{\theta}$ remained unaffected as the power law exponent changed. The plastic equivalent strain, $\overline{\epsilon}_f$ however, was affected.

Another important question is if the profile of the local neck is affected by the hardening parameter. This can be measured for specimens made of actual material, like API X70. For hypothetical materials only numerical results are available. The

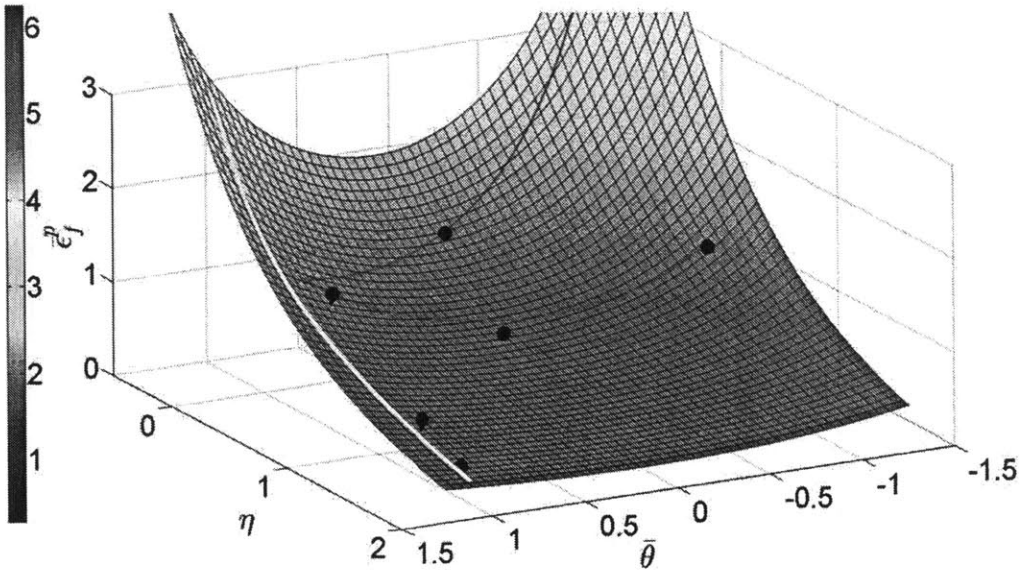

Figure 4-51: 3D Fracture locus for X70

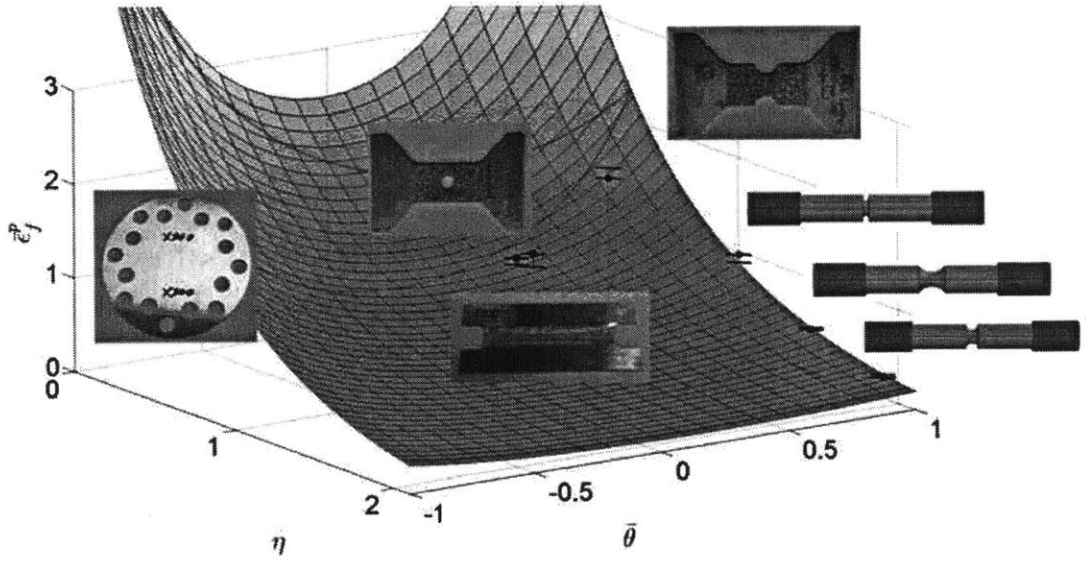

Figure 4-52: 3D Fracture locus for X100

answer to this question is positive, as shown in Fig. 4-54. The same figure proves that the present simulation predicted accurately the final shape of the neck at the point of fracture. Experimental results for X70 is seen to match well with numerical

Table 4.7: Fracture constant for X70 and X100.

.	X70	X100
C_1	0.05	0.029
C_2 [MPa]	454	535
C_3	0.91	0.9

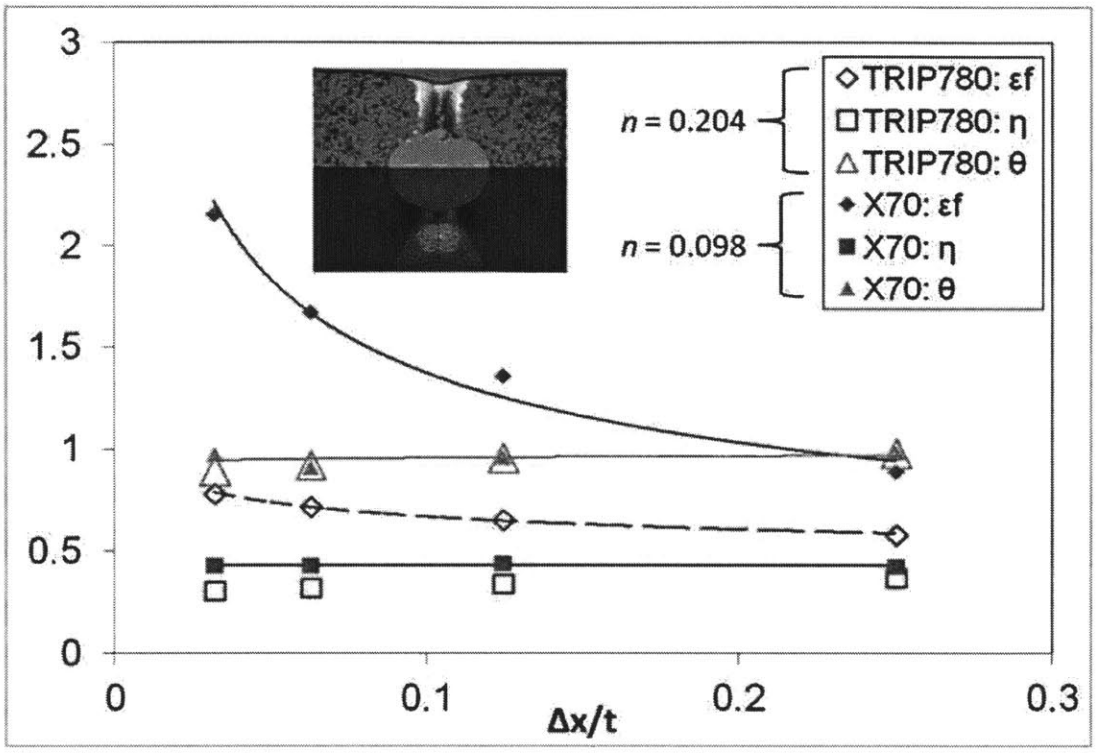

Figure 4-53: Difference in mesh-size dependence on plastic equivalent strain to fracture, η and $\overline{\theta}$ between API X70 and TRIP780.

simulation data for correct hardening exponent ($n = 0.098$) and a mesh size of $0.1mm$.

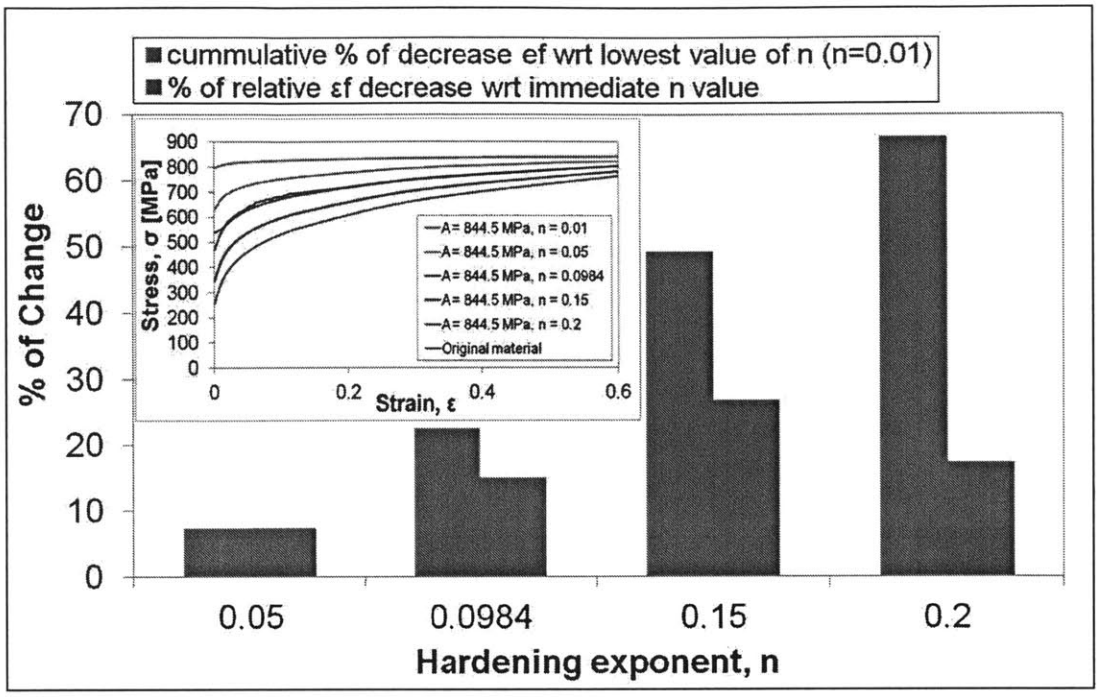

Figure 4-54: Five hypothetical materials with different values for the hardening exponent.

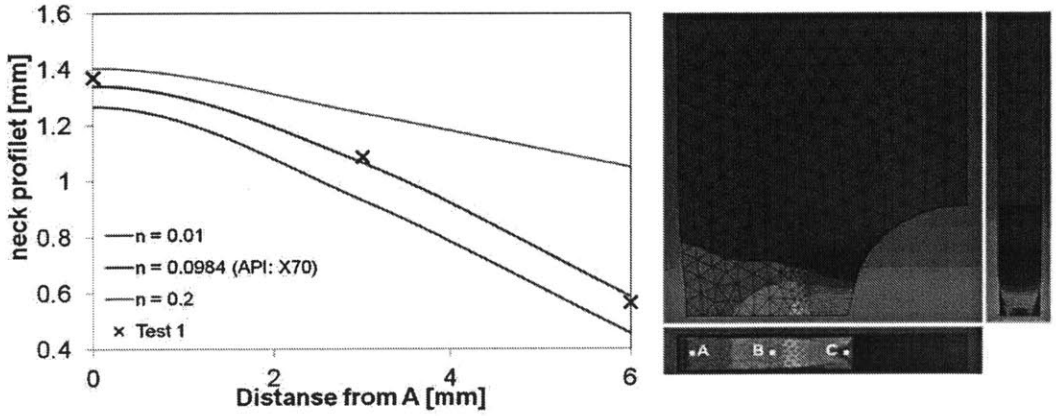

Figure 4-55: Dependence of hardening exponent on thickness to fracture for API X70 and two additional material variations, $n = 0.01$ and $n = 0.2$.

Chapter 5

Validation of Novel Approach of Structural Integrity on Pipelines and Risers

5.1 Fracture resistance prediction of SENT specimens

The objective of the proposed two-year study is to apply the new fracture technology developed at MIT for a class of Advanced High Strength Steels to new type of steels entering the Oil and Gas industry market. This technology departs radically from the traditional one-parameter characterization of material fracture (such as fracture toughness, or CTOA). It introduces a new three-parameter fracture model where fracture initiation and propagation is controlled by the accumulated plastic strain coupled with normalized hydrostatic pressure (stress tri-axiality) as well as with the measure of deviatoric stress (LODE angle). Presently, there is enough experimental evidences that reliable fracture prediction should include those two important parameters.

To make the best use of the capabilities of each team member, it was decided to study the equivalence of both technologies on an examples of Single Edge Notched Tensile test and Single Edge Notched Bending tests. The work on SENT is done

in collaboration with Dr. Nonn, while the SENB project is conducted jointly with Dr. Walters. Dr. Walters presented preliminary results of the above comparison in the recent OMAE in Rotterdam on the example on Weldox steel. We chose X70 as the baseline material wanting to accommodate our sponsor (Shell IRD, Deep Water Novel Development Systems) particular interest. The result of tests and numerical tests and numerical simulation of SENT and SENB tests will first be presented at the October meeting at MIT and the published in the Journal of Engineering Fracture Mechanics.

The final benchmarking of the MIT technology will be completed using a full scale test taken from the open literature. The difficulty in doing this is that the bursting tests available in the open literature were conducted for a similar (X65) but not exactly the same grade of steel, studied at ICL (X70). Despite this inconsistency, we will proceed with this task during the 2012 research.

The SENT and SENB specimens were extracted in the longitudinal direction from Shell pipe segments at the MIT Central Machine Shop. Eight SENT specimens were cut and sent to Germany and three SENB specimens were sent to TNO. Three SENT tests have already been conducted. The first one failed at the welded grips and therefore it was discarded. That event was a big disappointment and delayed the preliminary comparative study to be completed during Kirki summer internship. Partial results from the remaining two tests in the form of load versus clip-gage displacement were received by MIT in mid August. We are still waiting to get the load versus the crosshead displacement to use for comparison with our in house simulation results.

5.1.1 Introduction

The determination of the exact mechanical properties of material is essential for an optimal and safe design of linepipes. It is especially important for the prevention of over-engineering and the reliable assessment of complex accidental loading, such as extreme bending due to loss of buoyancy of support, or abrupt ground movement. Currently, the focus of research in offshore deepwater installations and linepipes is

towards pre-cracked structures with high triaxiality stress states and complex loading histories. At the same time, low triaxiality stress states must be correctly studied in order to represent shear dominated failure in pipes. A comprehensive experimental and numerical program was undertaken to determine the mechanical properties of the traditional API X70 grade of steel. The material was characterized for anisotropic plasticity, fracture initiation and uncracked ductility for various states of stress. The same material was also used for pre-cracked fracture toughness assessment. The experimental program included flat and round specimens. The first type of tests on flat butterfly-shaped, central hole, notched and circular disk specimens; were selected to address the low stress triaxiality range. Tests on round notched bar specimens and SENT fracture mechanics tests extended the characterization and verification process to higher stress triaxiality values. This program covered a wide range of stress conditions and demonstrated their effect on the material resistance to crack extension. Each test conducted was numerically simulated using solid finite element models, matching the exact geometric and loading history features. The numerical simulation provided information on the local stress and strain fields around the location of the potential or existing cracks. Based on the above hybrid experimental/numerical technique tailored for pipe applications, the MMC fracture model was calibrated. The model relates the material ductility not only to stress triaxiality but also to the Lode parameter. The predictive capabilities of the MMC were then evaluated in the case of SENT testing, used extensively in the pipeline industry. It was shown that the present fracture model calibration from uncracked specimens can predict with great accuracy all the features of the pre-cracked SENT experiments. One can conclude that, the MMC model has great potential as a practical tool in pipeline design.

5.1.2 Crack Driving Force and R-curves

Since the experimental determination of the R-curve for full-scale tests can be very time- and cost-intensive, especially in the view of parametric studies for different pipeline geometry, numerous computational fracture models have been developed within finite element framework aiming to characterize ductile fracture propagation

of steel materials for small and full-scale tests. There are two groups of models, fracture mechanics and damage mechanics based models. Typical example for the former is the mapping approach which interpolates ductile tearing between results of several simulations with fixed but different crack sizes [10]. There are several major limitations of the fracture toughness approach. First, it requires the presence of initial cracks and it will not work to predict initiation of fracture in crack-free bodies. Secondly, it only provides information of initial crack growth, thus falls short of predicting post-failure behavior of a given component all the way to a complete separation. Third, no constraint effect is considered explicitly, but has to be included via constraint normalized R-curve. Fourth, no direction of the crack propagation including crack path deviation can be predicted without a user-defined criterion. Finally and most importantly, the approach is restricted to the stress states at the crack tip generating merely Mode I fracture. By contrast, damage mechanics theory is able to describe crack initiation and propagation by allowing the damage evolution to take into account both the influence of local stress and strain variables. Hence, ductile crack propagation can be fully represented within a single simulation. One of these models is Gurson-Tvergaard-Needleman model [11], [12]; and [13] and its subsequent modifications. The GTN model and its extensions have removed all above mentioned limitation of the fracture mechanics based models but introduced several new issues. The micromechanics-based GTN model describes the failure mechanism as a sequence of void nucleation, growth and coalescence. Recent modifications of GTN, e.g. to account for shear-stress dominated fracture [14]; [15]; [16], lead to an increase of the additional phenomenological parameters and therefore lost its original appeal. The number of free parameters of the shear modified GTN model has increased to 13 from the original 7 in the GTN model. This creates difficulties in the calibration procedure which should be an integral part of all fracture modeling. Several disposable parameters in the GTN model are responsible for the coupling of fracture with plasticity. Recently [17] showed that this large set of parameters is not necessary for achieving a good correlation in the plastic and fracture range for low triaxiality levels. Another finding was that the GTN model and its derivative cannot

predict fracture in the combined regime of shear and compression loading. The next step in the development of fracture technology is the Modified Mohr-Coulomb model. This is a phenomenological but physics-inspired model. It requires the calibration of three free parameters and it is applicable to the whole spectrum of stress states from tension and tension/shear to pure shear, all the way to shear and compression. The two parameters are defining the classical Mohr-Coulomb fracture model and the third parameter is responsible for the local shape of the yield condition, introduced by [18]. It was successfully applied for the prediction of ductile fracture initiation and propagation in advanced high-strength sheet and low-strength aluminum materials [19]. This extended model describes the equivalent strain to fracture depending on stress triaxiality and Lode angle that is the normalized third invariant of deviatoric stress tensor. To derive the three-dimensional fracture locus, it is necessary to calibrate only three model parameters by at least the same number of experiments. The suitability of the MMC model to characterize ductile fracture has been demonstrated in many publications, primary for the ranges of low stress triaxiality ($< 2/3$) see (e.g. [24], [41]). On the other hand, there is little information about the accuracy of the model prediction for the high triaxiality range, ¿ 1.0, which is very important for analysis of cracked structures. Recent results on the case on API X100 was given in [20] validated by compact specimen experimental and numerical results. The present section is extending the applicability of the MMC model to the range of high stress triaxiality. This is the area so far dominated almost exclusively by the fracture toughness method and the GTN approach. After the brief description of the MMC model, a comprehensive experimental program is described to characterize anisotropic plasticity and fracture in the wide range of stress triaxiality 0¿¿2. The FE models of all six types of fracture specimens are developed and the model identifications are performed using the hybrid experimental/computational method using a weighted average optimization method to calculate the fracture parameters. Finally, the calibrated model is used to predict fracture initiation and propagation on SENT tests with very good accuracy. In order to make a convincing case to the O&G industry, all specimens were cut from offshore pipes made of API X70 grade

steel. The major benefit of using the MMC model is the capability to predict failure in both crack-free and pre-cracked bodies and the detailed evolution of crack surface for both initiation and propagation. Using the above physics-based model, fracture in a wide range of loading conditions including shear can be predicted with a good accuracy.

Usually in the framework of classical fracture mechanics, fracture toughness tests on Compact Tension and Single Edge Notched Bend specimens are used to measure crack extension resistance. In the area of pipelines, there exist recommended practices that resulted from the Fracture Control Joint Industrial Project [JIP]. The suggested geometry of the compact specimens selected for the toughness evaluation differs from one practice to another. In the case of pipelines, Single Edge Notch Tension and Bending specimens are commonly used to estimate their fracture resistance. In [27] and [28] the experimental process is presented along with a suitable calculation process that is customized for thick structures. The experimental resistance curves will be used to verify the SENT results. The SENT specimens are thought to be more suitable to measure fracture toughness properties of pipes that are exposed to bending, tensile or pressure loading.

5.1.3 Problem Description and Numerical Model

Usually in the framework of classical fracture mechanics, fracture toughness tests on CT and SENB specimens are used to measure crack extension resistance. In the area of pipelines, there exist recommended practices that resulted from the Fracture Control Joint Industrial Project. The suggested geometry of the compact specimens selected for the toughness evaluation differs from one practice to another. In the case of pipelines, SENT and SENB specimens are commonly used to estimate their fracture resistance. In [30] the experimental process is presented along with a suitable calculation process that is customized for thick structures. The experimental resistance curves will be used to verify the SENT results. The SENT specimens are thought to be more suitable to measure fracture toughness properties of pipes that are exposed to bending, tensile or pressure loading.

SENT API X70

The geometry of the X70 SENT specimen was defined by its width $W = 24mm$, thickness $B = 24$ mm and the length of the gauge section $L = 200mm$. The initial length of the pre-existing crack is $a = 12mm$ $(a/W = 0.5)$.The tensile load P was applied monotonically through a pair of pins (see Fig. 3-3).

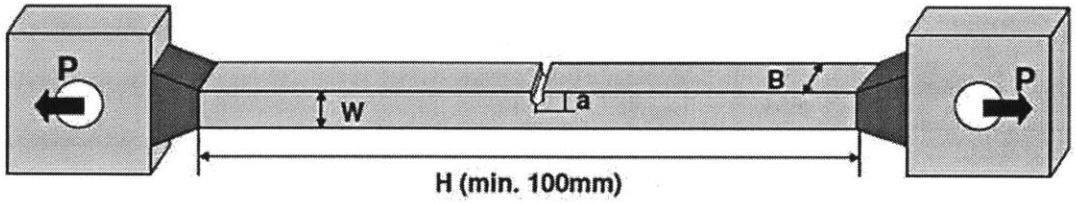

Figure 5-1: SENT specimen sketch with pin loading applied at the ends of the specimens.

The six tests on the pin-loaded SENT specimens were performed on API X70 at SZMF for the assessment of the applicability of the MMC model as a predictive tool of the fracture behavior of pipe materials in accordance with [30] for the determination of the crack extension resistance. Specimens were loaded monotonically to six different loading levels and then fully unloaded. Subsequently, the specimens were broken using liquid nitrogen to measure different crack extensions, Δa. Two clip opening displacements have been recorded continuously during testing by using clip-gauges mounted at 1.5mm (COD1) and 16.9mm (COD2) distance with respect to the specimen surface. Typically, the evaluation of the ductile fracture resistance of SENT specimens is conducted to determine the toughness values in terms of CTOD or J-integral versus Δa.

The FE analysis of the SENT specimen was conducted using three mesh sizes of 0.15, 0.3 and 0.6 mm for the near-the-notch area. The far-field mesh was much coarser to reduce computational time. Usually the same mesh size is used in both the calibration process and the application to eliminate mesh-size effect. Regardless of that, a mesh size study to verify these choices will be presented in the next section. One quarter of the actual specimen is modeled. Symmetry boundary conditions are used for the through-thickness (z-axis) and along-the-length (x-axis) directions. The

crack front is therefore forced to be flat with respect to the ZY-symmetry plane. The same frictionless loading conditions are implemented in the FE model. The frictionless pin is rigidly moved horizontally (Fig. 5-1) forcing the sharp crack at the symmetry plane to run through the thickness and the width in a practically Mode I failure. In the crack propagation area, a small amount of bending, induced by the machined notch and the pre-crack is superimposed on predominantly tensile deformations. One of the major features of the experiment is the tilting effect with respect to the longitudinal axis of the specimen. The tilting phenomenon was well represented in the FE simulation by applying the correct boundary conditions. The numerical simulation also verified the presence of a tunneling behavior. Because of the tunneling effect, a distinction should be made between the average (Δa_{ave}) and the maximum (Δa_{max}) crack extension. The Δa_{max} is defined at the middle of the width of the specimen while the Δa_{ave} is the averaged crack extension for a rectangular cracked area that has the same area as the actual cross-sectional crack propagation area, i.e. $A_{real} = A_{rectangular}$. Denoting the current shape of the advancing crack front by $\Delta a(y) = \Delta a_{max} \cdot f(y)$. The average crack extension is defined by Eq. (5.1).

$$\Delta a_{ave} = \frac{\Delta a_{max}}{b} \int_{-b/2}^{+b/2} f(y)\,\mathrm{d}y \tag{5.1}$$

where $f(y)$ is the normalized shape of the crack front with respect to the maximum crack extension, α and the breadth b and y is the direction of the crack propagation.

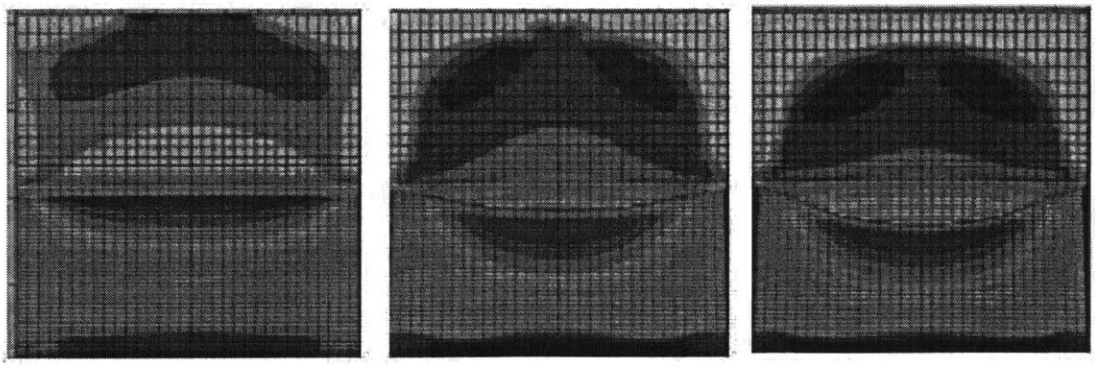

Figure 5-2: Time evolution of cracked surface normalized with respect to the Δ_{max} for time step 9 (left), $ts = 19$ (middle) and $ts = 23$ (right).

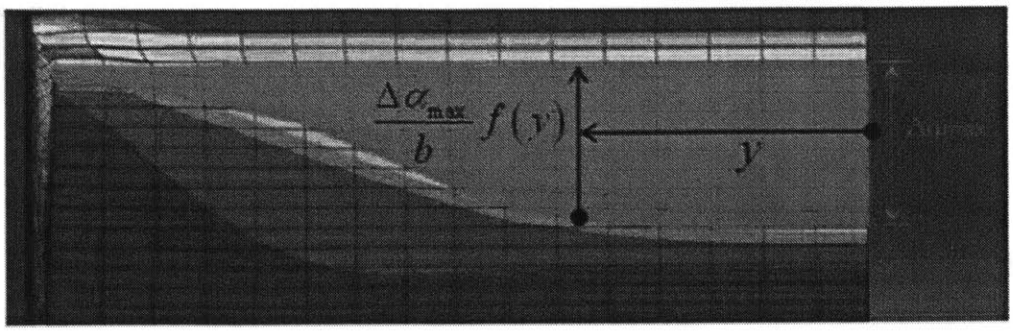

Figure 5-3: Sketch demonstration of Δ_{max} and Δ_{ave} for the time step ts = 23.

The time variable takes values from ts = 0, which corresponds to the unloaded/undeformed state, to ts = 100, which corresponds to the final displacement of the pins. At the initial state of failure, the fractured area emulates a rectangular area, $\Delta\alpha_{max} = \Delta\alpha_{ave}$ (Fig. 5-2). However, in the later stages of failure the fractured area is described better by a parabolic shape. $\Delta\alpha_{max} = \Delta\alpha_{ave}$ up to $ts = 15$ but they deviate significantly after that point. The history of stress triaxiality is monitored at the root of the crack. The values of the triaxiality are in the range of 1 to 2.2.

SENT API X100

For the case of API X100 eight tests on the pin-loaded SENT specimens were performed at SZMF as a validation of the applicability of the MMC model to describe fracture behavior of pipe materials. The SENT specimens are thought to be more suitable to measure fracture toughness properties of pipes that are exposed to bending, tensile or pressure loading. Compared to SENB specimens SENT specimens are able to represent the constraint that is actually observed in the pipe more realistically. Furthermore, the observed load in the pipe can better be described in a small scale test by a tensile load than by a bending load.

The test follows a procedure for determining the R-curve, using multiple specimen method in accordance with [30], in which the specimens are loaded monotonically to various loading levels and then fully unloaded after reaching different amounts of stable crack growth. Thereafter, the specimens are broken by using liquid nitrogen to measure different crack extensions Δa. The geometry of the tested specimens is

defined by the length of $L = 200mm$ without welded grips and the square cross-section of WxH is $13x13[mm^2]$ and $a/W = 0.5$. Two opening displacements have been recorded continuously during testing by using clip-gauges mounted at $1.5mm$ (COD1) and $16.9mm$ (COD2) heights with respect to the specimen surface.

The final initial crack size has been established by inserting the fatigue pre-crack of $2mm$. Typically, the evaluation of the ductile fracture resistance of SENT specimens is conducted to determine the toughness values in terms of CTOD or J-integral versus Δa. While the above relation has been established through the above tests, in this publication the main interest is in the comparison of measured and predicted force vs. COD as well as, COD versus Δa.

In the current study of X100, two FE models were developed with uniform mesh size of 0.3 and $1.5mm$ at the area of the sharp notch was used. In the present work, results from mesh size of 0.3 mm will be presented.

5.1.4 Resistance Curves and Fracture Surface Evolution

SENT API X70

The FE simulation predicted not only the pin force versus the crack opening displacement but also the evolution of the crack surface both quantitatively and qualitatively . The experimental crack growth is calculated using the British Standard [30]. The finite element results were compared to the experimental data for three different mesh sizes. The numerical simulation that includes the fracture information of the material follows the experimental results closely for the entire experimental procedure, as shown in Fig. 5-4.

SENT API X100

A study of the mesh size effect is a subject of current research and will be presented along with a detailed comparison in forthcoming publications.

As an outcome of the present simulation, the relationship between the calculated force on the SENT specimen were compared with the measured relationship. On

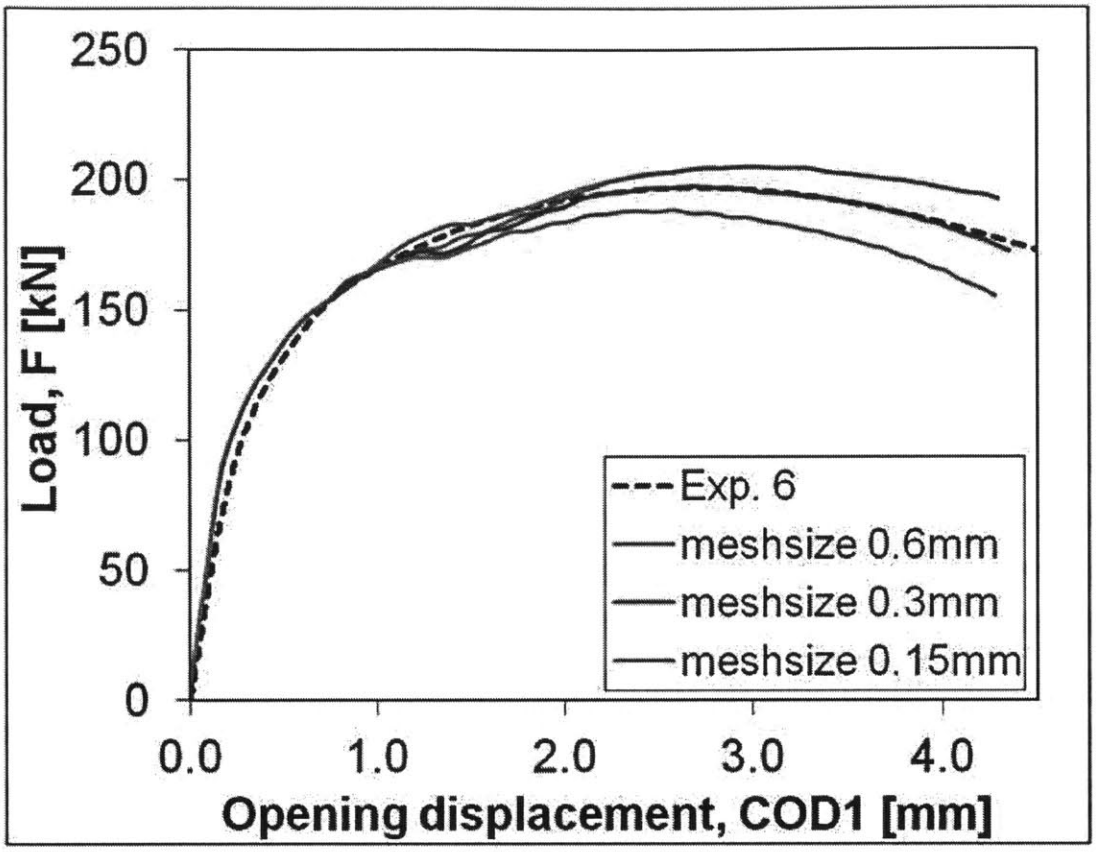

Figure 5-4: Comparison of FE results with experimental data predicting the initial crack growth rate.

same graph the FE prediction with the fracture option switched off is also shown.

The MMC Fracture model not only predicts the initiation and initial growth of the crack but also the propagation of the crack all the way to the back surface, until full separation occurs. The complete predicted load displacement curve is presented in Fig. 5-6, where several snapshots of crack extension are presented by inserts.

A pronounced tunneling effect is evident as a crack at the symmetry plane is propagating much faster than the edges of the free ends. The relationship between crack extension versus COD1 was also compiled from the numerical data and it is presented in Fig. 5-7. On the same figure superposed are points measured from the interrupted SENT tests.

The measured and predicted load displacement curve (Fig. 5-5) matches almost perfectly. Furthermore, the calculated crack extension is very close to the experi-

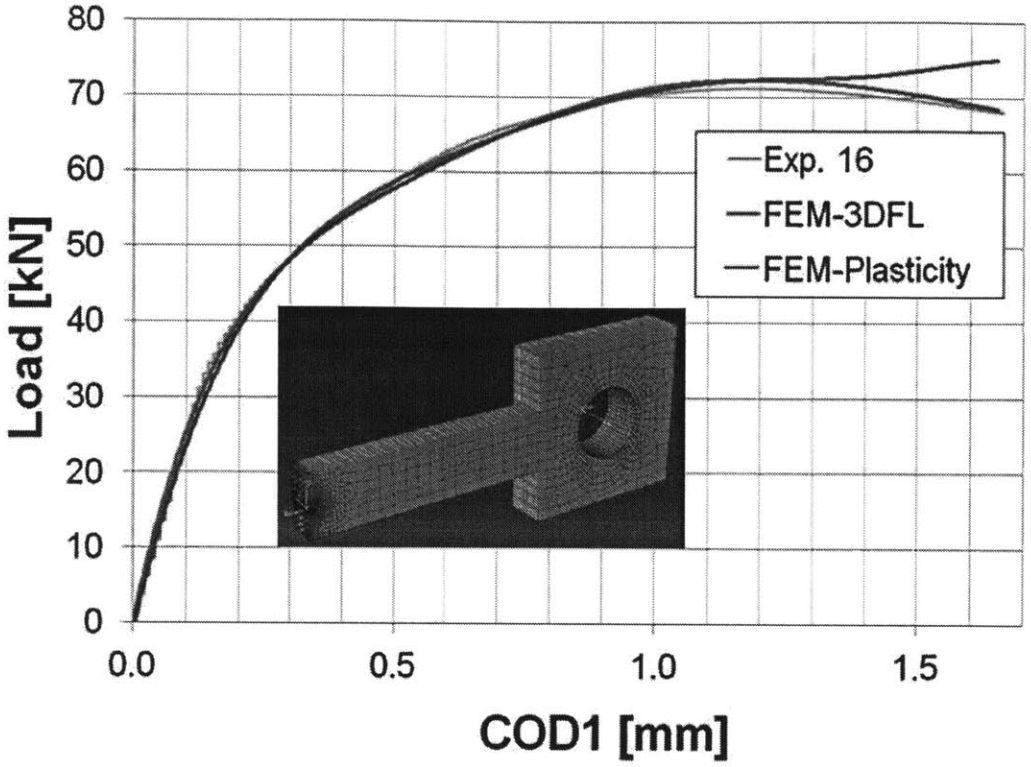

Figure 5-5: Initial crack growth of SENT specimens of API X100.

mental measurements, as evidenced in Fig. 5-7. Finally, the effect of tunneling is predicted correctly in terms of both magnitude and shape of fracture surface. The above FE results are very promising for the assessment of the crack resistance of various offshore and onshore structures.

5.1.5 SENT for the Prediction of Pipe Crack Resistance

As already addressed in the introduction, currently there are no suitable fracture/damage mechanics tools in the O&G industry which will allow for accurate and reliable prediction of the strain capacity and fracture resistance of pipelines subjected to complex loading scenarios. Even the widely used Gurson-Tvergaard-Needleman model despite the recent shear modification has proven not to be capable of capturing all constraint variations occurring in the pipelines, leading either to over-or under-conservative predictions. On the other hand, the accurate characterization of shear-type slant frac-

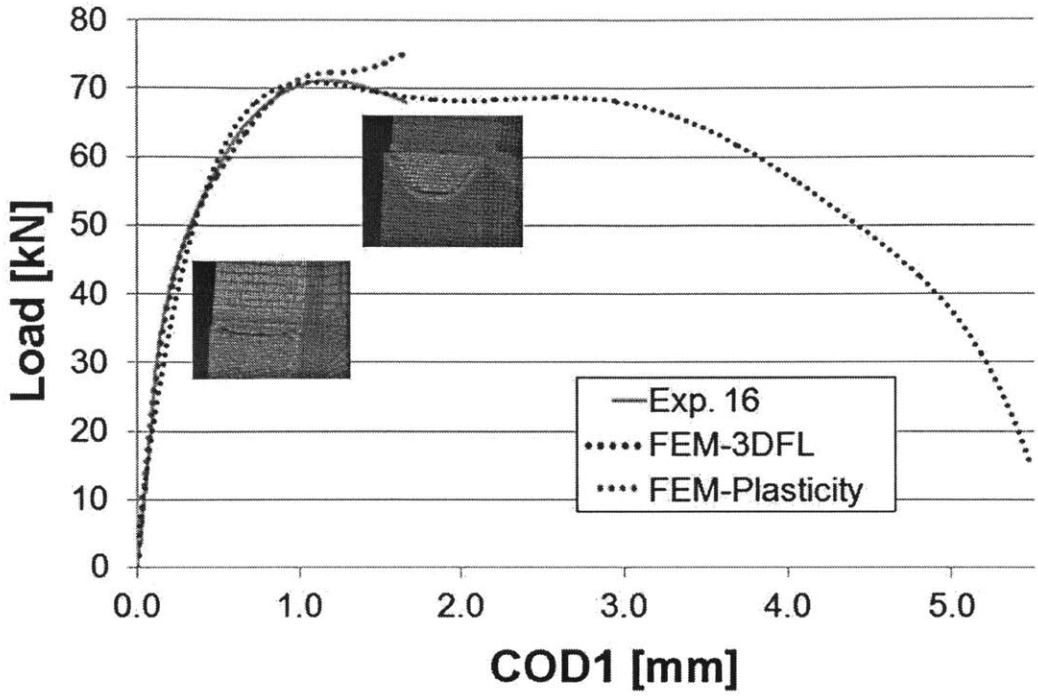

Figure 5-6: Predicted crack propagation of SENT specimen until final separation of API X100.

ture with localization of deformation becomes more important with increasing high strength of pipeline steels (¿X70) with decreasing strain hardening levels. In two earlier publication of the same team it was shown that the MMC model predicts accurately fracture of fracture of risers under extreme bending and shear ram cutting [62]. Given this fact, the suitable fracture models are urgently needed in the O&G industry which can be efficiently and successfully used for the estimation of strain capacity for different loading scenarios without performing cost-intensive full scale tests. The present results build a strong case of the applicability of the MMC fracture model for the prediction of pipe fracture in all triaxiality ranges relevant for the strain-based design. Previously, the MMC fracture model was applied mainly to thin walled structures for sheet metal forming applications where the range of stress parameters is limited ($0 < < 2/3$). In the present paper the comprehensive but at the same time pragmatic methodology was described for the calibration and validation of model parameters for parent materials which might be easily implemented

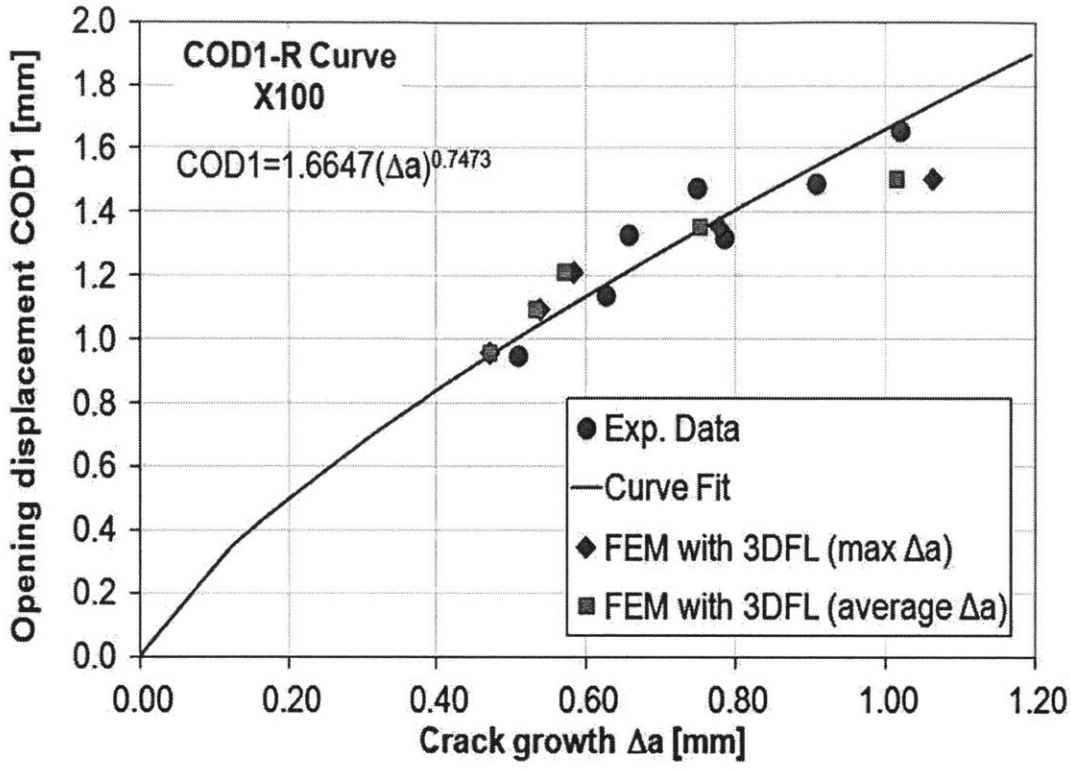

Figure 5-7: Comparison between numerically predicted initial crack growth and experimental data for API X100.

within the strain-based procedures. This methodology includes the calibration of the MMC fracture locus by performing tests covering a wide range of stress states ($-1 < \overline{\theta} < 1$ and $0 < \eta < 2$) and finally the validation of fracture locus on SENT specimens. At any given location there is an evolution of the stress state. All the above factors were taken into account in the general calibrated fracture locus. In the present computational model, crack propagation is predict by the element deletion method technique. The previous studies at ICL and also at other centers pointed out on a strong dependence on fracture initiation and propagation on mesh size. In the present paper, the mesh size effect has been reduced by selecting the same mesh size for the calibration and validation simulations. This method in conjunction with a suitable fracture subroutine, developed in ICL for Abaqus predicts correctly all the features of the structural response of the SENT specimens. It appears that now, one will be able to predict the fracture behavior of cracked specimens purely based on

testing on non-cracked specimens.

5.1.6 Conclusions

This paper provides the results from comprehensive characterization of pipeline steel X70 using experimental and numerical methods. Besides standard mechanical testing to obtain basic strength properties, different tests were performed to describe the existing anisotropic and fracture behavior of steel grades of interest. By conducting this experimental program, which includes tests on flat butterfly-shaped, punch, central hole and notched specimens for low stress triaxiality levels, as well as tests on the round notched bar specimens and standard SENT fracture mechanics tests for high triaxialities, a wide range of stress conditions has been covered demonstrating their effect on the material resistance. In parallel to the experimental study, detailed numerical investigations have been carried out with objective to quantify different stress states effect to calibrate and validate the employed MMC model. In contrast to in the pipeline industry which mainly uses toughness based approach, MMC is also capable of reproducing the crack initiation and propagation in the originally undamaged material accurately. This is done by taking into account not only the first two stress invariants but also the third stress invariant (Lode angle parameter). The achieved results show that the MMC model, in addition to an appropriately tailored calibration process for pipe applications, can be successfully applied to predict initiation and propagation of cracks in a pre-cracked structure configuration over a wide triaxiality range. The presented methodology on how to use the MMC model for the characterization of fracture behavior of pipes can be used as a basis for the development of the practical tool in the strain-based pipeline design. In order to confirm the expected capability of the MMC model to predict strain capacity of the pipelines subjected to large longitudinal deformations, future research work will focus on the modeling of fracture behavior of e.g. pre-cracked pressurized pipe under bending with possible fracture in the girth weld. Here, the major challenge will lie in the description of the material behavior of the heterogeneous girth weld with the proposed methodology. Once this challenge is met, MMC model could serve as reliable and efficient tool for

the prediction of pipeline capacity by capturing the phenomena influencing the overall fracture behavior such as e.g. path deviation of the crack from weld into the base metal.

5.2 Prediction of Bursting Pressure of Pipelines

The current section is involved with the process of wall-thickness estimation based on the material selected for the construction of a pipe. The main focus will be pipeline design against failure due to internal pressure. This is the most common design practice for pipe construction internationally. In the pipeline industry a wide range of design practices has developed to cover failure in all possible conditions (onshore, offshore, underground etc.). These practices are also used to assess reliably the fracture capacity of pipes subjected to internal pressure. Each design practice/standard proposes a safety factor that depends on the pipe geometrical features, the grade of steel used, the surrounding environment, the pipe manufacturing process and also past experience that is comparable with the new project. As far as the material dependence is concerned, only the yield stress is taken into account neglecting other information regarding the material behavior (such as damage, fracture initiation and anisotropy). In the following paragraph a short description of different design standards will be presented.

5.2.1 Yield Pressure assessment of Large-Scale Pipelines

The current design practices with respect pipe design against failure due to internal pressure aim to limit the hoop stress with respect to yield strength of the material. This is an overly safe approach that leads to over-engineered pipes and premature replacement of pipe components. This leads to costs in terms of maintenance and also of days of operation lost during the repair process. The main design pipeline codes are given below.

- ASME B31 Codes are the American standards that assess the pipe's safety

factor as a percentage of the yield pressure of the material for a specific geometry of the pipe. This is the first design code developed for the industry starting of with the B31 Code for pressurized pipes and branching out to B31.4 of Oil Transportation and B31.8 for Gas Transmission and Distribution Piping Systems. This was an early on tool for design of pipes that did not distinguish between onshore and offshore installations. The design internal pressure limit calculated by this standard is given by Eq. 5.2

$$p_d = \beta \cdot \frac{2t\sigma_y}{D - 2tY} \tag{5.2}$$

where p_d is the design pressure, t is the pipe thickness, D is the outside diameter of the pipe and β (ranging between 0.4-0.7 for thin pipes, i.e. $t/D \leq 6$ and given by an analytic expression for thicker pipes, see [20]) is a geometric parameter. For detail account of the calculation process of the design pressure, the reader is referred to [21].

- ISO DIS 13623 pipeline code is also for both onshore and offshore pipeline installation that employs structural reliability techniques moving from the stress based design towards limit state design. More specialized codes and standards have been developed for specific applications, such as offshore and underground. The design pressure according to this standard is given by Eq. 5.3

$$p_d = \frac{2}{\sqrt{3}} \frac{a_u}{\gamma_m \gamma_{sc} \gamma_{inc}} \frac{2t(\sigma_y - f_{y,t})}{D - t} \tag{5.3}$$

where a_u is a material parameter that is influenced by temperature (ranging between 0.96-1.00), γ_m is a material resistance parameter (ranging between 1.15-1.00), γ_{sc} is a safety factor (ranging between 1.040-1.308), γ_{inc} is a parameter affected by the loading condition (usually taken equal to 1.1) and $f_{y,t}$ is the yield strength derating value that is affected by temperature. A more detailed account is presented in [55] along with the ranges of all described parameters.

- API RP1111 is the American Petroleum Institute design standard for specif-

ically offshore pipelines and risers following the limit state design techniques also assuming that bursting and rupture are the failure modes of interest of the pipe. The expression of the design pressure for this standard is presented in Eq. (5.4).

$$p_d = A f_d f_e f_t p_b \tag{5.4}$$

where A is a safety factor (0.8), f_d internal pressure design factor (0.75 for risers - 0.9 for pipelines), f_e is the weld joint factor (only materials that have a value of 1.0 are accepted), f_t is the temperature de-rating factor (1.0 for $T < 121C$) and p_b is the specified minimum bursting pressure of the pipe.

- DNV-OS-F101 is the Det norske Veritas standard for offshore pipelines combining the ASME design and limit state design practices while taking into account the location of the pipeline, the transported product and environmental concerns.

Additional standards develop constantly with the aim of economic and safe design of pipes as part of joint industrial projects. The industry has slowly departed from the stress based design and has moved towards strain-based design as it is showed by many international conferences that host sessions on Strain-Based-Design , such as the International Society of Offshore (Ocean) and Polar Engineering Conference and the International Conference on Ocean, Offshore and Arctic Engineering (OMAE). The common denominator of stress based design techniques is demonstrated in Eq. (5.5)

$$p_d = \alpha p_y \tag{5.5}$$

where p_y is the yield pressure, p_d is the design pressure, α is the safety factor of the operational pressure as a function of the yield strenth of the material.

Prediction of first yield for pressurized pipes

In this paragraph the assessment tools of both thin- and thick-walled pipe yield pressure will be presented. For the calculation of first yield of a pipe that is subjected

to internal pressure, a yield criterion is required along with the stress state of an infinitesimal volume of the pipe. These two pieces of information lead to the calculation of the yield pressure p_{yield} as a function of the material strength against yield, the boundary conditions of the pipe and its geometry. In the following analysis, the von Mises yield criterion will be used covering cases ranging from thin to thick pipes. The von Mises yield condition is given by Eq. (5.6)

$$\sigma_y = \sqrt{\frac{1}{2}[(\sigma_\theta - \sigma_r)^2 + (\sigma_\theta - \sigma_z)^2 + (\sigma_z - \sigma_r)^2]} \tag{5.6}$$

where σ_y is the equivalent plastic stress, σ_θ is the circumferential (hoop) stress, σ_r is the radial stress and σ_z is the strenth in the direction of the longitudinal axis of the pipe. In the case of pressurized pipes, using the von Mises yield criterion, four distinct expressions exist for the calculation of yield pressure: i) thin-walled pressurized pipe with open ends, ii) thick-walled pressurized pipe with open ends, iii) thin-walled pressurized pipe with closed ends and finally iv) thick-walled pressurized pipe with closed ends. The difference between open and closed ends of the pressurized pipe, is the effect of the longitudinal stress component. The reason that the closed end condition is calculated, is that in experimental testing of pressurized pipes, the ends are usually fixed (see Fig. 5-9). In the open case of pressurized pipes, see Fig.

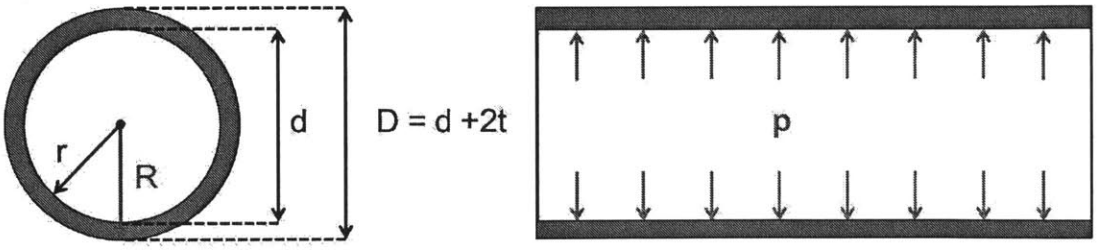

Figure 5-8: Schematic representation the main geometric features of a pressurized pipe with open ends.

5-8, σ_z is zero. In the case of closed end pipes subjected to internal pressure, the longitudinal component of stress, σ_z is calculated using a free body diagram in the longitudinal direction of the pipe. Assume that a pipe of outside diameter, R and

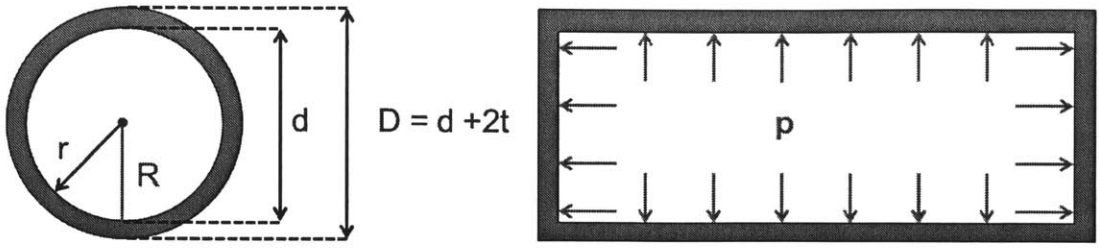

Figure 5-9: Schematic representation the main geometric features of a pressurized pipe with closed ends.

internal diameter r, with $R = r + t$. Then, in the z-direction the equilibrium of forces is given by Eq. (5.8)

$$p \cdot \pi r^2 = \sigma_z \cdot (\pi R^2 - \pi r^2) \tag{5.7}$$

$$\sigma_z = \frac{pr^2}{(\pi R^2 - \pi r^2)} \tag{5.8}$$

For $r >> R$, and $R, r > 0$, the thin-walled pipe condition for closed ends is recovered, Eq. (5.9).

$$\sigma_z = \frac{pR}{2t} \tag{5.9}$$

Combining the above results for all the possible combination of thickness consideration and end conditions, all possible analytical expressions for the yield pressure as a function of the material yield strength and pipe geometry is given below.

- Thin-walled with open ends:

$$p_y^{thin,open} = \frac{\sigma_y t}{r} \tag{5.10}$$

- Thick-walled with open ends:

$$p_y^{thick,open} = \frac{\sigma_y (R^2 - r^2)}{\sqrt{3(R^4 - r^4)}} \tag{5.11}$$

- Thin-walled with closed ends:

$$p_y^{thin,closed} = \frac{2}{\sqrt{3}} \cdot \frac{\sigma_y t}{r} = \frac{2}{\sqrt{3}} \cdot p_y^{thin,open} \tag{5.12}$$

Table 5.1: Finite Element Model Simulation Cases

Case name	Material	thickness [mm]
Case 1	X70	15.88
Case 2	X100	15.88
Case 3	X70	10.16
Case 4	X100	10.16
Case 5	X70	6.35
Case 6	X100	6.35

- Thick-walled with closed ends:

$$p_y^{thick,closed} = \frac{2}{\sqrt{3}} \cdot \frac{\sigma_y(R^2 - r^2)}{R^2} \tag{5.13}$$

In the analysis that follows, the difference in pressure between the yield pressure and the bursting pressure will be assessed using the calibrated material parameters for API X70 and X100. For the calculation of the yield pressure, Eq. (5.13) will be used. This pressure will be the safety benchmark for the pipes of interest. This analysis will be used in Chapter 6 to calculate the thickness reduction between X70 and X100 constructed pipes that are requested to allow for the same safety margin for the bursting pressure.

5.2.2 Numerical Model and Problem Description

In the current section a finite element model was developed to assess the effect of thickness to the bursting pressure of a pressurized pipe with closed ends. For that reason the same finite element model was modified for three different thickness values and ran using the material description for plasticity, anisotropy and fracture for both X70 and X100. The detailed naming of all cases for the three thickness values (Fig. 5-10) that were ran are presented in Table 5.1.

A solid element model, Fig. 5-11 was developed with uniform, homogeneous mesh. In order to drive the localization of damage, an artificial thickness reduction (deleting two elements, Fig. 5-11) was introduced using element deletion and a bottom-up

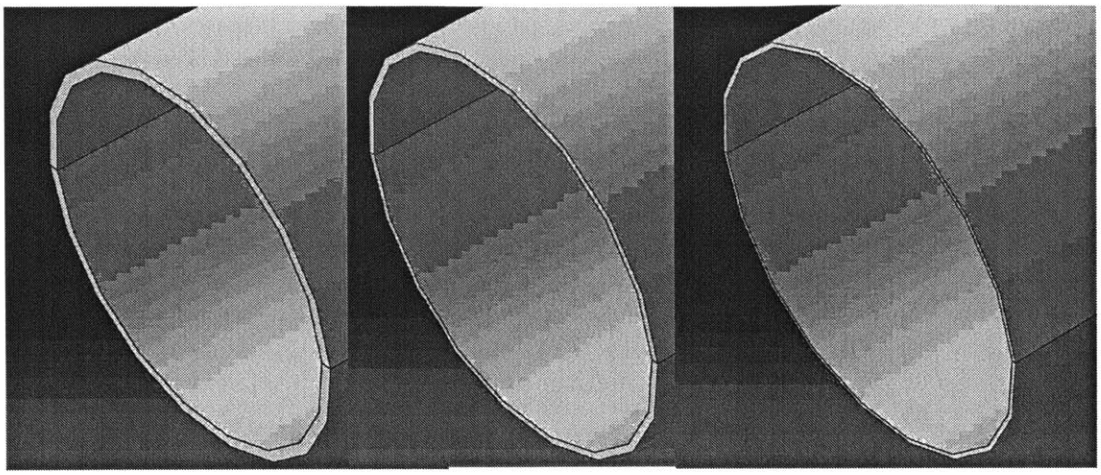

Figure 5-10: FEM models for the three different thickness cases, $t = 0.6$" (left), $t = 0.4$" (middle) and $t = 0.25$" (right).

mesh definition. The outer diameter to thickness ratio, $D/t = 31.3$ and $D = 21$" (533.4mm).

The geometry of the pipe was selected specifically to represent the casing pipe geometry of the Deepwater Horizon accident. The outside diameter was kept constant, while the internal was adjusted for three different thicknesses. The values for the different thickness values were selected based on [65]. Continuum, 3-D, 8-node, with reduced integration elements were used (C3D8R). A coarse mesh of 26mm x 68mm x 4mm was selected that calculated to a total of 8190 elements for the entire pipe. The mesh remained the same for all thickness cases. The end conditions were prescribed as closed ends, that is the usual boundary condition used in bursting experiments. The step used for the analysis was explicit dynamic and the time-like parameter was the increasing pressure applied in the internal surface of the pipe. The analytical prediction for the yield pressure were calculated using Eq. (5.13), ranged for API X70 between $p_y^t hick, closed = 13.11 - 32.12$MPa and for API X100 between $p_y^t hick, closed = 18.73 - 45.99$MPa. Therefore, the FEM ran for internal pressure increasing from 0 to 100MPa. Rupture and final bursting occurred in both material cases before the completion of the simulation.

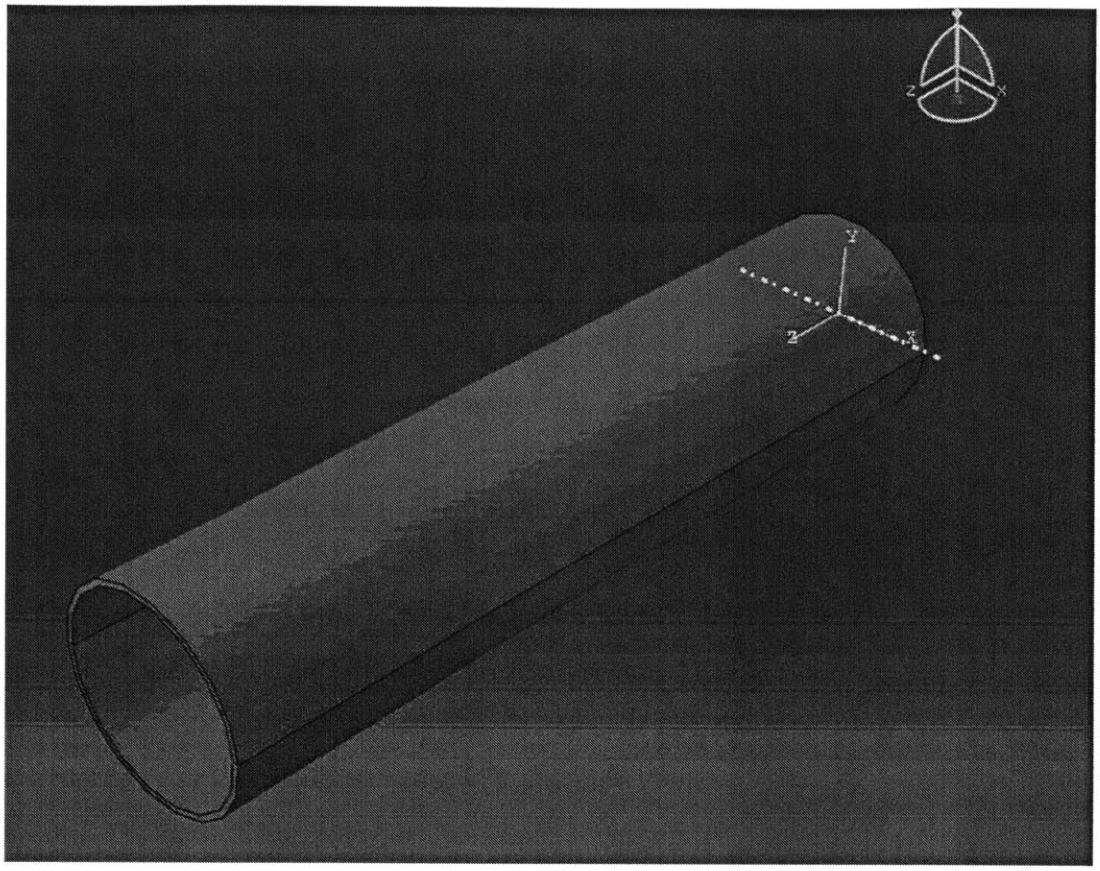

Figure 5-11: FEM bottom-up mesh and indication of element deletion for the initiation of damage localization, simulating pre-existing defect.

5.2.3 Effect of Anisotropy on the onset of fracture location

The two materials used were quite different in terms of anisotropy. X70 anisotropy analysis revealed a near to isotropic behavior, while X100 presented much more anisotropy. This difference is most probably due to the manufacturing process used for the two materials. The first pipe material came from a seamless pipe segments, while the second one originated from UOE pipe. This effect was demonstrated in the finite element simulations clearly. X70 FEM results showed that due to the fact that the material was considered isotropic, during the simulation, damage accumulated in the defect area leading to see-through crack that propagated from the defect zone towards the ends of the pipe. The crack propagation was stable and the qualitative results remain the same with reducing thickness (Figs. 5-12 and 5-13). However, in

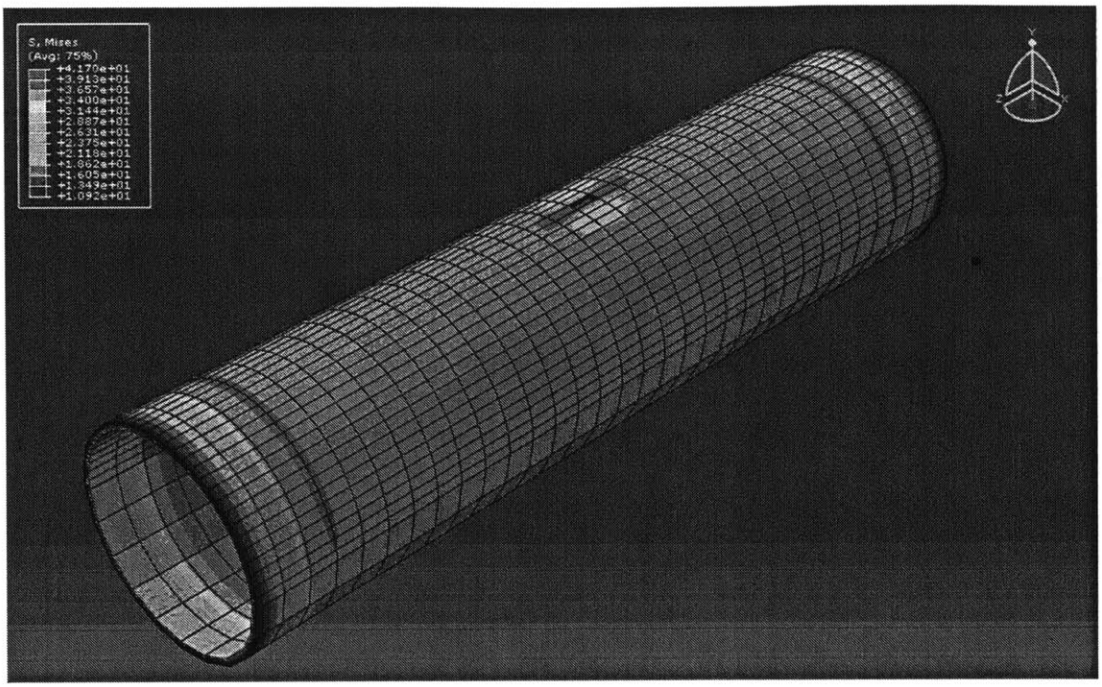

Figure 5-12: Localization of damage initiation of yield in the defect region demonstrated in the FEM simulation in terms of von Mises stress for Case 1.

the case of X100, the anisotropy effect was much stronger than the initial imperfection and failure location was driven according to the materials anisotropic features away from the defect area (Fig. 5-14). For computational time efficiency the original mesh was coarser on one side of the pipe and finer on the defected region to monitor better the crack propagation. After the original simulations indicated this weak dependence to the initial defect, however, the pipe was re-meshed with uniform mesh and was re-ran for all cases to exclude the mesh density effect from the results. Both the quantitative and qualitative results were not affected. Failure location in the X100 cases (Cases 2, 4 and 6) was driven by anisotropy. There is a a critical defect size that drives the fracture initiation and propagation in the defect area.

5.2.4 Effect of thickness on the bursting pressure

The most important effect in this current study is the effect of the thickness on the bursting pressure. It is expected that as the thickness value decreases, the bursting

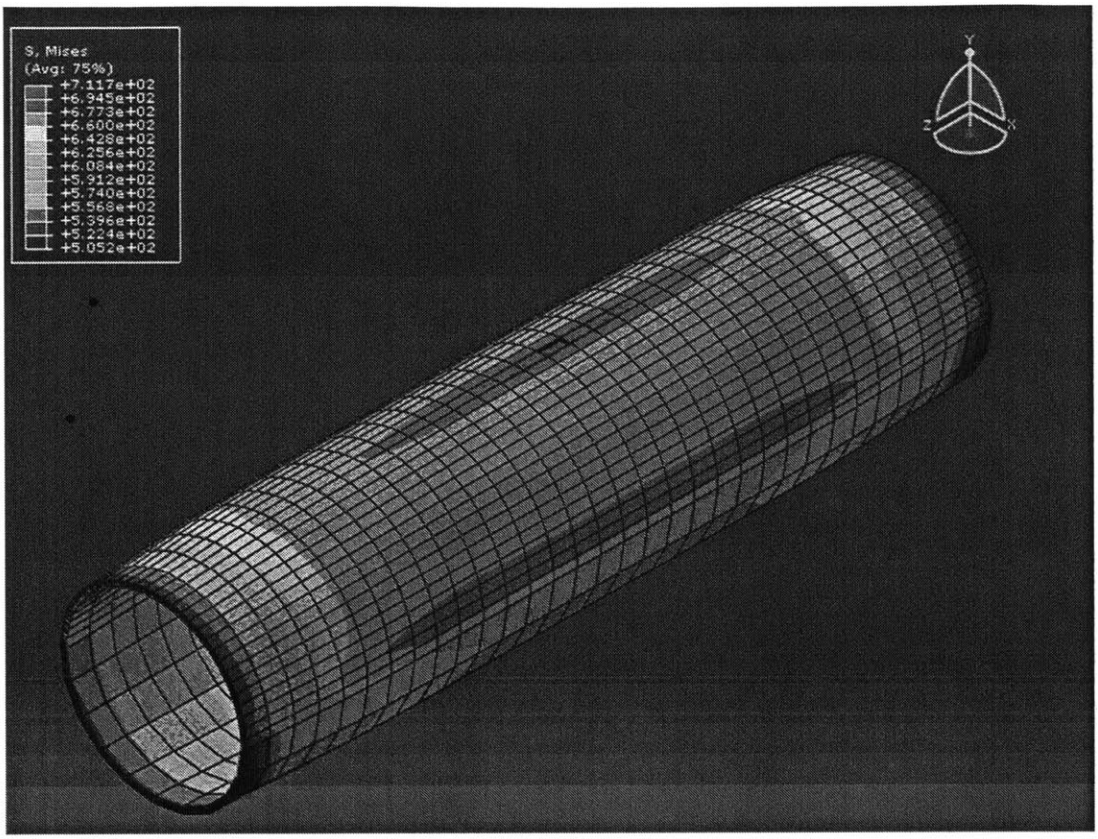

Figure 5-13: Localization of damage and crack initiation in the defect region demonstrated in the FEM simulation in terms of von Mises stress for Case 1.

pressure decreases assuming that all other parameters, material (pipe API grade material) and other geometric features (length of pipe and outside diameter). The interesting part of the analysis comes about when for the same geometry two different API grades of steel are considered. In order to make it clear, X70 and X100 are considered and their material descriptions are used to quantify that effect. FEM are run for the same geometry and the effect on their bursting pressure was evaluated. As it was expected, the bursting pressure decrease almost linearly with the thickness for X70 while the effect quadratic for X100 (see Fig. 5-15). The nonlinear relation of the $p_{bursting}$ and the t comes probably from the fact that the ductility of X100 is much smaller than that of X70. It is clear that the bursting pressure of grade X100 is larger for all thickness variations as it was expected. This additional strength can be used for reducing the amount of material used for the construction of a given pipe,

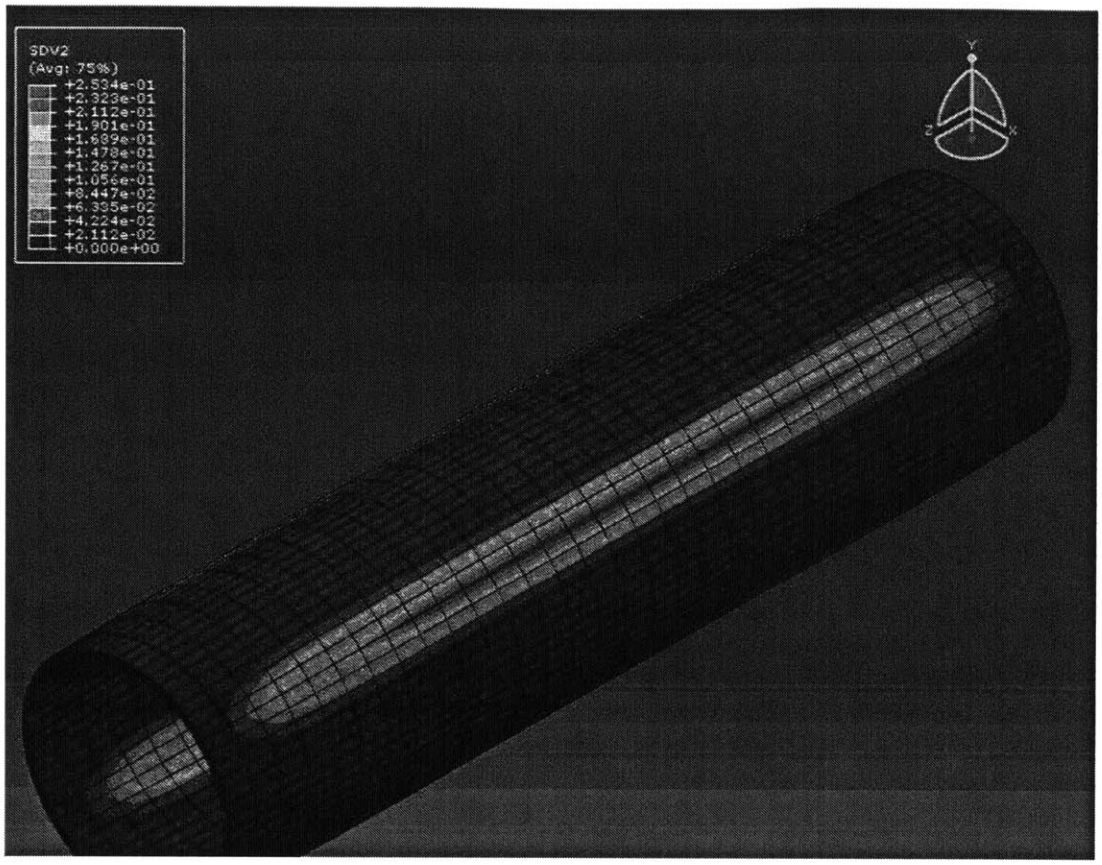

Figure 5-14: Localization of damage initiation of yield in the defect region demonstrated in the FEM simulation in terms of the damage factor for Case 2.

by replacing a lower grade steel, in this case X70, by a higher grade steel, X100. The financial effect of this will be full described in Chapter 6.

As it was mentioned earlier in this section, pipe design usually required the calculation of the safety factor of the pipe. According to different standards and guidelines the safety factor is evaluated based mostly on experience taking into account only the yield pressure of the pipe, while neglecting the rest of its material characteristics (anisotropy, fracture characterization). In section 5.2.1 this was described in detail. The current section offers a new method for evaluating the safety factor of a pipe. Since the calibration of a material takes place and therefore, the material description is detailed enough to encapsulate all its mechanical properties, it is possible to use results from bursting numerical experiments of the pipe of interest. Let us define this

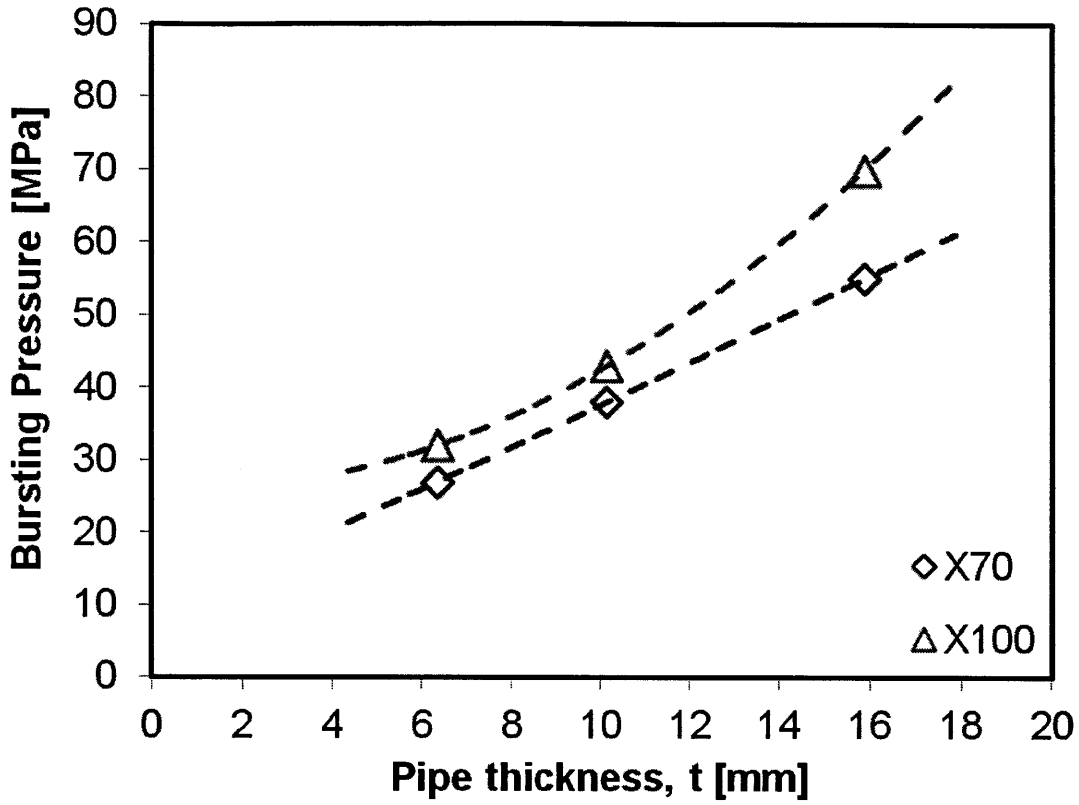

Figure 5-15: Effect of material and thickness on the bursting pressure of a pipe.

new safety factor, in Eq. 5.14.

$$\alpha = \frac{p_{bursting,FEM}}{p_{yield,analytic}} \tag{5.14}$$

The numerator of Eq. 5.14 includes all the material features and offers a reliable first estimate of the bursting pressure. For the denominator there is a multitude of different choices that is related to the thickness of the pipe and the end conditions. In testing procedure the best consideration for the end conditions is to consider that the ends closed. In operational conditions, open ends are usually considered. The difference between thin- and thick- stems in the calculation of the safety factor due to the fact that in the first case the denominator is calculated using Eq. (5.12), while in the later by Eq. (5.13). That effect is demonstrated in Fig. 5-16.

Each material has stores energy during its loading with internal pressure. Perma-

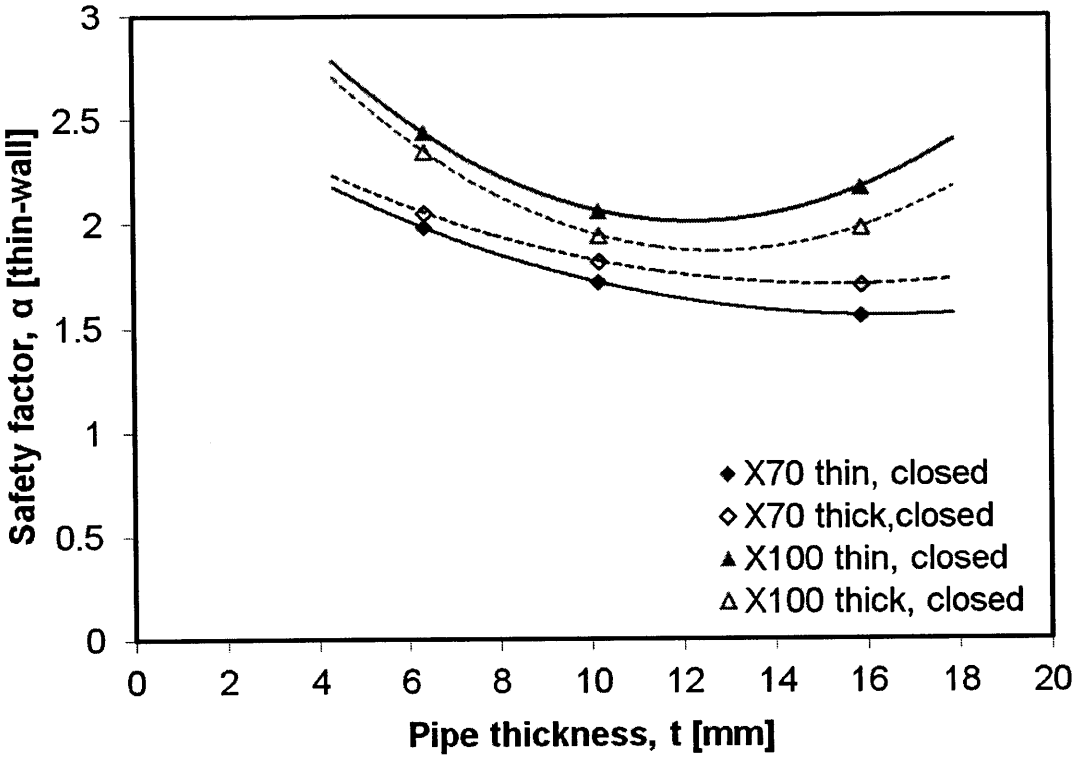

Figure 5-16: Difference in the safety factor evaluation between consideration of thin- and thick-walled pipes for X70 and X100.

nent damage starts after the onset of yield begins and extends until the initiation of failure (bursting). The amount of energy can be depicted by the difference in pressure between first yield at the internal surface of the pipe until the final bursting. The results for X70 and X100 is presented in Figs. 5-17 and 5-18 accordingly.

It is evident that the area reduces in the case of API X100, while the lines both for the yield and bursting pressure move upward between API X70 and X100 (Fig. 5-19). The area between the yield and the fracture lines decreases for higher grades, demonstrating the reducing ductility, while the upward trend between API steels demonstrates the increase in strength.

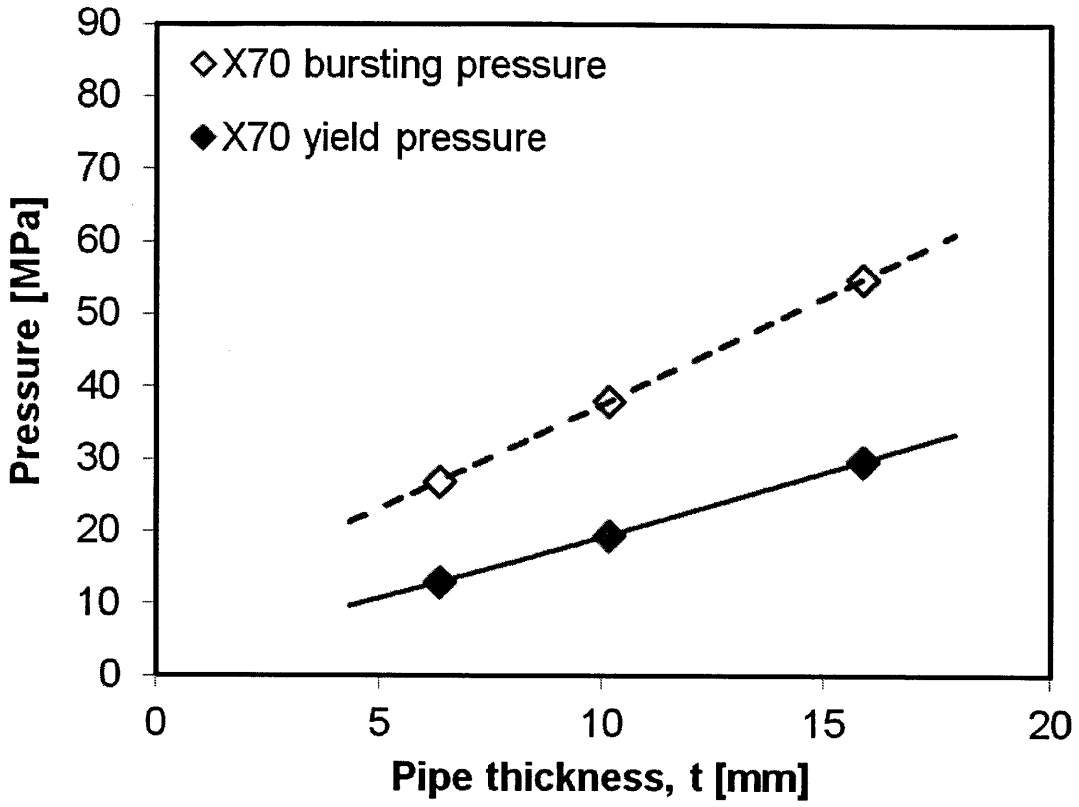

Figure 5-17: Difference between analytic yield pressure for thick pipes with closed ends and FEM predicted bursting pressure for three cases of API X70 (Cases 1, 3, 5).

5.2.5 Conclusion

In the current section is was proven that the MMC model calibrated for two API steels can offer a new design tool for pipes that is able to quantify the thickness reduction between grades for the same outside diameter of a pipe. This tools is based on the complete calibration of a set of parameters that enables the correct representation of the material behavior in terms of anisotropy, plasticity and fracture. That offers a new method for safety assessment of pipes that includes not only first yield but a range of mechanical properties of the material. This opens the way for reliable design and avoidance of over-engineering. Also, this methodology could be used in the assessment of remaining safety of existing pipes.

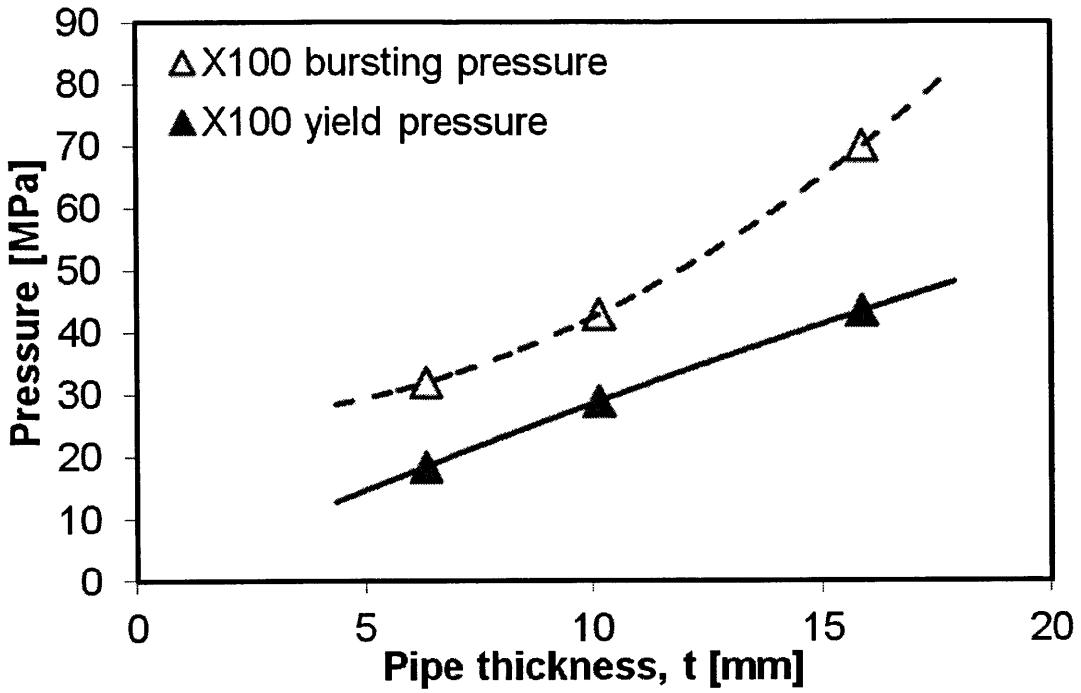

Figure 5-18: Difference between analytic yield pressure for thick pipes with closed ends and FEM predicted bursting pressure for three cases of API X100 (Cases 2, 4, 6).

5.3 Emergency Shearing for Oil Leak Prevention

The objective of the present paper is to summarize the MIT fracture technology and to show how this technology could be used to solve an important structural and material problem relevant to the DeepHorizon accident.

The ICL work on fracture modeling consists of four parts:

1. Physics-inspired fracture model
2. Unique experimental equipment and testing methods
3. General calibration procedure
4. FE implementation in several commercial finite element codes

In each of the above categories, the ICL methods and procedures have distinct advantages over those used by other leading industrial and academic labs around the

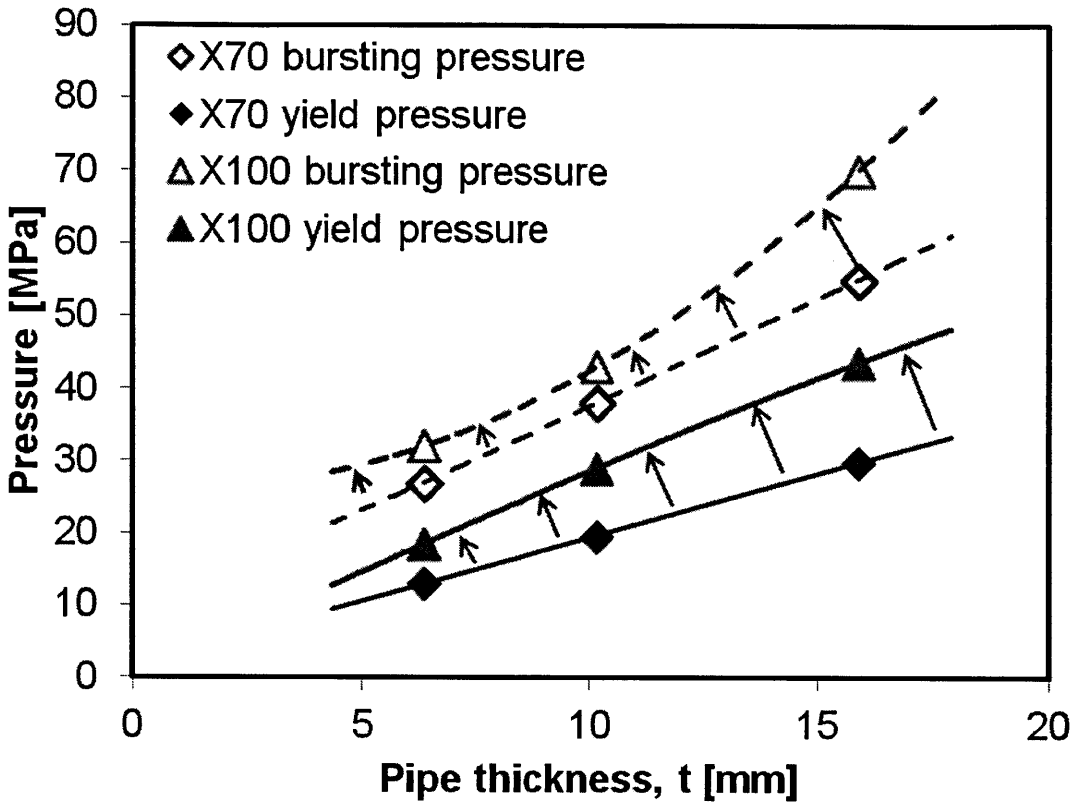

Figure 5-19: Difference between analytic yield pressure for thick pipes with closed ends and FEM predicted bursting pressure for six cases transitioning from of API X70 to X100.

world. The most important features of the above four components of our fracture modeling are briefly summarized for the benefit of the O&G community. This is followed by a case study involving numerical simulation and analytical solution of the process of shear ram cutting through a riser/drill pipe system for securing a well after an accidental pressure kick.

Over the past four years, ICL has been working on characterizing plastic properties of several grades of AHSS, including ThyssenKrupp TRIP 690, POSCO TRIP 780, POSCO DP590, ArcelorMittal DP980, US Steel DP780, ThyssenKrupp MS, ArcelorMittal SS3001LN. In all cases, the parameters of the power hardening law were determined, as well as the plastic anisotropy parameters. Work on steels for deep-water ocean applications has started in the lab only recently.

Presently, tensile tests were completed on X70 and X65 steels, according to the nomenclature used in the Oil and Gas industry. Work on characterizing fracture properties of those two materials is under way, but has not been complete to be included in the present paper. Therefore, it was decided to perform numerical simulations on ThyssenKrupp TRIP 690 steel, for which all data on plasticity and fracture are available and published in the open literature (see [63]).

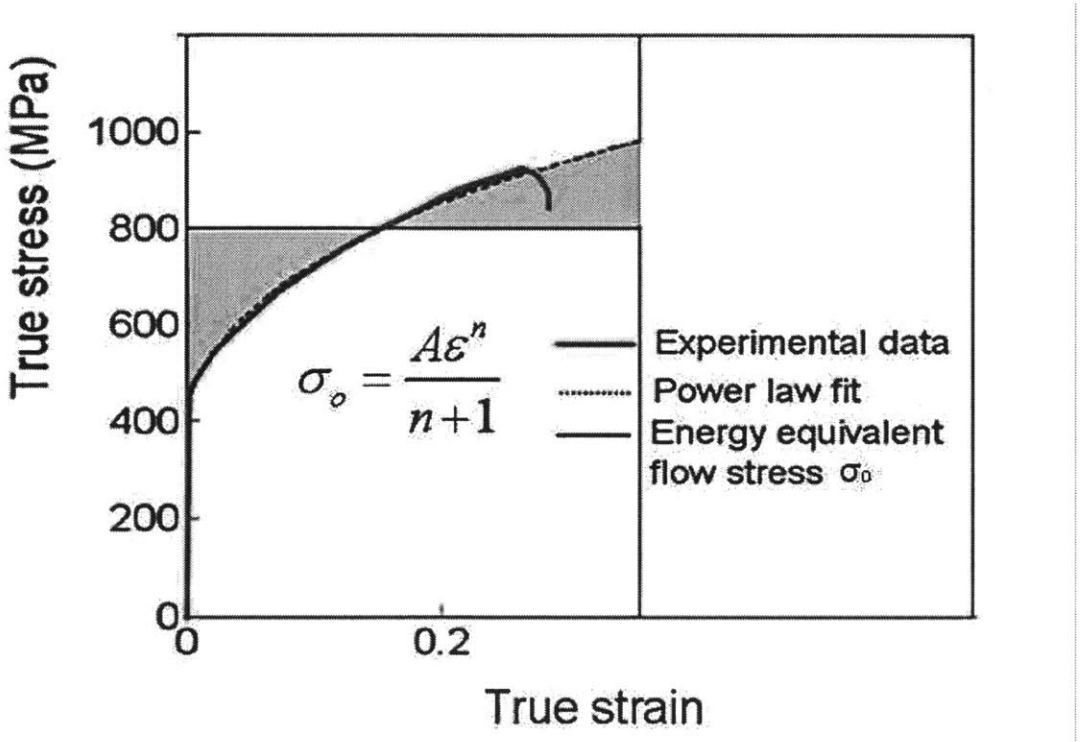

Figure 5-20: Power law fitting of the isotropic strain hardening behavior for TRIP690 and the concept of the energy equivalent flow stress [9].

The coefficients of the power hardening law for TRIP 690 are: A = 1276 MPa, n = 0.2655. This material has a similar yield stress to X70, but has much steeper hardening. Therefore, we decided to use this material for both the riser and the drilling pipe. The complete true stress strain curve of TRIP 690 is shown in Fig. 5-20. It was also found that TRIP 690 has a negligible amount of anisotropy. Therefore, a standard J2 plasticity theory was used in numerical calculations. The fracture parameters of TRIP690 are presented in Table 5.2 and are shown in Fig. 5-21

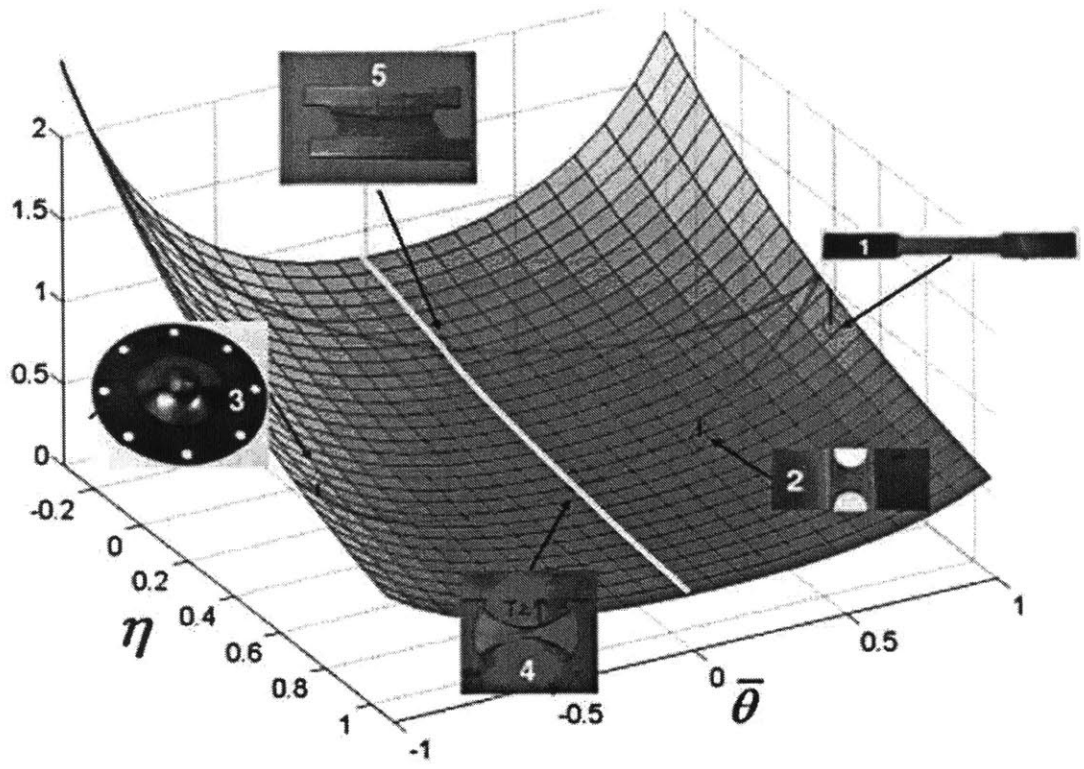

Figure 5-21: 3-D fracture locus in the space of the equivalent strain to fracture, stress triaxiality and Lode angle parameter for TRIP 690.

Table 5.2: Fracture parameters for TRIP 690.

C_1	C_2	C_3
0.12	720	1.095

The red line on the 3-D fracture locus corresponds to plain stress state, while the yellow line represents the plain strain condition. Plain stress will be prevailing during the initial lateral crushing of the tube, while plain strain will develop during the final cutting process. For bulk material such as heavy-wall pipes, different types of specimens could be machined such as notched and un-notched specimens and plain strain bending specimens. The above types of specimens were used in CSM to characterize fracture properties of one particular grade of stainless steel.

The results of the fracture calibration based on the measured fracture parameters are in very good correlation, $R_2 = 98\%$ as shown in Table 5.2.

Table 5.3: Geometry of the riser-drill pipe system.

	Outer Diameter [in]	Wall Thickness [in]
Drilling Riser Casing	21	0.675
Drill Pipe	6	0.6

5.3.1 Problem Description and Numerical Model

In this study, no reference is made to any particular design of shear ram blades. Instead, it is shown how efficient it is to predict all the stages of the cutting process using the general 3-D plasticity and fracture model developed at ICL. The exact outer diameter, D and wall thickness, t of the riser of the Deep Horizon drill platform was assumed to be identical to that of the sister platform Jim Cunninghan geometry that is available in the open literature [1]. Typical drill pipe geometry was taken from [77] and is presented in Table 5.3.

The same handbook provides a list of different materials typically used for deep-water drilling, such as API Steel Grade X95 that was selected for this study. TRIP 690 was the closest in terms of yield and UTS and it was chosen by the ICL fully characterized material database to be used for all the numerical simulation. The configuration of the concentric pipes/shear ram blades is shown in Fig. 5-22.

The blades were assumed to be perfectly rigid with an infinitesimal vertical gap between the blades in the model. Two types of Finite Element Model of the pipe were developed, a shell element model and a solid element model. In the shell element model both pipes were discretized by $80,000$ four node shell element with reduced integration points (S4R in Abaqus) with a mesh size of 5x5 mm.

It was found that the load level calculated using shell elements was unrealistically high compared to the solid model results (see below). This is because both pipes are relatively thick and the shell elements without out-of-plane degrees of freedom are much stiffer than the actual material elements.

The shell approximation of the outer pipe, with diameter to thickness ratio, $D/t = 31.3$, is acceptable. However, as far as the inner pipe with D/t = 10 is concerned, the

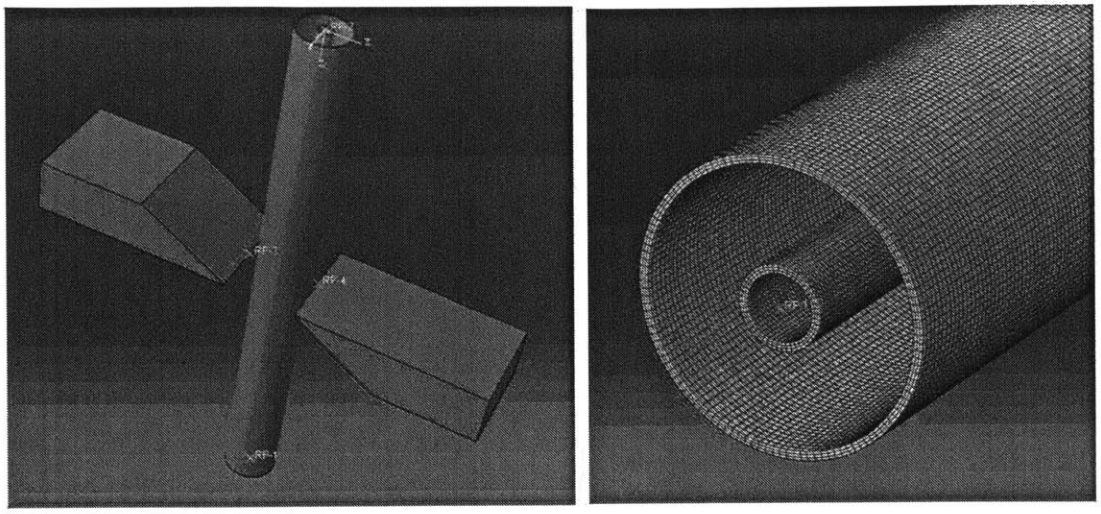

Figure 5-22: Initial configuration of the system of concentric pipes and shear ram blades and the solid element discretization of the system.

shell model is too crude and for that reason a solid element model was implemented. The solid model of both pipes was build using 8 node quadratic solid elements with reduced integration. Three elements were used through the thickness for both pipes (see Fig. 5-22). The size of the elements was approximately 5x5x5 mm. Surface to surface contact has been implemented to account for the interactions between inner/outer pipe and the outer pipe/blade. In addition, self-contact was introduced to model correctly the bottoming up of the interior of the respective pipes in the later stage of the deformation process.

The load was introduced through imposing a constant displacement rate of the blades. Mass scaling was applied in order to solve the quasi-static problem using Abaqus Explicit. The calculated load/displacement curve, up to the point of a complete flattening of both pipes, is shown in Fig.7. One can distinguish three phases of the deformation process.

5.3.2 Shearing Surface Representation and Shearing Force Prediction

In the first phase (shown by the yellow area in Fig. 7), there is a symmetric indentation of the outer pipe by two opposite wedges, much in the same way as the pinching process analysed in earlier publications [80] and [83].

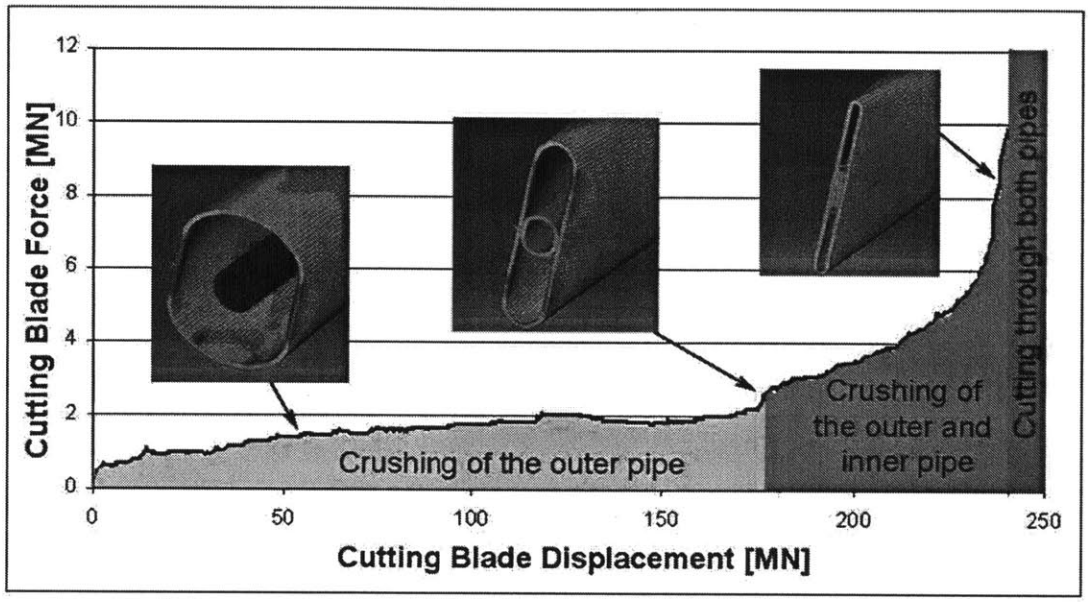

Figure 5-23: Three stages of the crushing/cutting process shown with removed cutting blades. Touching between the deformed outer pipe and un-deformed inner pipe is the starting point of stage two (orange area). Both pipes are then crushed together until complete flattening occurs.

Throughout the second phase, the shear force is rapidly increasing due to large membrane stretching and tightening of the bending radius of both tubes [81]. The crushing process terminated at about cutting blade displacement of 240mm. The 3-D view of the complete crushed tubes is shown in Fig. 5-24 in a longitudinal AA cut. From this point on, the process of cutting of both pipes initiates, producing much higher forces exceeding the scale of Fig. 5-23.

During the cutting process there is practically no more bending and in-plane membrane deformation of both pipes. The cutting process is essentially a plain strain process that should be modeled using plane-strain finite elements. The present finite

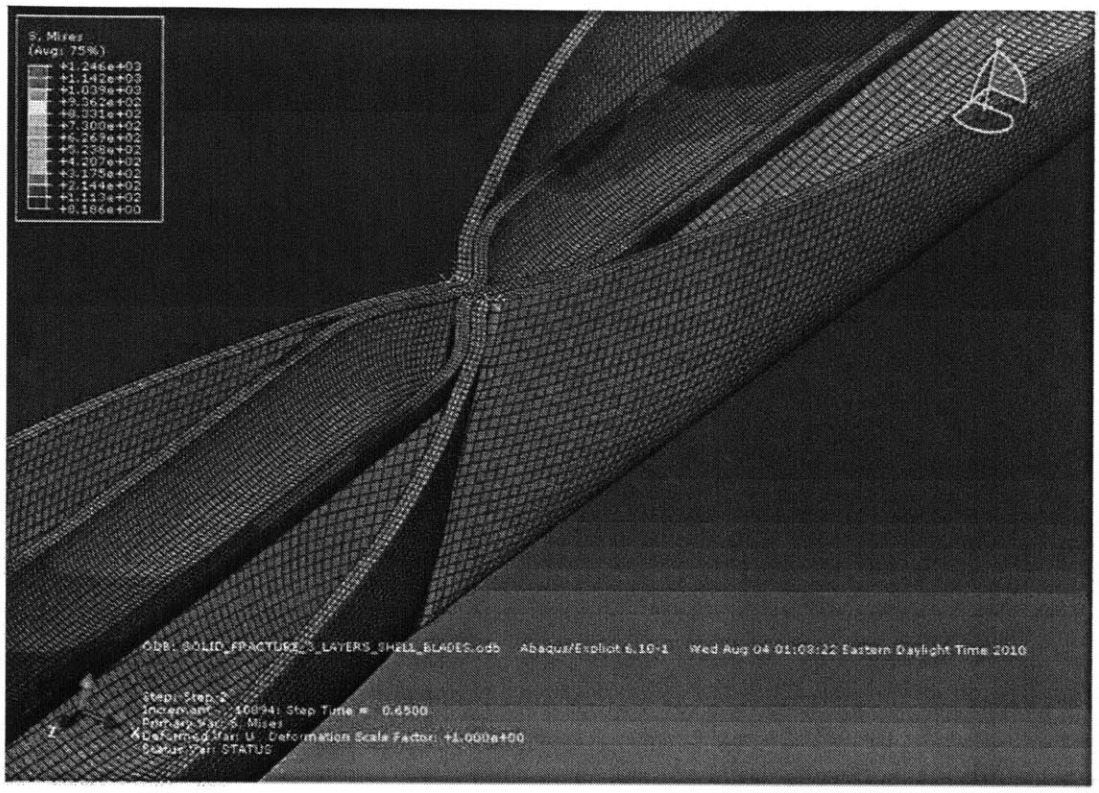

Figure 5-24: At the last stage of the crushing proceed both tube cross sections are completely flattened by wedge type of cutting blades.

element mesh shown in Fig. 5-25 is much too coarse to get a reliable prediction of the cutting force. A much finer mesh with a number of elements of twenty or more through the thickness should be introduced, as shown in Fig. 5-26.

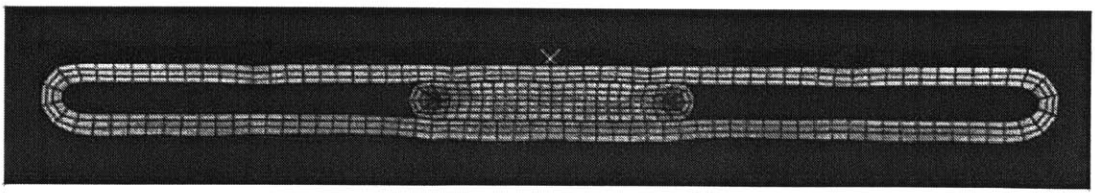

Figure 5-25: Onset of the cutting process with both pipes being completely locally flattened.

Elegant analytical solutions of the pinching and cutting process have been derived in the past by one of the co-authors of this paper. The load-displacement curve of the indentation of a tube by rigid shear ram blade, taken from reference [83] is of the

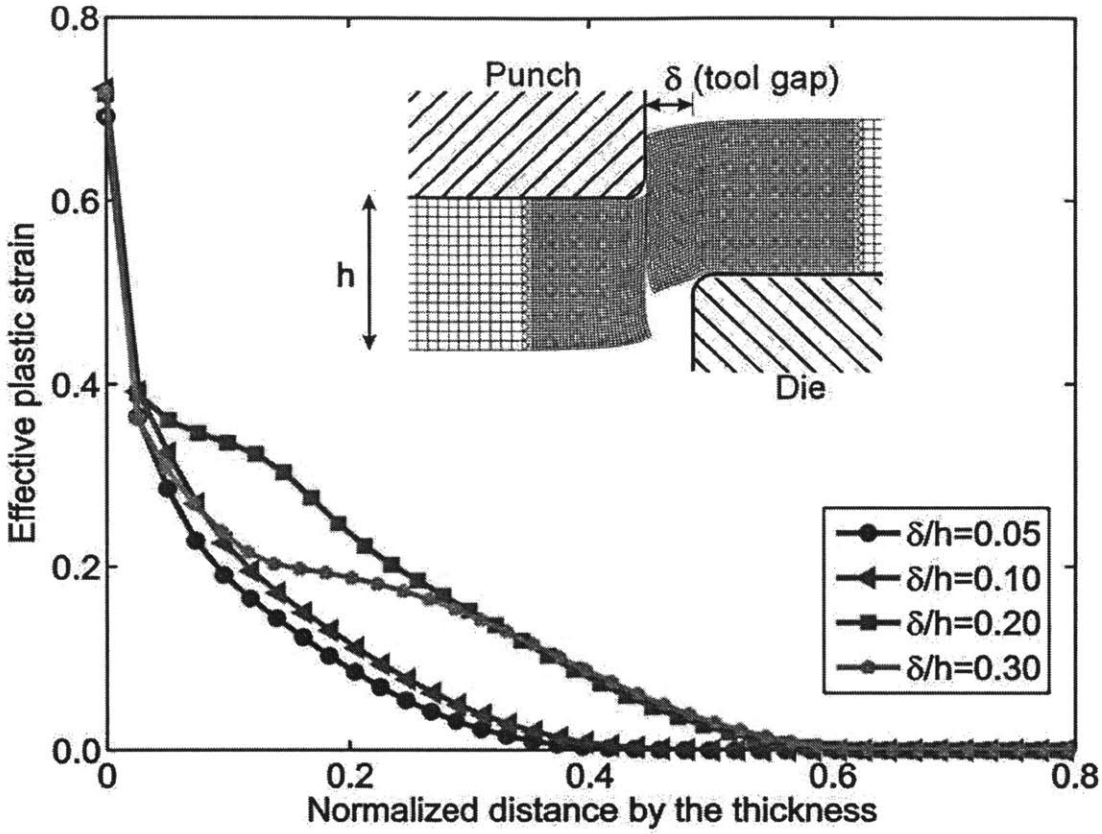

Figure 5-26: The distribution of equivalent plastic strain along the width of the cross section (taken from [82]).

form shown in Eq. (5.15).

$$P = 2\sqrt{2\pi}\sigma_o t^{3/2} u^{1/2} \tag{5.15}$$

where σ_o is the energy equivalent flow stress of the rigid plastic approximation (see Fig. 5-20) and u is the indentation depth. For the present parameters of the hardening law, the value of σ_o depends on the expected range of strain, ϵ_1 according to $\sigma_o = 1000\epsilon_1^{0.265}$. The solution in q. (5.15) is valid in the initial phase of pinching process indicated in Fig 5-23 by the yellow color. For the estimated range of strains, i.e. $\epsilon_1 = 0 - 0.15$, the corresponding energy equivalent stress is $\sigma_o = 600MPa$. In this phase, both bending and membrane action is taken into account.

In the second phase both the inner and outer pipe are been squeezed simultane-

ously. The major contributing factor to the crushing resistance of the system is the bending deformation due to the tightening radius. The solution of this problem was outlined in [81], so only the final results applicable to the two pipes is quoted here.

$$P = 6\pi\sigma_o t^2 \frac{R_i}{R_o - u} \tag{5.16}$$

where R_o and R_i are respectively the radii of the outer and inner pipe. The solution is seen to blow up to infinity for $u = R_i$. At this point the pipe is complete squeezed between the blades and the bending radii are comparable to the tube thickness t. Taking $\epsilon_1 = 0.43$ the value of equivalent flow stress becomes 800 Pa. The above values of were used to construct the analytical solutions. Finally, the maximum cutting force can be estimated from simplified solution due to Atkins [22], see Eq. (5.17).

$$P = \frac{4}{3} A h_o \frac{n^n}{(n+1)^{n+1}} \tag{5.17}$$

where A and n are the hardening law coefficients of TRIP 690. The comparison of the analytical solution is given by Eqs. (5.15), (5.16) and (5.17) with the present numerical solution shown in Fig. 5-27.

A close agreement between the close-formed solution and the results of numerical simulation provides a very useful crosscheck of the correctness of the above solutions. Analytical solutions are very useful in the phase of preliminary design, when decisions must be made on the thickness, radius and material of a pipe.

After the full collapse of the cross-section of both pipes, the cutting process takes place. The final shearing versus blade displacement is shown in Fig. 5-28.

5.3.3 History of Stress Triaxiality

The triaxiality history as a function of equivalent strain was monitored. Two points were selected, namely Point C and Point D, located on the riser and drill pipe respectively. The triaxiality monitored for both points lies in the are of $= 0$, which designates the shear stress state as it was expected in a cutting process.

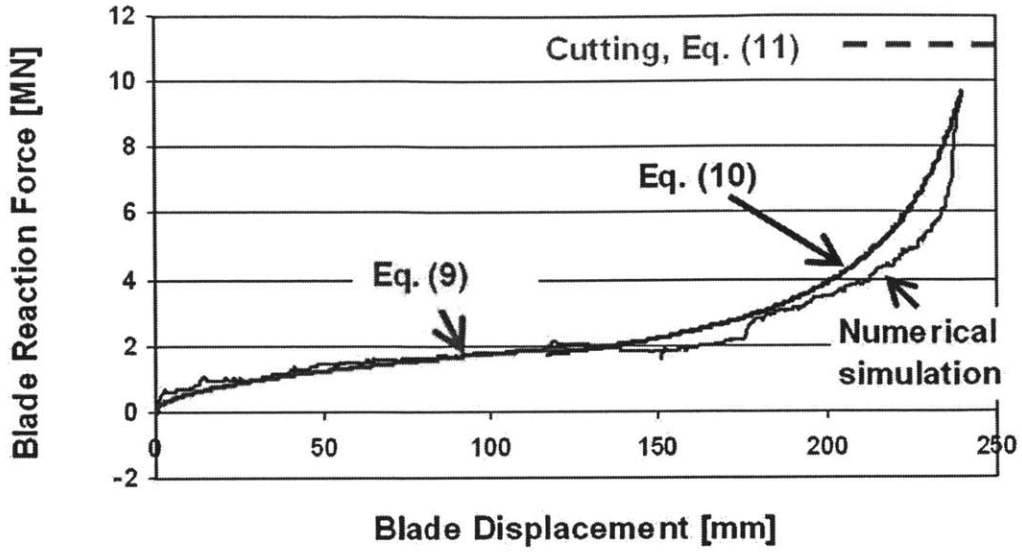

Figure 5-27: Analytical solution of the crushing/cutting process of the pipe superposed on the numerical solution.

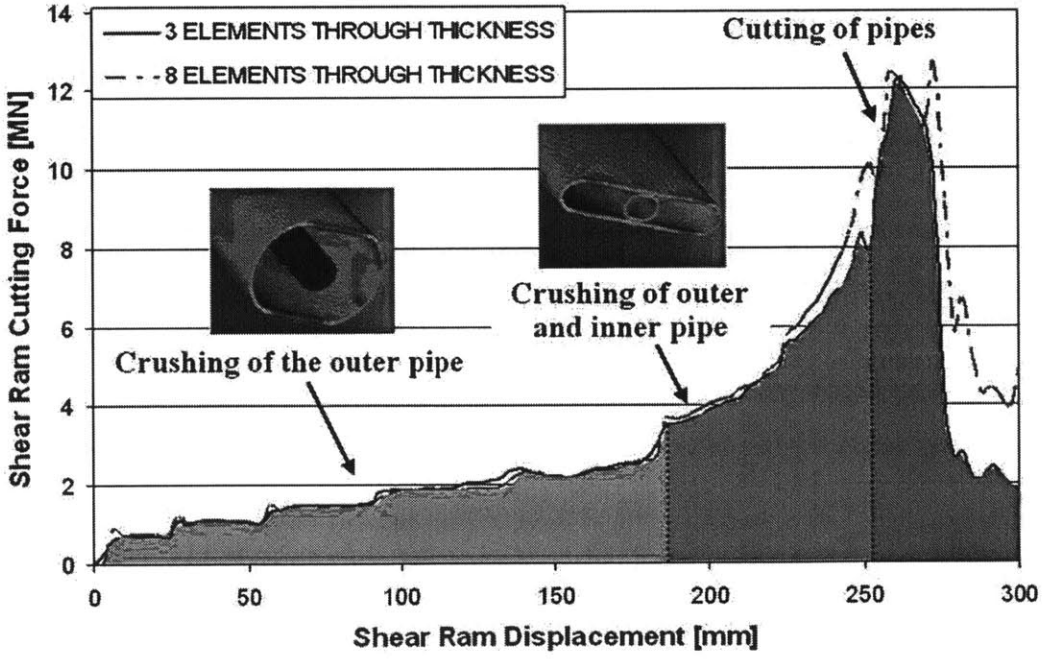

Figure 5-28: History of shearing force and three stages of the cutting process.

5.3.4 Conclusions

The O&G industry is striving to correctly predict the response of deep water installation to operational and accidental loads. The necessary fracture technology has

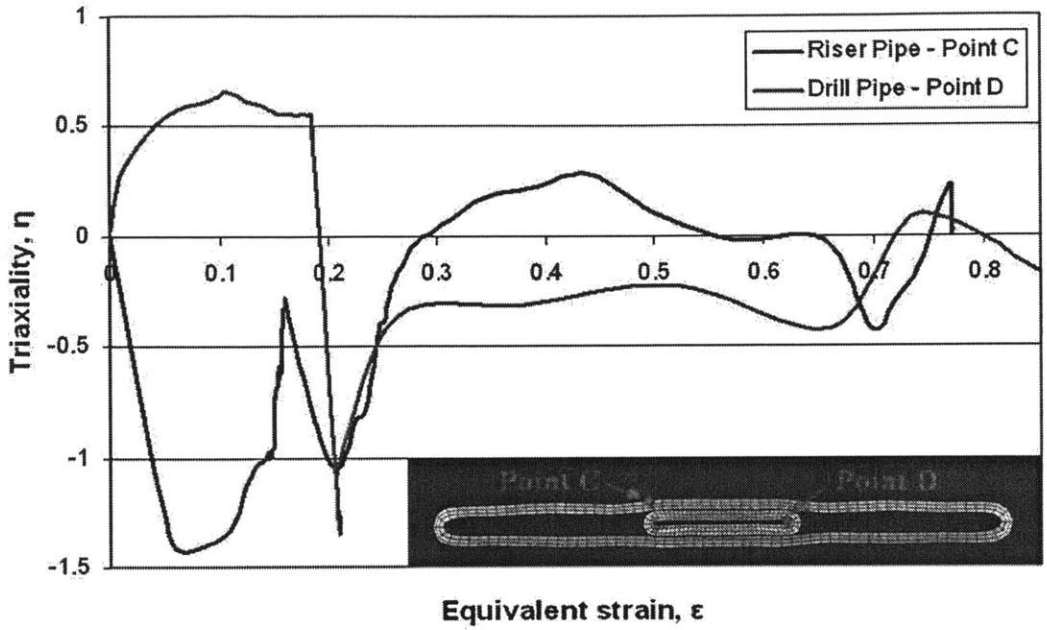

Figure 5-29: Triaxiality vs. equivalent strain to fracture for Point C (outer riser pipe) and D (inner drill pipe).

been independently developed at MIT and CSM. Work is in progress at both institutions to characterize plasticity and fracture properties of ultra high strength steels for deep-water applications. The interest towards reliable predictive tools has recently been renewed in connection to the DeepHorizon accident in the Gulf of Mexico. The results of the present pilot study on the numerical simulation of shear ram cutting through a riser and drill pipe system are very promising for the understanding of the mechanics of the process and the correct design of effective cutting hardware. Furthermore, the presented analytic solution should prove very useful in the preliminary stage of design. At the same time, virtual prototypes are speeding up the design cycle and are reducing expensive full-scale testing. It is seen from Fig. 11 that the cutting force is relatively low in the initial phase and then rapidly increases towards the end of the process. By changing the design of blades it is possible to exert a lower, more constant level of force throughout the whole cutting process.

5.4 Deepwater Horizon Platform Sinking Reconstruction

The intent was to address real-world case of operational and/or accidental loads were pipes were subjected to extreme loading. In April 2010, the BP accident presented itself as a perfect case study to focus Task 2 research. In order to explain the origin of the oil leak, we focused our attention on extreme bending of a riser containing a drill pipe. That was done when the plasticity and fracture properties of offshore grades of steel are not determined yet. Therefore, the original simulation was performed using material data from the automotive TRIP690 steel, which had similar mechanical properties to medium grade offshore steels. The MIT simulation predicted exactly the location of the fracture sight of the leaking pipe, released in the official BP website. The results were presented at the 21st ISOPE conference and captured the attention of the community and the media. This line of research will continue in the proposed Phase II research, as explained in what follows.

Extensive research in the area of plasticity and fracture modeling of high strength steels is been pursued in the Impact and Crashworthiness Lab at MIT. This project is supported by the international fracture consortium on AHSS funded by the automotive and steel industry. The MIT fracture model stems from the MMC criterion combined with a suitable biaxial testing program and a calibration procedure. The objective of this paper is to present the main components of this technology and show its capabilities in predicting onset and propagation of cracks in O&G offshore heavy wall pipes. Results are shown for the cases of extreme bending of two concentric pipes and of the shear ram induced cutting process which is a critical part of the blowout preventor function.

5.4.1 Problem Description and Numerical Model

In order to calibrate the fracture properties of TRIP 690 and X70 three different types of tests were performed. Details on the experimental procedure and on the

geometry of the specimens used can be found at [63]. This test procedure has been initially developed for metal sheets. It has been extended however for cylindrical geometry components to characterize plasticity and fracture of offshore steels such as X70 and X100. Equivalent strain to fracture was measured in each case using digital image correlation technique. The calibrated fracture parameters of TRIP 690 are given in Table 5.2. The stress strain curve was measured and reported in a number of earlier publications [63]. This curve can be described with good accuracy by the following hardening law, $\overline{\sigma} = A\epsilon^n$. The coefficients of the power hardening law where $A = 1276MPa$, $n = 0.2655$. The 3D fracture locus of TRIP 690 is shown in Fig. 5-21.

The geometry of the investigated concentric pipes was assumed to be identical to that of the sister platform, Deepwater Nautilus, of the Deep Horizon, available in the open literature [1]. This was cross-checked with dimensions given in the drilling data information handbook [77].

The information regarding the material of the pipes was taken from the drilling common practices data handbook [77]. This handbook provides a list of different materials typically used for deepwater drilling. For the numerical simulations, we have selected TRIP 690 that was studied and fully characterized at ICL and presents similar mechanical properties ($UTS = 900MPa$ and $\sigma_y = 500MPa$) with the offshore steel X95 in order to simulate the material behavior for the case study. The stress strain curve of TRIP 690 is presented at [60]. The fracture data are provided in Table 5.2.

The un-deformed geometric configuration of the concentric pipes is shown in Fig. 6. The left end is the symmetry plane, while the right end of the pipes is subjected to approximately a quarter-circular displacement (see insert in Fig. 5-30), similar to that expected in the case of a sinking platform.

The results from the finite element simulation were compared to the available images provided by Remotely Operated Vehicles (ROV) that investigated the leak of oil in the location of the accident. The outer pipe has a diameter to thickness ratio, $D/t = 31.3$, that would justify the use of shell elements. However, the inner pipe has

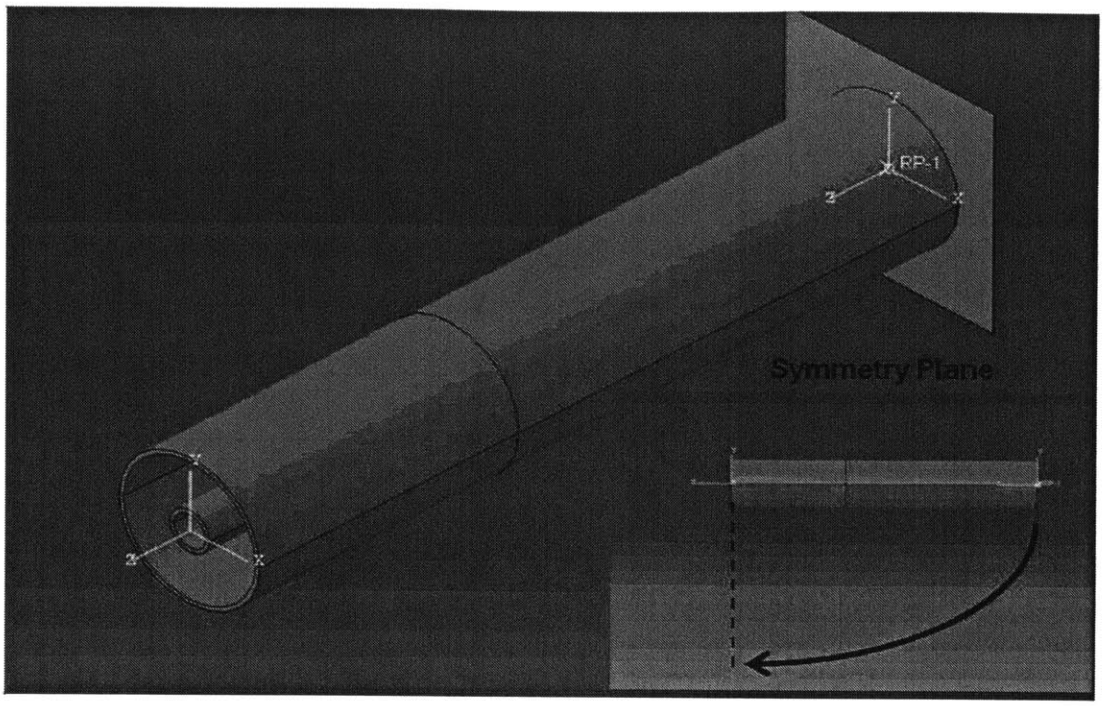

Figure 5-30: Geometrical configuration of the bending numerical simulation model.

$D/t = 10$ and thus it was decided to use solid element model throughout the whole simulation. The solid model of both pipes was build using 8 node quadratic solid elements with reduced integration.

For computational efficiency, only half of the length of the pipes was modeled and symmetric boundary conditions were prescribed on the cutting plane (Fig. 5-30). Furthermore, the half pipes were partitioned into two areas as it is shown in Fig. 5-31. Area 1 is the area of component failure located close to the symmetry plane while Area 2 is the remaining part of the pipe. In Area 2 coarse mesh size 15x15x15 mm (one element through the thickness) is used to reduce computational time. In area 1 however, 5x5x5, i.e. three elements through the thickness are used.

Surface to surface contact settings have been implemented to account for the interactions between inner and outer pipe. In addition, self-contact was introduced to model correctly the flattening and contact of the interior of both pipes in the later stage of the bending process.

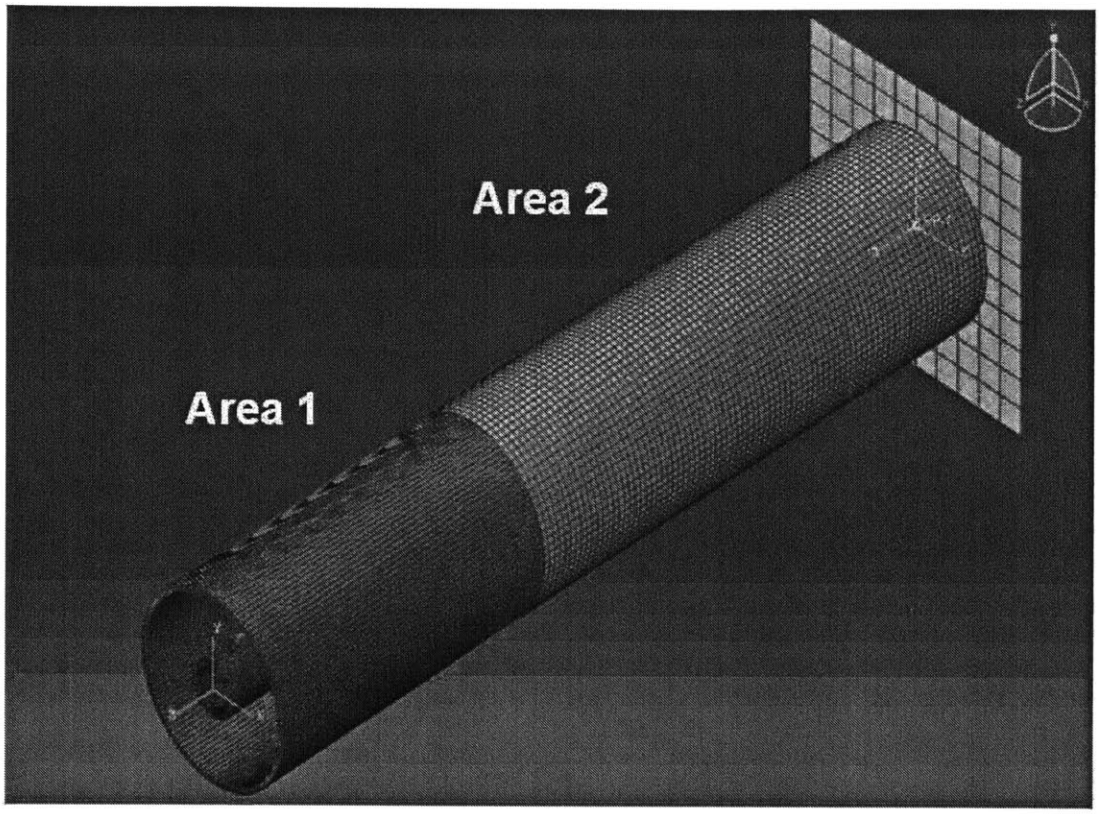

Figure 5-31: Finite element model mesh of the riser/ drill system with fine mesh size prescribed in Area 1 and coarse used in Area 2.

5.4.2 Leak location Prediction

The numerical results are presented in this subsection. The MIT fracture criterion is implemented in the material characterization and when the damage factor reaches a critical value, failure occurs. This leads to element deletion to visualize crack formation.

The progression of damage is shown above in Fig. 5-32. The entire pipe is shown using the available mirroring technique of the Abaqus 6.9. The red areas, that appearing in Figs. 5-32 (middle and right), indicate high values of equivalent strain and potential location of crack initiation. In order to follow the evolution of the cross-section, a cut was made on the symmetry plane, as shown in Fig. 5-33. As the bending progresses, there is an ovalization of the cross-section until complete flattening of the cross-section. The critical locations of high equivalent strain are

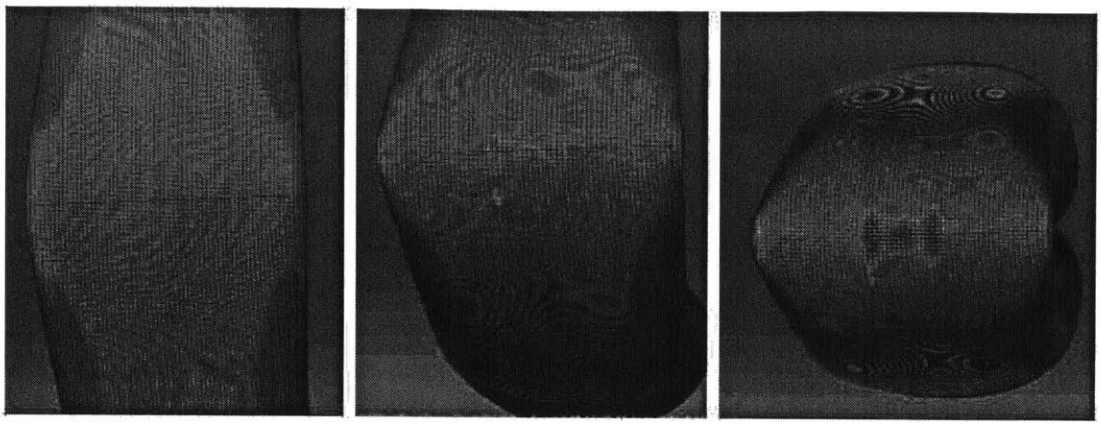

Figure 5-32: Progression of bending of the system of riser/drill and localization of damage.

again shown in red.

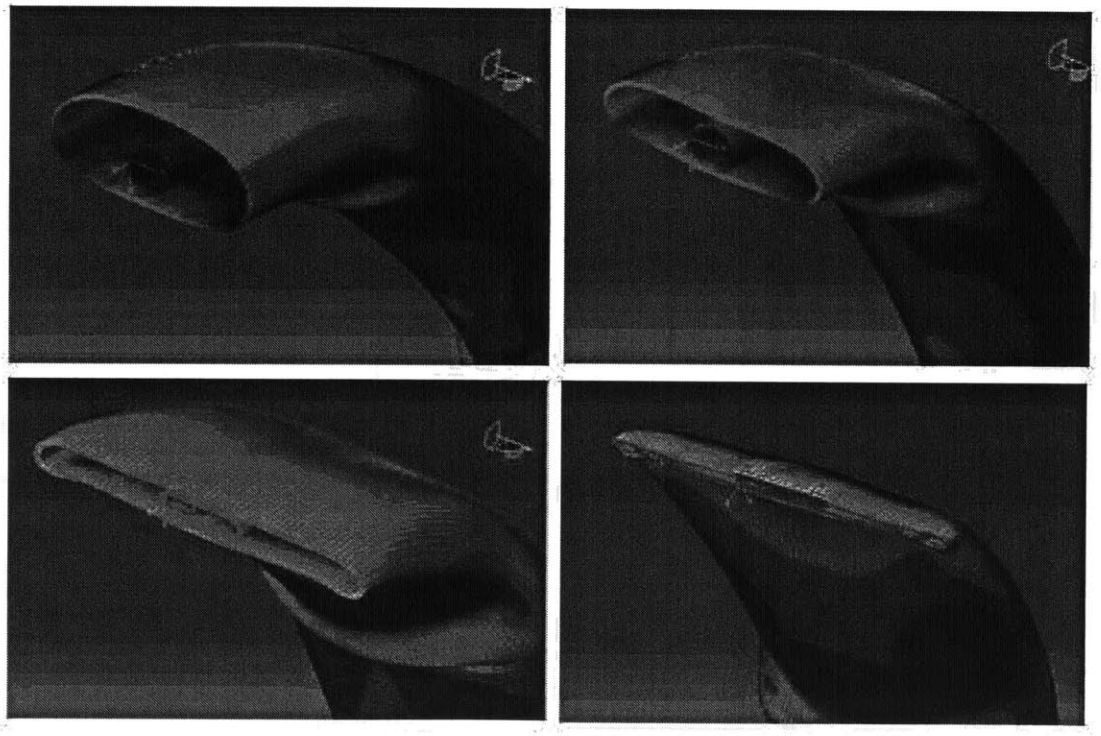

Figure 5-33: History of symmetry plane cross-section up until the onset of fracture.

The case of extreme bending and the possibility of fracture onset in the body of both the inner and outer pipe, was important in the case of the GoM accident, in order to reliably predict the location of leak and the amount of oil pouring our into the

ocean. The accurate prediction of the failure site was achieved and numerical results were compared with picture taken on the spot by ROVs see Fig. 5-34. These pictures were published on the official website of the owner company of the Deep Horizon platform. It is evident that there are four locations of fracture initiation situated symmetrically around the longitudinal axis. After failure of the outer element damage propagates through the thickness leading to see-through cracks and oil leak.

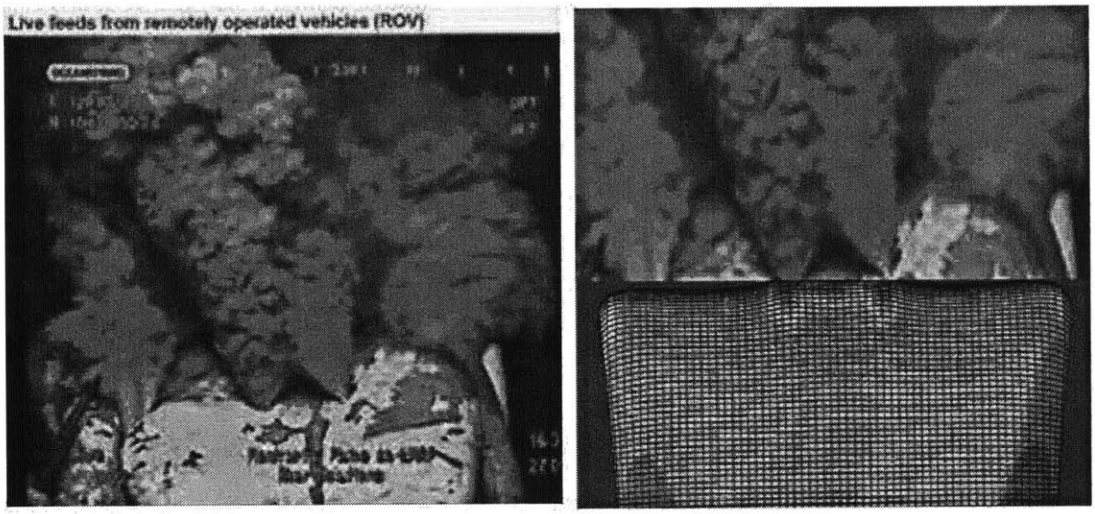

Figure 5-34: On the left: Picture taken from the riser leak location of the Deep-water Horizon platform by underwater ROV. On the right: Comparison of failure location predicted by the Finite Element simulation with the damaged Deep Horizon installation.

The comparison between the photographic evidence (taken from the daily live broadcasts of the owning company) and the numeric simulations are presented side-by-side in Fig. 5-34. The failure locations are correctly predicted (Fig. 5-34). The auxiliary pipes running along the main riser, visible in Fig. 5-34, are not modeled in the FE model but the results are not affected by those components.

5.4.3 History of Stress Triaxiality

In the extreme bending case, the history of stress state at the fracture location is quite complex. This fact emphasizes the need of a more intricate fracture model that can take into account the change of triaxiality and Lode angle dependence during the

bending and cutting process.

The history of triaxiality as a function of equivalent strain was monitored in specific points. Both points selected were located at the area where fracture initiated. More specifically, failure points on the outer pipe, Point A and Point B (see Fig. 5-35) where selected. The triaxiality history was recorded for both points during the finite element simulation. The results for point A are presented in Fig. 5-36.

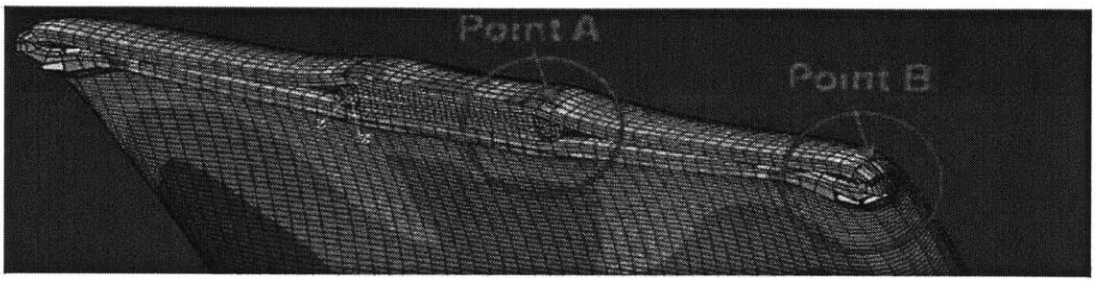

Figure 5-35: Location of failure positions, Point A and B situated on the symmetry plane of the bend pipe.

The history of triaxiality for both points indicates a shift from tension to shear. The triaxiality at Point A starts from $\eta = 0.33$ (representing uniaxial tension), then abruptly goes to the plain strain compression, $\eta = -\sqrt{3}/3 = -0.57$ and ends up with plain strain tension at $\eta = \sqrt{3}/3 = 0.57$. The zero stress triaxiality, characterizing pure shear, is crossed twice (Fig. 5-36).

At Point B on the other hand, the triaxiality starts from the equi-biaxial tension and monotonically decreases to negative values. Almost half of the loading history is dominated by shear superimposed on moderate compression. The above analysis emphasizes the importance of correctly modeling shear generated ductile fracture. The inclusion of the history dependent model in the current MIT fracture technology distinguishes it from all other fracture predictive technologies used currently in the O&G industry.

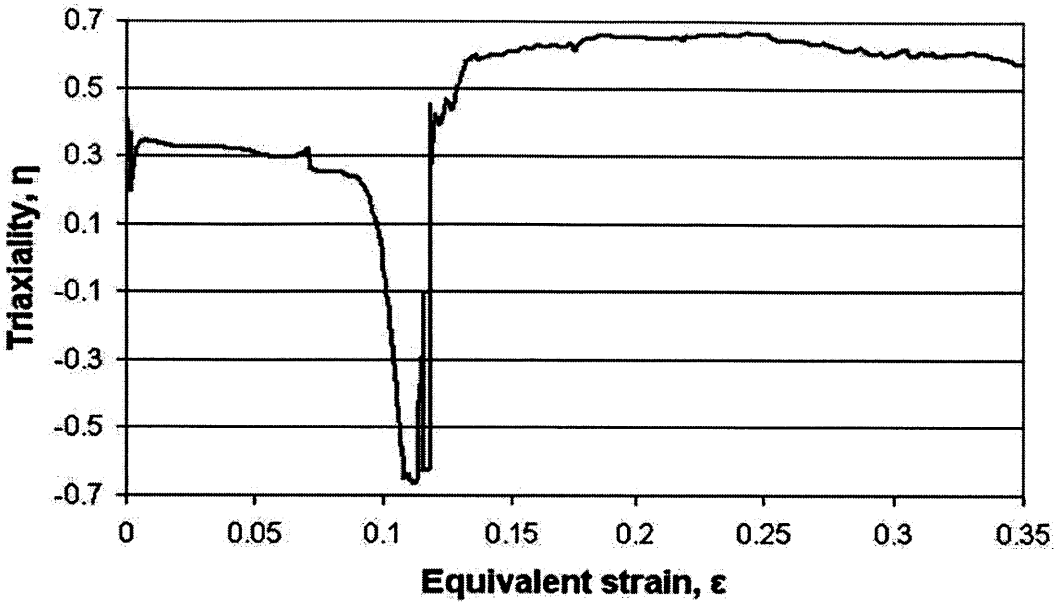

Figure 5-36: Tension dominated history of triaxiality at Point A, as a function of equivalent strain.

5.4.4 Conclusions

The capability of reliably predicting failure for non-monotonic and non-proportional loading is one of the advantages of the MIT fracture technology. The development of a new ductile fracture model that takes into account the loading history effect has been the focus of ICL for the past several years with application to steel, aluminum, automotive and aerospace industries. From the numerical simulation of the above two illustrative examples, it is clear that for the most part, damage is accumulated with negative or zero stress triaxiality. Fracture in these types of problems cannot be predicted by means of the classical of the GNT approach which is only applicable to the tension dominated regions. Likewise, the current JIPs deal with test and predictions of the tensile side of the pre-cracked pipes. Again the experience gained in these projects cannot be extended to the shear dominated failure of pipe components. Therefore, it is strongly recommended that a fracture model capable of including complex and nonlinear loading histories will become the new standard for the O&G industry.

Chapter 6

Financial Analysis Pipelines and Risers

Energy needs are constantly increasing globally and especially for oil and gas. It was estimated that the demand for natural gas is expected to double by 2030 [7]. The oil market is moving in parallel to that of natural gas, projecting similar demand increases. As it is presented in [53], the breakdown of the energy demand between oil, gas and coal, shows that 55% of the global energy demand supplied by oil and gas. Based on the US Energy Information Administration's World Energy Outlook, "fossil fuels will remain the primary sources of energy, meeting more than 90% of the increase in future energy demand". In order to deliver the demand for energy consumption, it is expected that the pipeline infrastructure will grow annually by around 7% projected until 2022, which is translated to more than 8000 km of new pipeline annually [53]. The need for safe, high-pressure pipelines transporting fossil fuel products calls for modern technical approaches assessing the safety and new higher grades of steel that will carry the load reliably.

Also, the ageing of existing pipeline infrastructure requrires the development of a plan for the estimation of its remaining life and the need for its replacement in the following decade. In 2007, the US gas pipeline infrastructure was estimated and presented by [53]. The data are presented in Tables 6.1 for onshore and 6.2 for offshore pipelines. The high pressure liquid transmission lines amount to about

Table 6.1: US onshore gas pipeline estimates for 2007, taken from [53]

Type of pipe	Length in km	Length in miles
Gas Transmission	472,000	295,000
Gas Gathering	34,000	21,000

Table 6.2: US offshore gas pipeline estimates for 2007, taken from [53]

Type of pipe	Length in km	Length in milles
Gas Transmission	10,000	6,000
Gas Gathering	10,000	6,000

251,000 km (157,000 miles). The low pressure gas pipelines amount to about 1,600,000 km (1,000,000 miles). It is evident that the transportation of oil and gas through pipelines both onshore and offshore is a very large market and as environmental restrictions become more strict, new safety assessment tools are essential.

The reduction of transportation costs for fossil fuels has been a major reason for their commercialization. Long-distance pipelines present a safe and at the same time economic means of transportation from the production site to the consumer location. As the sources of fossil fuels move to more hostile locations, the requirement for better pipe design is essential. New methods that are able to offer that safe design are necessary. This is where this work comes to play. Offering not only a new fracture technology for pipe design that assess both the crack resistance and actual strength capacity, but also a combination of the technical analysis with financial assessment. This approach offers a reliable tool that is able to quantify the balance between safety and economic design. It can also quantify the cost versus the benefit between different designs and material selections for a specific pipe installation project. As an illustrative example, the structural integrity against bursting of a pipeline of given geometry will be assessed using the proposed fracture technology. Its cost will be assessed and compared for the two studied grades of steel, X70 and X100. The first grade is a conventional grade of lower strength, while the second one is a relatively new API grade that offers more strength. The case study will include the evalua-

tion of thickness reduction of the original geometric design of the pipe as a benefit from using a grade with higher strength. The detailed description of the mechanical properties of both grades is presented in Chapter 4. This fracture method can offer a competitive advantage to the user, since it included all fracture material properties. These properties can then be implemented into a finite element model for multiple geometry and loading scenarios analysis.

As fossil fuel reserves move to remote locations and specifically deepwater environments, the importance of powerful technical tools for riser design are in need. The broad oil and gas pipe industry (pipeline, riser etc) has a lot to gain from exploring new methods of structural integrity assessment like the one proposed in this work. Deepwater exploration and production refers to water depths greater that 0.3km (1000ft) according to the US Bureau of Ocean Energy Management, Regulation and Enforcement. The increasing depths and relocation to more hostile environments (ultra-deep water, arctic etc.) call for both new fracture methods and higher grade steels, same as in the case of pipelines. Designs and standards are very different for pipelines and risers. The difference lies in the loading, boundary and environmental conditions as well as the materials used for each pipe type. Although, the codes are different, however the underling technical tools assessing the safety factors lag behind when compared to other industries, such as the aero/astro and automotive industries. The current thesis proposes the use of a powerful tool for the assessment of safety combined with a financial module that will readily assess the value of pipe-assets according to the design and material used. The verification of the technical methodology as a powerful safety assessment tool for pipes was completed in Chapters 4 and 5. In the current chapter, the quantification of the cost effect of constructing a pipeline subjected to internal pressure will be presented as an illustrative example, comparing results for API X70 and X100 . As it is already mentioned, there is a compromise between these two grades. X70 offers more ductility, therefore the pipe can sustain more strain during operation, while X100 offers more strength, allowing for higher operational loads. This difference is important for pipe construction. In the following sections two pipelines of the same original geometry will be studied and

their cost structures will be analyzed.

6.1 Current Approaches for Asset Valuation and Financial Analysis of Pipelines

The pipeline industry has been extensively using classical asset evaluation techniques for pipelines. More specifically, regarding the cost assessment, the concept of Net Present Value (NPV) is used. This idea is based on the time value of money, meaning that the value of a given amount of money, at any given currency, changes with respect to time. The value of one US dollar ($) today is different than that of one dollar in a year from now. The underlying reason is that within that year (or within any other time period) money can be invested. Therefore, a return is expected (positive or negative) according to the chosen investment. The value of future cash flows can be evaluated using the definition of NPV, Eq. (6.1).

$$NPV = \sum_{i=0}^{N} \frac{CF_i}{(1+r_i)^i} \tag{6.1}$$

where NPV is the value of the investment in today's money value, CF_i is the cash flow (positive for revenue, negative for cost) at the i_{th} time period in the timeline, r_i is the interest rate that quantifying the time value of money and i represents the index running through time periods (month, year, decade etc.). Usually, every investment has two main features. The expected return of the investment, that is how much the investment has produced or lost during a specific time-frame, and its associated risk. The term risk refers to the possibility of producing different outcomes by taking upon an investment. For example, when investing on a company's stock, there is a risk for bankruptcy. Different possible outcomes can provide different returns for a given investment. The expected return of this asset refers to the weighted average of all possible returns. The weights on this sum are the probabilities of each return actually materializing. As an example, an investment costs $100 (USD) and its possible returns in a year from now are i) $150 (USD) with probability 20%, ii) $200 (USD) with

probability 40% and iii) \$80 (USD) with probability 40%. The expected return of this investment is \$142 (USD) according to Eq. (6.2).

$$r_{exp} = \frac{\sum_{i=0}^{N} r_i p_i - C}{C} \tag{6.2}$$

where r_{exp} is the expected return, C is the price to buy the investment, r_i is the return of each outcome and p_i is the probability of each outcome. Each investment has it own risk and return structure. In a healthy market there is always a risk-free investment (i.e. savings account deposits) that is the lowest discount rate that can be used. Different companies/investors have access to different discount rates based on their credibility and special characteristics. In the current analysis, a starting value that was deduced by industry experts will be considered, $r_i = 10\%$. This will be used as the base scenario for the assessment of the sensitivity of the cost results with respect to r_i. Two additional values will be considered, namely $r_i = 8\% and 12\%$.

Returning to the asset evaluation in the case of pipelines, both the cost of installation, maintenance, operation and other costs and the revenue cash flows are in different points in time. In order to make decisions today for the value of a pipeline the NPV concept is used assessing the value of a pipeline in today's money. Usually, a pipeline is considered a good investment, when the NPV of its cost structure is outweighed by the expected future revenues. When various designs of a pipeline installation are under consideration for a specific projects, then each design can be considered as a different investment that can be assessed. Then, the comparison of these different designs can be done in terms of expected NPV for each one to make managerial decisions. This financial analysis is usually distinct from the technical analysis that ensures that pipelines have a certain level of safety.

Break-even analysis can be used, quantifying what is the time period required for the asset to repay its upfront investment cost and operating and maintenance costs. In order to make that calculation, it is required that certain information are known, such as the expected cost and revenue structure of the asset, the timeline of each expected cash flow and finally the time value of money of the company for

that specific investment. That is usually quantified by the cost of capital. Detailed information on basic financial calculations and definitions can be found in [13]. The timeline of the expected cash flows is defined by the expected life of the asset and the nature of the expected cost and revenue structures. In the case of pipeline, its expected operational life varies between 20 and 40 years. A simple estimate of the expected revenue structure is calculated using the daily production/transportation times the spot value of the contained fossil fuel. The expected cost structure will be presented in detail in the following section.

In this work, the two fields are brought together to offer a tool where safety of the asset is directly linked with its financial value. To illustrate the strength of this methodology, two identical pipes made of X70 and X100 subjected to the same internal pressure (operational load) will be assessed using this unique dual methodology. The balancing effect of safety and cost will be presented in detail.

Pipeline is considered an asset to the owning company and as an asset is required to be evaluated. Especially in the case of the construction of a new pipeline Cost Benefit Analysis (CBA) is used as the systematic approach for estimating and comparing benefits and costs between different suggested designs of pipelines. CBA was introduced by Jules Dupuit in 1848 and later on used by Alfred Marshall. It was originally used in policy related questions, however, its efficacy and applicability rendered it a useful and readily used tool for all kinds of project evaluations. The reason that this method is used is to not only assess and justify the feasibility of building the asset/pipeline but also to offer a comparative tool for different design options. It involves comparing the total expected cost of each different asset/investment against the total expected benefits stemming from its purchase, weighed against benefits to assess the net result. This net effect takes into account the time value of money by discounting each cash flow in present value terms.

In CBA it is not possible to correctly quantify all expected cash flows related to the investment. This approach offers, however, a method for assessing the value of an asset to the best of the analyst's knowledge. In the case of the pipeline example, there is uncertainty in the quantification of the exact cost breakdown, the positioning

of the negative cash flows in the timeline and also the expected revenues. That is due to the fact that, since the price of oil and gas fluctuates greatly with respect to time and cannot be correctly estimated for the life span of a pipeline. The derivative market, that is the market where one can close a given price for a given commodity, such as oil and gas, can provide forward price information for only a period of five years ahead. The uncertainty in price of fossil fuels and in other parameters, such as the discount rate in the NPV calculations can also be taken into account. To take this uncertainty into account a sensitivity analysis allows for the estimation of change in the final outcome with respect to different parameter values.

Coming back to the financial evaluation of pipeline projects, previous authors have focused on the cost side. In [11], the authors aimed to assess the cost structure of pipelines specifically regarding the installation and try to make an assessment based on material cost and the geometric features of the pipe. Other research groups, such as [10] and [7] followed the same idea trying to assess the possible benefit of different materials used for the pipe, quantifying the benefit of advanced strength steels in terms of weight reduction (Fig. 6-1).

In all the above-mentioned work, presenting the cost assessment of different pipeline projects with respect to material selection, the technical analysis was reduced to taking into account merely the nominal yield strength of the material in question. What is important to mention is that no other aspect of the material behavior was considered. Anisotropy and fracture material features were not taken into account which are very important material features for the estimation of the safety level of a pipeline. Therefore, the comparison of projects can be extending to include the entire material behavior. This is a usual method used in the pipeline industry for cost assessment of different projects. In the following section, a new mindset is presented. It is a holistic approach that combines lessons-learned from the technical part of this thesis with financial tools in order to make an assessment on the benefit of higher strength material for pipeline design against bursting (failure of pipes under internal pressure).

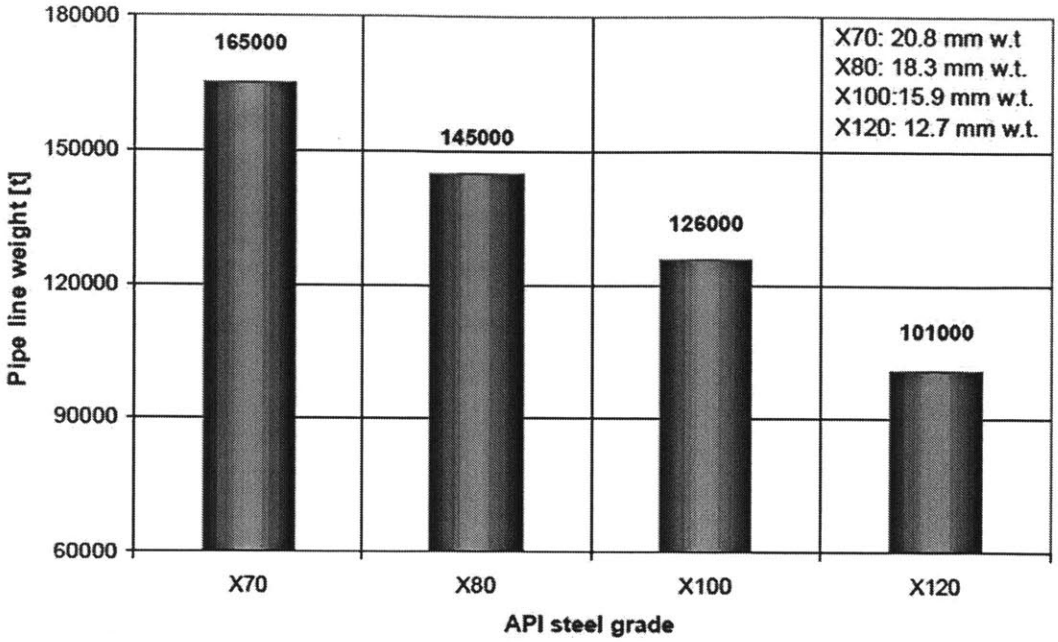

Figure 6-1: Weight reduction trend between pipelines made from different API grades taken from [10].

6.2 Financial Evaluation of Pipelines & Risers with Structural Integrity Input

In this section, the idea of using the results from the technical part of the thesis to assess the thickness reduction of an API X70 pipeline, when the material is replaced with X100, is presented in detail. The full characterization of both materials was the key, innovative component of the followed evaluation of two X70 and X100 pipeline projects. A safety margin factor, α was developed for pipelines based on a hybrid numerical/analytical approach. The safety margin of a pipeline is defined by Eq. (6.3). This is a new definition of safety that is proposed in the current thesis. The pipeline industry is usually using yield-based definitions of safety. As it was mentioned earlier in this chapter, the current thesis proposes a new method of defining safety incorporating all the material characteristics for anisotropy, plasticity and fracture,

through the calculation of the bursting pressure.

$$\alpha = \frac{p_{bursting,FEM}}{p_{yield,analytic}} \tag{6.3}$$

where α is the safety margin, $p_{bursting,FEM}$ is the bursting pressure calculated from finite element simulations and $p_{yield,analytic}$ is the analytic yield pressure. This safety margin factor demonstrates the safety capacity of a pipe subjected to internal pressure against bursting. Based on the results of the finite element simulations, it was possible to assess the following factors are usually considered in the decision process.

1. Pipeline design (diameter, thickness)
2. Pipeline material (traditional vs. AHSS)
3. Operational pressure (production level)
4. Other design aspects (temperature variations, other operating loads etc.)

In order to assess the thickness reduction between the two grades of steel, FEM were developed and ran for both material parameters. The technical part of this case study is presented in detail in Section 5.2. The same finite element model was modified for three different thickness values and ran using the material description for plasticity, anisotropy and fracture X70 and X100. Six cases were processed for the three thickness values (Fig. 6-2) and API grades (Table 6.3). The outer diameter to thickness ratio of the base case (Case 1) was $D/t = 31.3$ and $D = 21$" (533.4mm).

The outside diameter was kept constant, while the internal diameter was adjusted to accommodate for three different thicknesses. The values for the different thickness values were selected based on [65]. The complete information of the mesh and FEM features is presented also in Section 5.2.

The analytic prediction for the yield pressures, calculated using Eq. (5.13), ranged for API X70 between $p^{thick,closed}_{yield,analytic} = 13.11 - 32.12$MPa and for API X100 between $p^{thick,closed}_{yield,analytic} = 18.73 - 45.99$MPa for thickness values ranging between 6.35

Table 6.3: Finite Element Model Simulation Cases

Case name	Material	thickness [mm]
Case 1	X70	15.88
Case 2	X100	15.88
Case 3	X70	10.16
Case 4	X100	10.16
Case 5	X70	6.35
Case 6	X100	6.35

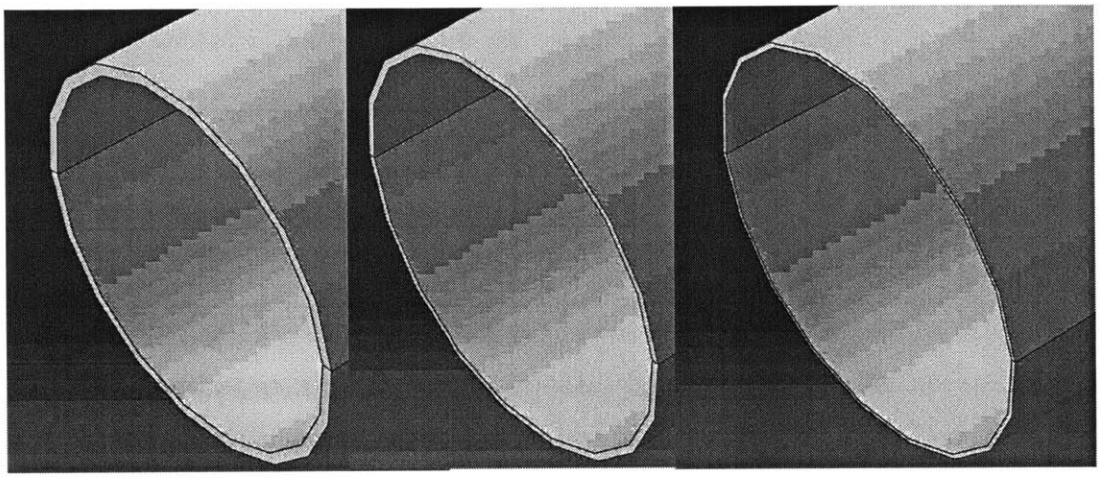

Figure 6-2: FEM models for the three different thickness cases, $t = 0.6$" (left), $t = 0.4$" (middle) and $t = 0.25$" (right).

to 15.88mm. The process of the evaluation of the thickness reduction between the low, X70 and the high grade, X100 steels is demonstrated in Fig. 6-3. It is clear that the bursting pressure of grade X100 is larger for all thickness variations as it was expected. This additional strength can be used for reducing the amount of material used for the construction of a given pipe, by replacing a lower grade steel, in this case X70, by a higher grade steel, X100. The financial effect of this will be full described in the following section.

The numerator of Eq. 6.3 includes all the material features (elasticity, anisotropic plasticity and fracture) offering a reliable first estimate of the bursting pressure. For the denominator there is a multitude of different choices that is related to the thickness of the pipe and end conditions. There are four different possible analytic estimation of

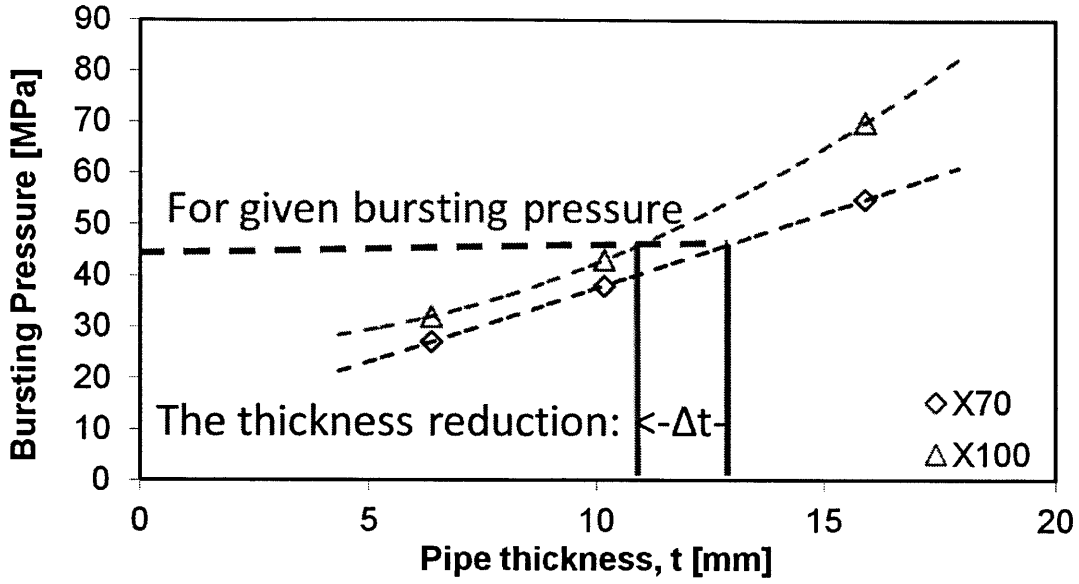

Figure 6-3: Evaluating the thickness reduction between X70 and X100 taking into account the full material characterization of both API grades.

yield pressure (thin-open, thin-closed thick-open, thick-closed). In testing procedure the usual consideration for the end conditions is to consider that the pipe ends are closed. In operational conditions, open ends are usually considered. The difference between thin- and thick- stems in the calculation of the safety factor due to the fact that in the first case the denominator is calculated using membrane theory, Eq. (5.12), while in the later by Eq. (5.13), based of a complete solution. That effect is demonstrated in Fig. 6-4

Each grade dissipates energy during its loading with internal pressure. Permanent damage starts after the onset of yield begins and extends until the initiation of cracks and subsequent through-thickness fracture. The difference in pressure between first yield at the internal surface of the pipe and the final bursting is an indication of the pressure capacity of the pipe. The results for X70 and X100 are presented in Fig. 6-5.

It is evident that the area between the solid and dashed lines reduced in the case of API X100 (green), while the lines both for the yield and bursting pressure move upward between API X70 and X100 (Fig. 6-5). The area between the yield and the

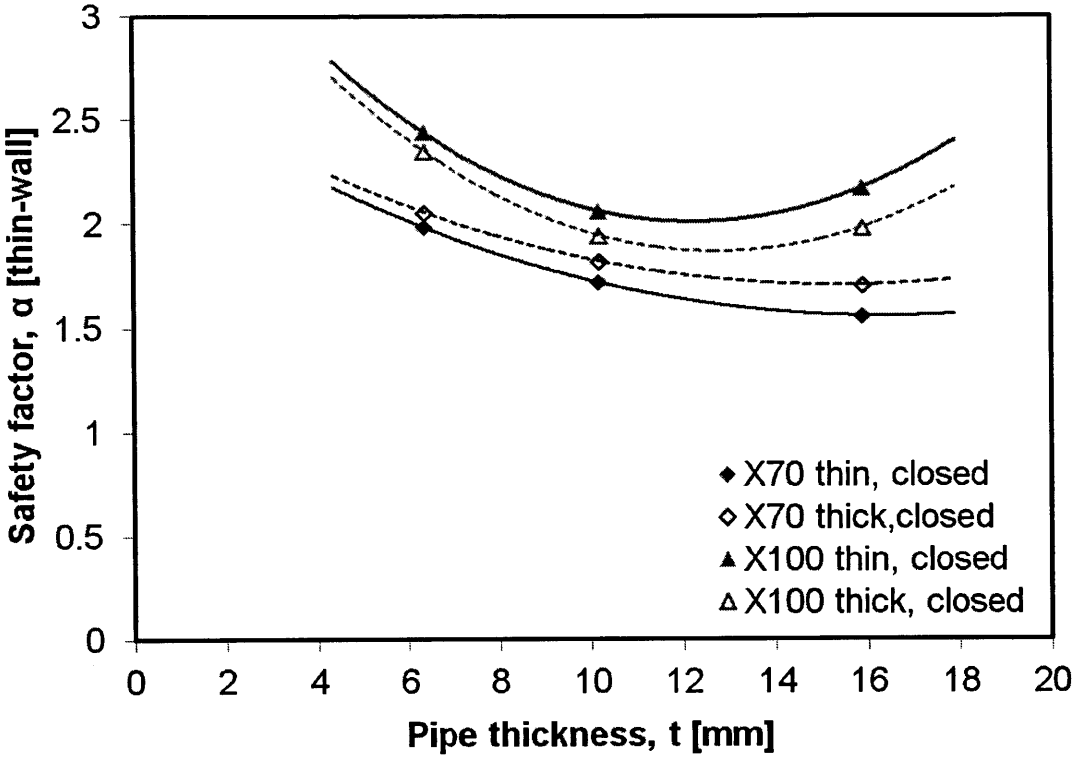

Figure 6-4: Difference in the safety factor evaluation between consideration of thin- and thick-walled pipes for X70 and X100.

fracture lines decreases for higher grades, demonstrating the reducing ductility, while the upward trend between API steels demonstrates the increase in strength.

Based on Fig. 6-3, the thickness of an original pipe ($t = 15.88mm$) can be reduced to $t_{reduced} = 13.1mm$ for X100 material replacement to sustain the same level of bursting pressure. The weight reduction per unit length of the pipe is This estimation is not merely based on yield pressure as other past approaches did, but it includes all material characteristics that stem from the analysis using the MIT fracture technology. This is a large stem towards inclusive approaches that combine engineering and finance for managerial decision making.

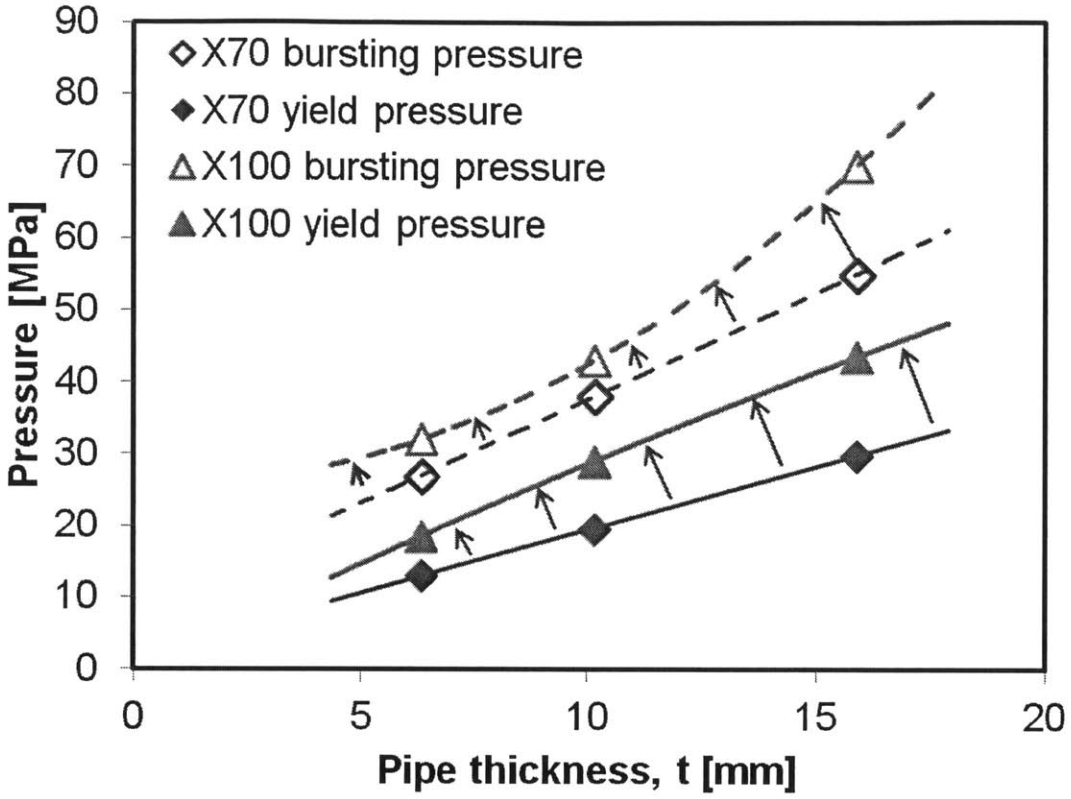

Figure 6-5: Difference between analytic yield pressure for thick pipes with closed ends and FEM predicted bursting pressure for six cases transitioning from of API X70 to X100.

6.2.1 Effect of Material Price

The first step of the cost-benefit analysis is the pipeline cost breakdown for the Capital Expenditures (CAPEX). CAPEX is the upfront cost for the installation and completion of the project. CAPEX consists of different cost components. These are i) construction (Right of Way: ROW), ii) material, iii) labor and iv) miscellaneous costs. This breakdown is standard and it is presented in many relevant papers, including [11]. In Fig. 6-6, a typical breakdown is presented for the CAPEX of pipelines.

The most important component that scales with the weight reduction of the amount of material used due to thickness reduction is the material cost. It is important to mention that although the amount of material used reduces for higher grades, however the price of higher grades steels is higher than that of conventional

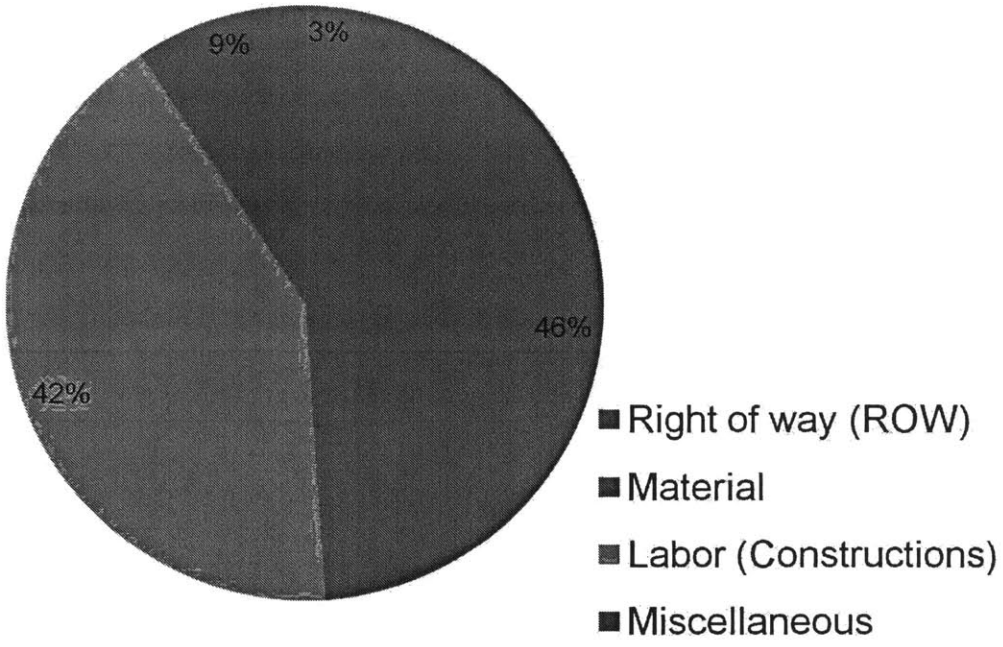

Figure 6-6: CAPEX breakdown for pipelines.

ones, justifying the intensive Research and Development investments on developing and standardizing new grades. Therefore, the material cost component of a new pipe design (AHSS pipe) is reduced provided that the new grade is not more expensive than a certain percentage of the cost of the original, low strength material. To explore that relation between the price difference of the two materials and the cost reduction a sensitivity analysis was conducted for different price differences of X70 and X100. For each case of price difference, the material cost was evaluated for both grades and cost reduction between the two grades was computed. Seven price scenarios were assumed. The price of X70 was used a benchmark and the price of X100 was evaluated in terms of % of increase with respect to X70 (Table 6.4).

The outcome of this analysis is presented in Fig. 6-7. The calculation of the cost reduction is done following industry assumptions about material prices ($Price_{X70} = \$700/metricton$). The evaluation of cost reduction is according Eq. (6.4).

Table 6.4: Results from sensitivity analysis of material price to the cost change between X70 and X100 pipelines of the same safety.

Price increase [%]	Cost reduction [%]
0	17.8
5	13.7
10	9.6
15	5.4
20	1.3
25	-2.8
30	-6.9

$$\frac{\delta Cost}{Cost_{X70}} = \frac{Cost_{X70} - Cost_{X100}}{Cost_{X70}} = \frac{(Area_{X70} \cdot Price_{X70}) - (Area_{X100} \cdot Price_{X100})}{Area_{X70} \cdot Price_{X70}} \tag{6.4}$$

where $Area_{X70}$ is the cross-sectional area of the original X70 pipe, $Area_{X100}$ is the cross-sectional area of X100 reduced thickness pipe, $Price_{X70}$ is the X70 material price and $Price_{X100}$ is the X100 material price, and P_i is the percentage increase of X100 with respect to X70. For the same price of the two grades the benefit of using higher grade steels is maximized. As the price of X100 increase with respect to the price of X70, the cost reduction diminishes. The interesting outcome of this analysis was that there is a price for API X100 for which the benefit of thickness reduction is evened out by the price effect. It was estimated that if the price of X100 is 22% higher than that of X70, then with regards only to the material cost component of CAPEX there is no financial incentive to switch to X100. However, higher grade steels offer other benefits that may reduce other aspects of the cost structure. Based on industrial data the current price increase of X100 with respect to X70 is around 15%.

The benefit of introducing advanced high strength steels in pipelines for the transportation of fossil fuels can be quantified not only in the material cost reduction but also in the reduction of labor (reduction of welding time), installation (larger pipe segments leading to fast installation times), and raw material transportation costs

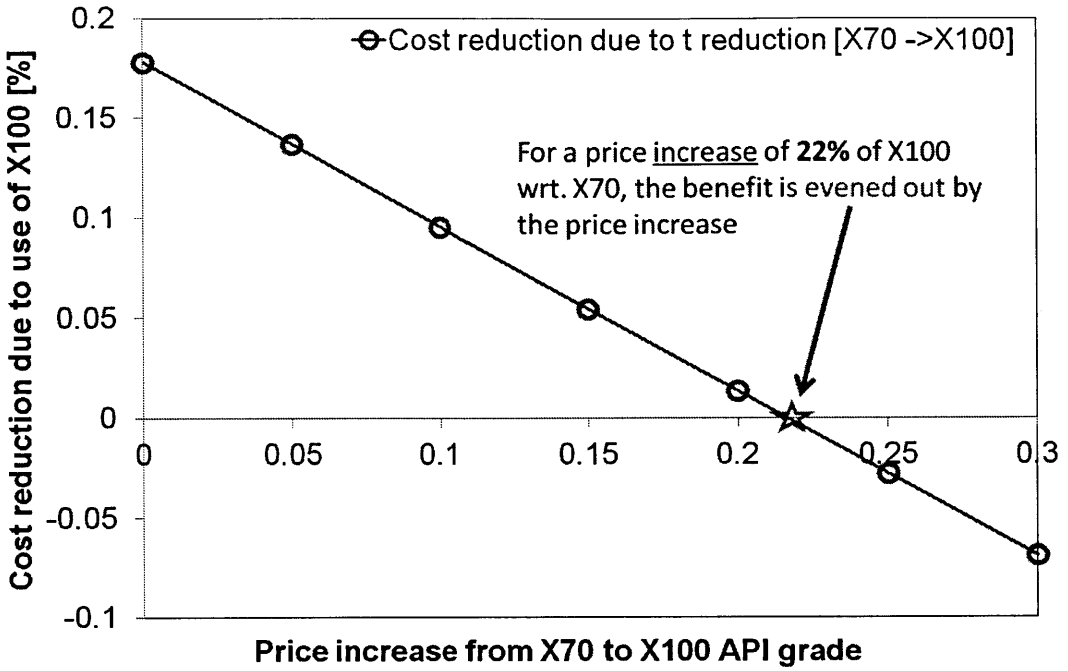

Figure 6-7: Effect of price ratio between X70 and X100 to the material cost.

(less routes for the transportation of the required material). This Section will not go into the detail of estimating the cost reduction of each component. These factor are independent of the pipe engineering. They depend heavily on economic factors, such as transportation rates, labor salaries, global economy etc.

6.2.2 Effect of Discount Rate

The last part of the financial analysis includes all costs throughout the operational life of the pipeline. The total cost includes CAPEX and yearly maintenance and operational. The basic reference providing data on annual maintenance and operational cost for pipelines for this analysis comes from the comparison of cost between pipeline and wire projects presented in [3]. The annual cost of maintenance and operations for pipelines is estimated to be $10,000 (USD) per pipeline mile. The expected life of a pipeline varies between twenty to forty years. In order to quantify today's value of the cost during the asset's life in today's money, all cash flows are discounted to time zero. This refers to the time of initiation of the project construction. The CAPEX are

Table 6.5: The effect of the discount rate in the Cost NPV

r [%]	Change of NPV_{X100} wrt. NPV_{X70} [%]
8	-2.8
12	2.2

separated in two equal parts and spread during the first two years. The construction period could vary from two to six years depending on the location difficulty (terrain, material transportation challenges etc.). For this analysis, the pipeline life is assumed to be forty years and cash flows occur in the first two years. Maintenance costs are considered the same between the two grades (same corrosivity and exposure to accidental events). The baseline of the discount rate was considered to be 10%. Two additional values for the discount rate were considered representing bad and good case scenarios. By replacing the original X70 with X100 and keeping the operational pressure constant, the effect of the discount rate, with respect to the baseline discount rate is shown in Table 6.5.

The discount rate and the cost NPV are variables inversely proportional, meaning that as the discount rate increases the NPV increases. By reducing the discount rate by 20% (from 10% to 8%), the NPV increased by about 3%. In the case of 20% (from 10% to 12%), increase the NPV decreased by around 2%. The reason for this is that the largest part of the cost is positioned on the first few years on the timeline, reducing the effect of the discount rate. In Table 6.6, the percentage of NPV material cost as part of the total NPV cost is presented. The material cost reduced by 3% for all values of the discount rate with respect to the total pipeline cost. It is also important to note that with increasing discount rate the material cost is becoming a larger percentage of the total cost.

Assuming a 1000 mile pipelines, the negative cash flows of the cost distribution in the timeline is shown in Fig. 6-8. All bars represent NPV of costs but are positioned in their actual time location to demonstrate that the NPV of CAPEX comes about early on compared to the maintenance and operational costs that spread evenly throughout the asset's life.

Table 6.6: Cost reduction estimations for different discount rates

r [%]	X70 Material Cost [%]	X100 Material Cost [%]
8	41	38
10	42	39
12	43	40

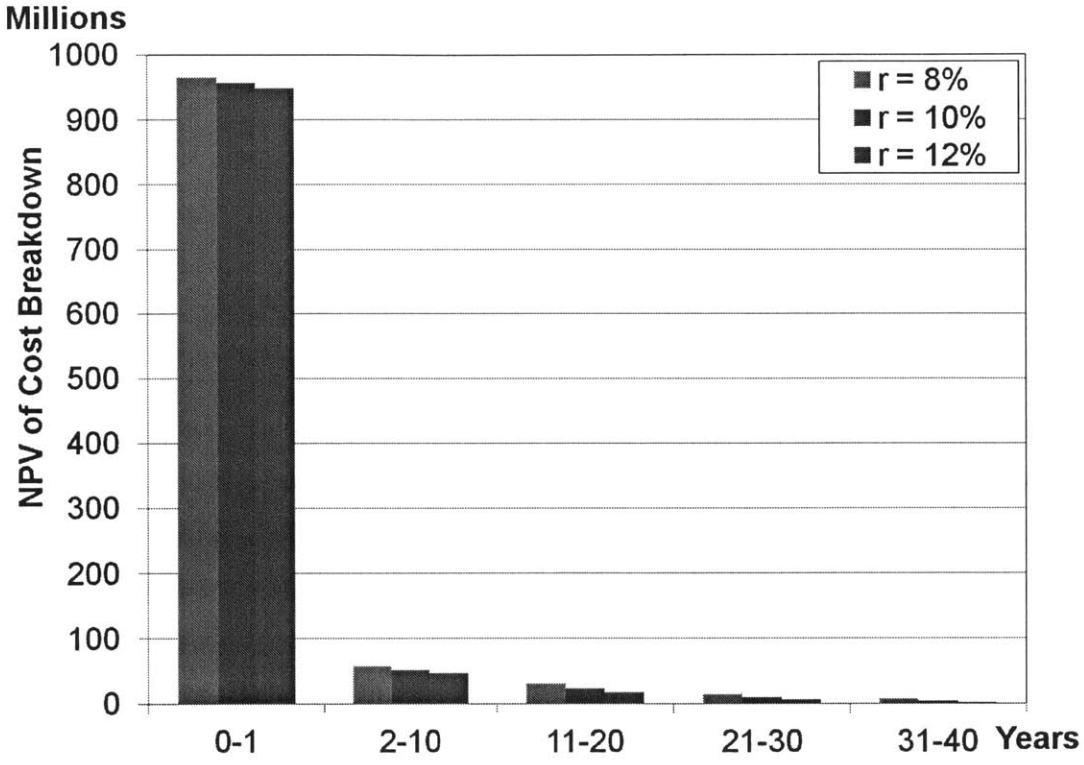

Figure 6-8: Effect of price ratio between X70 and X100 to the material cost.

In the current evaluation, onlythe cost side is addressed so far. The revenue cash flows in a pipeline project are expected to start in two to six years after the completion of the project and to continue throughout its operational life. The NPV of the revenues is expected to be greatly affected by the change in the discount rate, since the installments are expected for a large period of time. In order to quantify, the break-even point for such a project, it is important that we can assess the revenue structure. The NPV of the revenues is again inversely proportional to the discount rate, but the effect now is much stronger. For a 20% reduction of the discount rate the

NPV of the revenues increase by about the same percentage (24.3%) while for a 20% increase the NPV of revenues decrease by about the same amount (22%). A typical distribution of revenue during the operational life of the pipeline is demonstrated in Fig. 6-9. The effect of the discount rate on the revenue NPV is independent of the value of each cash flow provided that the distribution is as presented in Fig. 6-9.

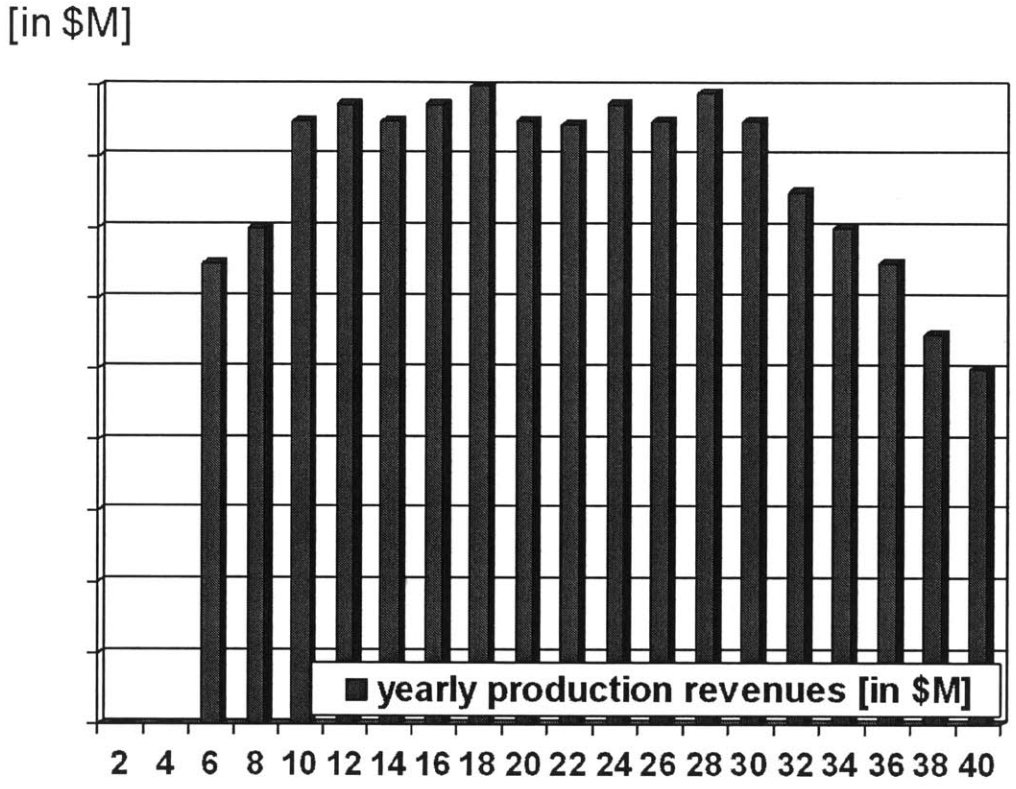

Figure 6-9: Expected revenue cash flows of a pipeline.

Therefore, the effect of the discount rate on the NPV is much stronger in the revenue side than in the cost side. That will affect the break-even analysis for each discount rate. In order to define the exact break-even point, that is the year for which the asset has made up completely for its cost, it is required that the value of the future revenue cash flows is determined in detail. This long unanswered question has troubled finance experts for many years and still a clear answer is not readily available. The main reason lies on the volatility of the energy market and its strong

dependence to global events such as catastrophic events and war, see Fig. 6-10.

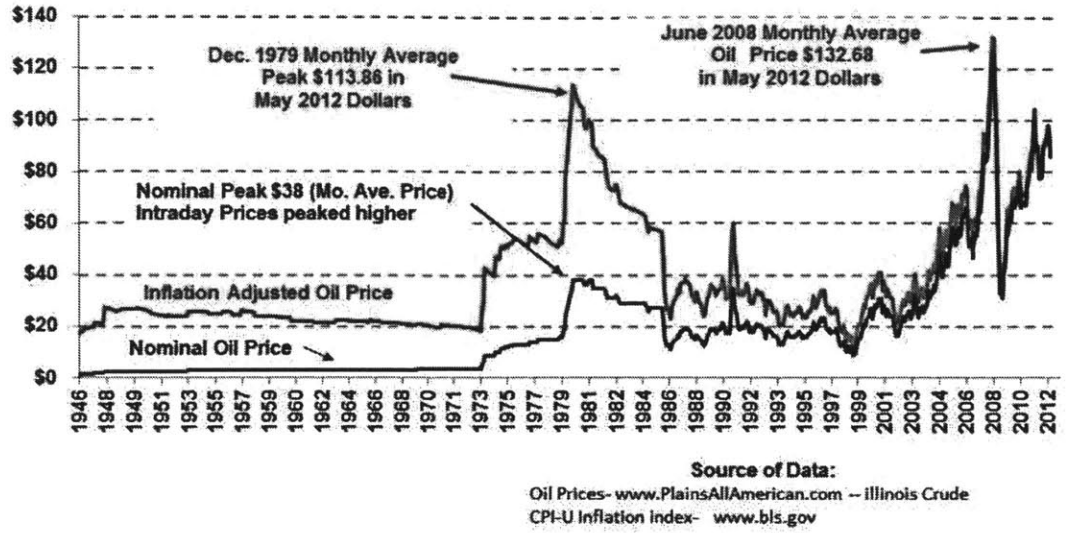

Figure 6-10: Historic data of oil price market between 1946 and 2012.

To the rescue comes the derivative market that can provide estimates of future prices of commodities, such as that of the oil and gas. However, this market can only offer looking-forward information for only a range of 5-10 years leaving a large part of the future revenue cash flow estimation uncovered. The present thesis will not address the question of price evaluation of oil and gas for the operational life of a pipeline. However, the results presented, so far, demonstrate the vast capability of intertwining engineering and finance for management decision making. This work aims to offer an example of the proposed mindset, hoping that other researcher working in the interface of engineering and finance will find this attempt interesting and useful.

6.3 Evaluating the API Trend towards Advanced High Strength Steels

The automotive industry was an inspiration to this work. The automotive industry trend towards advanced high strength steels is showed in Fig. 6-11. The major driver

was cost reduction through weight and fuel reduction. The same trend is observed in the pipe industry, especially for the case of onshore pipelines. Many publications have demonstrated that dynamic including

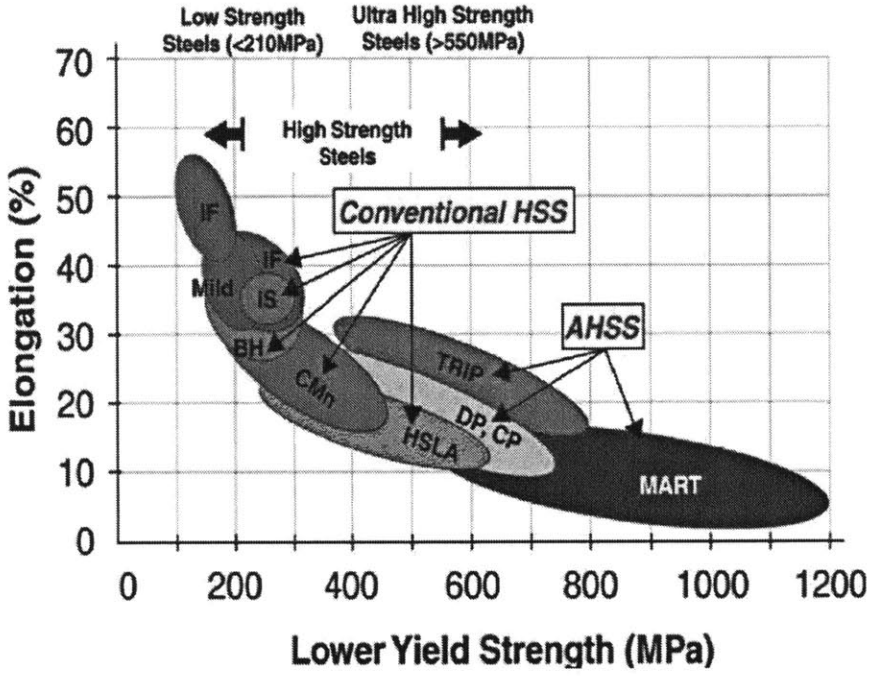

Figure 6-11: Trend towards AHSS observed in the automotive industry.

The API community has demonstrated a similar trend towards advanced high strength steel grades as shown in Fig. 6-12. The move was enforced by increasing demand for safer pipe operation, due to recent accidents and shifting to more challenging areas in terms of permanent environmental and operational loading.

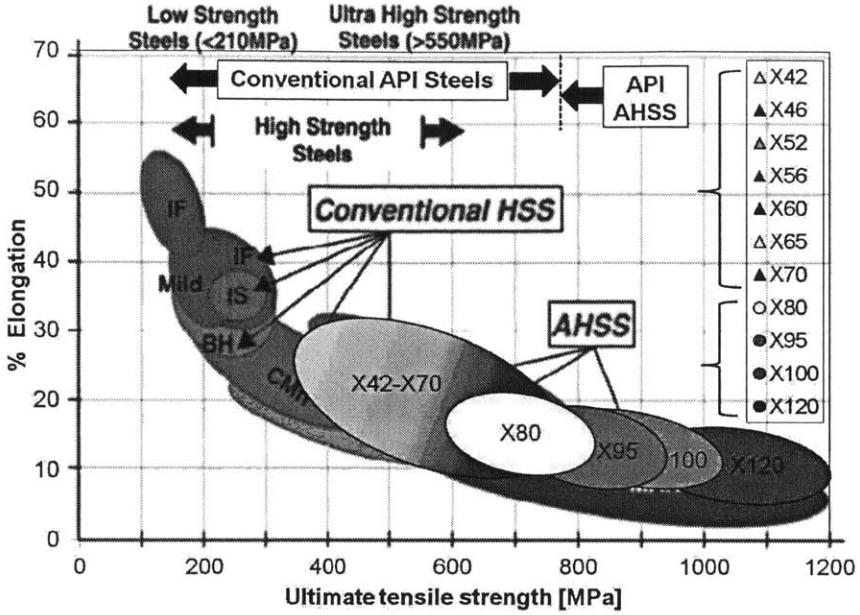

Figure 6-12: Common trend towards AHSS observed in the O&G and automotive industries.

6.3.1 Oil & Gas Infrastructure Evaluation Process

The process for evaluating the cost of construction of pipelines has been an important topic for the oil and gas community. The longer the distance the better the choice of pipelines are for the economic transportation of fossil fuels from the production location to the process facility to the end user. The importance of advanced high strength steels is pronounced in the case of transportation of gas especially for locations where a seaborne option is not available. This is rendering high pressure gas transportation via pipelines increasingly crucial to the energy community. Energy demand is forecast to be doubled by 2030 as it is estimated by various groups including [28]. The trend toward higher strength steels is facilitated by the development of new Advanced Strength steels including X100 and X70. Traditionally, new grades are facing the girth weldability issues, however the industry has worked towards that direction leading to the development of welding procedures for both automatic and manual procedures. It is important to note that other researchers have tried to quan-

tify the financial benefit of new API grades. More specifically, in [7], X80, X100 and X120 are evaluated in terms of cost reduction compared to the conventional X70 API grade. The estimated cost reduction for replacement of X70 to X100 is 30% based on the 30% yield strength increase. However, this is a very crude approximation that takes only into account the yield strength of the material and not both its plasticity and fracture characteristics. An important point that is made in this paper is that the pipe manufacturers are working to standardize fatigue, corrosion and ageing behavior of new API grades so that the effect of these factors can be adequately quantified in terms of operational cost. So far a complete analysis is not available but since the industry in working towards that direction, it will be assumed that the operational costs for both advanced and conventional API grades is the same. The increase of operational pressure leads to rise of daily production by $dpA_{cross-section}$, where $A_{cross-section} = \pi R^2$, dp is the pressure difference and R is the internal radius. The new AHSS grades cost more in absolute numbers but offer higher strength, therefore the cost per unit strength offered is a more appropriate way of evaluating cost. The main cost benefits stem from using less material and the reduction of construction cost. For the thickness reduction the same idea as in [7] is used for the 30% due to the difference in yield strength of 30 ksi from X70 to X100. However, as it was already mentioned, all mechanical properties including ductility reduction should be taken into account. This gap between conservative conventional approaches and new methodologies are bridged and fully explained in the current chapter. This chapter offers a new approach to financial analysis combined with the technical part of the investigation. The proposed idea of this thesis offers an advantage for managerial decision-making by combining lessons-learned from engineering with finance. Both existing and new infrastructure requires modern tools taking full advantage of the developments of engineering and finance for the design of safe and economic pipes.

6.4 Conclusions

The actual current market price for X100 is about 15% more than X70. Therefore, it is economically beneficial to move towards AHSS for pipelines. With time, it is expected that the price of X100 will drop further, therefore the benefits will be even more pronounced. As far as the NPV evaluation, the main conclusion is that the cost side is weakly effected by the discount rate, due to the fact that most of the volume of cost cash flows is positioned in the first few years of the project. In the revenue side the NPV of future revenues is strongly affected. In the overall, project assessment the discount rate is an important aspect that affects the final result of whether the replacement is worth-while.

Chapter 7

Conclusions and Recommendations

7.1 Summary of results

The current thesis offers a comprehensive study of two API grades of steel, X70 and X100, regarding their material properties with respect to anisotropic plasticity and fracture. Extensive experimental and numerical investigations were carried out, resulting in a complete characterization of those two grades. This was the first step into introducing a powerful hybrid tool for structural integrity assessment of thick-walled pipes subjected to complex loads. This fracture technology was originally developed at ICL, in the course of the past 10 years, for metal sheet applications. This method was used for the determination of the mechanical properties of these two grades. In the course of this study, an extension was required in the experimental part for the inclusion of important material behavior outside of the plane stress condition. This so-called extension led to the determination of the material identities, for API X70 and X100, that were subsequently used as a basis to demonstrate the capability of the proposed fracture methodology with respect to pipeline state-of-the-art fracture mechanics methods. Various case studies were carried out with main focus on standardizing the method with respect to current pipe codes. The validation and benchmark of the methodology came as a result of the numerical investigation of SENT specimens using the MIT fracture technology compared to experimental data in collaboration with Salzgitter Mannesmann Forschung Gmb. The outcome of this

study demonstrated the potential of the method to predict material crack resistance by capturing fracture initiation and propagation in pre-cracked SENT specimens. The investigation of the method's capabilities continued with the case study of pressurized pipes up until bursting that resulted in the verification of the method as a design tool for pipelines. The final dual case study focused on riser design under accidental load, leading to extreme bending and requiring urgent shearing for the closure of the connecting well. This study aimed to reconstruct the Deepwater Horizon accident and demonstrate the necessity for modern fracture mechanics approaches used in the design of emergency response plans. The proposed model was able not only to locate the oil leak location, but also access the required force for shearing of the casing and drill pipe to cap the well and contain the oil from polluting the environment. This extensive analysis proved the strength of the method as a structural integrity tool for pipes. The technical analysis of pipes was then combined with financial engineering for the evaluation of the economic benefit of altering the design of pressurized pipelines through material selection from low-grade (API X70) to higher grade (API X100).

7.2 Contributions

The major contributions of the current thesis are:

- Application of the existing MIT fracture technology for the full characterization of two API grades, X70 and X100 for anisotropy, plasticity and fracture for pipeline and riser applications.
- Extension of the applicability of the MIT fracture technology for the range of high triaxiality levels ($\eta \geq 1$) by including standard round notched specimens in the fracture calibration process.
- Validation of the extended material calibration for the prediction of crack resistance of single edge notched specimens subjected to tension for both API X70 and X100.

- Application of the material calibration for large-scale simulations of pressurized pipelines with initial imperfection and comparison of results with experimental and analytic results for both grades, in order to calculate the thickness reduction benefit from replacing API X70 steel grade with API X100, while ensuring structural integrity of pipelines against bursting.

- Application of the material calibration for large-scale simulations of casing containing a drill pipe, subjected to extreme bending, for the prediction of fracture with the objective to identify oil leak locations for the Deepwater Horizon Accident and determination of the shearing force level required for the emergency cut of both pipes.

- Development of a new methodology that combines the technical analysis with financial cost-benefit analysis tools in order to allow for safe and economic management decision-making through the evaluation of the economic benefit of replacing lower grades of steel with advanced strength API grades leading to cost reduction and revenue increase of pressurized oil and gas pipelines.

Each contribution will be presented in short in the following subsections.

7.2.1 MIT fracture technology for API grades

The determination of the exact mechanical properties of a material is essential for an optimal and safe design of pipes. It is especially important for the prevention of over-engineering and the reliable assessment of complex accidental loading, such as extreme bending due to loss of buoyancy of support, or abrupt ground movement. API grades are used for the construction of oil and gas pipes. Therefore their characterization is the first step towards the reliable design of pipes. The backbone of the MIT methodology is the Modified Mohr-Coulomb fracture criterion along with a suitable bi-axial testing program and a calibration procedure. A comprehensive experimental and numerical program was undertaken to determine for the first time the mechanical properties of the traditional API X70 and high strength API X100 grades of steel.

Both materials were characterized for anisotropic plasticity, fracture initiation and uncracked ductility for various states of stress. The outcome of the comprehensive experimental and numerical study resulted into the determination of the 3D fracture locus of both materials presented in Figs. 4-51 and 4-52. These 3D surfaces represent the fracture initiation criterion and offer the capability of realistic finite element simulations for the investigation of the behavior of tubular components of a given geometry subjected to a certain load profile.

7.2.2 Introduction of round notched fracture specimens

The focus of research in pipes lies on pre-cracked structures with high triaxiality stress states and complex loading histories. At the same time, low triaxiality stress states are also essential in order to represent shear-dominated failure in pipes. Impact and Crashworthiness Lab has been conducting work on ductile fracture for over ten years now, with a special focus on metal sheets. This work has been supported by the worldwide automotive and steel industry that is mainly concerned with sheet metal forming and crashability. The standardized fracture specimens used for the calibration of the 3D fracture surface are plane stress limiting the range of applicability of the model to low triaxiality levels. The suitability of the model to characterize ductile fracture has been demonstrated in many publications, primary for the ranges of low stress triaxiality ($\eta < 2/3$). This method was extended to the range of high stress triaxiality ($\eta > 1$), which is very important for analysis of cracked structures. In order to accomplish that both flat and round specimens (Fig. 4-29) were used for the fracture calibration of the API grades. Axisymmetric specimens have been used at ICL in the past but the study of the implications to high triaxiality application was addressed for the first time in the current work. The first type of tests on flat butterfly-shaped, central hole, notched and circular disk specimens; were selected to address the low stress triaxiality range, while tests on round notched bar specimens fracture mechanics tests extended the characterization and verification process to higher stress triaxiality values. The result of this part of the thesis along with the results of the previous subsection will be submitted for publication in the Journal of

Experimental Mechanics.

7.2.3 SENT versus MIT fracture technology for crack resistance prediction

The predictive capabilities of the proposed extended methodology were validated by the comparison of the FEM generated results with SENT tests measurements that are used extensively in the pipeline industry. The outcome of that study was that the present fracture model calibration from un-cracked specimens is able to predict with great accuracy all the features of the pre-cracked SENT experiments. This leads to the conclusion that, the extended calibration methodology that includes the round notched specimens in the calibration process, has great potential as a practical tool in pipeline design predicting reliably the crack resistance measured through SENT experiments. The results of this section resulted in two publications, [62], conference paper in the 22_{nd} ISOPE conference and [58], journal paper submitted and under review to the Journal of Pressurized Vessels and Piping.

7.2.4 Prediction of bursting pressure of pressurized pipelines

The proposed methodology was employed for the prediction of bursting pressure of pipelines. Both API grade characterizations were used and the effect of material mechanical properties and wall thickness on the bursting was determined. In order to induce localization of damage and final bursting, an initial imperfection (local thickness reduction) was introduced. Thickness reduction results between X70 and X100 pipelines resulting from finite element results were estimated and compared to open literature predictions that took only plasticity characteristics of the grades. Results from the analysis were used to assess the strength versus ductility difference between the two grades. The results of this study will be submitted for publication in Journal of Pressurized Vessels and Piping.

7.2.5 Prediction of failure in risers subjected to extreme accidental loading

The capability of reliably predicting failure for non-monotonic and non-proportional loading is one of the advantages of the MIT fracture technology. This new ductile fracture model, calibrated using only flat specimens, takes into account the loading history effect and focuses on shear dominated fracture and plane stress conditions. In order to demonstrate the capabilities of this methodology, material that was calibrated at ICL for the automotive industry, TRIP690, was used for the numerical simulation of extreme bending of two concentric pipes and of the cutting process for the complete separation that is required for the containment of the fossil fuel of the connected well. The reason for investigating these specific cases of accidental loads was the fact that the 2010 Deepwater Horizon accident occurred. Fracture in these types of problems cannot be predicted by means of the classical fracture mechanics methods which are usually only applicable to the tension dominated regions. By using a fracture model capable of including complex and nonlinear loading histories, shear dominated fracture was adequately predicted for both cases of extreme bending and complete shearing. The qualitative and quantitative results compared to the actual BP ROV pictures at the leak location for the first part and analytic estimations for the second part verified that the MMC model was able to predict shear dominated fracture. The results were presented in two conference publications, [60] to the High Strength 2010 Conference and [61], to the 2011 ISOPE conference.

7.2.6 Technical Analysis combined with Finance

After the completion of the technical analysis, the results of the proposed method were used for the improvement of the decision-making process of pipe design based on both its structural integrity and financial value. The selected case for which this mindset was tested, was the design of pressurized pipelines. The first step included technical investigation of the thickness reduction for the pipeline design against bursting of pipes with base material switching from X70 to X100. This employed the capabilities

of the proposed fracture methodology and the full characterization of both API grades. The results of this analysis where subsequently used as input in a sensitivity analysis for the estimation of the value of the asset taking into account both the cost and touching upon the revenue structure during the pipe's operational life. The results demonstrated the trends of the asset's value as a function of the price of the base material and of the rate used to discount all future cash flows to the present.

7.3 MIT Fracture Technology for Pipes

There are many benefits of using the MIT fracture technology in the area of pipe design and structural integrity assessment. The major one is that the applicability of the underlying fracture criterion goes far beyond that of classical fracture mechanics. The Modifiend Mohr-Coulomb criterion can:

- Treat both cracked and un-cracked components.
- Predict not only initiation but also propagation of cracks.
- Predict the stability of crack propagation and its relation to the material properties.
- Offer ease of use since calibration occurs once but the resulting information is part-geometry and loading condition independent.

Another benefit is the reduction of the number of components and full-scale tests for the material configuration which decreases the cost of laboratory and field testing. Based on several validation cases performed under the scope of this thesis, it has been proven that SENT testing results are well predicted through numerical simulation using the material characterization that stems from the MIT fracture technology. The results of this thesis also quantify the safety factor of conventional and new pipe designs under operational loading scenarios. The use of the proposed numerical capabilities can offer a competitive advantage to users for challenging projects in which the current know-how does not allow for safe installation and operation. This method

offers a much higher level of understanding of material behavior, compared to previous methods. Upon completion of the characterization of a grade, the complete material behavior (plasticity and fracture under complex loading paths) is available. Currently, only limited material data are provided to the pipeline customers. Finally, the material parameters for description of anisotropic plasticity and fracture calibrated using uncracked specimens is applicable for the prediction of the response of cracked specimens (SENT) and structural components (pipeline with existing thickness reduction).

7.4 Recommendations on Pipelines & Risers

The current thesis has concluded on the following recommendations for the industry. The trend towards AHSS should materialize for the design and construction of new pipelines and risers in order to take advantage of the benefit in terms of increased pipe strength, that leads to the potential increase of the operating pressure. This leads to increased asset value due to the resulting increased daily production. At the same time, there are significant cost reductions for the use of high strength grades due to resulting design with lower amount of base material used. The current thesis offers sufficient evidence that the suggested fracture methodology can develop into a new standard for the safe, reliable and economic operation of pipes. It is essential that the oil and gas and pipeline industries follow the trend of other industries to move away from outdated and old-fashioned procedures and embrace the future side by side with researchers in the field. Also, one of the conclusions of this work was that it is necessary to create an environment for the free flow of research and information across the academic and industrial barrier for sake of modern and safe design of large-scale metal structures, so that lessons learned from major accidents are efficiently transferred across the entire field to avoid additional catastrophic events due to lack of communication.

7.5 Future Research

Further research should be conducted in the following topics.

- Classification and characterization of weldments (effect of HAZ and welding imperfections)
- Study of the ductile to brittle transition (manifold approach) due to:
  - Addition of dynamics loading effects and study of strain rate.
  - Study of temperature effect in the ductile to brittle transition.
  - Study the effect of increasing stress constrain.
- Investigate the possibility of laboratory material design for a given application through the combination of metallurgy and mechanical property knowledge for the correlation of micro-structure and macro-behavior.
- Study and include the effect of material aging to the mechanical property characterization.
- Transition to fracture methodology for the characterization for anisotropic plasticity and fracture of composite pipes.
- Apply the fracture methodology to other areas of large-scale metal structures such as sky-scrapers, bridges and ships for their structural integrity assessment.

Bibliography

[1] Accessed: 6/25/2010.

[2] Application of the modified coulomb-mohr model to ductile fracture. *Engineering Fracture Mechanics*, May.

[3] Comparing pipes wires - a capital cost analysis of energy transmission via natural gas pipelines and overhead electric wire lines.

[4] Mechanik der festen krper im plastisch deformablen zustand.

[5] *Linepipe Property Issues in Pipeline Design and Reestablishing MAOP*, International Congress on Pipelines. PEMEX, 14-16 November 2001.

[6] *Developments in fracture control technology for gas pipelines utilizing high strength steels*, Tokyo, 2003. 22nd World Gas Conference.

[7] *High Strength large-diameter pipe for long-distance high pressure gas pipelines*, Honolulu, Hawai, USA, 2003. 13th International Offshore and Polar Engineering Conference.

[8] Modeling of plane strain ductile rupture. *International Journal of Plasticity*, 19(10):1517 – 1541, 2003.

[9] *Validation of FE models of pipelines with localized metal loss.* SEM Annual Conference & Exposition on Experimental and Applied Mechanics, 2003.

[10] *Development of grade X120 material for high pressure gas transportation lines*, Ostend, Belgium, 2004. 4th International Conference on Pipeline Technology.

[11] *High-strength Steel Pipeline Economics*, Toulon, France, 2004. 14th International Offshore and Polar Engineering Conference.

[12] *Strain Based Design - What the contribution of a pipe manufacturer can be*, Lisbon, Portugal, 2007. 17th International Offshore and Polar Engineering Conference.

[13] *Financial Modeling.* New York, 3rd edition edition, 2008.

[14] Modification of the gurson model for shear failure. *European Journal of Mechanics - A/Solids*, 27(1):1 – 17, 2008.

[15] *Test methods for characterization of strain capacity: comparison of Rcurves from SENT/CWP/FS tests*, Pipeline Technology Conference, Ostend, 12-14 October 2009. IPC.

[16] Failure by void coalescence in metallic materials containing primary and secondary voids subject to intense shearing. *International Journal of Solids and Structures*, 48(9):1255 – 1267, 2011.

[17] On the predictive capabilities of the shear modified gurson and the modified mohr-coulomb fracture models over a wide range of stress triaxialities and lode angles. *Journal of the Mechanics and Physics of Solids*, 59(7):1374 – 1394, 2011.

[18] P. Hopkins A. Cosham and K.A. Macdonald. Best practice for the assessment of defects in pipelines - corrosion. *Engineering Failure Analysis*, 14(7):1245 – 1265, 2007.

[19] American Petroleum Institute Washington. *Recommended Practice 579, Fitness For Service*, January 2000.

[20] API. *API RP1111, Design Construction, Operation and Maintenance of Offshore Hydrocarbon Pipelines*, 1998 edition.

[21] ASME. *ASME-B31.13-1999, Process Piping, ASME Code for Pressure Piping, B31 an American National Standard*, 2001 edition.

[22] A.G. Atkins. On cropping and related processes. *International Journal of Mechanical Sciences*, 22(4):215 – 231, 1980.

[23] Z. L. Zhang B. Nyhus and C. Thaulow. Normalisation of material crack resistance curves by the t stress. In *2nd International Symposium on High Strength Steel*, Verdal, Norway, 23-24 April 2002.

[24] Yuanli Bai. *Effect of loading history in necking and fracture.* PhD thesis, Massachusetts Institute of Technology, 2008.

[25] Yuanli Bai and Tomasz Wierzbicki. A new model of metal plasticity and fracture with pressure and lode dependence. *International Journal of Plasticity*, 24(6):1071 – 1096, 2008.

[26] Yuanli Bai and Tomasz Wierzbicki. Application of extended mohr-coulomb criterion to ductile fracture. *International Journal of Fracture*, 161:1–20, 2010.

[27] Yuanli Bai and Tomasz Wierzbicki. Partially coupled anisotropic fracture model for aluminum sheets. *Engineering Fracture Mechanics*, 77(7):1128 – 1152, 2010.

[28] Bernstein. Oil market report, October 2008. McKinsey Global Institute Global Energy Demand Model 2009.

[29] British Energy Generation Ltd. *Assessment of the integrity of structures containing defects, R6-Revision 3*, 1999.

[30] BSI. *BS 7448: Part 4 Fracture mechanics toughness tests*, 1997.

[31] BSI. *Guide to methods for assessing the acceptability of flaws in metallic structures*, July 2005.

[32] P.J. Budden. Failure assessment diagram methods for strain-based fracture. *Engineering Fracture Mechanics*, 73(5):537 – 552, 2006.

[33] Canadian Standards Association, Ontario, Canada. *Oil and gas pipeline systems, CSA Z662*, 2007.

[34] Center for Reliable Energy Systems (CRES). *Validation and Documentation of Tensile Strain Limit Design Models for Pipelines*, 2007.

[35] J Chattopadhyay, B.K Dutta, and H.S Kushwaha. Experimental and analytical study of three point bend specimen and throughwall circumferentially cracked straight pipe. *International Journal of Pressure Vessels and Piping*, 77(8):455 – 471, 2000.

[36] McKinsey & Company. Unlocking energy efficiency in the u.s. economy. July 2009.

[37] T. Coppola, L. Cortese, and P. Folgarait. The effect of stress invariants on ductile fracture limit in steels. *Engineering Fracture Mechanics*, 76(9):1288 – 1302, 2009.

[38] Rudi Denys and Antoon Lefevre. Ugent guidelines for curved wide plate testing. In *Pipeline Technology 2009, Proceedings*, page 21, 2009.

[39] Det Norske Veritas. *Recommended Practice - DNV-RP-F101 - Corroded Pipelines*, October 2010.

[40] Vieira R. D. Castro J. T. Benjamin A. C. Freire J. L. F. Diniz, J. L. C. Stress and strain analysis of pipelines with localized metal loss. *Experimental Techniques*, 46(6):765–775, 2006.

[41] M. Dunand and D. Mohr. Ductile fracture of ahss sheets under multi-axial loading: Experiments and modeling. *AIP Conference Proceedings*, 1383(1):484–491, 2011.

[42] K.R. Jayadevan Erling Ostby and Christian Thaulow. Fracture response of pipelines subject to large plastic deformation under bending. *International Journal of Pressure Vessels and Piping*, 82(3):201 – 215, 2005.

[43] Vieira R.D. Freire, J.L.F. and Benjamin A.C. Experimental strain analysis of metal loss defects in pipeline. *Experimental Techniques*, 30(5):42–47, 2006.

[44] Vieira R.D. Freire, J.L.F. and A.C. Benjamin. Experimental techniques in the field of pipeline integrity. *Experimental Techniques*, 30(4):44–50, 2006.

[45] Vieira R.D. Castro J.T.P. Freire, J.L.F. and A.C. Benjamin. Burst tests of pipeline with extensive longitudinal metal loss. *Experimental Techniques*, 30(6):60–65, 2006.

[46] Vieira R.D. Castro J.T.P. Freire, J.L.F. and A.C. Benjamin. Rupture tests of pipeline containing complex-shaped metal loss defects. *Experimental Techniques*, 31(2):57–62, 2007.

[47] GKSS Research Centre. *Fitness for service procedure*, January.

[48] A. L. Gurson. Continuum theory of ductile rupture by void nucleation and growth: Part i—yield criteria and flow rules for porous ductile media. *Journal of Engineering Materials and Technology*, 99(1):2–15, 1977.

[49] D. Hardie, E.A. Charles, and A.H. Lopez. Hydrogen embrittlement of high strength pipeline steels. *Corrosion Science*, 48(12):4378 – 4385, 2006.

[50] Stijn Hertelé. *Coupled experimental-numerical framework for the assessment of strain capacity of flawed girth welds in pipelines.* PhD thesis, Ghent University, 2012.

[51] R. Hill. A theory of the yielding and plastic flow of anisotropic metals. *Proc. Roy. Soc. London*, 193:281297, 1948.

[52] P. Hopkins. Comprehensive structural integrity - the structural integrity of oil and gas transmission pipelines. *Elsevier Science Ltd.*, 2003.

[53] P. Hopkins. Oil and gas pipelines: Yesterday and today. 2007.

[54] Sueyoshi H. Ishikawa, N. and S. Igi. Application of damage mechanics modeling to strain based design with respect to ductile crack initiation. In *8th International Pipeline Conference*, Alberta, Canada, 2010.

[55] ISO. *Petroleum and Natural Gas Industries - Steel Pipes for use as Casing or Tubing for Wells*, 2004 edition.

[56] J. Jackiewicz. Use of a modified Gurson model approach for the simulation of ductile fracture by growth and coalescence of microvoids under low, medium and high stress triaxiality loadings. *Engineering Fracture Mechanics*, 78:487–502, 2011.

[57] K.R Jayadevan, Erling Ostby, and Christian Thaulow. Fracture response of pipelines subjected to large plastic deformation under tension. *International Journal of Pressure Vessels and Piping*, 81(9):771 – 783, 2004.

[58] A. Nonn K. Kofiani and T. Wierzbicki. New calibration method for high and low triaxiality and validation on sent specimens of api x70. *International Journal of Pressure Vessels and Piping.* Under review.

[59] Sandeep Kibey, Xiangyu Wang, Karel Minnaar, Mario L. Macia, Doug P. Fairchild, Wan C. Kan, Steve J. Ford, and Brian Newbury. Tensile strain capacity equations for strain-based design of welded pipelines. *ASME Conference Proceedings*, 2010(44236):355–363, 2010.

[60] Evangelos Koutsolelos Kirki N. Kofiani and Tomasz Wierzbicki. Multi-axial fracture of advanced high strength steels. In *2nd International Conference of Super-High Strength Steels, month =*.

[61] Evangelos Koutsolelos Kirki N. Kofiani and Tomasz Wierzbicki. Shear generated fracture in predicting oil leak in accidents involving sinking platforms. In *21nd International Offshore and Polar Engineering Conference, month =*.

[62] Nonn A. Wierzbicki T. Kalwa C. Kofiani, K. and C. Walters. Experiments and fracture modeling of high-strength pipelines for high and low stress triaxialities.

[63] Yaning Li and Tomasz Wierzbicki. Prediction of plane strain fracture of ahss sheets with post-initiation softening. *International Journal of Solids and Structures*, 47(17):2316 – 2327, 2010.

[64] Mannesmann. *Steel Tube and Pipe Manufacturing Processes.*

[65] E. W. McAllister, editor. *Pipeline rules of thumb handbook : quick and accurate solutions to your everyday pipeline problems.* Gulf Professional Pub., Boston, 2002.

[66] Shinohara Y. Sakamoto S. Tsuru E. Asahi H. Nagai, K. and T. Hara. Anisotropy of the stress-strain curves for line pipe steels. *ASME Conference Proceedings*, 2010:59–65, 2010.

[67] Kalwa C. Nonn, A. Modeling of damage behavior of high strength pipeline steel. In *18th European Conference on Fracture of Materials, year = 2010, address =*.

[68] U.S. Department of the Interior. Assessment of undiscovered technically recoverable oil and gas resources of the nations outer continental shelf, February 2006.

[69] E. Ostby. Fracture control offshore pipelines - phase ii, 2007.

[70] H. Pisarsky. Flaw tolerance in pipeline girth welds subjected to axial straining and internal pressure, 2007.

[71] T. A. Bubenik R. J. Eiber, W. A. Maxey. Final report on fracture control technology for natural gas pipelines, 1993.

[72] Andreas Sandvik, Erling Ostby, and Christian Thaulow. A probabilistic fracture mechanics model including 3d ductile tearing of bi-axially loaded pipes with surface cracks. *Engineering Fracture Mechanics*, 75(1):76 – 96, 2008.

[73] Bo Cerup Simonsen and Rikard Tornqvist. Experimental and numerical modelling of ductile crack propagation in large-scale shell structures. *Marine Structures*, 17(1):1 – 27, 2004.

[74] Benjamin A.C. Vieira R.D. Freire J.L.F. Souza, R.D. and J.T.P. Castro. Rupture tests of pipeline segments containing long real corrosion defects. *Experimental Techniques*, 31(1):46–51, 2007.

[75] Steglich and Brocks. Micromechanical modelling of damage and fracture of ductile materials. *Fatigue & Fracture of Engineering Materials & Structures*, 21(10):1175–1188, 1998.

[76] B. Tanguy, T.T. Luu, G. Perrin, A. Pineau, and J. Besson. Plastic and damage behaviour of a high strength x100 pipeline steel: Experiments and modelling. *International Journal of Pressure Vessels and Piping*, 85(5):322 – 335, 2008.

[77] Technip. *Drilling data handbook*, 8th edition edition.

[78] V Tvergaard. On Localization in Ductile Material Containing Spherical Voids. *International Journal of Fracture*, 18(4):237–252, 1982.

[79] V Tvergaard and A Needleman. Analysis of the Cup-Cone Fractrure in a Round Tensile Bar. *Acta Metallurgica*, 32(1):157–169, 1984.

[80] A.R. Watson, S.R. Reid, W. Johnson, and S.G. Thomas. Large deformations of thin-walled circular tubes under transverse loadingii: Experimental study of the crushing of circular tubes by centrally applied opposed wedge-shaped indenters. *International Journal of Mechanical Sciences*, 18(78):387 – 397, 1976.

[81] Abramowicz W. Wierzbicki, T. *The mechanics of deep plastic collapse of thin-walled structures.* Wiley, New York, 1989.

[82] Dirk M. Wierzbicki, T. Mit industrial fracture proposal, July 2010.

[83] T. Wierzbicki and M.S. Suh. Indentation of tubes under combined loading. *International Journal of Mechanical Sciences*, 30(34):229 – 248, 1988.

[84] David Wilson. Gulf of mexico oil spill causes $95 billion in stock damage: Chart of day, May 2010.

[85] Liang Xue and Tomasz Wierzbicki. Ductile fracture initiation and propagation modeling using damage plasticity theory. *Engineering Fracture Mechanics*, 75(11):3276 – 3293, 2008.